

**CHEMICAL SYNTHESIS AND BIOLOGICAL
EVALUATION OF INHIBITORS AND SUBSTRATE OF
CYTOSOLIC PHOSPHOLIPASE A₂**

NG CHENG YANG

(B.Sc.(Hons.), NUS)

**A THESIS SUBMITTED
FOR THE DEGREE OF DOCTOR OF PHILOSOPHY
DEPARTMENT OF CHEMISTRY
NATIONAL UNIVERSITY OF SINGAPORE**

2016

DECLARATION

I hereby declare that this thesis is my original work and it has been written by me in its entirety, under the supervision of A/P Lam Yulin, (in the laboratory S5-03-19/03), Chemistry Department, National University of Singapore, between 2012 and 2016.

I have duly acknowledged all the sources of information which have been used in the thesis.

This thesis has also not been submitted for any degree in any university previously.

The content of the thesis has been partly published in:

Chem. Commun. **2017**, 53, 1813-1816

Ng Cheng Yang

02/06/2016

ACKNOWLEDGEMENT

I would like to express my deepest gratitude to my supervisor, Associate Professor Lam Yulin. The past few years of my Ph.D. had been incredibly hectic and without her patience and guidance, this work would not have materialized. This is especially so during the final phase of the Ph.D. and I am very grateful for her support, constant encouragement and invaluable advices. I would also like to thank my co-supervisor, Associate Professor Low Chian Ming for all the invaluable support and advices he had given.

I would also like to express my deepest appreciation to my group members in chemistry, Dr Wong Lingkai, Dr Sanjay Samantha, Dr Woen Susanto, Dr Hadhi Widjaya, Dr Ang Wei Jie, Dr Poh Zhong Wei, Gan Chin Heng, Chng Yong Sheng, Maximillian Viera, Tan Yu Jia, Ong Wee Yong, Cliff Anderson, Eric Lee Jing Xiang, Niu Zilu, Kevin Timothy Fridianto, Ian Seet Hua En, Timothy Kwok Xiong Wei, Wilson Toh Ghim Hon, Teng Yi Feng, Albertus Triadhi Pradintyo and Cao Xujun for all their help and guidance in the lab. Thanks for all the insightful discussion especially with Dr Ang Wei Jie. I would also like to express my deepest gratitude to Dr Francis Tan Chee Kuan for all the help given, from the most basic to all the works in biology conducted in the thesis. Without his patience in explaining the concepts as well as the long hours of discussion, everything would not have been possible. My deepest appreciations to the admin and staffs of chemistry and pharmacology department, Miss Suriawati Binte Saad, Dr Wu Ji'En, Dr Yuan Chenghui, Mdm Han Yanhui, Mdm Wong Lai Kwai and Miss Cheong Yoke Ping for all their help in administrative matters as well as NMR and Mass analysis of the compounds synthesized.

Finally, I would like to thank my family and friends for their support and encouragement throughout my study. They are Wesley Yu, Choong Ping Sen, Hung Hui Yi, Kelvin Lim, Mark Seow and HBI. Last but not least to my fiancée, Miss Tay Manjun for all the support, help and encouragements. Thank you for being with me during the darkest days and helping me in any ways possible to make this journey more endurable.

TABLE OF CONTENTS

ACKNOWLEDGEMENTS	i
TABLE OF CONTENTS	ii
ABSTRACT	vi
LIST OF TABLES	vii
LIST OF FIGURES	viii
LIST OF SCHEMES	x
LIST OF ABBREVIATIONS (CHEMISTRY)	xi
LIST OF ABBREVIATIONS (BIOLOGY)	xiv
LIST OF PUBLICATIONS	xvii
CHAPTER 1: INTRODUCTION	
1.1 Phospholipase A ₂ and Its Functions	1
1.1.1 Inflammation and Arachidonic Acid Cascade	2
1.1.2 sPLA ₂	3
1.1.3 iPLA ₂	3
1.1.4 cPLA ₂	4
1.1.4.1 cPLA ₂ isoforms and substrate specificity	4
1.1.4.2 Activation Mechanism of cPLA ₂	5
1.2 cPLA ₂ in Neuroinflammation	7
1.3 cPLA ₂ in Alzheimer's Disease	8
1.4 Current Developments in cPLA ₂ Inhibitors	
1.4.1 Trifluoromethylketones	10
1.4.2 Oxoamides	12
1.4.3 Indoles and Derivatives	14
1.4.4 Pyrroles	17
1.4.5 Pyrrolidines	18

1.4.6	Other inhibitors	19
1.5	Fluorogenic Inhibitors and Substrates of PLA ₂	
1.5.1	Principles of Fluorescence	22
1.5.2	Fluorophores and Immunofluorescence	23
1.5.3	Fluorogenic PLA ₂ probes	26
1.6	Objectives of Research	28
1.7	References	29

**CHAPTER 2: CHEMICAL SYNTHESIS AND STRUCTURE-ACTIVITY RELATIONSHIP
STUDIES OF ARACHIDONIC ACID ANALOGUES AS CYTOSOLIC PHOSPHOLIPASE A₂
INHIBITORS**

2.1	Introduction	36
2.2	Chemical Synthesis	
2.2.1	Retrosynthetic Analysis of AACOCF ₃	37
2.2.2	Synthesis of AACOCF ₃ and Trifluoromethylketone-based Analogues	39
2.2.3	Synthesis of Arachidonyl-based Amide Analogues	42
2.3	Biological Results of cPLA ₂ Assay	45
2.4	MTS Assay	51
2.5	Selectivity Against sPLA ₂	53
2.6	Inhibition of iNOS Production via LPS stimulation of BV-2 Cells	54
2.7	ROS Production	57
2.8	In Vitro Evaluation of the Blood-brain Barrier Permeation	58
2.9	In-silico Docking Analysis	59
2.10	Conclusion	63
2.11	Experimental - Chemistry	64
2.12	Docking	99
2.13	Experimental - Biology	
2.13.1	EnzchekPhospholipase A ₂ Fluorogenic Assay (% Activity)	101

2.13.2	Enzchek Phospholipase A ₂ Fluorogenic Assay (IC ₅₀)	101
2.13.3	Enzchek Phospholipase A ₂ Fluorogenic Assay (selectivity)	102
2.13.4	Cell-culture and LPS treatment	102
2.13.5	MTS Assay	103
2.13.6	BCA Assay	103
2.13.7	Western Blot	104
2.13.8	ROS Assay	104
2.14	References	106

CHAPTER 3: CHEMICAL SYNTHESIS AND BIOLOGICAL EVALUATION OF FLUOROGENIC CYTOSOLIC PHOSPHOLIPASE A₂ INHIBITORS AND SUBSTRATE

3.1	Introduction	111
3.2	Chemical Synthesis	
3.2.1	Synthetic Strategy	112
3.2.2	Synthesis of the Inhibitor Probe	112
3.3	Biological Result of cPLA ₂ Assay and sPLA ₂ selectivity	114
3.4	Inhibitory Ability of 7OHCou-AACF3	116
3.5	7OHCou-AACF3 as a Fluorescent Dye for Imaging	117
3.6	Design and Synthesis of Substrate Probe Flu7OHCou	119
3.7	MTS Assay of 7OHCou-AACF3 and Flu7OHCou	122
3.8	Flu7OHCou as a Substrate for Monitoring cPLA ₂ Activity	124
3.9	Experimental - Chemistry	128
3.10	Experimental - Biology	
3.10.1	EnzchekPhospholipase A ₂ Fluorogenic Assay (% Activity)	148
3.10.2	Enzchek Phospholipase A ₂ Fluorogenic Assay (IC ₅₀)	148
3.10.3	Enzchek Phospholipase A ₂ Fluorogenic Assay (selectivity)	149
3.10.4	Cell Culture	149

3.10.5	MTS Assay	150
3.10.6	BCA Assay	151
3.10.7	Western Blot	151
3.10.8	Cell Staining	152
3.10.9	Photophysical Property of 7OHCou-AACF3	152
3.10.10	Assay With Positive Control Bee Venom PLA ₂	153
3.10.11	Assay for cPLA ₂ Enzyme With and Without Triton X-100	153
3.10.12	Assay for Selectivity Test With Flu7OHCou	153
3.10.13	Assay to Determine IC ₅₀ of AACOCF ₃ With Flu7OHCou	154
3.11	References	155

CHAPTER 4: CONCLUSION AND FUTURE PERSPECTIVES

4.1	Conclusion	157
4.2	Future Perspectives	157

ABSTRACT

Cytosolic phospholipase A₂ (cPLA₂) is an important class of enzyme involved in the inflammatory pathway. In various disease states such as arthritis and neuroinflammation models, cPLA₂ was found to have elevated expression or increased activity. As a result, this influenced the production of inflammatory markers such as prostaglandins and eicosanoids which in long-term would be detrimental to the disease state. Suitable pharmacological interventions for identifying cPLA₂ as a target have been shown to relieve the effects of inflammation. In this thesis, arachidonyl trifluoromethyl ketone was chosen as the scaffold and a library of analogues was synthesized as inhibitors of cPLA₂. Structure activity relationship (SAR) study was conducted with the use of a biochemical assay to identify new leads and effectiveness of cPLA₂ inhibition in which the successfully developed compound was evaluated on a neuroinflammatory model. In addition, a set of fluorogenic inhibitors and substrate of cPLA₂ were synthesized and demonstrated to be potential imaging tools for detecting cPLA₂.

LIST OF TABLES

Table 1-1	<i>In vitro</i> and <i>in vivo</i> activities of 2-oxoamides tested on Edema induced rats
Table 1-2	<i>In vitro</i> and <i>in vivo</i> studies for functionalized sulfonamide analogues
Table 1-3	IC ₅₀ of pyrrolidene derived inhibitors in different assay conditions
Table 1-4	Inhibition by 1,3-disubstituted propanones in various assay conditions
Table 1-5	Inhibition data and pharmacokinetic parameters of indonyl propanone inhibitors
Table 2-1	Optimization for the hydrogenation of compound 8a
Table 2-2	Potency of 1 at 10 μM and their physicochemical properties
Table 2-3	Potency of 2 at 10 μM and their physicochemical properties
Table 2-4	Effective Permeabilities (P _e) of test compounds at 6 h and 16 h
Table 3-1	% activity of cPLA ₂ in the presence of different test compounds at 10μM were tested in a PLA ₂ assay at n=4

LIST OF FIGURES

- Figure 1-1 Simplified structure of different isoforms of cPLA₂
- Figure 1-2 Cascade of neurotoxic events leading to neuroinflammation
- Figure 1-3 Perrin-Jablonski energy diagram
- Figure 1-4 Fluorescence images of cells
- Figure 2-1 Functionalities on AA that could be varied
- Figure 2-2 Structures of all synthesized inhibitors
- Figure 2-3 Dose-dependent inhibitory plot of **1a**, **2g** and **2i**.
- Figure 2-4 MTS assay
- Figure 2-5 sPLA₂ activity of the respective compounds at 10 μ M
- Figure 2-6 Time point changes of protein expression level in BV-2 cells after 2 μ g/mL of LPS stimulation
- Figure 2-7 Changes in protein expression level of BV-2 cells at 14 h after 2 μ g/mL of LPS stimulation with different dose treatment of **2i**
- Figure 2-8 ROS production of BV-2 cells after a 14 h 2 μ g/mL LPS insult
- Figure 2-9 Predicted binding mode of compound **1a**, **2d**, **2g**, **2i**, **2n** docked into cPLA₂ with key interacting residues highlighted
- Figure 3-1 Structure of **AACOCF₃** and inhibitor probes
- Figure 3-2 IC₅₀ of **7OHCou-AACF3** determined to be 12.5 \pm 1.0 μ M at n=4
- Figure 3-3 Inhibition activity of **7OHCou-AACF3** on sPLA₂ at 10 μ M compared with sPLA₂ specific inhibitor Thioetheramide-PC (Thio-PC) at 10 μ M
- Figure 3-4 Western blot of 3 independent experiments showing protein bands of iNOS and GAPDH
- Figure 3-5 Western blot and fluorescence imaging of BV-2 and SHSY5Y cells
- Figure 3-6 Absorbance and Emission graphs of donor and acceptor of the substrate **Flu7OHCou**.

- Figure 3-7 MTS assay conducted on AACOCF₃, **7OHCou-AACF3** and **Flu7OHCou** on 2 different cell lines at different time points
- Figure 3-8 Absorbance and Emission of the substrate probe **Flu7OHCou** in aqueous Tris-buffer, 1% Triton X
- Figure 3-9 Photophysical property of **Flu7OHCou**
- Figure 3-10 IC₅₀ of AACOCF₃ determined from a liposomal substrate solution of **Flu7OHCou**
- Figure 3-11 Absorbance and Emission graphs of the inhibitor probe **7OHCou-AACF3** in water

LIST OF SCHEMES

Scheme 1-1	Metabolites produced after the arachidonic acid cascade
Scheme 1-2	Structure of trifluoromethyl ketones inhibitors of cPLA ₂
Scheme 1-3	Structures of potent oxoamides inhibitors of cPLA ₂
Scheme 1-4	Structure of indole inhibitors of cPLA ₂
Scheme 1-5	Structures of Ecopaldib, WAY-196025, Efipladib and Giripladib
Scheme 1-6	Structures of pyrrole derivatives as inhibitors of cPLA ₂
Scheme 1-7	Structures of 1-12, Pyrroxyphene, RSC-3388 and Pyrrophoneone
Scheme 1-8	Structures of 1,3-disubstituted propanones derivatives as inhibitors of cPLA ₂
Scheme 1-9	Structures of 1-17 to 1-23 as cPLA ₂ inhibitors
Scheme 1-10	Structure of methyl arachidonyl fluorophosponate, a non-selective PLA ₂ inhibitor
Scheme 1-11	Structures of fluorogenic substrates of PLA ₂
Scheme 2-1	Retrosynthesis of 2-1
Scheme 2-2	Synthesis of AACOCF ₃ and analogues
Scheme 2-3	Synthesis of 1m to 1o
Scheme 2-4	Synthesis of arachidonyl based amide analogues
Scheme 2-5	Synthesis of 2p and 2q
Scheme 3-1	Synthesis of common intermediates before coupling with fluorogenic probes.
Scheme 3-2	Synthesis of inhibitor probes 12a-f via amide coupling.
Scheme 3-3	Synthesis of inhibitor probe 12g
Scheme 3-4	Synthesis of carboxylic acid 20
Scheme 3-5	Synthesis of fluorogenic carboxylic acids 24
Scheme 3-6	Synthesis of substrate probe Flu7OHCou
Scheme 3-7	Synthesis of Coumarin Analogues
Scheme 3-8	Synthesis of Fluorescein 18

LIST OF ABBREVIATIONS (Chemistry)

δ	Chemical Shift
Ac	Acetyl
AcOH	Acetic Acid
Bn	Benzyl
Bu ₃ SnH	Tributyltinhydride
CBr ₄	Tetrabromomethane
(CD ₃) ₂ CO	Deuterated Acetone
(CD ₃) ₂ SO	Deuterated Dimethylsulfoxide
CD ₃ OD	Deuterated Methanol
CDCl ₃	Deuterated Chloroform
CHCl ₃	Chloroform
(COCl) ₂	Oxalyl Chloride
Cs ₂ CO ₃	Cesium Carbonate
CuI	Copper(I) Iodide
d	Doublet
dd	Doublet of Doublet
dt	Doublet of Triplet
DABCYL	4-((4-(Dimethylamino)phenyl)azo)benzoic Acid
DCC	<i>N,N'</i> -Dicyclohexylcarbodiimide
DCM	Dichloromethane
DIPEA	<i>N,N</i> -Diisopropylethylamine
DMAP	4-Dimethylaminopyridine
DMPU	1,3-Dimethyl-3,4,5,6-tetrahydro-2(1H)-pyrimidinone
DMF	Dimethylformamide
DMSO	Dimethylsulfoxide
EA	Ethyl Acetate
EDC.HCl	Ethylcarbodiimide Hydrochloride

EI	Electron Ionization
en	Ethylenediamine
Eq	Equivalent
ESI	Electrospray Ionization
Et	Ethyl
Et ₂ O	Diethyl ether
EtOH	Ethanol
FRET	Förester resonance energy transfer
FT-IR	Fourier Transform Infrared Spectroscopy
HCl	Hydrochloric Acid
H ₂ SO ₄	Sulphuric Acid
HMPA	Hexamethylphosphoramide
HOBt	Hydroxybenzotriazole
K ₂ CO ₃	Potassium Carbonate
KOH	Potassium Hydroxide
M	Molar
MeOH	Methanol
m	Multiplet
Me	Methyl
MeCN	Acetonitrile
MHz	MegaHertz
M.W	Microwave
MS	Molecular Sieve
NaCl	Sodium Chloride
NaHCO ₃	Sodium Hydrogencarbonate
NaI	Sodium Iodide
NaOH	Sodium Hydroxide
NBD	7-Nitrobenzo-2-oxa-1,3-diazole amine

n-BuLi	n-Butyllithium
NH ₃	Ammonia
NH ₄ Cl	Ammonium Chloride
NMR	Nuclear Magnetic Resonance
PPh ₃	Triphenylphosphine
Ph	Phenyl
Pyr	Pyridine
Rpm	Revolutions Per Minute
rt	Room Temperature
s	Singlet
t	Triplet
TBAF	Tetrabutylammonium Fluoride
td	Triplet of Doublet
<i>t</i> BuOK	Potassium <i>Tert</i> -butoxide
TEA	Triethylamine
TFAA	Trifluoroacetic Anhydride
TMSCl	Trimethylsilyl Chloride
TMS	Tetramethylsilane
THF	Tetrahydrofuran
TLC	Thin Layer Chromatography
TsOH	<i>p</i> -Toluenesulfonic acid

LIST OF ABBREVIATIONS (BIOLOGY)

AA	Arachidonic Acid
AACOCF ₃	Arachidonyl Trifluoromethylketone
A β	Amyloid Beta
AD	Alzheimer's Disease
ASP	Aspartic Acid
BBB	Blood–brain Barrier
BCA	Bicinchoninic Acid
BEL	Bromo-enol Lactone
BSA	Bovine Serum Albumin
BV-2	C8-4 Cell-line
CNS	Central Nervous System
CO ₂	Carbon Dioxide
cPLA ₂	Cytosolic Phospholipase A ₂
D549	Aspartic Acid-549
DAPI	4', 6-Diamidino-2-phenylindole Dihydrochloride
DMEM	Dulbecco's Modified Eagle Medium
DNA	Deoxyribonucleic Acid
DOPC	1,2-Dioleoyl-sn-glycero-3-phosphocholine
DOPG	1,2-Di-(9Z-octadecenoyl)-sn-glycero-3-phospho-(1'-rac-glycerol)
DTT	Dithiothreitol
E418	Glutamic Acid-418
ECL	Enhanced Chemiluminescence
EDTA	Ethylenediaminetetraacetic Acid
ERK	Extracellular signal-regulated Kinase
FBS	Fetal Bovine Serum
G197	Glycine-197
G198	Glycine-198

GFAP	Glial Fibrillary Acidic Protein
HEK293T	Human Embryonic Kidney 293 T
IC ₅₀	Concentration of Inhibitor where Response is Reduced by Half
ICC	Immunocytochemistry
IgG	Immunoglobulin Subtype Gamma
IHC	Immunohistochemistry
iNOS	Inducible Nitric Oxide Synthase
iPLA ₂	Calcium-independent Phospholipase A ₂
LB Broth	Luria Bertani Broth
LPC	Lysophosphatidylcholine
LPS	Lipopolysaccharides
MAPK	Mitogen-activated Protein Kinase
MTS	3-(4,5-dimethylthiazol-2-yl)-5-(3-carboxymethoxyphenyl)-2-(4-sulfophenyl)-2H-tetrazolium)
MD	Molecular Dynamics
NMDA	N-methyl-D-aspartate
PBS	Phosphate Buffer Saline
PC	Phosphatidylcholine
PMSF	Phenylmethylsulfonyl Fluoride
R200	Arginine-200
RIPA	Radioimmunoprecipitation Assay
rmsd	Root-mean-square Deviation
ROS	Reactive Oxygen Species
SAR	Structure Activity Relationship
SDS	Sodium Dodecyl Sulphate
SDS-PAGE	Sodium Dodecyl Sulphate Polyacrylamide Gel Electrophoresis
Sema3A	Semaphorin 3A
S228	Serine-228

S577	Serine-557
SER	Serine
sPLA ₂	Secretory Phospholipase A ₂
TBST	Tris-buffered saline with Tween 20
Tris-Gly	Tris-Glycine

LIST OF PUBLICATIONS

1) Ng, C. Y., Kwok, T. X. W., Tan, F. C. K., Low, C.M., Lam, Y. Fluorogenic Probes to Monitor Cytosolic Phospholipase A₂ Activity, *Chem. Commun.* , **2017**, 53, 1813-1816.

2) Ng, C. Y., Kannan, S., Chen, Y. J., Tan, F. C. K., Ong, W. Y., Verma, C. S., Go, M. L., Low, C. M., Lam, Y. A New Generation of Arachidonic Acid Inhibitors as Potential Neurological Agent Targeting Cytosolic Phospholipase A₂. (Submitted)

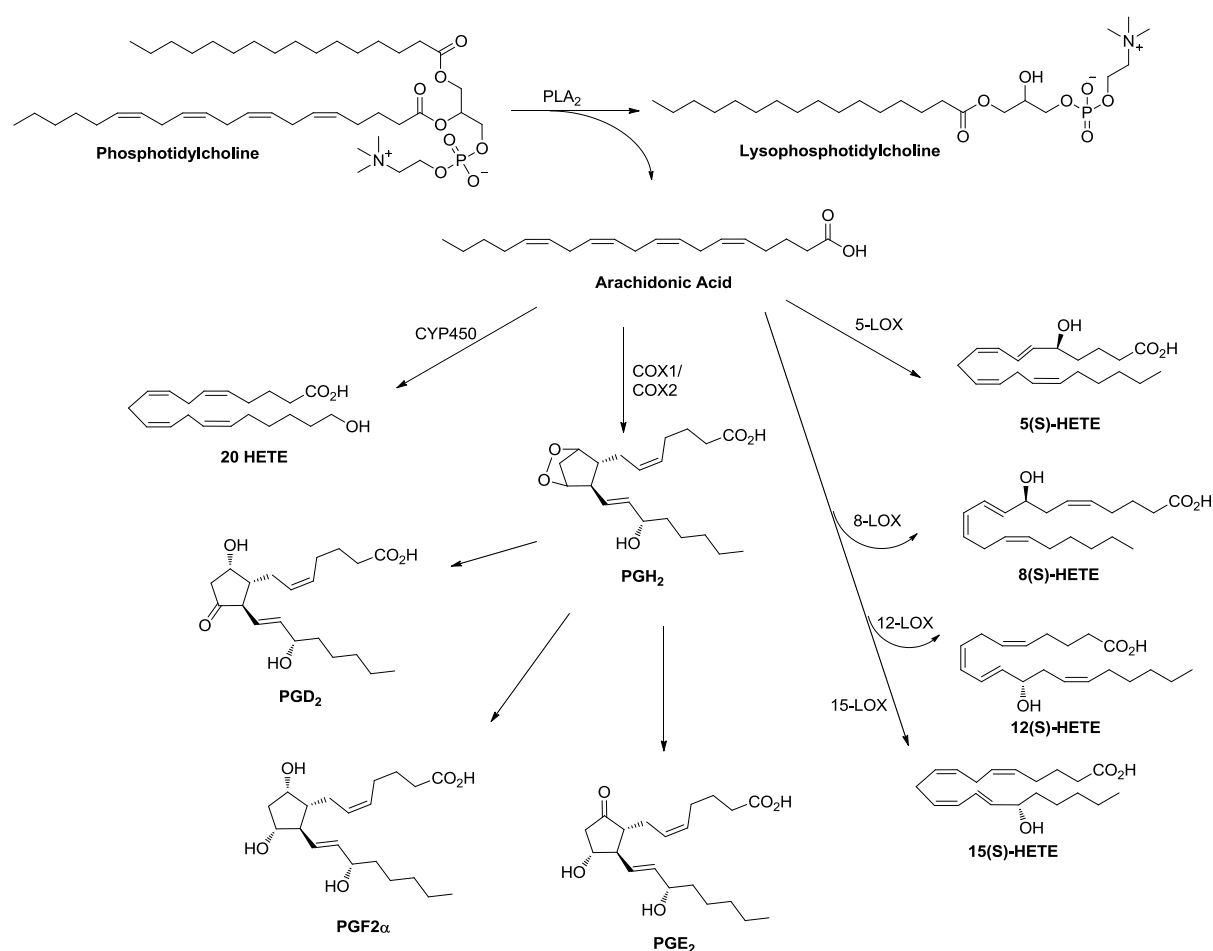
CHAPTER 1: INTRODUCTION

1.1 Phospholipase A₂ and its functions

Phospholipase A₂ (PLA₂) belongs to a superfamily of phospholipases catalyzing its substrate specifically at the sn-2 position of the acyl bond. The metabolites from the hydrolysis of PLA₂ are lysophospholipids and long chain fatty acids which are mainly long chain polyunsaturated fatty acids (LCPUFA) of arachidonic acid (AA) and docosahexaenoic acid (DHA). Lysophospholipids function as precursors for platelet activating factors (PAF) and in other reactions ranging from metabolism of intracellular phospholipid to growth-factor-like extracellular mediators.¹ LCPUFA which are found in various parts of the body especially in the neural membrane of the Central Nervous System (CNS), act as precursors for inflammatory mediators such as eicosanoids and prostaglandins. For instance, AA are usually found esterified on membrane phospholipids, and basal levels are converted into inflammatory mediators required for bodily functions.² Being a part of membrane phospholipids, the cis nature of the double bonds on AA also affects membrane fluidity. PLA₂s are therefore important modulators in phospholipid turnover and maintain the levels of free LCPUFA, indirectly serving its roles in altering membrane fluidity and permeability.

It has been reported that neuroinflammation is strongly influenced by both the activity and downstream metabolite produced by PLA₂.^{2,3} PLA₂ levels were found to be up-regulated in the event of neurodegenerative diseases, which generally involve a sizeable amount of inflammatory and oxidative components in their pathways, resulting in severe oxidative stress in the brain.³ Several neurodegenerative diseases such as ischemia, multiple sclerosis, Alzheimer's disease, prion diseases and schizophrenia have been found to be attributed to neuroinflammation. Hence, it is of paramount importance to understand the activity of PLA₂ in the CNS. Three most important classes of PLA₂, namely cPLA₂, sPLA₂ and iPLA₂, were discussed in the sections that followed.

1.1.1 Inflammation and Arachidonic Acid Cascade



Scheme 1-1: Metabolites produced after the arachidonic acid cascade. ^{4, 5}

A large proportion of phospholipids, in particular phosphatidylcholine, have an arachidonate ester at the *sn*-2 position of phospholipids. After their hydrolysis by PLA₂, free fatty acid AA is commonly released and acts as the main precursor to the formation of pro-inflammatory eicosanoids such as prostaglandins and leukotrienes. Upon the release of AA, 5-lipoxygenase (5-LOX) converts it into 5-hydroperoxyeicosatetraenoic acid (5-HETE), which is then converted into leukotrienes. Similarly, other lipoxygenases (8-LOX, 12-LOX, 15-LOX) also act on AA to produce different isomers of HETE as shown in Scheme 1-1.^{4,5} On the other hand, production of prostaglandin PGH₂, is controlled by the activity of COX1/COX2. This highly unstable endoperoxide is rapidly converted to PGE₂, PGD₂, PGF₂α.⁶ Strict control of the levels of AA and lysophospholipids is therefore crucial to maintain normal brain function. This implies that PLA₂ activity also needs to be strictly modulated so as to ensure their optimum levels.³

1.1.2 Secretory Phospholipase A₂

Secretory phospholipase A₂ (sPLA₂) is one of the most well-studied class of PLA₂ with lower molecular weight ranging from 14-18kDa.⁷ They contain 6-8 disulphide bridges and are originally isolated and characterized from both cobra and rattlesnake venom.⁸ sPLA₂ is calcium dependent and possess calcium binding sites for activation. By having a conserved calcium binding loop and a catalytic site involving histidine and aspartic acid, they differ from the typical serine proteases which utilized acyl enzyme intermediate in the hydrolysis.⁸ A water molecule is first polarized in the dyad via a calcium dependent mechanism, which then attacks the carbonyl ester of the phospholipid substrates. This class of enzyme has no distinct preference for its substrates, unlike cPLA₂ which are highly specific for arachidonyl substrate at the sn-2 of phospholipids.

In general, sPLA₂ was found to be implicated in various inflammatory and autoimmune diseases. Among the various isoforms, sPLA₂-IIA is the most extensively studied. This isoform was first discovered in atherosclerotic lesions and has its role as inflammatory marker protein in atherosclerosis.⁸ Synovial fluids of people suffering from rheumatoid arthritis also had elevated levels of sPLA₂-IIA while mice which were deficient of this enzyme had reduced symptoms of arthritis.⁹ In addition to eicosanoid and prostaglandins production, this class of enzyme was also capable of inducing various proinflammatory mediators generation from many cells types such as neutrophils, monocytes, macrophages etc.¹⁰

1.1.3 Calcium-independent Phospholipase A₂

Calcium-independent Phospholipase A₂ (iPLA₂) was originally isolated from macrophage. Calcium binding is not a necessary condition for its activation however; its activity can still be regulated by calcium binding proteins such as calmodulin or ATP for stabilization.¹¹ Structurally, the catalytic site of iPLA₂ is similar to cPLA₂ bearing an active serine that participates in the hydrolysis. However, the serine in iPLA₂ lies in a more exposed position, resulting itself to be more accessible to solvents as compared to cPLA₂. This could shed light on the low substrate specificity of iPLA₂ towards AA.⁷ iPLA₂ does not require calcium for its activation, and is regulated in processes such as iPLA₂

oligomerization, caspase cleavage and ATP binding resulting in iPLA₂ activation. iPLA₂ has several isoforms such as iPLA₂β, iPLA₂γ, iPLA₂δ, iPLA₂ε, iPLA₂ζ, iPLA₂η with iPLA₂β being the most well-studied. It is possible for iPLA₂β to bind with ATP resulting in structural stabilization and enzyme activation.¹²

1.1.4 Cytosolic Phospholipase A₂

Cytosolic phospholipase A₂ (cPLA₂) is a widely distributed phospholipase that is ubiquitous throughout the body. Among the three major phospholipases (sPLA₂, iPLA₂, cPLA₂) mentioned, cPLA₂ play a vital role in releasing AA specifically in the pro-inflammatory signalling pathway. Though sPLA₂ and iPLA₂ are also capable of mediating such release, selectivity in particular fatty acyl chain could not be identified. This selectivity might arise due to the structures of the different PLA₂ isoforms.

1.1.4.1 cPLA₂ Isoforms and substrate specificity

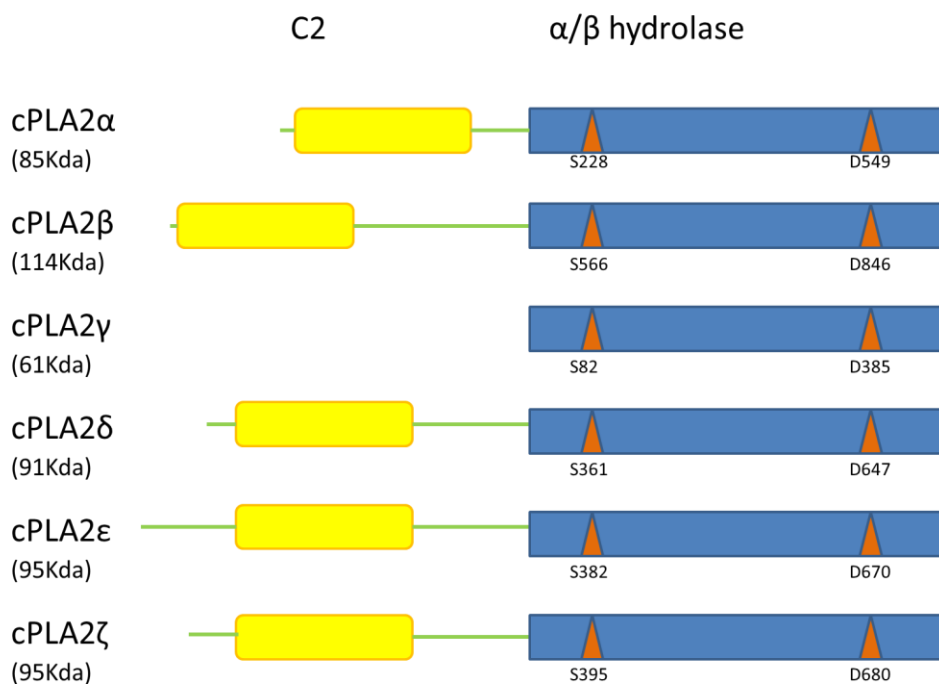


Figure 1-1: Simplified structure of different isoforms of cPLA₂. Close structural resemblance was observed in C2 and α/β domains among the isoforms bearing a catalytic dyad of Ser and Asp. Red triangle refers to the active site.^{6,7}

cPLA₂ contains 6 subgroups, namely α , β , δ , γ , ϵ and ζ . In the brain, 3 specific paralogs, cPLA₂ α , cPLA₂ β and cPLA₂ γ are present.^{6,7} They are specifically expressed in the amygdale, corpus callosum, hippocampus, substantia nigra, subthalamic nucleus and thalamus.¹³ cPLA₂ α is the most well-studied among the isoforms and is ubiquitously expressed in most human tissues.⁶ Structurally, they contain the same catalytic dyad of serine and aspartic acid enabling their role as phospholipase. However, the molecular weight of the various enzyme isoforms ranges from 61kDa in cPLA₂ γ to 114kDa for cPLA₂ β . The crystal structure of cPLA₂ α derived from E5-CHO cells had been published.¹⁴ A novel structure containing a C2 domain which exhibits lipid-binding and calcium-dependency characteristic in cPLA₂ α was identified from the crystal structure together with a catalytic domain. This topology revealed the presence of a flexible lid that regulates the access of its substrate to the catalytic domain bearing the active site. A deep hydrophobic funnel selectively limits arachidonyl substrate entrance into the enzyme, while actual catalysis of the substrate occurs at the heart of this funnel. Comparing with other serine proteases, cPLA₂ α differs in that it contained a catalytic dyad consisting of Ser and Asp instead of the normal Ser-His-Asp triad. Presence of Ca²⁺ binding on the C2 domain is important in promoting the translocation of cPLA₂ to approach the membrane. Upon a series of phosphorylation and subunit binding, repositioning of the catalytic domain to the membrane surface will then occur, leading to the catalytic action of cPLA₂.¹⁵ Among the different paralogs, only cPLA₂ γ does not contain the calcium binding C2 domain. This might also explain why it is calcium independent for its activation. The catalytic dyad of Ser and Asp are conserved for all the paralogs.

1.1.4.2 Activation mechanism of cPLA₂

Previous studies reported that cPLA₂ perform important functions related to membrane regulation.⁷ Thus, cPLA₂ activity is tightly regulated. One major approach to control cPLA₂ activity is by regulating the activation of cPLA₂. There are several proposed models of cPLA₂ activation. Most of them are in agreement that cPLA₂ activation involves two key post-translational modifications: the binding of calcium and phosphorylation of key residues. The presence of calcium has been shown to be essential for cPLA₂ activity.¹⁶ For example, production of AA, a product of cPLA₂, has been demonstrated to be triggered by calcium mobilizing agonists.¹⁷ Research has also shown that calcium

binds to the C2 domain of cPLA₂, triggering a Ca²⁺ dependent translocation from the cytosol to the intracellular membranes in order of preference of the Golgi apparatus, endoplasmic reticulum and the nucleus.^{15, 18} This does the essential function of bringing cPLA₂ into contact with its substrates; membrane phospholipids. There are two known stages of calcium release.¹⁶ Firstly, a rapid intracellular release of calcium triggers the translocation of cPLA₂ to the intracellular membranes. The second stage involves a sustained influx of external Ca²⁺ which results in stable binding to membrane. This mechanism has been supported by studies illustrating that both stages of calcium release are needed for cPLA₂ function. The application of a serum that increases intracellular calcium stimulates the release of AA. However, this effect is inhibited by the addition of chelators that remove extracellular calcium.¹⁹ Likewise, external release of calcium alone results in a slow rate of cPLA₂ translocation with a corresponding low cPLA₂ activity and low release of AA.

cPLA₂ activity can also be regulated by phosphorylation of key serine residues in the catalytic domain, namely Ser505, Ser727 and Ser515. This is supported by the association of several kinases with cPLA₂ activation in a variety of cell types, and the loss of cPLA₂ activity in the presence of phosphatases.¹⁷ Ser505 is the site of action for mitogen activated protein kinases (MAPK).²⁰ Phosphorylation of Ser505 leads to an increase in catalytic activity of cPLA₂, thereby resulting in enhanced release of arachidonic acid.^{20, 21} Studies have suggested that phosphorylation at Ser505 enables cPLA₂ to achieve its optimal orientation, and increases its binding affinity to phospholipids at low calcium levels.¹⁷ Phosphorylation at Ser727 is the site of action for MAPK downstream kinases. Ser727 has been shown to be a functionally important residue that regulates protein-protein interaction. One method to demonstrate phosphorylation at Ser727 regulates cPLA₂ activity is by relieving the inhibition by the p11-annexin A2 complex.²² Studies done on rabbit vascular smooth muscle cells have also established the crucial role of Ser515 phosphorylation on cPLA₂ activity.²³ Mutant S515A reduced phosphorylation at Ser505, suggesting that Ser515 phosphorylation is upstream of Ser505 phosphorylation and that phosphorylation at both sites are needed for cPLA₂ activity.²⁴ One of the enzymes that could act on Ser515 has been shown to be CamKII.^{23, 24}

1.2 cPLA₂ in neuroinflammation

Various reports have surfaced recently on the link between cPLA₂ and neuroinflammation.^{3, 25-27} It has been shown that overexpression of cPLA₂ led to an increase in pro-inflammatory cytokine production, leading to subsequent pathological changes in the neurodegenerative process.³ Aberrant activation of cPLA₂ has been demonstrated in various examples such as stimulation of the MAPK signalling pathway for cPLA₂ activation via reactive oxygen species (ROS), S-nitrosylation of cPLA₂ and COX-2 by inducible nitric oxide synthase (iNOS) to magnify inflammatory responses etc.¹³ By attacking membrane phospholipids, cPLA₂ produces pro-inflammatory precursors of lysophospholipids and free fatty acids.²⁸ In particular, cPLA₂ cleaves phosphatidylcholine to form lysophosphatidylcholine and arachidonic acid.²⁹ Sundaram et al. has demonstrated that an increase in cPLA₂ activity could result in an increase production of lysophosphatidylcholine. Being a soluble lipid mediator released by neurons, cPLA₂ could activate glia cells and release pro-inflammatory cytokines, causing ROS production and neuronal damage that would in long term lead to neuroinflammation.^{3, 30}

AA itself also plays a role in neuroinflammation. AA is a free fatty acid that is an important component of neuronal membranes.³¹ Therefore an overproduction of AA would potentially result in a huge increase in prostaglandin and leukotrienes which in long-term would lead to neurodegeneration. Studies have shown such elevated levels of prostaglandin E₂ in patients with probable Alzheimer's Disease (AD), while beneficial effects on the development of AD was observed when downstream COX inhibitors was used. Animal studies have also shown that deletion of prostaglandin receptors lead to decrease oxidative damage and $\alpha\beta$ peptides, indicating that immune-activated oxidative damage is present in neuroinflammation.^{32,33} In addition to being a precursor, AA has been shown to be involved in mitochondrial dysfunction, and acting as a retrograde messenger implicated in memory function.³⁴ Toxic and trophic effects were found on neurons after exposure and this also include membrane fluidity alteration, protein kinases activation and regulation of gene expression. cPLA₂ is thus an important regulator in this inflammatory pathway by modulating the level of AA.

Membrane phospholipids which are substrates of cPLA₂ could be affected when a change in cPLA₂ activity occur. As a result, this causes phospholipid remodelling and membrane perturbations, ultimately affecting membrane protein functions. For instance, prolonged activation of cPLA₂ can potentially skew the balance of membrane phospholipids in the CNS resulting in their long-term destruction. Electron transport chain and other related protein would be directly impacted. Finally, alterations in membrane phospholipids can result in increasing membrane permeability and synaptic loss.^{2, 28} Curtailing cPLA₂ activation to only basal level might therefore be important in reversing the harmful effects of long-term neuroinflammation.

1.3 cPLA₂ in Alzheimer's Disease

cPLA₂ is known as a contributing factor to neurodegenerative diseases such as AD, Parkinson's disease and multiple sclerosis.^{2, 25, 35-36} Activity of cPLA₂ showed to increase in brain fractions of AD patients as compared to that of healthy controls.³⁷ In addition, changes in cPLA₂ expression had been localized to areas of the brain such as the hippocampus and amygdala. The hippocampus, in particular, is an area that suffers significant neuronal damage in AD. Conversely, iPLA₂ and sPLA₂ are ubiquitously expressed throughout the brain with sPLA₂ largely localized to synaptic vesicles.²⁵ Traditional models which associated cPLA₂ overactivation in AD with $\alpha\beta$ and NMDA receptors have been proposed. There is a strong case supporting the involvement of $\alpha\beta$ in cPLA₂ activation - the inhibition of $\alpha\beta$ leading to a decrease in cPLA₂ activity. This is further supported by evidences of $\alpha\beta$ inducing reactive oxygen species (ROS) production and calcium influx in astrocytes.³⁸ As cPLA₂ activation has a similar effect of triggering inflammatory processes and the production of ROS, cPLA₂ may be a downstream effector of $\alpha\beta$ pathology. $\alpha\beta$ and NMDA receptor stimulation have been shown to induce the release of AA. It has been proposed that this stimulation is activated by kinases, such as MAPK and PKC.^{39, 40}

In addition, $\alpha\beta$ exposure leading to downstream glutamate excitotoxicity and neuronal damages was shown to activate cPLA₂.^{13, 41, 42} This established a link between oxidative/nitrosative pathway to that of $\alpha\beta$ cytotoxicity and inflammatory response from cPLA₂ activation. Re-examining the pathology of

Alzheimer's disease also suggested direct implications of $\alpha\beta$ neurotoxicity, arising from cPLA₂ dysregulation.^{25, 42, 43} One possible mechanism to explain the aberrant activation of cPLA₂ has been proposed by Shelat et al.⁴⁴ Shelat et al illustrated that $\alpha\beta$ and NMDA receptors are associated with ROS production through NADPH oxidase, presenting a parallel pathway to cPLA₂ activation. $\alpha\beta$ acts on NADPH oxidase, producing ROS that activates ERK1/2, a known activator of cPLA₂.

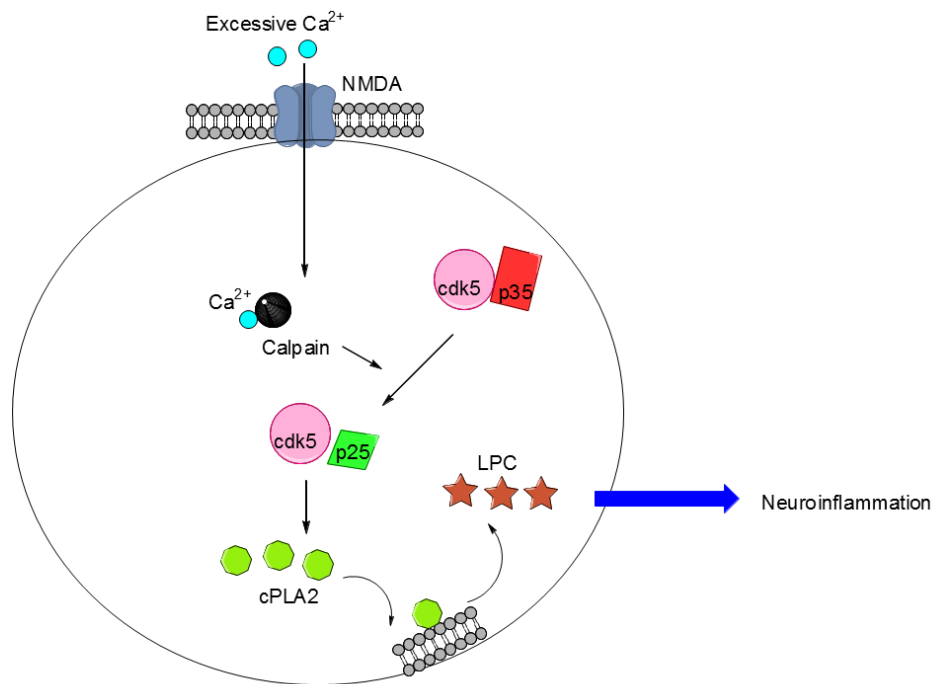


Figure 1-2: Cascade of neurotoxic events leading to neuroinflammation

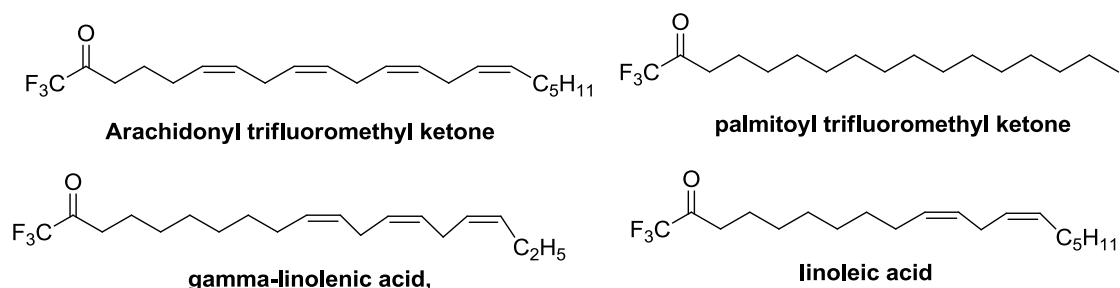
Nevertheless apart from $\alpha\beta$, Sundaram et al. have also elucidated a novel pathway involving cPLA₂ and p25/Cdk5 mediated neuroinflammation (Figure 1-2).³ Sundaram et al. established the link between hyperactivated p25/Cdk5 complex to neuroinflammation through cPLA₂. Neurotoxic insults lead to an influx of calcium ions, activating Calpain. Calpain cleaves p35, the physiological regulator of Cdk5, to form p25, resulting in the formation of the p25/Cdk5 complex. This activates downstream signalling events which in turn result in an increased cPLA₂ activity. As cPLA₂ catalyses the formation of lysophosphatidylcholine (LPC) from phosphatidylcholine (PC), the release of LPC leading to glia cell activation was observed by detecting an upregulation of glial fibrillary acidic protein (GFAP) expression.⁴⁵ Currently, it is not yet known if these pathways occur independently of each other, or are linked in an upstream or downstream manner. Nevertheless, this evidence of linking

the increased activation of cPLA₂ to neurodegeneration has highlighted the need to understand the role of cPLA₂ in AD pathology as well as the potential of cPLA₂ as a promising therapeutic target.

1.4 Current developments in cPLA₂ inhibitors

Identifying cPLA₂ as a potential therapeutic target is important as this allows for pharmacological intervention that could reduce the harmful effects brought about in a dysregulated system. Inhibition can thus be readily achieved using small molecules with high selectivity against cPLA₂. Currently, considerable efforts had been targeted at generating different scaffolds which could exhibit high potency and selectivity on cPLA₂ against other phospholipases. Given the ubiquity of this phospholipase, various classes of compound synthesized were tested on different cell-lines containing the same enzyme to investigate their pharmacokinetic properties. A brief summary of these classes of compounds is shown in the following section.

1.4.1 Trifluoromethyl ketones



Scheme 1-2: Structure of trifluoromethyl ketones inhibitors of cPLA₂

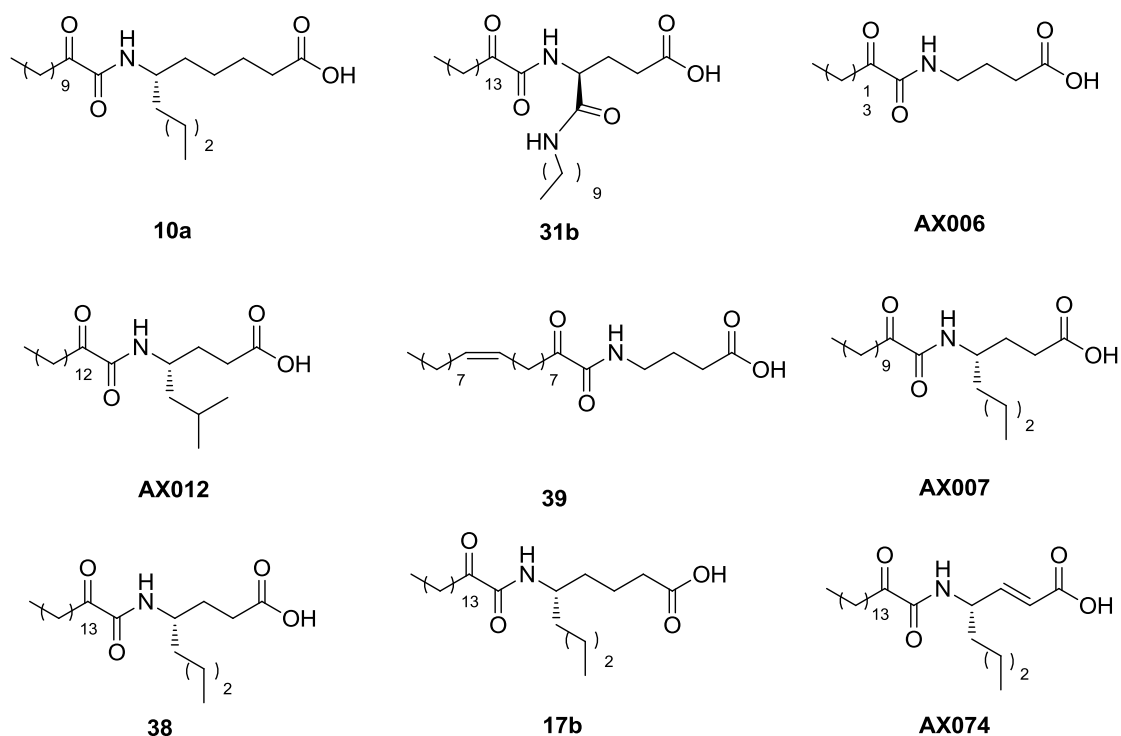
Arachidonyl trifluoromethyl ketone (AACOCF₃), is a trifluoromethyl ketone known to be a potent inhibitor of phospholipase A₂. Capable of inhibiting cPLA₂ and iPLA₂ with IC₅₀ values of 1.5 μM and 6 μM respectively, AACOCF₃ is also 500 fold more selective for cPLA₂ over sPLA₂ in terms of potency.² AACOCF₃ is widely used as a standard during the screening of inhibitors for *in vitro* or *in vivo* studies on cPLA₂ inhibition. The high potency of AACOCF₃ could be due to its close structural resemblance with the AA, which was generated after cPLA₂ hydrolysis of the membrane substrate. Replacing the carboxylic acid with a trifluoromethyl ketone increases the electrophilicity of the

carbonyl carbon, resulting in a different form of interaction with the nucleophilic Ser228 residue at the catalytic site as compared with the membrane phospholipid substrate. AACOCF₃ forms a new covalent bond after a nucleophilic attack by Ser228 OH in cPLA₂ providing a negatively charged hemiketal that is stabilized by two positive arginine residues, hence achieving cPLA₂ inhibition.

Inhibition of cPLA₂ by AACOCF₃ has been demonstrated to have high potencies in various cells, providing anti-inflammatory protection to downstream targets. In primary neuronal culture containing short-chain peptide oligomers, a dose-dependent and time-dependent increase in phosphorylated cPLA₂ was detected when treated with synthetic $\alpha\beta$.⁴³ This resulted in an increase in AA concentration. Pre-treatment with AACOCF₃ caused a reduction in AA release and an increase in $\alpha\beta$ induced cell death while treatment with the iPLA₂ inhibitor, bromoenol lactone (BEL) had no effects. These results demonstrated the selectivity of AACOCF₃ and its ability to provide neuroprotection by inhibiting cPLA₂. In another series of experiments, treatment of AACOCF₃ on rat dorsal root ganglion neuron culture prevented growth cone collapse when stimulated by the repellent Semaphorin 3A (Sema3A).⁴⁶ Growth cones are axons containing amoeboid tips, which under the actions of eicosanoid such as 12(S)-HETE, downstream kinase activation and phosphorylation leading to cone detachment occur. As a competitive inhibitor to cPLA₂, AACOCF₃ prevented the stimulation of phospholipase activity by Sema3A, thereby limiting the extent of growth cone collapse.

Other trifluoromethylketone analogues have also been synthesized and tested for their inhibitory activity against cPLA₂. Amongst them are close structural analogues such as gamma-linolenic acid, palmitoyl trifluoromethyl ketone and linoleic acid which were tested on different assay systems including mixed-micelle, DOPM/GLU vesicle as well as natural membrane systems from U937 cells.⁴⁷ It was found that they have a certain degree of selectivity towards iPLA₂ instead of cPLA₂ limiting their effectiveness towards cPLA₂ inhibitors.

1.4.2 Oxoamides



Scheme 1-3: Structures of potent oxoamides inhibitors of cPLA₂

Table 1-1: *In vitro* and *in vivo* activities of 2-oxoamides tested on Edema induced rats.⁴⁸⁻⁵⁰

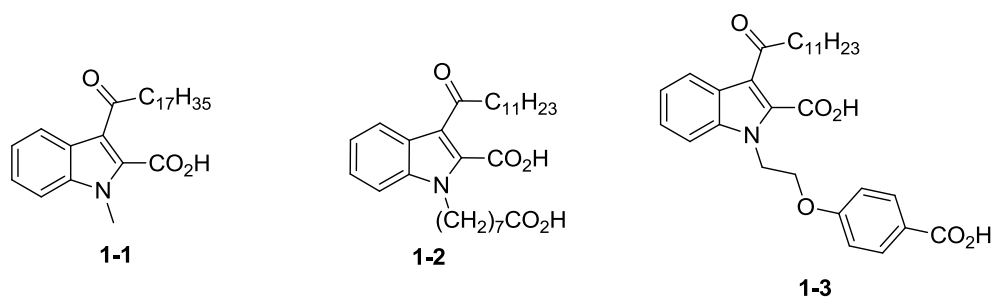
Name in paper	X _I (50) ^b	Anti-inflammatory activity ED ₅₀ (mmol/kg)	Analgesic activity(%)
10a	0.025 ± 0.013	0.01	33
31b	0.025 ± 0.012	0.0165	11
AX006	0.017 ± 0.009	0.01	93
AX012	0.017 ± 0.006	0.008	69
39	0.011 ± 0.003	0.0001	53
AX007	0.009 ± 0.004	0.1	63
38	0.008 ± 0.003	0.008	65
17b	0.005 ± 0.002	0.00005	71
^a AX074	0.003 ± 0.001	-	-

^aAX074 had not been tested on *in vitro* systems

^b $X_I(50)$ refers to the inhibitor's concentration giving rise to 50% inhibition with units of mole fractions determined by taking the moles of inhibitor divided by total moles of substrate plus inhibitor plus detergent.

In 2002, G. Kokotos and E.A. Dennis et al developed 2-oxoamides as a novel class of cPLA₂ inhibitor.⁵¹ Its structure mimics the substrate phosphatidylcholine by possessing isosteric replacement of various functional groups. The sn-2 ester of the phosphatidylcholine is replaced by an oxoamide functionality which could interact with the OH of Ser228 in cPLA₂ while the phosphate on the substrate is changed to a carboxylate moiety. In addition, incorporation of two alkyl chains resembles the two fatty acid segments on phosphatidylcholine, enabling penetration of the molecule into hydrophobic regions within cPLA₂.⁵² Various modifications on this class of inhibitor have so far been carried out. The lead compound **AX007** containing a L- γ -norleucine moiety was found while screening a library of novel 2-oxoamides and gave a highly potent $X_I(50)$ of 0.009 mole fraction.⁵¹ Such a biological evaluation was performed by determining $X_I(50)$ in a Phospholipase A₂ assay containing mixed micelles of substrate instead of the conventional IC₅₀ and K_i. $X_I(50)$ measurement is a more appropriate technique as surface concentration of the inhibitor is more important than the bulk concentration due to the primary activity of cPLA₂ on the interface. Extensive studies which were subsequently performed led to the discovery of more potent analogues such as **AX007**, **17b** and **AX074**.⁵² In addition to the need for a non-bulky side chain beside the nitrogen, chirality beside the amide was also an important feature to achieve high potency. It was also found that 2-oxoamide have a certain degree of inhibition for sPLA₂ while iPLA₂ inhibition was minimal. Analogues possessing free carboxyl groups are highly selective for cPLA₂ inhibition over other phospholipases.⁵³

1.4.3 Indoles and derivatives



Scheme 1-4: Structure of indole inhibitors of cPLA₂

This class of analogues was first reported by Lehr et al. when a library of indole-2-carboxylic acid was screened.⁵⁴ By measuring AA release from calcium ionophore A23187-induced bovine platelets, **1-1** was identified with an IC₅₀ of 8 μM. The extent of cell lysis by the compounds was also reported to prevent false positives due to reduced AA formation from lysed cells. Subsequently, further investigative studies showed that the carboxylic acid group was important for inhibition. This implies that a positive residual in the vicinity of the binding pocket while the acyl containing the carbon chain were important for the interaction with OH of Ser228 in cPLA₂. Indole N must also be substituted for potency to be observed. This substitution required carbon of a certain number, at the same time possessing a polar moiety at the chain end such as carboxylic acid giving rise to **1-2** and **1-3** with potency of 1.6 μM and 0.5 μM respectively.⁵⁵

Functionalized indole sulfonamide was developed from Wyeth, starting off as a substrate mimetic exercise on indole compounds.⁵⁵ Compounds possessing good pharmacokinetic (PK) properties were evaluated with a primary “coumarin assay” and cell-based assays, identifying **1-4** as a lead with good potency and PK parameters. IC₅₀ values obtained from the coumarin assay reached 0.8 μM while a mast cell line, MC-9 assay similarly gives 0.8 μM.⁵⁶ Compound **1-5** and **1-6** bearing the sulfoxide moiety were subsequently found to have IC₅₀ of 0.8 μM and 0.5 μM respectively in a GLU micelle assay.⁵⁷ To further enhance the interaction of the compound with cPLA₂, substitution on the C2 of indole was extensively explored. The result was the development of a sulfonamide class of compound with the following pharmacophore, N-benzhydryl moiety, C2 sulfonamide and C3 benzoic acid. With

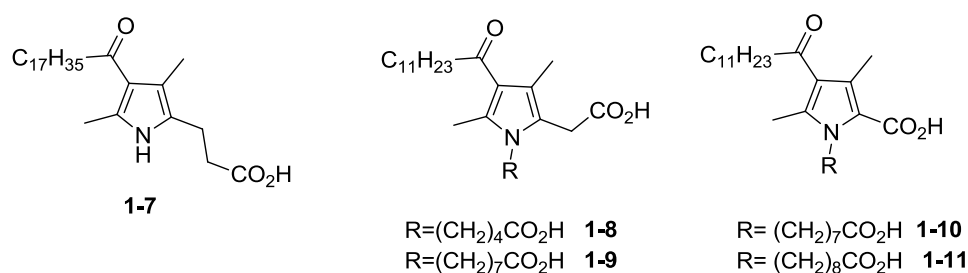
Table 1-2: *In vitro* and *in vivo* studies for functionalized sulfonamide analogues

Compound	IC ₅₀ /μM		%F ^c	Rat IV Cl ^e (mL/min/kg)
	GLU ^a	RWB ^b		
1-4	160	>400	63(10mg/Kg)	-
1-5	0.8	2.0	39 ^d	44
1-6	0.5	0.8	11 ^d	47
Ecopladib	0.15	0.11	29.0(5mg/kg)	14
			8.0(20mg/kg)	
Efipladib	0.040	0.070	1.0(25mg/kg)	5.0
WAY-196025	0.010	0.030	6.0(25mg/kg)	6.1
Giripladib	0.27	0.15	-	-

^a GLU micelle assay ^b Rat Whole Blood assay ^c Oral Bioavailability of compound on rats using MC/Tween formulation ^d Dosage was not stated ^e Clearance level

Efipladib was found to have applications in cancer research in terms of preventing the proliferation and angiogenesis of cancer via eicosanoid pathways.⁶² Treatment of Efipladib on prostate cancer cell lines caused a surge in COX-1 protein and PGE2 level as well as a reduction in lipoxigenase products. The possible induced production of COX-1 could enable the mechanism of prostate cancer cell survival and proliferation to be elucidated.⁶³ WAY-196025, on the other hand, was found to be useful such as in asthma treatment. *In vitro* allergen stimulation on human blood samples obtained from asthmatic and healthy individuals were performed in assay added with the inhibitor to block 5-lipoxygenase production. It was reported that although allergen regulated gene expression was not significantly influenced, various allergen-dependent and asthma associated modifications in gene expression were identified.⁶⁴

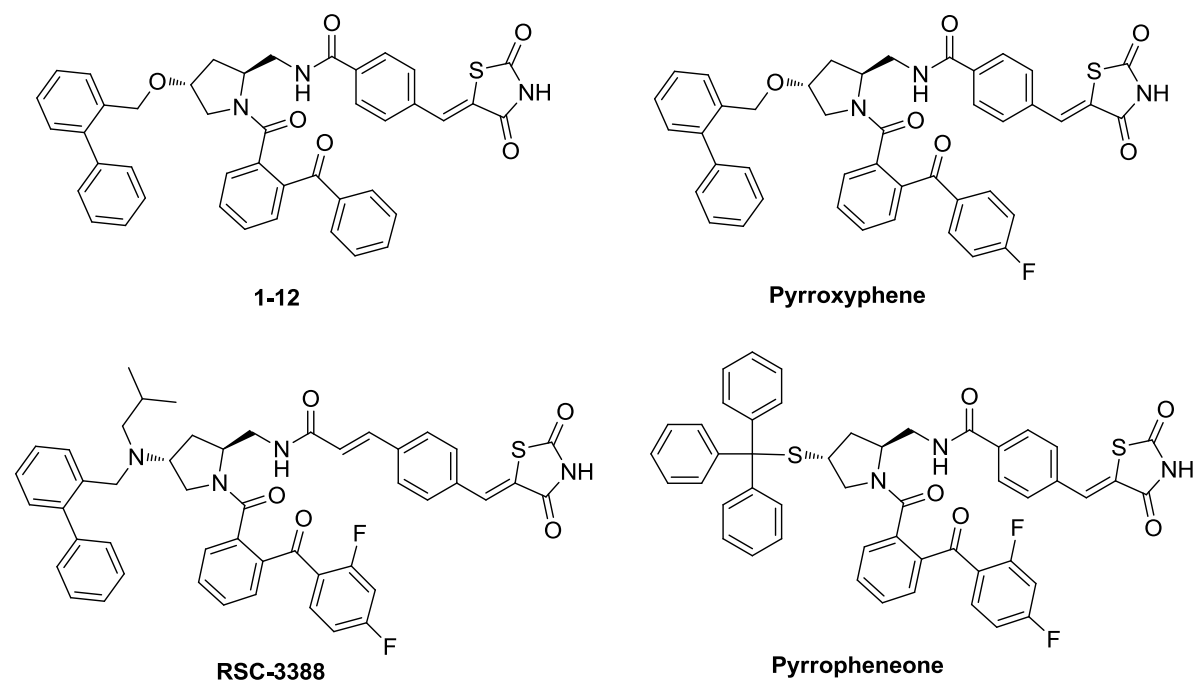
1.4.4 Pyrroles



Scheme 1-6: Structures of Pyrrole derivatives as inhibitors of cPLA₂

Lehr first introduced the pyrrole series of inhibitor as a structure mimetic of cPLA₂ substrates, achieving **1-7** which gave an inhibition value of 24 μ M when the AA released from bovine platelets was measured after A23187 calcium ionophore stimulation.^{54, 65} Further SAR studies showed that the introduction of an acyl group on N led to loss in potency, leading to the use of solely alkyl substitution to preserved activity.⁵⁴ An extensive SAR exercise was conducted by varying the long alkyl chain at the C3 positions, length of the carboxylic acid at C2 as well as length of the alkyl moiety at the 2 remaining sites on the pyrrole. It was found that a propionic acid chain was the optimum length for C2 while substitution on the N experienced a significant increase in potency when it ends with a carboxylic acid moiety giving compounds **1-8** to **1-11** with IC₅₀ ranging between 3.9-3.3 μ M.^{66, 67} The methyl group which is less hindered is important to maintain potency of the series.⁶⁷ Due to the close structural similarity of indole analogues from the same group, they were postulated to exhibit similar binding mode with the target enzyme.

1.4.5 Pyrrolidines



Scheme 1-7: Structures of **1-12**, **Pyrroxyphene**, **RSC-3388** and **Pyrrophenoneone**

Table 1-3: IC₅₀ of pyrrolidene derived inhibitors in different assay conditions

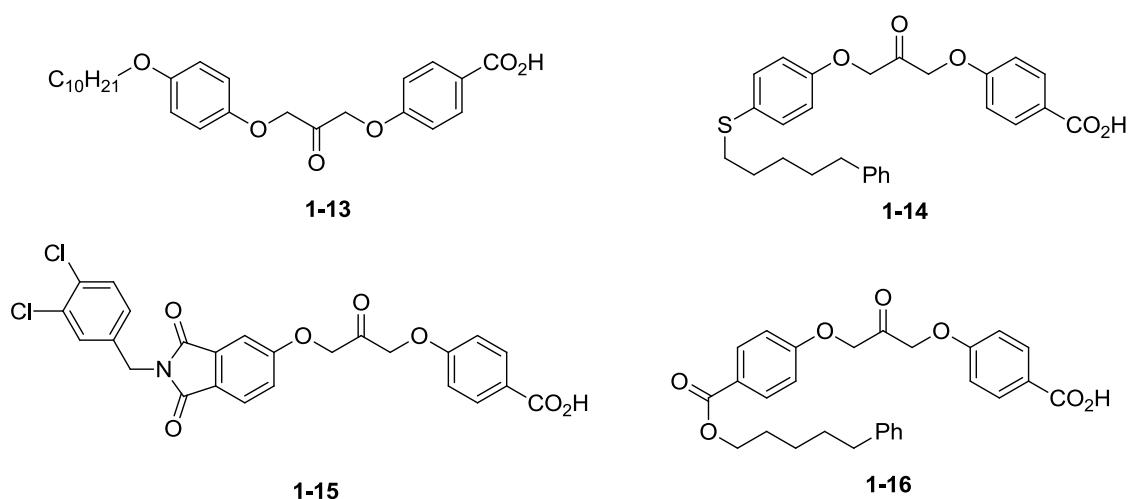
Name	IC ₅₀ /nM			
	PC/DOG	THP-1	PGE ₂	LTC ₄
1-12	165 ± 20	670 ± 70	410 ± 70	370 ± 70
Pyrroxyphene	78 ± 9	320 ± 30	260 ± 110	260 ± 60
RSC-3388	1.8 ± 0.5	22 ± 1	31 ± 43	13 ± 1
Pyrrophenoneone	4.2 ± 2.6	24 ± 1.7	25 ± 19	14 ± 6.7

Ono and co-workers have developed pyrrolidine derivatives as potential cPLA₂ inhibitors.⁶⁸ By incorporating a thiazolidinedione into the molecule, this serves as an acid-base interaction with Arg 200. In addition, the carbonyl on the *o*-(benzoyl)-benzoyl moiety, which was bonded to N of pyrrolidine, binds with the OH of Ser228, thus occupying the catalytic site of cPLA₂ entirely. Highly potent inhibitors were developed from this scaffold with **1-12** bearing an IC₅₀ value of 670 nM in AA production inhibition assays derived from THP-1 cells, surpassing the commercial inhibitor. Further modifications of the pharmacophores which include the introduction of F on the benzene, increasing

the steric bulkiness on the biphenyl as well as lengthening the thiazolidinedione via double bond insertion gave pyrroxyphene and RSC-3388 which gave IC₅₀ values of 320 nM and 22 nM respectively under the same assay condition. Furthermore, the cPLA₂ activity was evaluated with the PC/DOG assay on RSC-3388, giving an IC₅₀ value of 1.8 nM.⁶⁸

Due to the promising results obtained, pyrrophenone was synthesized by replacing the biphenyl functionality on the first three analogues with an S-trityl group to provide a sterically crowded and lipophilic moiety. This enabled pyrrophenone to achieve potency comparable to RSC-3388. (Table 1-3).^{69, 70} Computational studies performed on docked cPLA₂ using pyrrophenone also suggested that steric bulkiness in functionally allowed region could increase the potency of the drug.⁷¹ Moreover, the compound was also a selective cPLA₂ inhibitor over sPLA₂ and porcine pancreatic lipase.⁷⁰ Pyrrophenone has since been used as a commercial inhibitor for cPLA₂, finding applications in various biological experiments, such as regulating intercellular adhesion molecule 1 expression, mitochondrial Ca²⁺ uptake, orexin signalling and associated pathways derived from AA cascade.^{2, 72-74}

1.4.6 Other Inhibitors



Scheme 1-8: Structures of 1,3-disubstituted propanones derivatives as inhibitors of cPLA₂

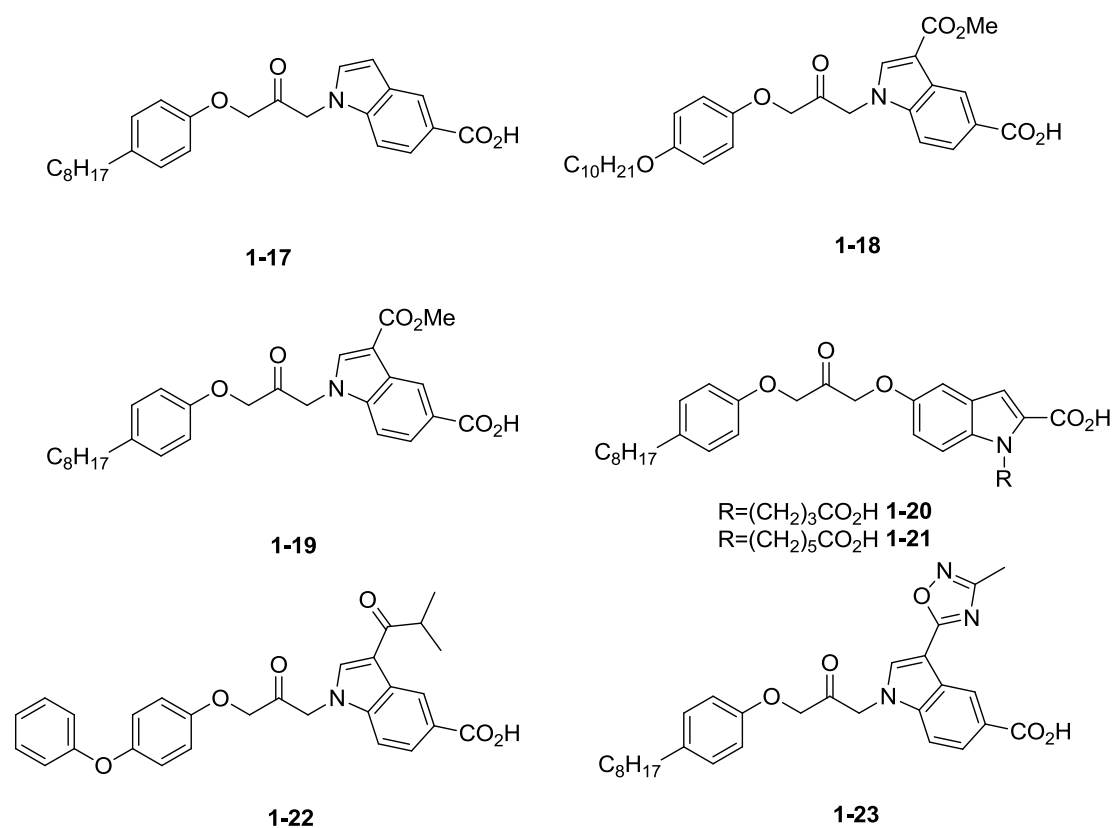
Connolly *et al* have developed various novel inhibitors mimicking the substrate in terms of its phosphate group, arachidonic acid as well as a serine trap. Such characteristics led to the design of compounds bearing a carboxylate, aromatic backbone as well as an electrophilic ketone moiety.

Extensive work were then performed to probe the pharmacophore of the inhibitor, in terms of lipophilicity of the aromatic backbone, electrophilicity of the ketone and acidity of the carboxylate, etc.⁷⁵ This gave rise to **1-13** and **1-14** which showed nanomolar inhibition of cPLA₂ in a bilayer assay and low nanomolar inhibition in a soluble substrate assay. Efforts to reduce the lipophilicity of the scaffold was achieved by introducing heterocyclic moiety into the structure in **1-15**, giving comparable potency in soluble substrate assay while low micromolar inhibition was achieved in HL90 cell assay for **1-16**.⁷⁶

Table 1-4: Inhibition by 1,3-disubstituted propanones in various assay conditions

Compound	Bilayer Assay IC ₅₀ /nM	Soluble Assay IC ₅₀ /nM	HL 90 cell assay IC ₅₀ / μM
1-13	8	30	2.8
1-14	4	80	-
1-15	-	560	1.0
1-16	-	50	1.3

With the high potency achieved for the 1,3-disubstituted propanone series, indonyl propanone analogues **1-17** was first synthesized and found to have IC₅₀ of 35 nM. SAR studies resulted in the highly potent **1-18** and **1-19** when tested by vesicle assay on purified enzymes and cellular assay containing human platelets. IC₅₀ of less than 5 nM was reported for both compounds in the vesicle assay while less than 2 nM inhibition was achieved in the cellular assay with phorbol ester (TPA) as stimulant.⁷⁷ Further modifications involving bioisosteric replacement of the carboxylic acid with amide, sulfonamide, thiazolidine and oxadiazole etc did not improve the potency satisfactorily.⁷⁸ In a bid to improve the solubility of the compound in water, a novel class utilizing the attachment of the propanone to other sites on the benzene ring rather than substitution on the indole-N was developed. Although the IC₅₀ values and metabolic stability of **1-20** and **1-21** in an *in vitro* environment of rat liver microsomes were not as favourable as **1-17**, they possessed much improved solubility in an aqueous medium.^{79, 80}



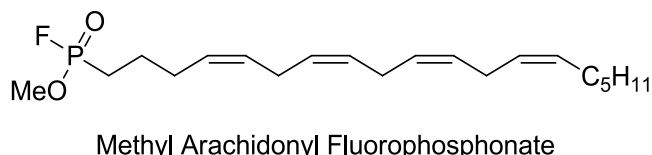
Scheme 1-9: Structures of **1-17** to **1-23** as cPLA₂ inhibitors

Table 1-5: Inhibition data and pharmacokinetic parameters of indonyl propanone inhibitors

Compound	Vesicle assay with isolated enzyme IC ₅₀ /nM	Cellular assay with intact human platelets (stimulant TPA ^a) IC ₅₀ /nM	Metabolic Stability/%	Thermodynamic solubility(μg/ml)
1-17	35	18	<5	8.4 ± 2.0
1-18	4.3	0.9	-	-
1-19	4.9	1.1	-	-
1-20	400	300	<5	30 ± 2.5
1-21	600	500	<5	17 ± 0.6
1-22	12	-	30	212 ± 15
1-23	2.1	-	81	<1

^aTPA (phorbol ester 12-*O*-tetradecanoylphorbol-13-acetate)

1-22 and **1-23** with low nanomolar inhibitory activities of 12nM and 2.1nM respectively were also reported. Both compounds were the most potent compounds from their respective libraries.^{81, 82, 83} **1-22** possessed a modest metabolic stability but an excellent solubility of 212µg/ml while **1-23** had a high metabolic stability of 81% but relatively low solubility.



Scheme 1-10: Structure of methyl arachidonyl fluorophosphonate, a non-selective PLA₂ inhibitor

Based on arachidonyl selectivity of cPLA₂ and the need for a Ser residue involvement during hydrolysis, Huang *et al* developed methyl arachidonyl fluorophosphonate (MAFP) which was shown to have good blocking effects for cPLA₂.⁸⁴ Being an irreversible inhibitor, a covalent phosphonoester bond would likely be formed when the OH of Ser228 was substituted with the F on MAFP. As a result, MAFP was also a good active site titrator of cPLA₂ activities.⁸⁴ Although it possesses high inhibitory action on cPLA₂ (IC₅₀ = 0.5 µM), it could similarly inhibit iPLA₂ in a time-dose dependent manner of up to 0.75 µM, making it an unselective inhibitor.² In addition, it was also a potent irreversible antagonist of the anandamide amidase whose substrate is arachidonyl ethanolamide.⁸⁴ Due to its non-specificity, this property of dual inhibition of iPLA₂ and cPLA₂ is also frequently utilized to quench effects of phospholipase A₂ entirely.

1.5 Fluorogenic inhibitors and substrates of PLA₂

1.5.1 Principle of Fluorescence

Photoluminescence refers to the phenomenon where the excitation of an electron from the ground state to a higher energy state via absorption of electromagnetic radiation resulted in the emission of photons. Whether the excitation of the electron into higher electronic states actually leads to an eventual emission of light is dependent on various factors. Emission of light may not occur when

excited electron relaxes to the ground state through non-radiative means such as interconversion, intersystem crossing and vibrational relaxation, as illustrated via the Perrin-Jablonski diagram (Figure 1-3).⁸⁵ When the electronic transition from the excited state to the ground state proceeds via radiative means, photoluminescence could be observed. This could broadly be classified into fluorescence and phosphorescence. Due to the difference in the type of excited state the electron is residing in, there is a difference in the timescale for light emission to occur. Fluorescence occurs when electronic transition to the ground state proceeds readily upon electronic excitation while a delayed one is observed for phosphorescence.⁸⁶

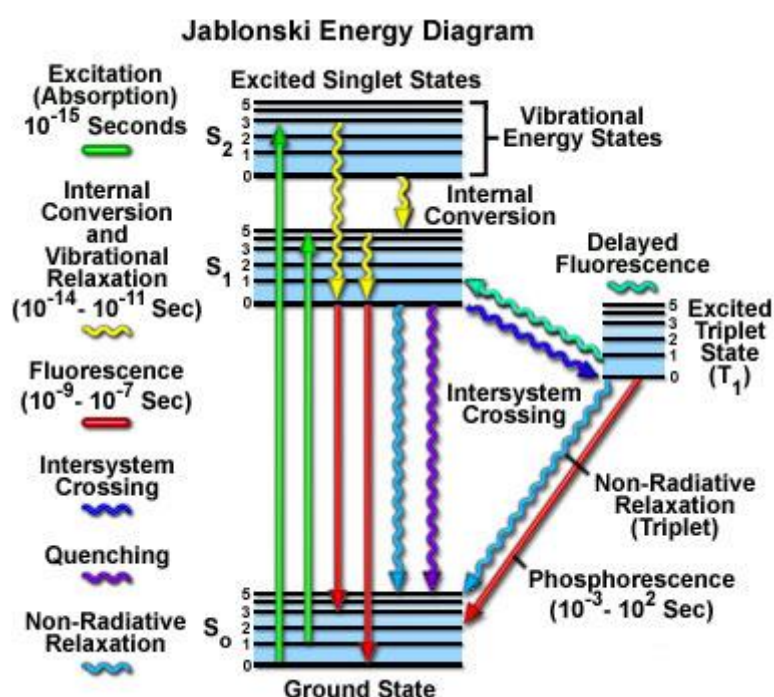


Figure 1-3: Perrin-Jablonski Energy diagram⁸⁷

1.5.2 Fluorophores and immunofluorescence

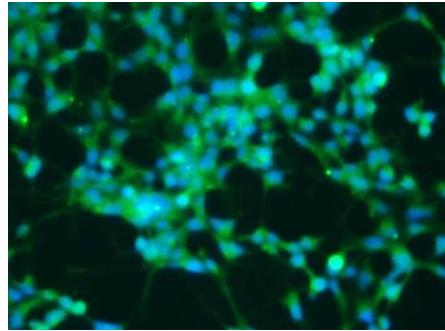
Fluorophores are compounds which produce fluorescence when excited by light. Organic molecules in particular possessing extended conjugated π -system are typical examples of fluorophores. The use of fluorophores is especially important in the field of bio-imaging. Ideal fluorophores should possess the following requirements. They should have high quantum yield with large extinction coefficient at the excitation wavelength. In addition, photo-stability of the molecule is important to reduce the extent of photo-bleaching.⁸⁸

In the field of immunofluorescence, fluorophores conjugated to antibodies are frequently used to label target antigenic sites. This powerful imaging technique picks up the emitted fluorescence by imaging instruments such as fluorescence/confocal microscopy, array scanner and flow cytometers, enabling researchers to elucidate cellular structures and visualize intracellular processes.⁸⁸ Under the umbrella of immunofluorescence, labelling of antigens on cells is termed as immunocytochemistry (ICC) while tissue staining is known as immunohistochemistry (IHC). Immunofluorescence could be performed via a direct method or indirect method. For direct immunofluorescence, primary antibodies of target antigens are directly conjugated with the desired fluorophores. This has advantages of shorter labelling time and reduced procedures while handling the sample. However, this method suffers from high cost and lower signal strength. On the contrary, the indirect method involves an initial use of an unlabelled primary antibody, followed by incubation of the sample with a secondary anti-immunoglobulin antibody that is conjugated with a fluorescent dye. With the second method, signal amplification could be achieved as one primary antibody had multiple binding sites for the secondary to attach itself on. A wide array of different coloured dyes could be chosen from different secondary antibodies that could be attached to the same primary. It has thus found widespread uses accompanied with its huge economical saving.

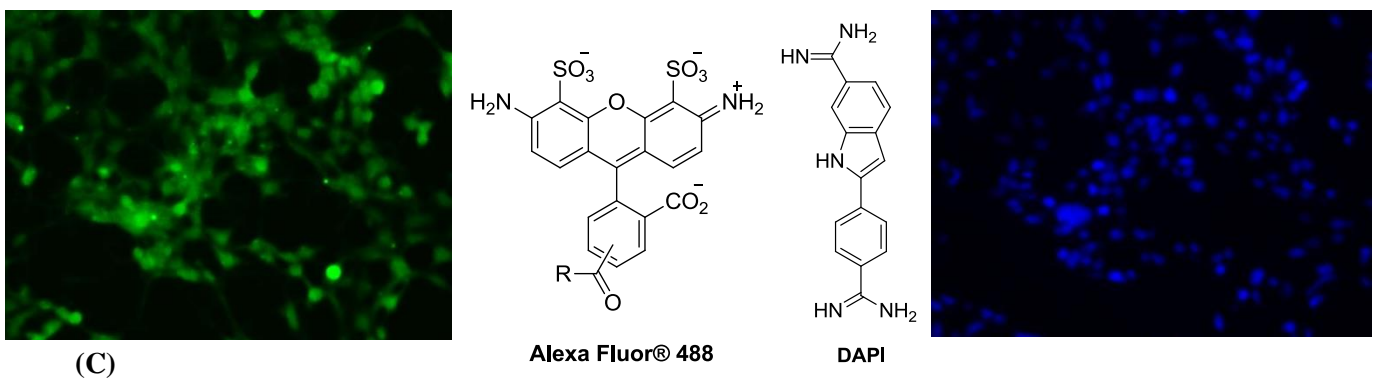
On the side-line, nuclear staining technology also plays an important role in bio-imaging. Cell-penetrant nuclei selective probes allow cells to be stained without much processing required. In addition, these probes have minimal effects on cell functions, enabling nuclear processes such as mitosis or cytokinesis to be monitored real-time. By using contrasting dyes to label different organelles, eg. Nuclei and mitochondria, multicolour images could be generated, allowing a complete visualization of the cell. Commonly used nuclear acid stains include DAPI (4',6-diamidino-2-phenylindole) and Hoechst stains (bis-benzimidazole derivatives) which intercalates with AT regions of the DNA.⁸⁹ Researchers commonly use such probes together with immunofluorescence to visualize localizations of cellular processes. For example in Figure 1-4, the use of a secondary antibody conjugated to Alexafluor® 488 and DAPI enables the simultaneous staining of both the cellular nuclei as well as cPLA₂ in SHSY5Y cells. Both dyes have distinctly different excitation and emission, as

such it could be detected at different wavelength upon applying the right type of filter. Visualization of the location of cPLA₂ (appeared green in Figure 1-4) was observed to be at the cytoplasm, separated from the nuclei (appeared blue), with distinctly defined neurites-like structures.

(A)



(B)



(C)

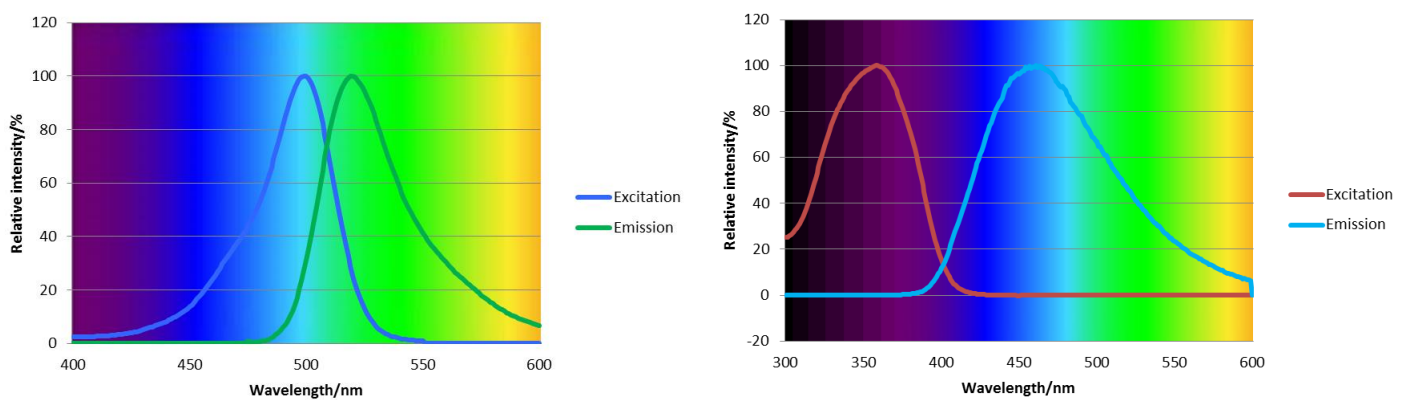
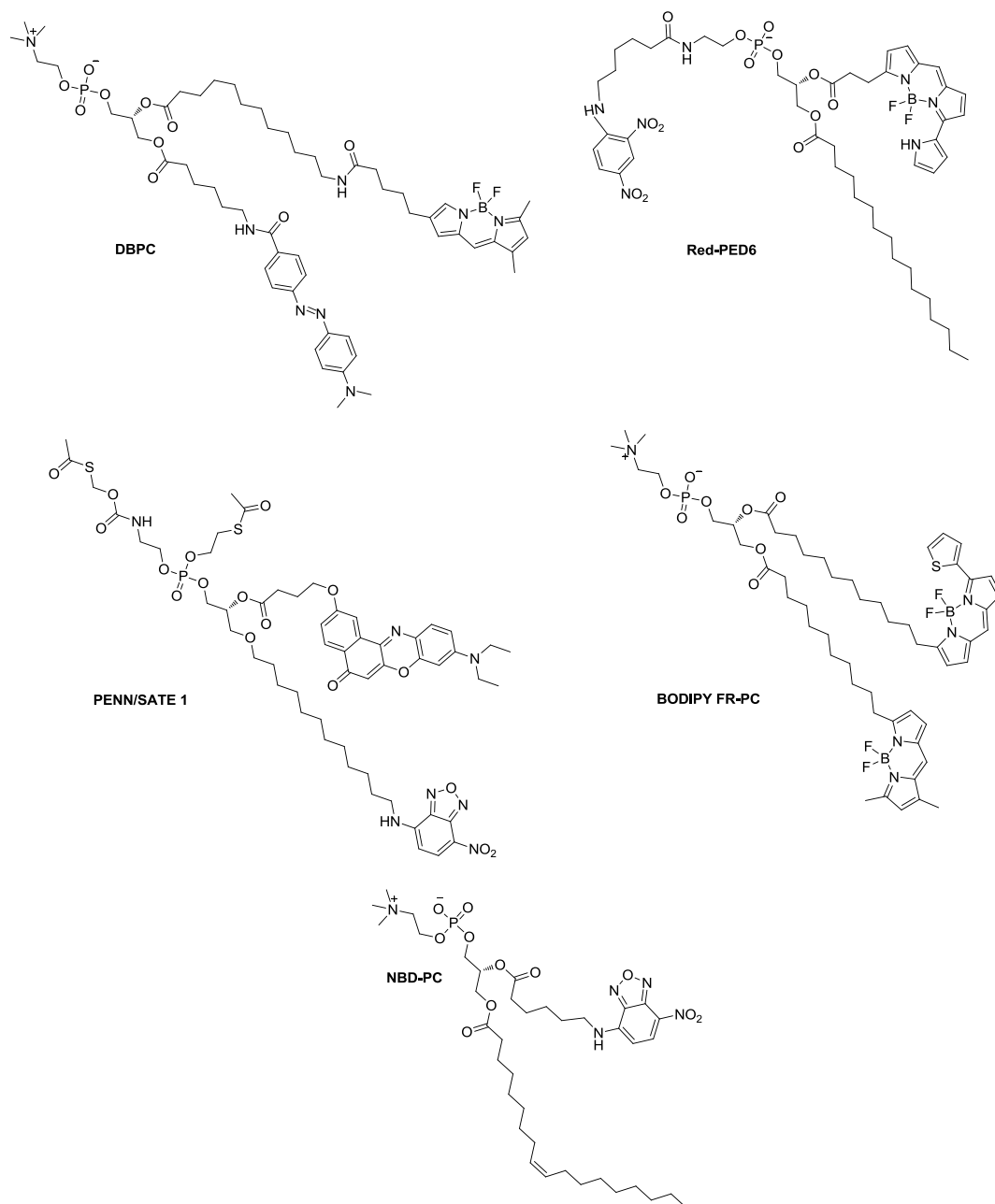


Figure 1-4: Fluorescence images of cells (A) Overlay image of Immunofluorescence of SHSY5Y cells between two channels. (B)(Left) Stained cPLA₂ on SHSY5Y cells via secondary antibody conjugated to Alexafluor 488. Image captured via FITC channel. (Right) Stained nuclei of SHSY5Y

cells via DAPI. Image captured via DAPI channel. Images were obtained from control experiments performed in chapter 4. (C) Absorption and Emission spectra of Alexa Fluor ® 488 and DAPI.^{90, 91}

1.5.3 Fluorogenic PLA₂ probes



Scheme 1-11: Structures of Fluorogenic substrates of PLA₂: DBPC, RED-PED6, PENN/SATE 1, BODIPY FR-PC and NBD-PC^{92- 96}

Various fluorogenic probes of PLA₂ had been previously synthesized.⁹²⁻⁹⁶ They are substrates of PLA₂ bearing fluorophores which could be used to track the real-time activity of PLA₂ and localization of the enzyme. At the same time, such compounds could also be utilized in fluorogenic assays. In the past, radiometric assay measuring the level of released radioactive fatty acid from cells was used to measure PLA₂ activities. This technique was dangerous and failed to give unambiguous determination of the type of PLA₂ responsible for the reaction. On the other hand, fluorogenic probes assays are rapid and highly sensitive, aiding in high throughput screening of enzyme samples or synthesized compounds. This would be important for *in vitro* drug discovery and research of PLA₂ in cellular signalling applications. There were a few strategies that were employed when designing the substrates. DBPC and Red-PED6 were designed by attaching quencher groups on the tail end of sn-1 acyl group.⁹²⁻⁹³ Fluorophores attached on the sn-2 tail end were quenched due to the close proximity of the quencher such as the DABCYL group on DBPC and the multiple nitro groups on Red-PED6.⁹³ Upon PLA₂ hydrolysis, the non-quenched fluorogenic carboxylic acid would be able to exhibit fluorescence, thus giving a direct indication of enzymatic activity. A 25-fold increase in fluorescence level by bee venom PLA₂ was observed upon hydrolysis of DBPC with bee venom PLA₂.⁹² Activity of cPLA₂ was subsequently visualized in bradykinin-inducible canine kidney cell line (MDCK-D1) with confocal microscopy.

FRET transition was another strategy employed. By pairing two different fluorophores of overlapping absorption and emission spectra, detection of hydrolytic changes could be done at two different channels, eg increase in intensity of donor emission or drop in intensity of acceptor emission. Probes such as PENN/SATE 1 and BODIPY FR-PC are good examples of this. PENN/SATE 1 contains a NBD as a FRET donor and Nile red moiety as the acceptor. NBD has an emission at 543 nm, which coincides with the excitation of Nile red at 540 nm. With an emission at 640 nm, an excitation at NBD's absorption will lead to a FRET transition leading to this emission in the probe. The authors were able to demonstrate the probe as cell penetrant and tracked the expression of PLA₂ in the growth of Medaka fish embryos.⁹⁴⁻⁹⁵ The BODIPY FR-PC utilized 2 derivatives of the BODIPY group having absorption and emission of 505/512 and 558/568 respectively. It had been shown to be capable of

tracking endogenous PLA₂ activity in zebrafish.⁹³ Recently, the group from Chen et al had demonstrated the use of FRET using NBD-PC and quantum dot loaded cluster of CdSe/ZnS compacted within a phospholipid micelles. A low background fluorescence with a low limit of detection of 3UL⁻¹ for PLA₂ was achieved.⁹⁶

1.6 Objectives of Research

The aim of this thesis is therefore to synthesize small molecule inhibitors of cPLA₂ which are structurally similar to its natural substrate. By evaluating the biological activity of these compounds, our aim is to determine the structure activity relationship (SAR) of the inhibitors on cPLA₂ to better understand the active site and binding pocket of the enzyme. This could provide future insight to develop a more potent and selective inhibitor. Molecular modelling would be an essential part to rationalize and further identify the possible residues involve in the inhibition. From the hit compound, selectivity and cytotoxicity tests would be performed to evaluate its feasibility as a drug and subsequently in a neuroinflammatory model.

Another objective of this thesis is to develop fluorogenic inhibitors and substrate of cPLA₂. Current design of fluorogenic substrates are based on criteria such as cell-permeability and the quantum yield of the respective fluorophores. This thesis aimed to develop a library of fluorogenic inhibitors of cPLA₂ which could perform its function as an inhibitor and at the same time as a tool in bio-imaging. From the most potent inhibitor obtained from biochemical screening, the fluorophore was incorporated into the substrate that was synthesised. This aimed to provide a more guided approach to the selection of fluorophore in synthesizing a fluorogenic substrate for cPLA₂.

1.7 References

1. Goetzl, E. J.; An, S. *FASEB J.* **1998**, *12* (15), 1589-1598.
2. Farooqui, A. A.; Ong, W. Y.; Horrocks, L. A. *Pharmacol. Rev.* **2006**, *58* (3), 591-620.
3. Sundaram, J. R.; Chan, E. S.; Poore, C. P.; Pareek, T. K.; Cheong, W. F.; Shui, G.; Tang, N.; Low, C. M.; Wenk, M. R.; Kesavapany, S. *J. Neurosci.* **2012**, *32* (3), 1020-34.
4. Kim, H.W.; Rapoport, SI; Rao, J. S. *Mol. Psychiatry* **2011**, *16* (4), 419-28
5. Tassoni, D.; Kaur, G.; Weisinger, R. S.; Sinclair, A. J. *Asia Pac. J. Clin. Nutr.* **2008**, *17* (1), 220-228.
6. Shimizu, T.; Ohto, T.; Kita, Y. *IUBMB Life* **2006**, *58* (5-6), 328-333.
7. Burke, J. E.; Dennis, E. A. *J. Lipid Res.* **2009**, *50*, S237-S242.
8. Dennis, E. A.; Cao, J.; Hsu, Y. H.; Magriotti, V.; Kokotos, G. *Chem. Rev.* **2011**, *111* (10), 6130-85.
9. Seilhamer, J. J.; Pruzanski, W.; Vadas, P.; Plant, S.; Miller, J. A.; Kloss, J.; Johnson, L. K. *J. Biol. Chem.* **1989**, *264*, 5335-5338.
10. Granata, F.; Nardicchi, V.; Loffredo, S.; Frattini, A.; Ilaria Staiano, R.; Agostini, C.; Triggiani, M. *Immunobiology* **2009**, *214*(9-10), 811-821.
11. Burke, J.; Dennis, E., *Cardiovas. Drug Ther.* **2009**, *23* (1), 49-59.
12. Winstead, M. V.; Balsinde, J.; Dennis, E. A. *Biochim. Biophys. Acta* **2000**, *1488*, 28-39.
13. Sun, G. Y.; Shelat, P. B.; Jensen, M. B.; He, Y.; Sun, A. Y.; Simonyi, A. *Neuromolecular Med.* **2010**, *12* (2), 133-48.
14. Hardy, J. *Trends Neurosci.* **1997**, *20* (4), 154-159.
15. Dessen, A. a.; Tang, J.; Schmidt, H.; Stahl, M.; Clark, J. D.; Seehra, J.; Somers, W. S. *Cell* **1999**, *97*, 349-360.
16. Channon, J. Y.; Leslie, C. C. *J. Biol. Chem.* **1990**, *265*(10), 5409-5413.
17. Clark, J. D.; Schievella, A. R.; Nalefski, E. A.; Lin, L.-L. *J. Lipid Mediat. Cell Signal.* **1995**, *12* (2-3), 83-117.
18. Evans, J. H.; Spencer, D. M.; Zweifach, A.; Leslie, C. C. *J. Biol. Chem.* **2001**, *276* (32), 30150-60.

19. Hirabayashi, T.; Kume, K.; Hirose, K.; Yokomizo, T.; Iino, M.; Itoh, H.; Shimizu, T. *J. Biol. Chem.* **1999**, *274* (8), 5163-5169.
20. Lin, L. L.; Wartmann, M.; Lin, A. Y.; Knopf, J. L.; Seth, A.; Davis, R. J., *Cell* **1993**, *72*, 269-278
21. Tucker, D. E.; Ghosh, M.; Ghomashchi, F.; Loper, R.; Suram, S.; John, B. S.; Girotti, M.; Bollinger, J. G.; Gelb, M. H.; Leslie, C. C. *J. Biol. Chem.* **2009**, *284* (14), 9596-611.
22. Tian, W.; Wijewickrama, G. T.; Kim, J. H.; Das, S.; Tun, M. P.; Gokhale, N.; Jung, J. W.; Kim, K. P.; Cho, W. *J. Biol. Chem.* **2008**, *283* (7), 3960-71.
23. Pavicevic, Z.; Leslie, C. C.; Malik, K. U. *J. Lipid Res.* **2008**, *49* (4), 724-37.
24. Muthalif, M. M.; Hefner, Y.; Canaan, S.; Harper, J.; Zhou, H.; Parmentier, J. H.; Aebersold, R.; Gelb, M. H.; Malik, K. U. *J. Biol. Chem.* **2001**, *276* (43), 39653-60.
25. Gentile, M. T.; Reccia, M. G.; Sorrentino, P. P.; Vitale, E.; Sorrentino, G.; Puca, A. A.; Colucci-D'Amato, L. *Mol. Neurobiol.* **2012**, *45* (3), 596-604
26. Hsieh, H.-L.; Yang, C.-M. *BioMed Res. Int.* **2013**, *2013*, 18
27. Tajuddin, N.; Moon, K.-H.; Marshall, S. A.; Nixon, K.; Neafsey, E. J.; Kim, H.-Y.; Collins, M. A. *PloS One* **2014**, *9* (7), | e101223.
28. Pettegrew, J. W.; Panchalingam, K.; Hamilton, R. L.; McClure, R. J. *Neurochem. Res.* **2001**, *26* (7), 771-782.
29. Clark, J. D.; Ling, L. L.; Kriz, R. W.; Ramesha, C. S.; Sultzman, L. A.; Lin, A. Y.; Milona, N.; Knopf, J. L. *Cell* **1991**, *65*, 1043-1051.
30. Sheikh, A. M.; Nagai, A.; Ryu, J. K.; McLarnon, J. G.; Kim, S. U.; Masuda, J. *Glia* **2009**, *57* (8), 898-907.
31. Janssen, C. I.; Kiliaan, A. J. *Prog. Lipid Res.* **2014**, *53*, 1-17.
32. Liang, X.; Wang, Q.; Hand, T.; Wu, L.; Breyer, R. M.; Montine, T. J.; Andreasson, K. J. *Neurosci.* **2005**, *25* (44), 10180-7.
33. Shi, J.; Wang, Q.; Johansson, J. U.; Liang, X.; Woodling, N. S.; Priyam, P.; Loui, T. M.; Merchant, M.; Breyer, R. M.; Montine, T. J.; Andreasson, K. *Annal. Neurol.* **2012**, *72* (5), 788-98.

34. Hillered, L.; Chan, P. H. *J. Neurosci. Res.* **1988**, *20*, 451-456.
35. Lee, H. J.; Bazinet, R. P.; Rapoport, S. I.; Bhattacharjee, A. K., *Neurochem. Res.* **2010**, *35* (4), 613-9.
36. Kalyvas, A.; Baskakis, C.; Magrioti, V.; Constantinou-Kokotou, V.; Stephens, D.; Lopez-Vales, R.; Lu, J. Q.; Yong, V. W.; Dennis, E. A.; Kokotos, G.; David, S. *Brain* **2009**, *132* (Pt 5), 1221-35.
37. Ong, W.-W.-Y. O.; Lu, X.-R.; Horrocks, L. A.; Farooqui, A. A.; Garey, L. J. *Exp. Neurol.* **2003**, *183* (2), 449-457.
38. Abramov, A. Y.; Duchon, M. R, *Philos. Trans. R. Soc. Lond., B, Biol. Sci.* **2005**, *360* (1464), 2309-14.
39. Xu, J.; Weng, Y.-I.; Simoni, A.; Krugh, B. W.; Liao, Z.; Weisman, G. A.; Sun, G. Y. *J. Neurochem.* **2002**, *83*, 259-270.
40. Sun, G. Y.; He, Y.; Chuang, D. Y.; Lee, J. C.; Gu, Z.; Simonyi, A.; Sun, A. Y. *Mol. Neurobiol.* **2012**, *46* (1), 85-95
41. Singh, I. N.; Sorrentino, G.; Sitar, D. S.; Kanfer, J. N. *Neurosci. Lett.* **1997**, *222* (1), 5-8
42. Kriem, B.; Sponne, I.; Fifre, A.; Malaplate-Armand, C.; Lozac'h-Pillot, K.; Koziel, V.; Yen-Potin, F. T.; Bihain, B.; Oster, T.; Olivier, J.-L.; Pillot, T. *FASEB J.* **2004**.
43. Sanchez-Mejia, R. O.; Newman, J. W.; Toh, S.; Yu, G.-Q.; Zhou, Y.; Halabisky, B.; Cisse, M.; Scarce-Levie, K.; Cheng, I. H.; Gan, L.; Palop, J. J.; Bonventre, J. V.; Mucke, L. *Nat. Neurosci.* **2008**, *11* (11), 1311-1318.
44. Shelat, P. B.; Chalimoniuk, M.; Wang, J. H.; Strosznajder, J. B.; Lee, J. C.; Sun, A. Y.; Simonyi, A.; Sun, G. Y. *J. Neurochem.* **2008**, *106* (1), 45-55.
45. (a) Carson, M. J.; Thrash, J. C.; Walter, B., *Clin. Neurosci. Res.* **2006**, *6* (5), 237-245. (b) Sanford, S. D.; Yun, B. G.; Leslie, C. C.; Murphy, R. C.; Pfenninger, K. H. *J. Neurochem.* **2012**, *120* (6), 974-984.
46. Ghomashchi, F.; Richard Loo; Balsinde, J.; Bartoli, F.; Apitz-Castro, R.; Clark, J. D.; Dennis, E. A.; Gelb, M. H. *Biochim. Biophys. Acta* **1999**, *1420* (1-2), 45-46.

47. Kokotos, G.; Six, D. A.; Loukas, V.; Smith, T.; Constantinou-Kokotou, V.; Hadjipavlou-Litina, D.; Kotsovolou, S.; Chiou, A.; Beltzner, C. C.; Dennis, E. A. *J. Med. Chem.* **2004**, *47* (14), 3615-3628
48. Six, D. A.; Barbayianni, E.; Loukas, V.; Constantinou-Kokotou, V.; Hadjipavlou-Litina, D.; Stephens, D.; Wong, A. C.; Magrioti, V.; Moutevelis-Minakakis, P.; Baker, S. F.; Dennis, E. A.; Kokotos, G. *J. Med. Chem.* **2007**, *50* (17), 4222-4235
49. Stephens, D.; Barbayianni, E.; Constantinou-Kokotou, V.; Peristeraki, A.; Six, D. A.; Cooper, J.; Harkewicz, R.; Deems, R. A.; Dennis, E. A.; Kokotos, G. *J. Med. Chem.* **2006**, *49* (9), 2821-2828.
50. Kokotos, G.; Kotsovolou, S.; Six, D. A.; Kokotou, V. C.; Beltzner, C. C.; Dennis, E. A., *J. Med. Chem.* **2002**, *45* (14), 2891-2893.
51. Mouchlis, V. D.; Michopoulou, V.; Constantinou-Kokotou, V.; Mavromoustakos, T.; Dennis, E. A.; Kokotos, G. *J. Chem. Infor. Model.* **2012**, *52* (1), 243-54.
52. Barbayianni, E.; Stephens, D.; Grkovich, A.; Magrioti, V.; Hsu, Y. H.; Dolatzas, P.; Kalogiannidis, D.; Dennis, E. A.; Kokotos, G. *Bioorg. Med. Chem.* **2009**, *17* (13), 4833-43.
53. Lehr, M. *Arch. Pharm.* **1996**, *329*, 386-392.
54. Lehr, M. *J. Med. Chem.* **1997**, *40* (17), 2694-2705.
55. McKew, J. C.; Lovering, F.; Clark, J. D.; Bemis, J.; Xiang, Y.; Shen, M.; Zhang, W.; Alvarez, J. C.; Joseph-McCarthy, D. *Bioorg. Med. Chem. Lett.* **2003**, *13* (24), 4501-4504.
56. McKew, J. C.; Foley, M. A.; Thakker, P.; Behnke, M. L.; Lovering, F. E.; Sum, F.-W.; Tam, S.; Wu, K.; Shen, M. W. H.; Zhang, W.; Gonzalez, M.; Liu, S.; Mahadevan, A.; Sard, H.; Khor, S. P.; Clark, J. D. *J. Med. Chem.* **2006**, *49* (1), 135-158.
57. Lee, K. L.; Foley, M. A.; Chen, L.; Behnke, M. L.; Lovering, F. E.; Kirincich, S. J.; Wang, W.; Shim, J.; Tam, S.; Shen, M. W. H.; Khor, S.; Xu, X.; Goodwin, D. G.; Ramarao, M. K.; Nickerson-Nutter, C.; Donahue, F.; Ku, M. S.; Clark, J. D.; McKew, J. C. *J. Med. Chem.* **2007**, *50* (6), 1380-1400.
58. McKew, J. C.; Lee, K. L.; Shen, M. W. H.; Thakker, P.; Foley, M. A.; Behnke, M. L.; Hu, B.; Sum, F.-W.; Tam, S.; Hu, Y.; Chen, L.; Kirincich, S. J.; Michalak, R.; Thomason, J.; Ipek, M.;

- Wu, K.; Wooder, L.; Ramarao, M. K.; Murphy, E. A.; Debra G. Goodwin; Albert, L.; Xu, X.; Donahue, F.; Ku, M. S.; Keith, J.; Nickerson-Nutter, C. L.; Abraham, W. M.; Williams, C.; Hegen, M.; Clark, J. D. *J. Med. Chem.* **2008**, *51* (12), 3388-3413.
59. Lee, K. L.; Behnke, M. L.; Foley, M. A.; Chen, L.; Wang, W.; Vargas, R.; Nunez, J.; Tam, S.; Mollova, N.; Xu, X.; Shen, M. W.; Ramarao, M. K.; Goodwin, D. G.; Nickerson-Nutter, C. L.; Abraham, W. M.; Williams, C.; Clark, J. D.; McKew, J. C. *Bioorg. Med. Chem.* **2008**, *16* (3), 1345-58.
60. Thotala, D.; Craft, J. M.; Ferraro, D. J.; Kotipatruni, R. P.; Bhave, S. R.; Jaboin, J. J.; Hallahan, D. E., *PLoS One* **2013**, *8* (7), e69688.
61. Dannenberg, A. J.; Altorki, N. K.; Boyle, J. O.; Dang, C.; Howe, L. R.; Weksler, B. B.; Subbaramaiah, K. *Lancet Oncol.* **2001**, *2* (9), 544-551.
62. Niknami, M.; Vignarajan, S.; Yao, M.; Hua, S.; Witting, P. K.; Kita, Y.; Shimizu, T.; Sved, P.; Patel, M. I.; Dong, Q. *Biochim. Biophys. Acta* **2010**, *1801* (7), 731-7.
63. Whalen, K. A.; Legault, H.; Hang, C.; Hill, A.; Kasaian, M.; Donaldson, D.; Bensch, G. W.; Bensch, G.; Baker, J.; Reddy, P. S.; Wood, N.; Ramarao, M. K.; Ellis, D. K.; Csimma, C.; McKee, C.; Clark, J. D.; Ryan, J.; Dorner, A. J.; O'Toole, M. *Clin. Exp. Allergy* **2008**, *38* (10), 1590-605.
64. Lehr, M. *Eur. J. Pharm. Sci.* **1994**, *2*, 89-97.
65. Lehr, M. *Eur. J. Med. Chem.* **1997**, *32* (10), 805-814;
66. Lehr, M. *J. Med. Chem.* **1997**, *40* (21), 3381-3392.
67. Seno, K.; Okuno, T.; Nishi, K.; Murakami, Y.; Watanabe, F.; Matsuura, T.; Wada, M.; Fujii, Y.; Yamada, M.; Ogawa, T.; Okada, T.; Hashizume, H.; Kii, M.; Hara, S.-i.; Hagishita, S.; Nakamoto, S.; Yamada, K.; Chikazawa, Y.; Ueno, M.; Teshirogi, I.; Ono, T.; Ohtani, M. *J. Med. Chem.* **2000**, *43* (6), 1041-1044.
68. Seno, K.; Okuno, T.; Nishi, K.; Murakami, Y.; Yamada, K.; Nakamoto, S.; Ono, T. *Bioorg. Med. Chem. Lett.* **2001**, *11* (4), 587-590
69. Ono, T.; Yamada, K.; Chikazawa, Y. U., Masahiko ; Nakamoto, S.; Okuno, T.; Seno, K. *Biochem. J.* **2002**, *363*, 727-735.

70. Burke, J. E.; Babakhani, A.; Gorfe, A. A.; Kokotos, G.; Li, S.; Jr., V. L. W.; McCammon, J. A.; Dennis, E. A. *J. Am. Chem. Soc.* **2009**, *151* (23), 8083-8091.
71. Wan, R.; Liu, Y.; Li, L.; Zhu, C.; Jin, L.; Li, S. *J. Mol. Endocrinol.* **2014**, *52* (1), 43-53.
72. Yun, B.; Lee, H.; Ghosh, M.; Cravatt, B. F.; Hsu, K.-L.; Bonventre, J. V.; Ewing, H.; Gelb, M. H.; Leslie, C. C. *J. Biol. Chem.* **2014**, *289* (3), 1491-1504.
73. Kukkonen, J. P. *Biochimie* **2014**, *96* (0), 158-165.
74. Connolly, S.; Bennion, C.; Botterell, S.; Croshaw, P. J.; Hallam, C.; Hardy, K.; Hartopp, P.; Jackson, C. G.; King, S. J.; Lawrence, L.; Mete, A.; Murray, D.; Robinson, D. H.; Smith, G. M.; Stein, L.; Walters, I.; Wells, E.; Withnall, W. J. *J. Med. Chem.* **2002**, *45* (6), 1348-1362.
75. Walters, I.; Bennion, C.; Connolly, S.; Croshaw, P. J.; Hardy, K.; Hartopp, P.; Jackson, C. G.; King, S. J.; Lawrence, L.; Mete, A.; Murray, D.; Robinson, D. H.; Stein, L.; Wells, E.; John Withnall, W. *Bioorg. Med. Chem. Lett.* **2004**, *14* (14), 3645-9.
76. Ludwig, J.; Bovens, S.; Brauch, C.; Elfringhoff, A. S.; Lehr, M. *J. Med. Chem.* **2006**, *49* (8), 2611-2620.
77. Hess, M.; Schulze Elfringhoff, A.; Lehr, M., *Bioorg. Med. Chem.* **2007**, *15* (8), 2883-91.
78. Fritsche, A.; Elfringhoff, A. S.; Fabian, J.; Lehr, M., *Bioorg. Med. Chem.* **2008**, *16* (7), 3489-500.
79. Fabian, J.; Lehr, M. *J. Pharm. Biomed. Anal.* **2007**, *43* (2), 601-5.
80. Bovens, S.; Kaptur, M.; Elfringhoff, A. S.; Lehr, M. *Bioorg. Med. Chem. Lett.* **2009**, *19* (8), 2107-11.
81. Bovens, S.; Schulze Elfringhoff, A.; Kaptur, M.; Reinhardt, D.; Schafers, M.; Lehr, M. *J. Med. Chem.* **2010**, *53* (23), 8298-308
82. Drews, A.; Bovens, S.; Roebrock, K.; Sunderkotter, C.; Reinhardt, D.; Schafers, M.; van der Velde, A.; Schulze Elfringhoff, A.; Fabian, J.; Lehr, M. *J. Med. Chem.* **2010**, *53* (14), 5165-78.
83. Huang, Z.; Payette, P.; Abdullah, K.; Cromlish, W. A.; Kennedy, B. P., *Biochemistry* **1996**, *35*, 3712-3721.

84. Deutsch, D. G.; Omeir, R.; Arreaza, G.; Salehani, D.; Prestwich, G. D.; Huang, Z.; Howlett, A., *Biochem. Pharm.* **1997**, *53* (3), 255-260.
85. Lakowicz, J. R., *Principles of Fluorescence Spectroscopy*. 3rd edition.; Springer-Verlag: New York, USA, **2006**, 643.
86. Valeur, B.; Berberan-Santos, M. N., *Molecular Fluorescence*. 2nd edition.; Wiley-VCH: Weinheim, Germany, **2012**, 569.
87. <http://www.olympusmicro.com/primer/java/jablonski/jabintro/>
88. Johnson ID. *Practical Considerations in the Selection and Application of Fluorescent Probes*. In: *Handbook of Biological Confocal Microscopy*. 3rd edition (J.B. Pawley. Ed); Plenum Press. New York, **2006**. 362-363.
89. Invitrogen. *Molecular Probes™ Handbook. A Guide to Fluorescent Probes and Labeling Technologies*. 11th edition; ThermoFisher Scientific, **2010**, chapter 12
90. <http://www.atdbio.com/content/34/Alexa-dyes>
91. <https://www.thermofisher.com/order/catalog/product/D1306>
92. Li, F.; Manabe, K.; Shope, J. C.; Widmer, S.; DeWald, D. B.; Prestwich, G. D. *Chem. Biol.* **2002**, *9*, 795-803
93. Manna, D.; Cho W. *Methods Enzymol.* **2007**, *434*, 15-27
94. Wichmann, O.; Wittbrodt, J.; Schultz, C., *Angew. Chem. Int. Ed.* **2006**, *45*, 508-512
95. Wichmann, O.; Gelb, M. H.; Schultz, C. *ChemBioChem.* **2007**, *8*, 1555-1569
96. Li, J.; Zhang Y.; Ai, J.; Gao, Q.; Qi, H.; Zhang, C.; Cheng, Z. *RSC Advances*, **2016**, *6*, 15895-15899

CHAPTER 2: CHEMICAL SYNTHESIS AND STRUCTURE-ACTIVITY RELATIONSHIP STUDIES OF ARACHIDONIC ACID ANALOGUES AS CYTOSOLIC PHOSPHOLIPASE A₂ INHIBITORS

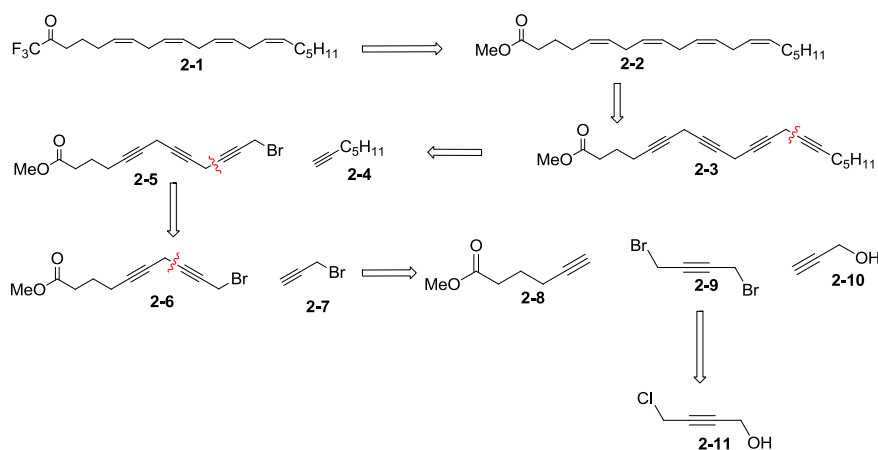
2.1 Introduction

Phospholipases A₂ (PLA₂s) are a superfamily of enzymes characterized by their ability to hydrolyze the acyl ester bond at the sn-2 position of glycerophospholipids to yield polyunsaturated fatty acids (PUFAs) and a lysophospholipid.¹ The mammalian PLA₂ family comprises five main types of enzymes, namely the secreted small molecular weight sPLA₂, the larger cytosolic Ca²⁺-dependent cPLA₂, the Ca²⁺-independent iPLA₂, the platelet-activating factor acetylhydrolases PAF-AH and the lysosomal PLA₂. Of these PLA₂ enzymes, the ubiquitous cPLA₂ is found to be responsible for the release of arachidonic acid (AA), an important PUFA which serves as the precursor for the synthesis of eicosanoids and prostanoids that mediate a wide variety of inflammatory responses.² In the central nervous system, cPLA₂ activation has been implicated in the pathogenesis of a number of neurodegenerative (Alzheimer's disease, Parkinson's disease and prion diseases) and neuropsychiatric (schizophrenia and depressive disorder) diseases.³ Effects of inflammation and its involvement in nitrosative/oxidative signaling pathways for example had been frequently cited as a pathogenetic link to Aβ-amyloid production due to the actions of cPLA₂. A direct effect of a sustained, aberrant cPLA₂ activation could result in enhanced neural membrane destruction eventually comprising functions on membranal ion receptors, leading to cell death.³ Thus cPLA₂ is an important target for drug discovery, and for the development of new therapeutics to treat neurodegenerative and neuropsychiatric disorders. An ideal cPLA₂ inhibitor should not only reach the site where inflammatory processes are taking place (this may be achieved through improved drug delivery systems), they should also inhibit inflammation, block oxidative stress and cross the blood-brain barrier. To-date, various organic compounds have been shown to inhibit cPLA₂ selectively.⁴ However, some of these compounds provide unfavorable side-effects⁵ while others suffer from solubility and metabolic stability problems.⁶ Thus there is a need to examine other compounds for their activities and suitability as cPLA₂ inhibitor. As part of our efforts to develop cPLA₂ inhibitors as potential drug candidates for the

treatment of neurological disorders, we have synthesized a new series of AA analogues and evaluated them for their inhibitory activities. In our inhibitor design, we have included the arachidonyl trifluoromethyl keto pharmacophore, as earlier studies have shown that arachidonyl trifluoromethyl ketone (AACOCF₃) is a potent but non-selective inhibitor of cPLA₂ that has been applied to various neurological studies.⁷ Bearing close structural resemblance with the substrate of cPLA₂ - phosphatidylcholine (PC), it had been shown to be cell-penetrant and effective in reducing the undesirable effects of a dysregulated cPLA₂ system.⁸ These include cell models, lysate systems as well as in vivo studies of CNS systems demonstrating its potential in breaching the blood brain barrier.⁸⁻⁹ We hoped to utilize the relevant pharmacophores of AACOCF₃ to achieve its potent and cell-penetrant capability, at the same time develop a selective inhibitor of cPLA₂ through our study. We herein present the synthesis of AA analogues **1a-o**, **2a-q** and **20c** as well as the investigation of these compounds for their (i) inhibition of cPLA₂, (ii) cytotoxicity, (iii) specific functionality to the inhibitory function, and (iv) ability to cross the blood-brain barrier.

2.2 Chemical Synthesis

2.2.1 Retrosynthetic Analysis of AACOCF₃



Scheme 2-1: Retrosynthesis of **2-1**

The retrosynthetic analysis of **2-1** (AACOCF₃) and its analogues was envisioned to be synthesized from **2-2**, where ester could be subsequently converted into a trifluoromethylketone group. **2-2** could be synthesized from **2-3**, via a controlled hydrogenation to form the all-cis tetraene functionality.

Disconnection at the appropriate positions on the skipped alkyne **2-3** could form the individual alkyne fragments **2-8**, **2-10** and **2-11**, which are commercially available. Through a series of cross-coupling and bromination reactions as shown in earlier studies, **2-1** and its analogues could be synthesized.¹⁰ Using AA as a scaffold, we sought to enhance the potency and selectivity of the cPLA₂ inhibitors. The inhibitor design involves the modification of AA at different selected positions of the compound (Figure 2-1).

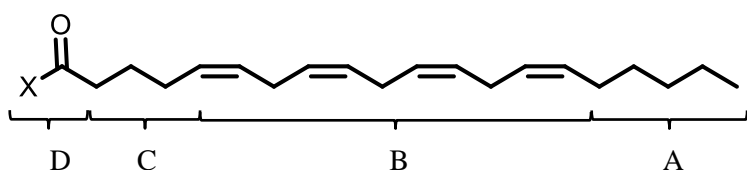
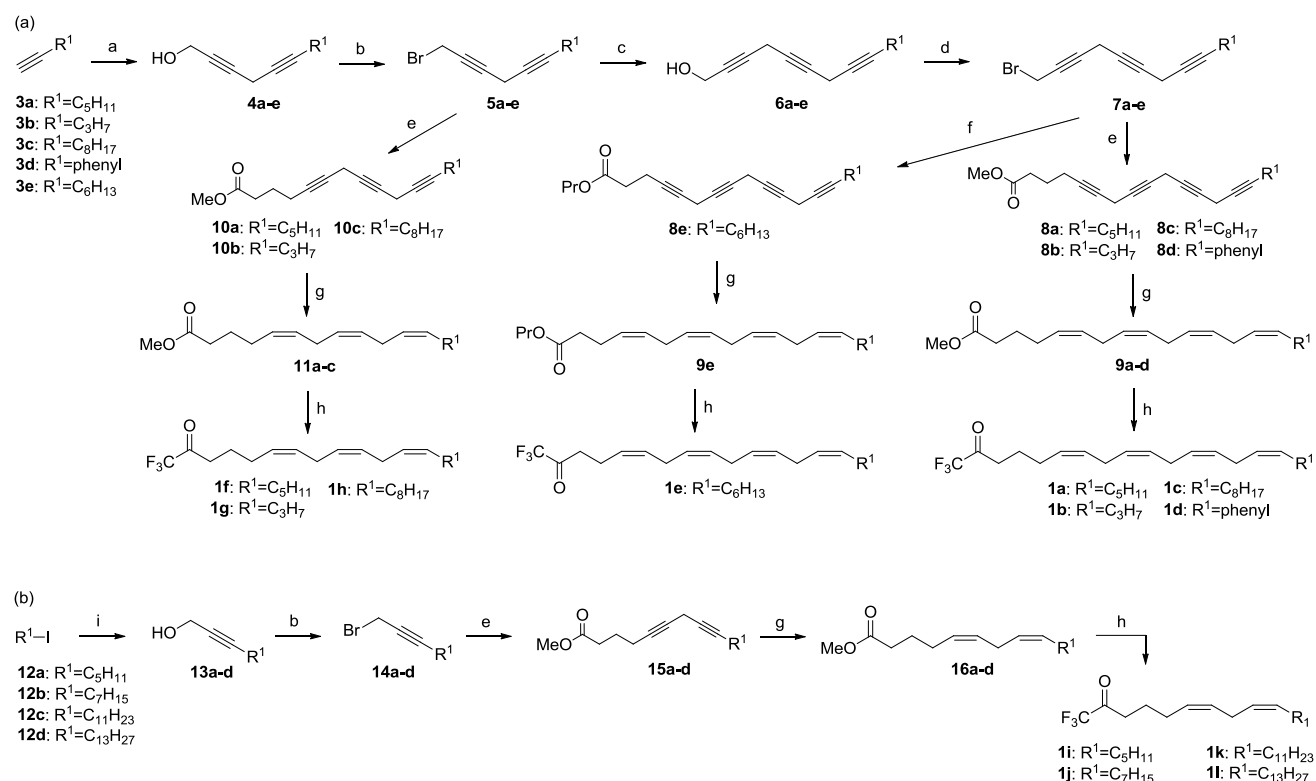


Figure 2-1: Functionalities on AA that could be varied: A – tail length, B – number of double bonds, C – number of methylene groups between the first double bond and the carbonyl group, and D – functionality on the carbonyl group.

2.2.2 Synthesis of AACOCF₃ and trifluoromethylketone based analogues



Scheme 2-2. Synthesis of AACOCF₃ and analogues (a) 4-Chloro-2-butyn-1-ol, CuI, NaI, K₂CO₃, DMF, rt, overnight (b) CBr₄, PPh₃, CH₂Cl₂, -40°C to -20°C, 1 h (c) Propargyl alcohol, CuI, NaI, K₂CO₃, DMF, rt, overnight (d) CBr₄, PPh₃, CH₂Cl₂, -40°C to -20°C, 1 h (e) Methyl 6-hexynoate, CuI, NaI, K₂CO₃, DMF, rt, overnight (f) Propyl 5-pentynoate, CuI, NaI, K₂CO₃, DMF, rt, overnight (g) H₂, Ni(OAc)₂·4H₂O, NaBH₄, en, 95% EtOH, rt, 2 h (h) i) NaOH, MW 120°C, 1 h ii) Trifluoroacetic anhydride, Pyridine, , CH₂Cl₂, rt, 2 h (i) Propargyl alcohol, n-BuLi, HMPA, THF, -78°C to rt, overnight

Modification of the tail length (A): AACOCF₃ **1a** was prepared by assembling alkynes together through a series of coupling and bromination reactions according to the synthetic strategy shown in Scheme 2-2a.¹⁰ A total of 3 coupling and 2 bromination reactions were performed to reach the skipped diyne **8a**. **8a** was initially hydrogenated with Brown's P2 nickel catalyst in ethanol according to a published procedure.^{10d} However this did not provide the desired compound **9a** (Table 2-1, entry 1). It was observed that decreasing reaction time improved the yield as over-hydrogenated side products were being reduced (Table 2-1, entry 2-4). Optimization of the hydrogenation reaction by varying the

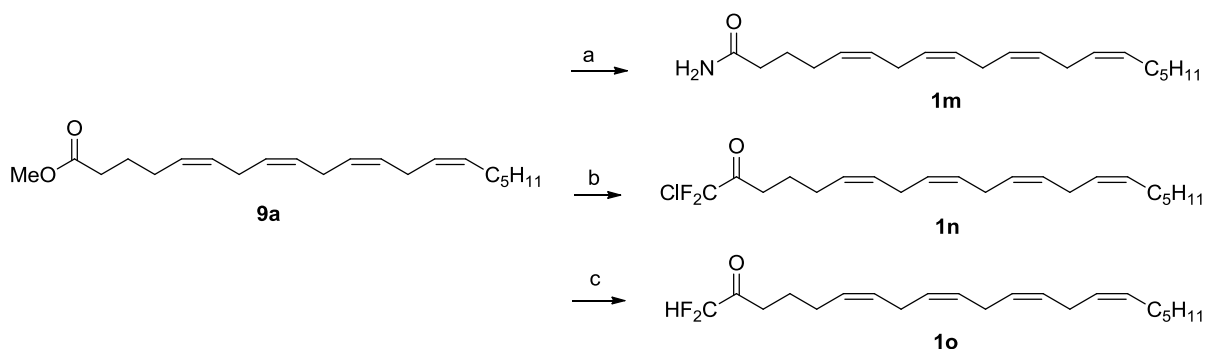
equivalent of the catalyst and reaction conditions (Table 2-1) eventually provided **9a** in 68% yield. Initial attempts to trifluoromethylate **9a** by stirring TMSCF₃ and CsF as a TMS activator with the ester in CHCl₃ at room temperature did not yield **1a**.^{11a} Replacing CsF with TBAF also failed to provide the desired compound.^{11b} We attempted to convert **9a** to the corresponding carboxylic acid and then treating it with LDA and EtO₂CCF₃.^{11c} However this too did not yield **1a**. Finally we tried to trifluoromethylate the intermediate carboxylic acid with pyridine and TFAA¹² and gratifyingly this gave **1a** in 48% yield (over 2 steps). Analogues **1b - 1d** containing the tetraene was synthesized in the same manner by varying the alkyne **3** in the first step of the reaction. Analogues **1f - 1h** containing the triene was synthesized by reducing the number of coupling and bromination steps to reach a skipped diyne **10a-c** before hydrogenation and trifluoromethylation to obtain the respective compounds.

Table 2-1: Optimization for the hydrogenation of compound **8a**

Entry	Equivalents of Brown's P2 nickel catalyst	Solvent	Time (h)	Yield (%)
1 ^{9d}	0.32	Pure EtOH	8	-
2	2.24	95:5 EtOH-2 M NaOH	8	-
3	2.24	95:5 EtOH-2 M NaOH	3	19
4	2.24	95:5 EtOH-2 M NaOH	1	63
5	1.5	95:5 EtOH-2 M NaOH	1	68

Modification of the number of double bonds (B): In the synthesis of analogues **1i-l** which contain two double bonds, the precursor intermediate **13a-d** is not commercially available and was synthesized by treating alkyl halide **12a-d** with propargyl alcohol in the presence of butyllithium and an additive as a solvating agent. Initially *N,N'*-dimethylpropyleneurea (DMPU) was used as the additive but it gave **13b** in only 20% yield. Hence we tried hexamethylphosphoramide (HMPA) which provided **13b** in 86% yield. This may be attributed to the increased polarity of the P=O bond in HMPA as compared to the C=O in DMPU, which stabilizes the acetylide to a greater extent. HMPA was thus used as an additive for the synthesis of intermediate **13a-d**.

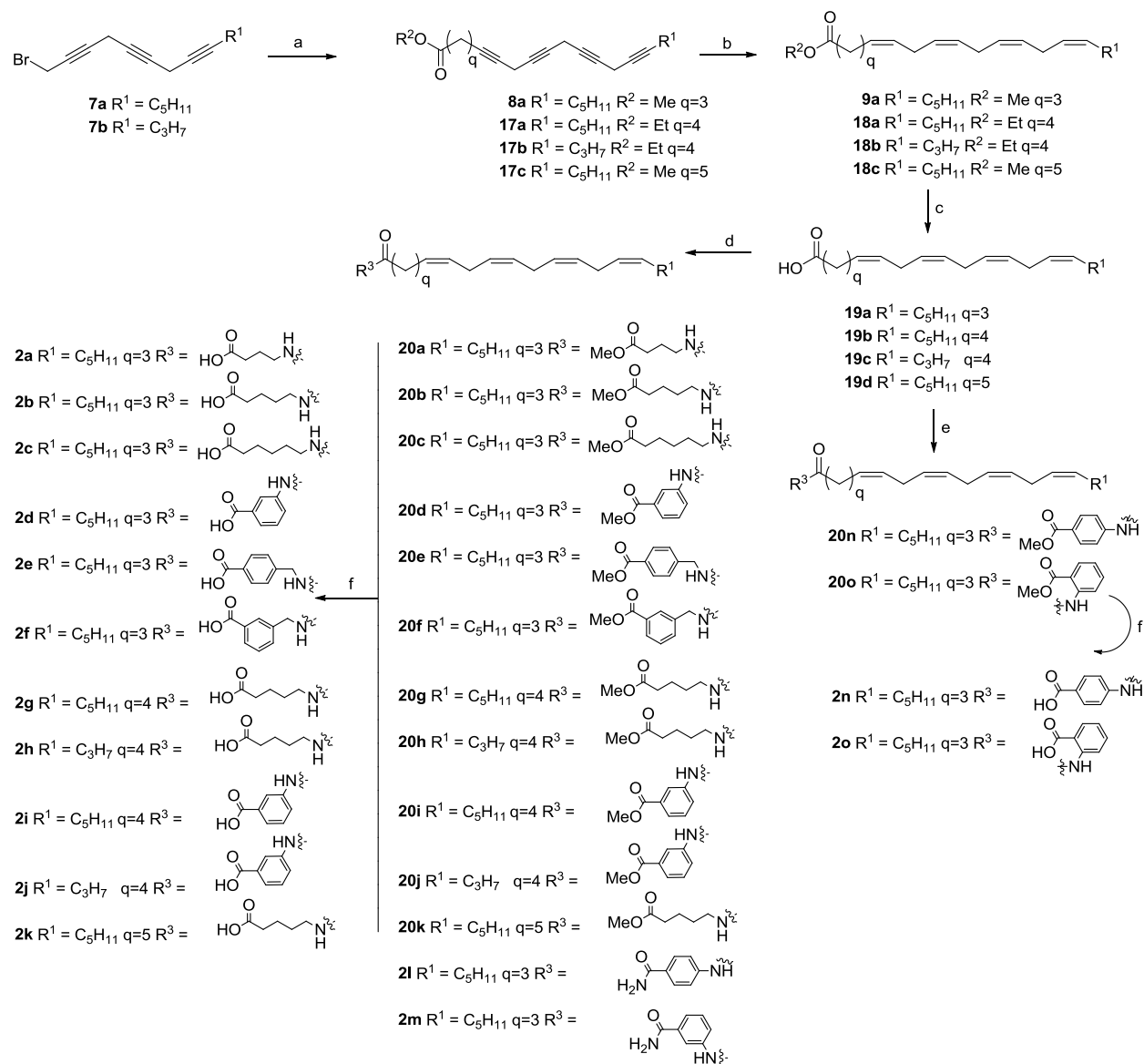
Modification of the number of methylene groups between the first double bond and the carbonyl group (C): The synthesis of **1a-d** and **1f-l** involved the coupling of methyl 6-hexynoate to the brominated intermediate before hydrogenation. To synthesize **1e** with reduced carbons between the carbonyl and first double bond, coupling of **7e** to propyl 5-pentynoate yielded the skipped diyne **8e** which was hydrogenated and trifluoromethylated to give **1e**.



Scheme 2-3. Synthesis of **1m** to **1o** (a) NH_3 , $\text{Mg}(\text{OMe})_2$, MeOH , 80°C , overnight (b) i) NaOH , MW 120°C , 1 h ii) Chlorodifluoroacetic anhydride, Pyridine , CH_2Cl_2 , rt, overnight (c) i) NaOH , MW 120°C , 1 h ii) Difluoroacetic anhydride, Pyridine , CH_2Cl_2 , rt, overnight.

Modification of the functionality on the carbonyl group (D): To form a primary amide **1m**, tetraene **9a** underwent amidation by heating it with a solution of ammonia dissolved in methanol and $\text{Mg}(\text{OMe})_2$ overnight at 80°C . The chlorodifluoroketone and difluoroketone functionalities in **1n** and **1o** were respectively synthesized by hydrolyzing the ester **9a** to the corresponding carboxylic acid followed by a reaction with the respective anhydrides with pyridine and dichloromethane under room temperature.

2.2.3 Synthesis of Arachidonyl based amide analogues



Scheme 2-4. Synthesis of Arachidonyl based amide analogues (a) $CH\equiv C-(CH_2)_qCO_2R^2$, CuI, NaI, K_2CO_3 , DMF, rt, overnight (b) H_2 , $Ni(OAc)_2 \cdot 4H_2O$, $NaBH_4$, en, 95% EtOH, rt, 2 h (c) MeOH/NaOH, rt, 3 h (d) NH_2 -Alk- CO_2Me or NH_2 -Ar- CO_2Me or NH_2 -Ar- $CONH_2$, EDC.HCl, HOBt, TEA, DMF, rt, overnight (e) i) $(COCl_2)$, catalytic DMF, CH_2Cl_2 , rt, 1 h ii) NH_2 -Ar- CO_2Me , TEA, THF, rt, overnight (f) MeOH/NaOH, rt, 3 h

huge decrease in electron density of the amine, affecting its reactivity. As such, a harsher amidation condition was required. **20n** and **20o** were then hydrolyzed to the free acid form **2n** and **2o**. **2q** was synthesized by coupling **7a** with the amine **23** followed by hydrogenation and hydrolysis. The full structures of all synthesized analogues are as shown in figure 2-2.

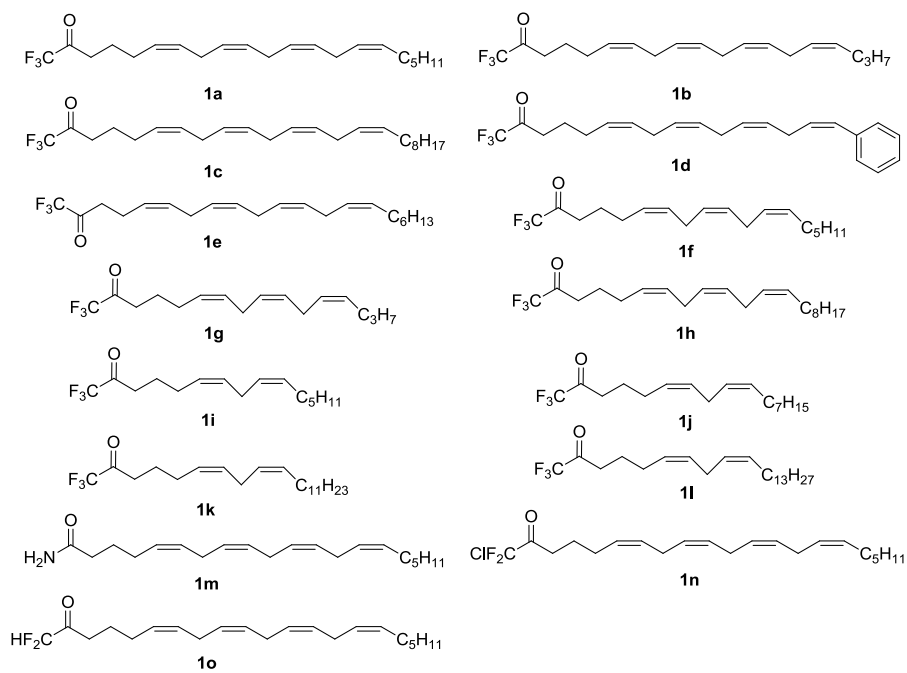


(Table 2-2, Cpd **1a-1c**). Nevertheless, a slight increase in potency was seen when the C8 (**1c**) alkyl chain was decrease to a C3 (**1b**) chain. The same trend was also observed for the diene series (**1i – 1l**). Increasing the alkyl chain length from C5 (**1i**) to C13 (**1l**) chain length resulted in a huge decrease in potency from 63.6% inhibition to 27.6%. A small increase in the potency from C5 (**1i**) to C7 (**1j**) was visibly detected although the increase is within the margin of error. **1d** possessing a phenyl moiety instead of the alkyl chain has the highest potency within the trifluoromethylketone series (Table 2-2). The highest potency could be attributed to additional interactions with cPLA₂ (*vide infra*).

Modification of the number of double bonds (B): The skipped alkene functionality in the arachidonyl backbone causes **1a** to be light and oxygen sensitive.¹³ We hypothesized that reducing the number of skipped alkenes on the backbone would improve the compound's stability. Hence analogues with a reduced number of double bonds **1f-1** were synthesized (Schemes 2-2a and 2-2b). Comparing their potencies with **1a**, the improvement in the potencies were less impressive. Nevertheless an increase in potency was detected when the number of double bonds increased from two (**1k**) to four (**1a**) while maintaining the number of carbons unchanged. A plausible explanation could be an increased in rigidity of the compound with more double bonds, making it less rotatable hence improving its binding affinity with the enzyme pocket.

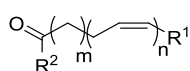
Modification of the number of methylene groups between the first double bond and the carbonyl group (C): Earlier studies have shown that the number of methylene groups between the carbonyl carbon and the first double bond (Figure 2-1) is important for enzyme recognition.¹⁴ To better understand the effects of these methylene groups on the inhibitory properties of the compound, **1e** with two methylene groups was synthesized. Results obtained showed that **1e** had the same potency as **1a** (Table 2-2). This suggested that the position of the double bonds from the carbonyl for enzyme recognition might not be as important as it was previously postulated.¹⁴

Modification of the functionality on the carbonyl group (D): Earlier studies have shown that the presence of a trifluoro moiety confers a very high electrophilicity on AA.¹⁵ This can result in the keto existing largely in the hydrated form, thus reducing the concentration of the active species. To vary

the electrophilicity of the carbonyl group, we have modulated the number of fluorine atoms or replaced the trifluoro moiety with other functionalities (Table 2-2, Cpd **1m-1o**). Reducing the electrophilicity of the carbonyl group by reducing the number of fluorine atoms on the trifluoromethyl moiety also did not result in a more potent cPLA₂ inhibitor (Table 2-2, Cpd **1n-1o**). Similarly a drop in potency to 39.3% inhibition was observed in **1m** when the carbonyl was converted into a primary amide.

Studies by Pickard *et al*¹⁶ have shown that site-directed mutagenesis of Arg200 in cPLA₂ severely affected its catalytic property. Since this amino acid residue is positioned near the mouth of the active site cleft, it was proposed that Arg200 plays a stabilizing role by interacting with the phosphate group on phosphatidylcholine, a glycerophospholipid that is hydrolysed by cPLA₂.¹⁷ We postulated that replacing the trifluoromethyl moiety with a group containing a negatively charged functionality that can interact with Arg200 would improve the compound's potency. Encouraged by these results, we decide to pursue the synthesis of amide analogues containing functionalities that could stabilize Arg200. Various analogues containing an alkyl extension ending with either a carboxylic acid, ester or amide functionality were thus synthesized (Schemes 2-4 and 2-5).

Table 2-2: Potency of **1** at 10 μM and their physicochemical properties



<i>Cpd</i>	R^2	m	n	R^1	<i>cPLA</i> ₂ <i>Activity (%)</i>	<i>Percentage inhibition (%)</i>
1a	CF ₃	2	4	C ₅ H ₁₁	40.0 ± 0.9	60.0
1b	CF ₃	2	4	C ₃ H ₇	37.0 ± 3.9	63.0
1c	CF ₃	2	4	C ₈ H ₁₇	45.0 ± 3.5	55.0
1d	CF ₃	2	4	phenyl	31.8 ± 2.0	68.2
1e	CF ₃	1	4	C ₆ H ₁₃	40.5 ± 3.6	59.5
1f	CF ₃	2	3	C ₅ H ₁₁	33.8 ± 2.2	66.2
1g	CF ₃	2	3	C ₃ H ₇	42.5 ± 0.3	57.5

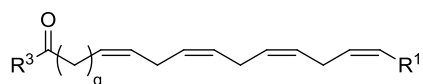
1h	CF ₃	2	3	C ₈ H ₁₇	45.6 ± 2.8	54.4
1i	CF ₃	2	2	C ₅ H ₁₁	36.4 ± 3.3	63.6
1j	CF ₃	2	2	C ₇ H ₁₅	33.9 ± 4.8	66.1
1k	CF ₃	2	2	C ₁₁ H ₂₃	54.0 ± 6.9	46.0
1l	CF ₃	2	2	C ₁₃ H ₂₇	72.4 ± 12.9	27.6
1m	NH ₂	2	4	C ₅ H ₁₁	60.7 ± 1.9	39.3
1n	CClF ₂	2	4	C ₅ H ₁₁	49.2 ± 4.5	50.8
1o	CHF ₂	2	4	C ₅ H ₁₁	40.2 ± 0.5	59.8

We started the investigation by synthesizing **2a-2c** which contained an extra carboxylic acid to provide additional interaction with Arg200 (Scheme 2-4). **2b** containing 4 methylene groups between the free carboxylic acid and amide was synthesized as the distance of these 4 methylene groups is approximately equal to the distance between the arachidonate ester and phosphate group of the substrate phosphatidylcholine. Such consideration ensures that **2b** fit into the binding pocket of cPLA₂ in the same manner as what the natural substrate does. A SAR on the carbon length between the carboxylic acid to the amide was performed by changing the number of methylene groups from 3 to 5 for **2a** and **2c** respectively. As anticipated, **2b** possessed the highest potency (Table 2-3). This suggests that an optimum number of methylene groups between the amide and carboxyl is 4, while deviating from this number cause the potency to drop. To examine if the carboxylic acid's interaction with Arg 200 was responsible for increasing potency, **20c** containing the ester instead of the carboxylic acid was also screened. A huge decrease in potency to 15.2% inhibition occurred, confirming the hypothesis. Next, our efforts were directed at determining the importance of number of methylene groups between the first double bond and the carbonyl group. Although it was concluded in previous section that this effect is insignificant, presence of the extension to reach out to Arg 200 has resulted in a distinct elongation of the molecule with respect to compounds **1a - o** in general. Comparing between **2b**, **2g**, **2k** and **2q** when methylene groups increase from 2 to 5, potency increased tremendously peaking at 4 methylene groups (**2g**) but dropped again when it was further

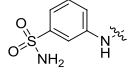
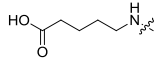
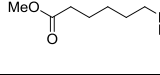
increase to 5 (**2k**). This point towards 4 methylene groups as the number for optimal interactions with the enzyme. Changing the tail length from C5 to C3 in **2h** didn't improve the potency.

At the same time, further rigidification of the molecule in hope of improving potency was achieved by introducing phenyl moiety instead of alkyl chains to link the amide and carboxylic acid together. 3 analogues containing a meta-directed (**2d**), para-directed (**2n**) and ortho-directed (**2o**) carboxylic acid were designed. Ortho substitution suffers from a huge loss in cPLA₂ inhibition. Meta-substitution (**2d**) was found to give the best result, providing a 2.5 fold higher potency than **1a**. When the free carboxylic acid was replaced by an amide, a lower potency was seen. Similar trend was also observed in the meta- and para-substituted amide where the meta amide **2m** has a higher potency than **2n**. To further improve the cell-penetrant ability of the compound, allosteric replacement of the carboxylic acid was made with sulphonamide **2p**. However an improvement of potency compared with **1a** was not observed. Since it was determined that 4 methylene groups between the amide and first double bond was optimum for binding, **2i** and **2j** with different alkyl tail end was synthesized. **2i** having a potency of 88.5% inhibition was discovered as the most potent compound. From the 2 tables, three compounds **2d**, **2g** and **2i** which significantly decreased the cPLA₂ activity, were identified (Table 2-3). Since **2d** and **2i** are structurally analogous, only the stronger inhibitor **2i** was selected for further studies. Thus using the fluorogenic PLA₂ assay and recombinant cPLA₂, the IC₅₀ of **2g** and **2i** were determined to be 5.3 ± 0.3 and 2.9 ± 0.2 μ M respectively, indicating that these compounds are more potent against cPLA₂ than **1a** (IC₅₀ = 16.5 ± 3.0 μ M) (Figure 2-2). This increase in potency of the compounds supported our hypothesis that the presence of a carboxylate group could interact with Arg200 to improve the compound's potency.

Table 2-3: Potency of **2** at 10 μ M and their physicochemical properties



<i>Cpd</i>	R^3	<i>q</i>	R^1	<i>cPLA</i> ₂ Activity (%)	Percentage Inhibition (%)
2a		3	C ₅ H ₁₁	39.7 ± 2.6	60.3
2b		3	C ₅ H ₁₁	26.7 ± 0.1	73.3
2c		3	C ₅ H ₁₁	40.9 ± 1.1	59.1
2d		3	C ₅ H ₁₁	13.2 ± 1.2	86.8
2e		3	C ₅ H ₁₁	25.8 ± 0.1	74.2
2f		3	C ₅ H ₁₁	35.6 ± 2.1	64.4
2g		4	C ₅ H ₁₁	15.5 ± 0.3	84.5
2h		4	C ₃ H ₇	43.6 ± 0.2	56.4
2i		4	C ₅ H ₁₁	11.5 ± 1.0	88.5
2j		4	C ₃ H ₇	16.5 ± 1.2	83.5
2k		5	C ₅ H ₁₁	37.7 ± 1.5	62.3
2l		3	C ₅ H ₁₁	67.4 ± 5.7	32.6
2m		3	C ₅ H ₁₁	57.5 ± 1.4	42.5
2n		3	C ₅ H ₁₁	33.3 ± 0.9	66.7
2o		3	C ₅ H ₁₁	65.5 ± 4.0	34.5

2p		3	C ₅ H ₁₁	53.9 ± 2.7	46.1
2q		2	C ₅ H ₁₁	56.6 ± 4.9	43.4
20c		3	C ₅ H ₁₁	84.8 ± 1.0	15.2

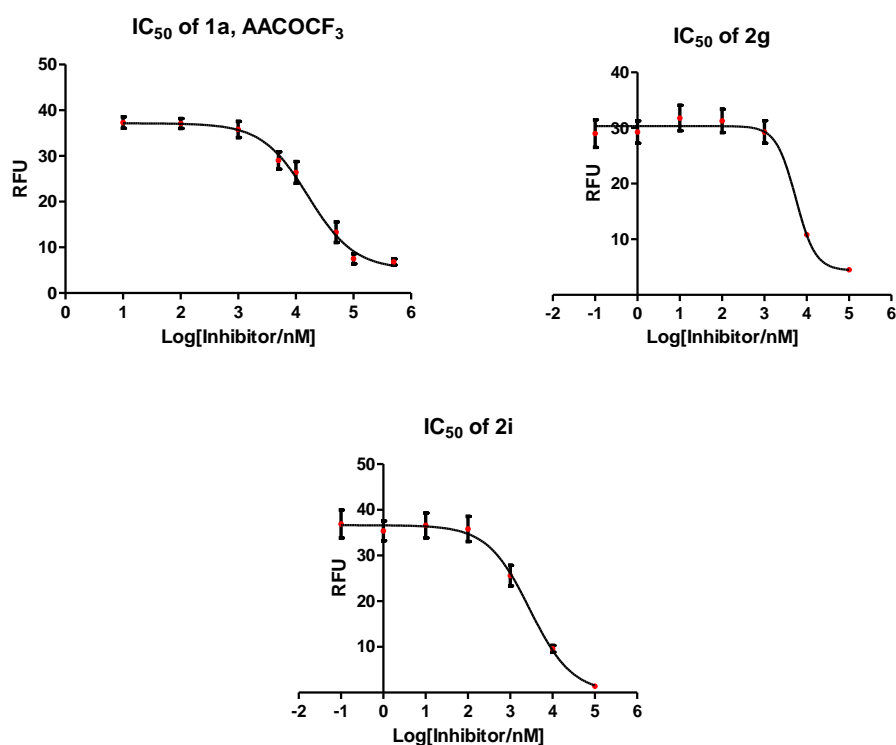
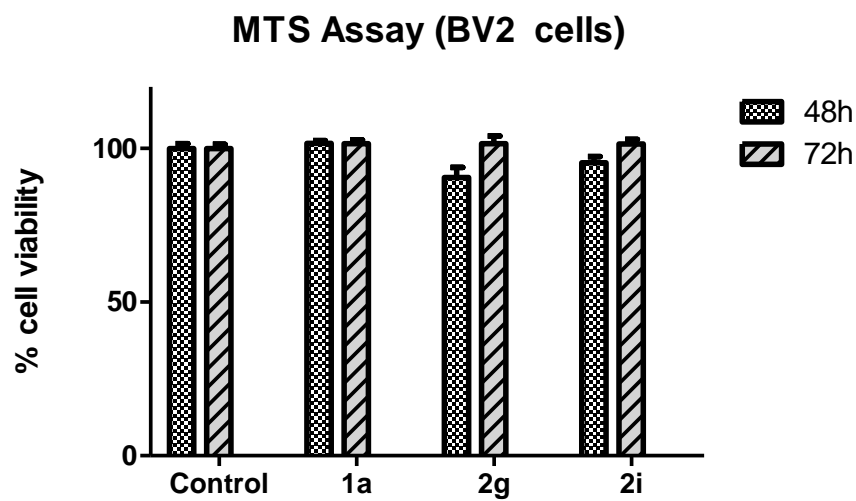


Figure 2-3: Dose-dependent inhibitory plot of **1a**, **2g** and **2i**.

2.4 MTS Assay

MTS assay were conducted with **1a**, **2g** and **2i** at 48 h and 72 h using BV-2 cells, a murine microglial cell derived from post-natal mouse cerebella, and HEK293T cells which are from the human embryonic kidney (Figure 2-4). Vehicle control, dimethyl sulfoxide (DMSO), was also included to serve as control as the compounds were dissolved in DMSO. The amount of DMSO used in the assay was limited to 1% of the total volume to ensure that it does not result in cytotoxicity of cells. Both **2g** and **2i** showed no toxicity effect on BV2 and HEK293T cells.

(A)



(B)

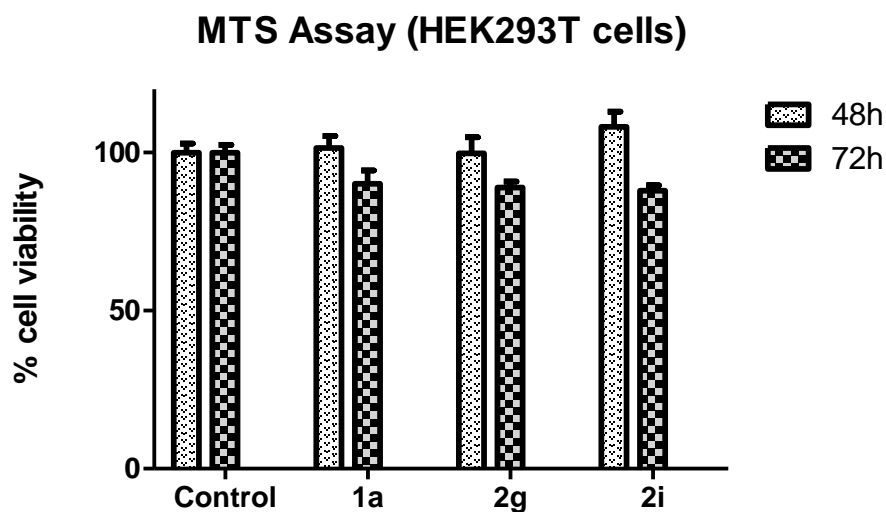


Figure 2-4: MTS assay - conducted on the **1a**, **2g** and **2i** on 2 different cell lines at different time points. Compounds were adjusted to a final concentration of 10 μ M. Results were obtained from three independent biological repeats.

2.5 Selectivity against sPLA₂

To further explore their selectivity towards cPLA₂, compounds **2g** and **2i** were evaluated for their activities against sPLA₂ at 10 μM concentration using a fluorogenic PLA₂ assay and recombinant sPLA₂ (Figure 2-5). Thioetheramide-PC, a specific inhibitor of sPLA₂ (IC₅₀ = 2 μM)¹⁸ was used as a comparison and showed a 62% reduction of sPLA₂ activity. Compound **2i** did not provide a significant change in sPLA₂ activity, indicating that it is not sPLA₂ selective. However compound **2g** showed a significant increase of sPLA₂ activity to 184%, implying that it could possibly be a sPLA₂ agonist. With the elimination of compound **2g** as a potential inhibitor of cPLA₂ through the sPLA₂ assay, compound **2i** was assessed for its ability to oppose microglia activation via cPLA₂ inhibition.

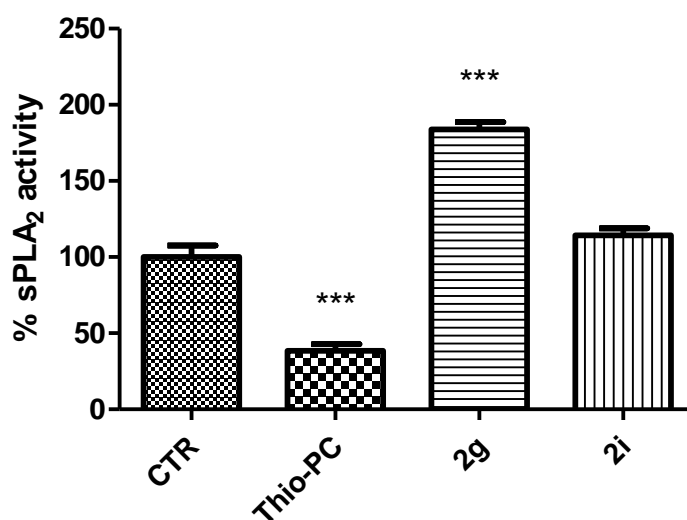
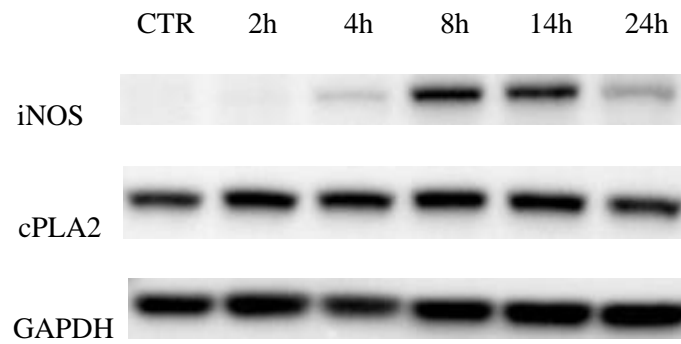


Figure 2-5: sPLA₂ activity of the respective compounds at 10 μM. Control refers to the set when only enzyme and substrate are present. Thio-PC refers to the sPLA₂ selective inhibitor thioetheramide-PC. Data analyzed by one-way ANOVA with Bonferroni's Multiple Comparison Test against the Control set indicates statistical differences between DMSO control versus Thio-PC and **2g** (***) (***P<0.01)

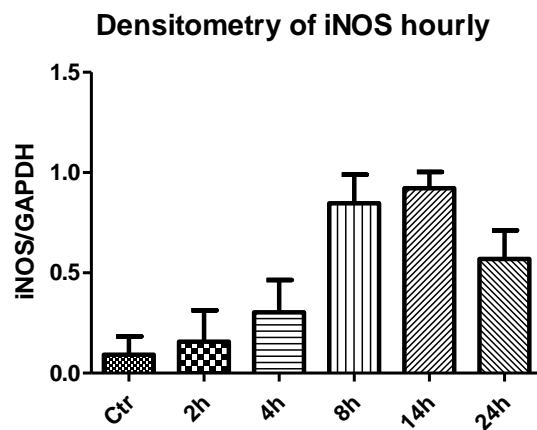
2.6 Inhibition of iNOS Production via LPS Stimulation of BV-2 Cells

It is well established that reactive oxygen species (ROS) and nitric oxide (NO), produced during microglia activation, contribute to inflammatory response and cytotoxic damage to surrounding neurons and neighboring cells.¹⁹ Recent studies have shown that BV-2 microglial cell could serve as an *in vitro* model to mimic such neuroinflammatory states when stimulated with lipopolysaccharide (LPS).²⁰ LPS activates BV-2 cells by triggering a cascade of inflammatory events which includes the production of NO. This event is characterized by the generation of the biomarker, inducible nitric oxide synthase (iNOS), as well as reactive oxygen species (ROS). Chuang *et al*²¹ have also shown that cPLA₂ is a major contributor in this pathway and inhibiting this enzyme reduces the production of the neurotoxic mediators and provide neuroprotective effects. Thus to investigate the ability of **2i** to inhibit cPLA₂ in a neuroinflammatory model, BV-2 cells were treated with LPS (2 µg/mL), incubated for different timepoints, collected and lysed for protein extraction. Western blots conducted showed that the iNOS level was highest between 8-14 h (Figure 2-6A). Densitometry analysis showed that there were no statistical differences in the iNOS levels between the 8 and 14 h timepoints (Figure 2-6B). The cPLA₂ level was also determined and found to be constant throughout the entire activation process (Figure 2-6C). Next, compound **2i** (20 µM) was incubated together with LPS in the BV-2 cells for 14 h. Under the same condition, the LPS-induced iNOS expression was significantly reduced by 50% (Figure 2-7). Varying the concentration of **2i** from 1-20 µM showed a dose-dependent decrease in the iNOS level, indicating that **2i** was capable of reducing iNOS production.

(A)



(B)



(C)

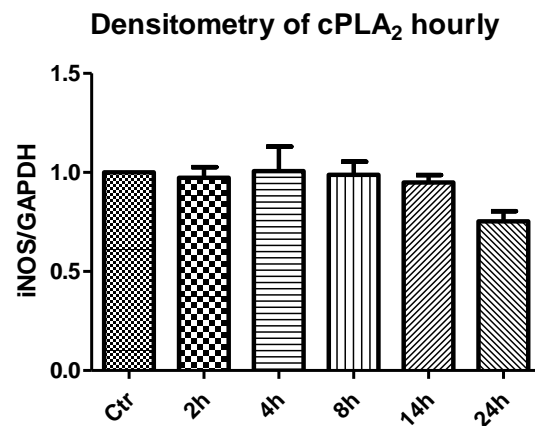
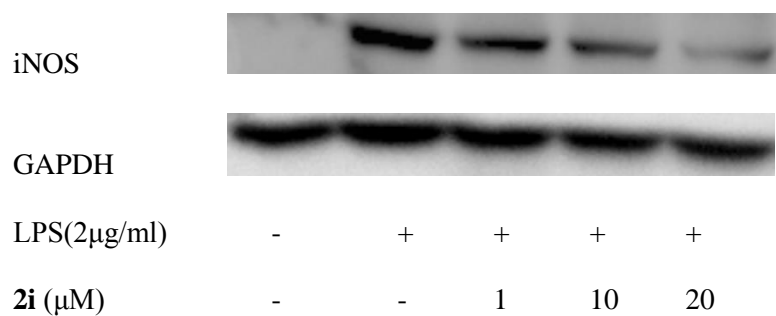
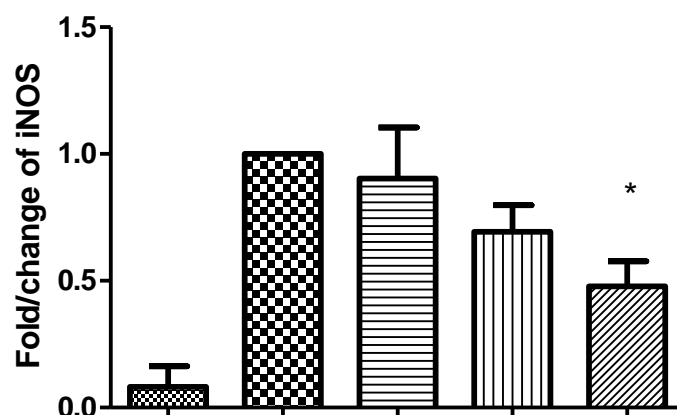


Figure 2-6: Time point changes of protein expression level in BV-2 cells after 2 $\mu\text{g}/\text{mL}$ of LPS stimulation. BV-2 cells were lysed at the respective time points, protein levels were normalized and western blot was performed (A) - Representative western blot out of 3 independent experiments showing protein bands of iNOS, cPLA₂ and GAPDH. (B) - Densitometry analysis of iNOS. (C) - Densitometry analysis of cPLA₂.

(A)



(B)



LPS (2μg/ml)	-	+	+	+	+
2i (μM)	-	-	1	10	20

Figure 2-7: Changes in protein expression level of BV-2 cells at 14 h after 2 μg/mL of LPS stimulation with different dose treatment of **2i**. BV-2 cells were lysed and protein levels were normalized and western blot was performed. (A) - Representative western blot out of 3 independent experiments showing protein bands of iNOS, cPLA₂ and GAPDH. (B) - Densitometry analysis of iNOS. . Data analyzed by one-way ANOVA with Dunnett's Multiple Comparison Test indicates statistical difference between LPS treated versus LPS treated with 20 μM of **2i** (*P<0.05)

2.7 ROS Production

CM-H2DCFDA was used as the main detection reagent for ROS for this study. Being a chloromethyl derivative of the conventional H2DCFDA, it is better retained in the cells due to the reactions of its chloromethyl group with intracellular thiol species. In addition, esterase present in the cells would convert acetate group found in CM-H2DCFDA into carboxylic acid, further retaining it in the cell. To investigate the ROS production by BV-2 cell stimulated with LPS, intracellular ROS was measured 14 h post-stimulation with CM-H2DCFDA fluorescence. A 2-fold increase in ROS was detected as compared to the control. When compound **2i** at 3 different concentrations (2-20 μM) was incubated together with LPS with the BV-2 cells for 14 h, a dose-dependent decrease in ROS was observed (Figure 2-8), indicating the compounds **2i** could reduce ROS production under neurotoxic conditions. However, residual ROS might still be observed for samples treated with compound **2i**. This could be because the activation of ROS production might not be solely due to the inflammatory pathway mechanism involving cPLA₂. It was reported in previous studies that a multitude of several other processes producing ROS may be at work.²²

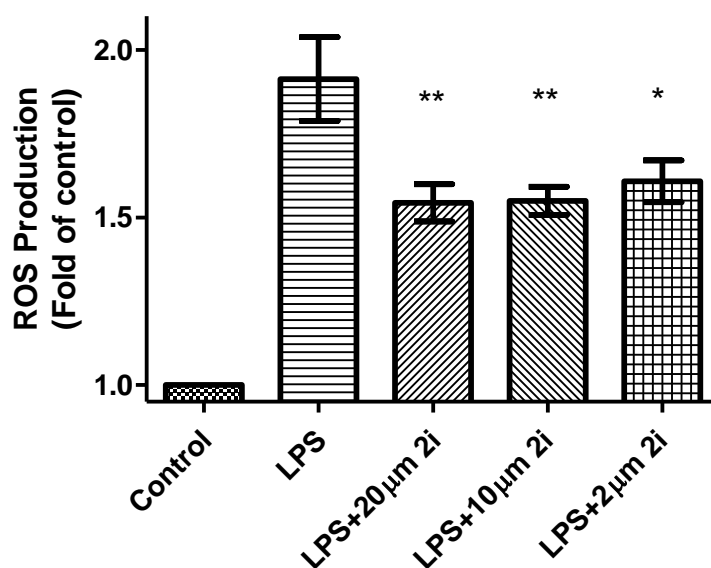


Figure 2-8: ROS production of BV-2 cells at 14 h after 2 µg/mL of LPS stimulation. Respective concentrations of **2i** was dissolved together with LPS in DMEM. Control set was added with vehicle DMSO. Data analyzed by one-way ANOVA with Bonferroni's Multiple Comparison Test indicate statistical difference when comparing between LPS-treated versus LPS-treated with respective concentration of **2i** (**P<0.01, *P<0.05).

2.8 *In vitro* Evaluation of the Blood-brain Barrier Permeation^a

^aThis part of the project was carried out in collaboration with Prof. Go Mei Lin

(Department of Pharmacy, NUS).

A major requirement for the development of a successful drug for the treatment of central nervous system (CNS) disorder is its ability to passage through the BBB to reach the therapeutic target. Hence screening for its ability to penetrate the BBB is of great importance. To explore whether compound **2i** is able to penetrate into the brain, we used a parallel artificial membrane permeation assay (PAMPA)²³ to assess its BBB permeability.

Since poor water solubility and insoluble precipitates can cause false positives in bioassays, we carried out a kinetic solubility test to determine the aqueous solubility of compound **2i** before proceeding to the PAMPA assay. Using the multiscreen filter plates from Millipore, the solubility of **2i** was found to be $65.6 \pm 5.1 \mu\text{M}$ ($28.7 \pm 2.2 \mu\text{g/mL}$) and $>100 \mu\text{M}$ ($>43.8 \mu\text{g/mL}$) at 3 h and 24 h respectively, at pH 7.4. Next, the *in vitro* permeability (P_e) of **2i** and five standard compounds (caffeine, carbamazepine, quinidine, dopamine and propranolol) were determined at 6 h and 16 h (Table 2-4). Compound **2i** was found to have much greater permeability ($12.34 \pm 1.46 \times 10^{-6} \text{ cm/s}$) at 16 h than the other compounds tested. Since earlier studies have shown that compounds with a permeability $>7.0 \times 10^{-6} \text{ cm/s}$ would be able to cross the BBB by passive permeation,²³ this implies that **2i** has the potential to across the BBB.

Table 2-4: Effective Permeabilities (P_e) of test compounds at 6 h and 16 h

Compound	P_e (pH 7.4) (10^{-6} cm/s)	$\text{Log } P_e$	P_e (pH 7.4) (10^{-6} cm/s)	$\text{Log } P_e$
Time	6 h		16 h	
2i	2.19 ± 0.22	-5.66 ± 0.04	12.34 ± 1.46	-4.91 ± 0.02
Propranolol	11.67 ± 0.29	-4.93 ± 0.01	11.26 ± 0.74	-4.95 ± 0.03
Carbamazepine	10.24 ± 0.28	-4.99 ± 0.01	9.86 ± 0.28	-5.01 ± 0.01
Quinidine	2.93 ± 0.12	-5.53 ± 0.02	4.14 ± 0.32	-5.38 ± 0.03
Caffeine	0.64 ± 0.40	-6.27 ± 0.33	2.12 ± 0.54	-5.69 ± 0.25
Dopamine	1.27 ± 0.18	-5.90 ± 0.06	0.46 ± 0.07	-6.34 ± 0.06

All values were obtained from 3 separate determinations made from a single stock solution of test compound

2.9 In-silico Docking Analysis^b

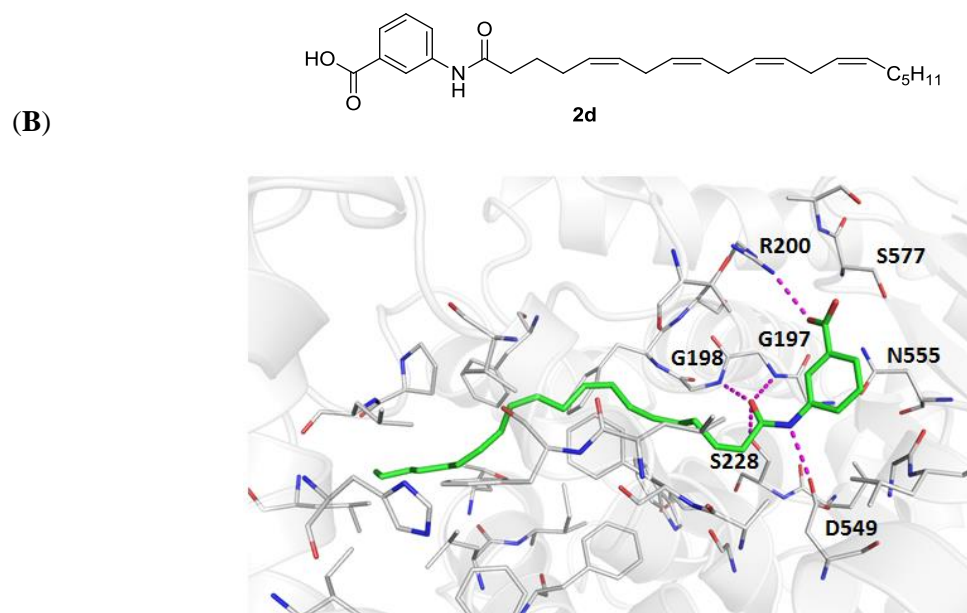
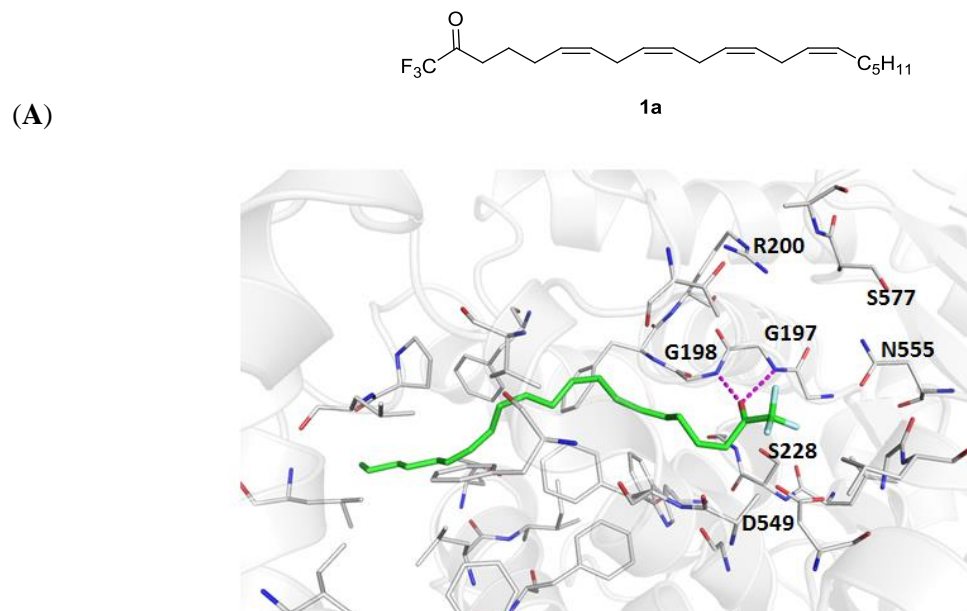
^bThis part of the project was carried out in collaboration with Prof. Chandra S Verma (Bioinformatics Institute, Agency for Science, Technology and Research (A*STAR)).

A docking study was performed to rationalize the inhibitory activities and to identify the possible binding sites of compounds **2g** and **2i** on the cPLA₂ enzyme. The crystal structure of cPLA₂ in its apo

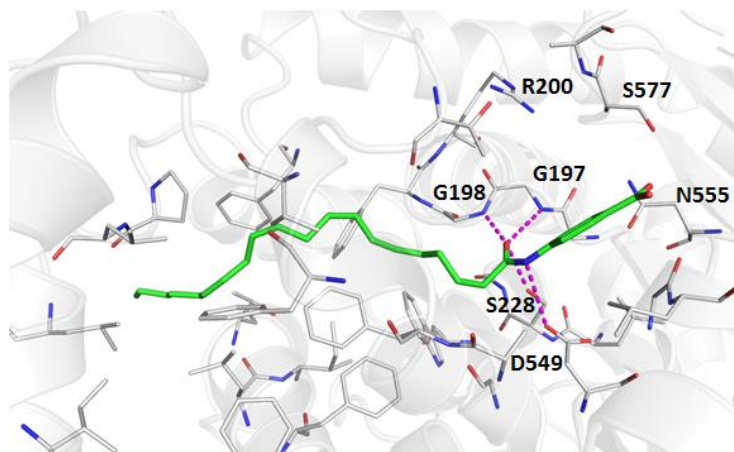
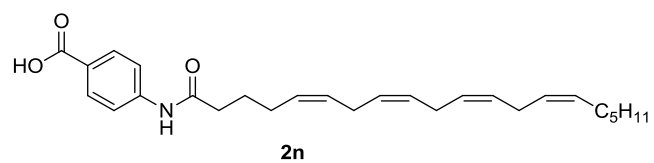
form and with a few missing regions was obtained from the protein data bank.²⁴ The missing regions were modelled and the complete structure was subjected to molecular dynamics (MD) simulations. The complete mode of cPLA₂ remained stable during simulation. The conformations sampled during the last 50 ns of the MD simulations were clustered into conformational sub-states using the Kclust programme from the MMTSB tool set, with an rmsd of 2 Å set as cutoff. The cluster centroids of the top 5 most populated clusters were used for docking calculations. The cPLA₂ binding has distinct properties - highly negatively charged at one side, slightly positive charged at the other side and a long, narrow and hydrophobic tunnel that connects both the charge ends. Since there are no co-crystal structures of cPLA₂-inhibitor available, various analogues of **1** and **2** were docked and the results obtained were compared to the experimental data to understand the binding of the designed compounds.

From the docking calculations, a binding site was defined around the catalytic important residue Ser228.¹⁶ Docking calculations with **1a** showed the compound penetrating into the deep hydrophobic pocket of cPLA₂ and the carbonyl group interacting with Ser 228 to provide a slow and tight binding via hydrogen bonds and van der Waals contacts (Figure 2-9A). Using this docking protocol, analogues of **1** and **2** were docked around this region. Docking calculations were repeated with different conformations of cPLA₂ as identified through clustering the MD simulation trajectories. Ten poses for each compound were computed and the best docking pose for each compound was chosen by ranking the computed binding energy (docking score). Analysis of the top scored solutions (lowest energy solutions) showed that all the compounds bind similarly in the active sites of cPLA₂ with (i) the electrophilic carbon of the substituted ketone in **1** or amide in **2** being in close proximity to Ser228, and (ii) Gly197/198 interacting with the carbonyl oxygen of **1** or the amide oxygen of **2**. In addition, docking analysis of **2** shows the carboxylic acid moiety interacting with the side chains of Arg200. For the aminobenzoic acid analogues **2d** and **2n**, the carboxylic acid functionality is in closer proximity to Arg200 when it is in the meta position than the para position (Figures 2-9B and 2-9C). This results in a stronger attractive interaction which could contribute to the stronger inhibitory property of **2d**. Furthermore, the interactions between the carboxylic acid moiety, Arg200 provide a

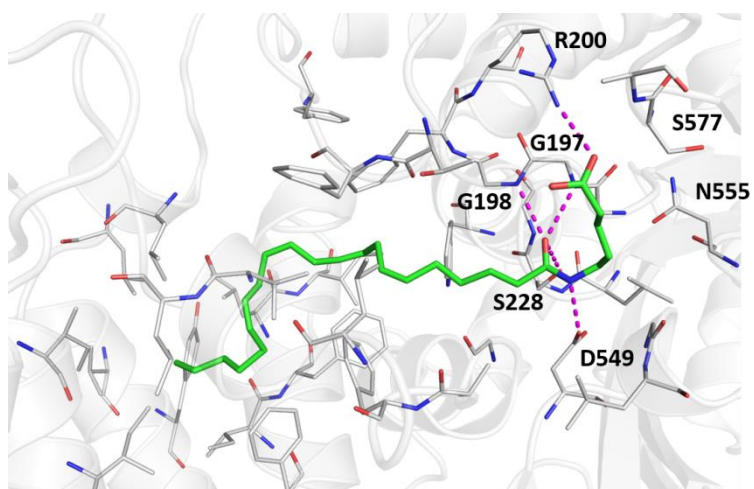
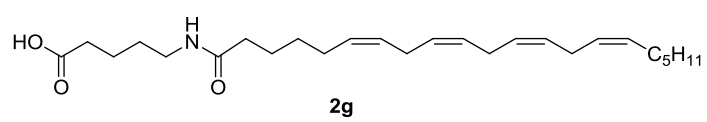
tighter binding for **2g** and **2i** than **1a** (Figures 2-9D and 2-9E). Compound **2i**, which has its carboxylic acid moiety closest to Arg200, has the most favourable interaction with cPLA₂. These results support our experimental cPLA₂ inhibition assay data which show **2i** as the strongest cPLA₂ inhibitor.



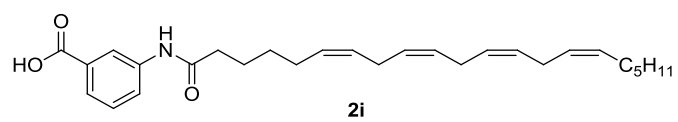
(C)



(D)



(E)



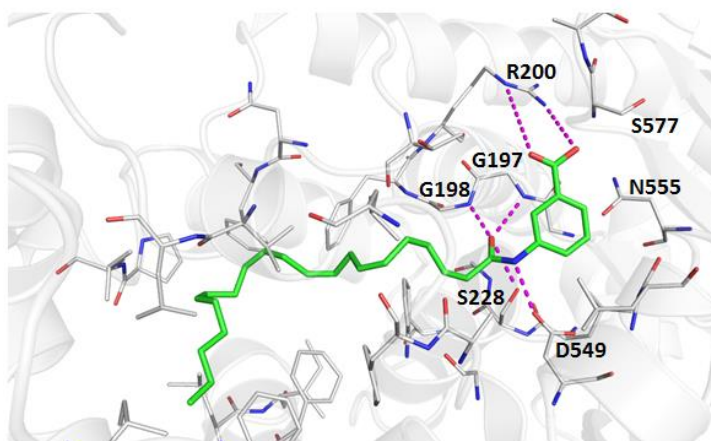


Figure 2-9: Predicted binding mode of compound **1a**, **2d**, **2g**, **2i**, **2n** docked into cPLA₂ with key interacting residues highlighted. Residues in the active sites are shown as lines; hydrogen bonds are indicated by dashed lines (magenta); protein residues involved in hydrogen bond interactions are labelled accordingly.

2.10 Conclusion

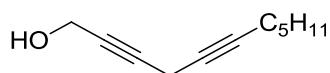
cPLA₂ activation has been shown to be critically important in the regulation of homeostatic processes and disease pathogenesis. Thus, cPLA₂ represents a potential novel therapeutic target to treat a wide range of diseases from cancer to neurodegenerative diseases such as Alzheimer's disease and multiple sclerosis.²⁵ In our efforts to develop potential drug candidates to treat neurological disorders, we have synthesized a new class of AA analogues and identified one compound **2i** that is a non-cytotoxic, cPLA₂-selective inhibitor which inhibits the enzyme more potently than AACOCF₃. Compound **2i** is also brain penetrant and able to reduce ROS and NO production in LPS-stimulated BV-2 microglial cells. Further studies are presently ongoing to develop the compound as a lead compound. Understanding its *in vivo* effect will be crucial in evaluating its clinical potential.

2.11 Experimental - Chemistry

Commercially available reagents were bought from Sigma Aldrich, Alfa Aesar, Acros and Tokyo Chemical Industry and used without purification. Solvents such as hexane, ethyl acetate, dichloromethane, and methanol were pre-distilled while others were used without further purification. Flash column chromatography was carried out on Merck silica gel 60. Thin-layer chromatography (TLC) was performed on precoated F254 silica plates from Merck and visualized with UV light. TLC were heated with potassium permanganate stain whenever necessary. Prep TLC were from Analtech Silica GEL GP (Cat 02015). ^1H and ^{13}C NMR spectra were recorded on Bruker ACF300 (300MHz) or AMX 500 (500MHz) spectrometer at 298K. All J values are reported in Hz and chemical shift (δ) reported in parts per million (ppm) relative to tetramethylsilane (TMS). Mass spectra were determined by high resolution mass spectrometry (HRMS) electron impact ionization (EI) or electrospray ionization (ESI) or atmospheric-pressure chemical ionization (APCI).

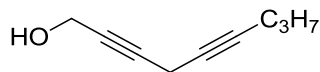
General procedure for the synthesis of 4a-e, 6a-e, 8a-e, 10a-c, 15a-d, 17a-d and 23

A mixture of the terminal alkyne (17.41 mmol), allylic halide (11.61 mmol), CuI (3.32 g, 17.41 mmol), NaI (2.61 g, 17.41 mmol) and K_2CO_3 (2.41 g, 17.41 mmol) were dissolved in DMF (36 mL) and stirred overnight at room temperature. The reaction mixture was then quenched by adding an equal volume of ethyl acetate and the organic layer was washed with saturated NH_4Cl (3 x 20 mL) and brine (3 x 20 mL). The organic layer was then dried using anhydrous MgSO_4 , concentrated and purified using flash column chromatography to afford the product as either a yellow oil or a yellow solid. The following cross-coupled products, **8a-e**, **10a-c**, **15a-d**, **17a-d** and **23**, were not isolated and were used directly for the next step of the reaction.

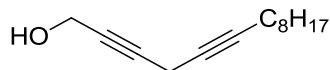


Undeca-2,5-diyne-1-ol (4a): Yellow oil, 88% yield, eluent system: 5:1 hexane-EA, ^1H NMR (500 MHz, CDCl_3) δ 4.26 (t, $J = 2.1$ Hz, 2 H), 3.23 – 3.14 (m, 2 H), 2.22 (s, 1 H), 2.15 (tt, $J = 7.1, 2.3$ Hz,

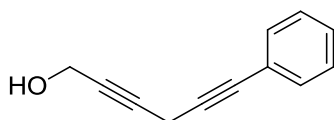
1 H), 1.56 – 1.43 (m, 1 H), 1.39 – 1.24 (m, 2 H), 0.89 (t, $J = 7.0$ Hz, 3 H); ^{13}C NMR (125 MHz, CDCl_3): δ 81.12, 80.71, 78.37, 73.23, 51.14, 31.02, 28.77, 22.15, 18.64, 13.97, 9.71.



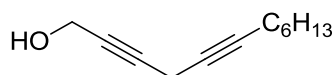
Nona-2,5-diyne-1-ol (4b): Pale yellow oil, 96% yield, eluent system: 5:1 hexane-EA, ^1H NMR (300 MHz, CDCl_3) δ 4.19 (t, $J = 2.2$ Hz, 2H), 3.13 (dd, $J = 4.6, 2.3$ Hz, 2H), 2.77 (s, 1H), 2.11 – 2.00 (m, 2H), 1.54 – 1.34 (m, 2H), 0.90 (t, $J = 7.4$ Hz, 3H). ^{13}C NMR (75 MHz, CDCl_3) δ 80.76, 80.35, 78.25, 73.38, 50.78, 21.91, 20.44, 13.27, 9.59.



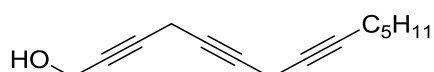
Tetradeca-2,5-diyne-1-ol (4c): Yellow oil, 74% yield, eluent system: 5:1 hexane-EA, ^1H NMR (300 MHz, CDCl_3) δ 4.17 (t, $J = 2.1$ Hz, 2 H), 3.11 (dd, $J = 4.5, 2.2$ Hz, 2 H), 2.07 (tt, $J = 7.1, 2.3$ Hz, 2 H), 1.39 (dd, $J = 14.6, 7.1$ Hz, 2 H), 1.32 – 1.08 (m, 10 H), 0.80 (t, $J = 6.7$ Hz, 3 H); ^{13}C NMR (75 MHz, CDCl_3) δ 80.85, 80.19, 78.24, 73.20, 50.60, 31.63, 28.98, 28.91, 28.70, 28.50, 22.43, 18.43, 13.83, 9.55.



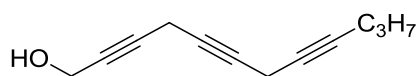
6-phenylhexa-2,5-diyne-1-ol (4d): Yellow oil, 79% yield, eluent system: 5:1 hexane-EA, ^1H NMR (500 MHz, CDCl_3) δ 7.44–7.42 (m, 2H), 7.30 – 7.29 (m, 3H), 4.29 (t, $J = 2.1$ Hz, 2H), 3.45 (t, $J = 2.1$ Hz, 2H), 1.83 (s, 1H). ^{13}C NMR (126 MHz, CDCl_3) δ 131.72(2C), 128.26(2C), 128.21, 122.93, 83.06, 80.90, 79.90, 78.92, 51.27, 10.60.



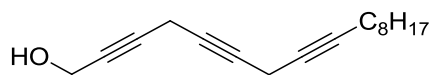
Dodeca-2,5-diyn-1-ol (4e): Pale yellow oil, 86% yield, eluent system: 5:1 hexane-EA, ^1H NMR (300 MHz, CDCl_3) δ 4.21 (t, $J = 2.2$ Hz, 2H), 3.14 (p, $J = 2.3$ Hz, 2H), 2.61 (s, 1H), 2.10 (tt, $J = 7.2, 2.4$ Hz, 2H), 1.48 – 1.34 (m, 2H), 1.33 – 1.21 (m, 6H), 0.84 (t, $J = 6.9$ Hz, 3H). ^{13}C NMR (75 MHz, CDCl_3) δ 81.05, 80.49, 78.28, 73.23, 50.89, 31.21, 28.53, 28.44, 22.41, 18.53, 13.89, 9.67.



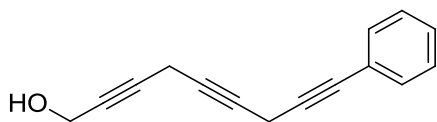
Tetradeca-2,5,8-triyn-1-ol (6a): Yellow oil, 87% yield, eluent system: 5:1 hexane-EA, ^1H NMR (300 MHz, CDCl_3) δ 4.23 (t, $J = 1.9$ Hz, 2 H), 3.27 – 3.00 (m, 4 H), 2.11 (ddd, $J = 9.2, 4.6, 2.3$ Hz, 2 H), 1.45 (dd, $J = 13.9, 6.9$ Hz, 2 H), 1.37 – 1.14 (m, 4 H), 0.87 (t, $J = 6.9$ Hz, 3 H); ^{13}C NMR (75 MHz, CDCl_3) δ 80.87, 79.71, 78.63, 75.40, 73.61, 73.44, 50.79, 30.93, 28.26, 22.06, 18.50, 13.81, 9.70, 9.55.



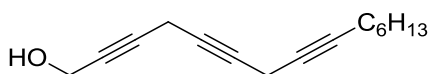
Dodeca-2,5,8-triyn-1-ol (6b): Yellow oil, 66% yield, eluent system: 5:1 hexane-EA, ^1H NMR (300 MHz, CDCl_3) δ 4.25 (t, $J = 2.1$ Hz, 2H), 3.38 – 2.95 (m, 4H), 2.13 (tt, $J = 7.1, 2.4$ Hz, 2H), 1.91 (s, 1H), 1.51 (dd, $J = 14.5, 7.2$ Hz, 2H), 0.96 (dd, $J = 9.7, 5.0$ Hz, 3H). ^{13}C NMR (75 MHz, CDCl_3) δ 80.83, 80.11, 78.64, 75.55, 73.62, 51.21, 22.09, 20.65, 13.47, 9.87, 9.71.



Heptadeca-2,5,8-triyn-1-ol (6c): Pale yellow solid, 62% yield, eluent system: 5:1 hexane-EA, ^1H NMR (300 MHz, CDCl_3) δ 4.20 (dd, $J = 7.6, 6.1$ Hz, 2 H), 3.19 – 2.97 (m, 4 H), 2.43 (s, 1 H), 2.08 (ddd, $J = 11.7, 9.3, 7.1$ Hz, 2 H), 1.51 – 1.00 (m, 12 H), 0.91 – 0.67 (m, 3 H); ^{13}C NMR (126 MHz, CDCl_3) δ 81.33, 81.08, 75.80, 75.57, 73.42, 73.13, 31.84, 29.19, 29.11, 28.90, 28.71, 22.66, 18.70, 14.69, 14.10, 10.14, 9.75.



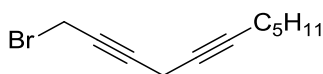
9-phenylnona-2,5,8-triyn-1-ol (6d): Yellow oil, 75% yield, eluent system: 5:1 hexane-EA, ^1H NMR (500 MHz, CDCl_3) δ 7.43 – 7.41 (m, 2H), 7.30 – 7.26 (m, 3H), 4.25 (t, $J = 2.1$ Hz, 2H), 3.39 (t, $J = 2.3$ Hz, 2H), 3.24 – 3.22 (m, 2H), 2.46 (s, 1H). ^{13}C NMR (126 MHz, CDCl_3) δ 131.73(2C), 128.27(2C), 128.18, 123.00, 83.44, 80.78, 79.84, 78.94, 74.68, 74.41, 51.07, 10.51, 9.93.



Pentadeca-2,5,8-triyn-1-ol (6e): Yellow oil, 77% yield, eluent system: 5:1 hexane-EA, ^1H NMR (500 MHz, CDCl_3) δ 4.26 (s, 2H), 3.21-3.19 (m, 2H), 3.14 (p, $J = 2.3$ Hz, 2H), 2.16 – 2.13 (m, 2H), 1.51 – 1.45 (m, 2H), 1.38 – 1.35 (m, 2H), 1.34 – 1.24 (m, 4H), 0.88 (t, $J = 7.0$ Hz, 3H). ^{13}C NMR (126 MHz, CDCl_3) δ 81.05, 80.14, 78.66, 77.26, 77.00, 76.75, 75.57, 73.61, 73.47, 51.25, 31.33, 28.66, 28.55, 22.53, 18.69, 14.03, 9.88, 9.74.

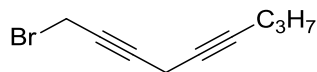
General procedure for the synthesis of 5a-e, 7a-e and 14a-d

The respective alcohol (6.124 mmol) and CBr_4 (4.062 g, 12.25 mmol) were dissolved in CH_2Cl_2 (5.2 mL) and cooled to -40°C . PPh_3 (3.213 g, 12.25 mmol) was dissolved in CH_2Cl_2 (5.2 mL) and added dropwise via a cannula to the reaction mixture, which was then stirred for 1h at -20°C . Upon completion of the reaction, hexane was added to the reaction mixture, resulting in the precipitation of PPh_3O . The resulting suspension was filtered through Celite, concentrated and purified by flash column chromatography using a 99:1 hexane-ethyl acetate eluent system to afford the respective product as either a yellow or colourless oil.

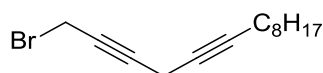


1-bromoundeca-2,5-diyne (5a): Yellow oil, 73% yield. ^1H NMR (500 MHz, CDCl_3) δ 3.91 (dd, $J = 3.0, 1.5$ Hz, 2 H), 3.20 (dd, $J = 3.2, 1.5$ Hz, 2 H), 2.17 – 2.08 (m, 2 H), 1.51 – 1.43 (m, 2 H), 1.38 –

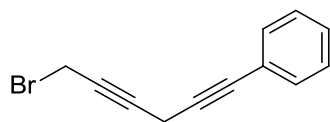
1.24 (m, 4 H), 0.86 (t, $J = 6.95$ Hz, 3H); ^{13}C NMR (125 MHz, CDCl_3) δ 82.10, 81.38, 75.23, 72.77, 31.04, 28.35, 22.20, 18.62, 14.85, 13.96, 10.07.



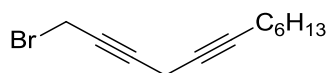
1-bromonona-2,5-diyne (5b): Yellow oil, 77% yield. ^1H NMR (500 MHz, CDCl_3) δ 3.90 (t, $J = 2.3$ Hz, 2H), 3.29 – 3.14 (m, 2H), 2.11 (tt, $J = 7.1, 2.4$ Hz, 2H), 1.59 – 1.35 (m, 2H), 0.94 (t, $J = 7.4$ Hz, 3H). ^{13}C NMR (125 MHz, CDCl_3) δ 81.98, 81.07, 75.12, 72.83, 21.96, 20.52, 14.76, 13.35, 9.95.



1-bromotetradeca-2,5-diyne (5c): Yellow oil, 60% yield. ^1H NMR (300 MHz, CDCl_3) δ 3.88 (t, $J = 2.3$ Hz, 2 H), 3.17 (dd, $J = 4.6, 2.3$ Hz, 2 H), 2.10 (tt, $J = 7.1, 2.3$ Hz, 2 H), 1.43 (dd, $J = 14.5, 7.1$ Hz, 2 H), 1.37 – 1.13 (m, 10 H), 0.84 (t, $J = 6.6$ Hz, 3 H); ^{13}C NMR (75 MHz, CDCl_3) δ 81.94, 81.22, 75.09, 72.62, 31.71, 29.07, 28.98, 28.75, 28.54, 22.54, 18.53, 14.69, 13.96, 9.94.

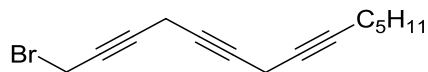


(6-bromohepta-1,4-diyne-1-yl)benzene (5d): Yellow oil, 65% yield. ^1H NMR (500 MHz, CDCl_3) δ 7.44 – 7.42 (m, 2H), 7.30 (dd, $J = 5.0, 1.8$ Hz, 3H), 3.94 (t, $J = 2.3$ Hz, 2H), 3.48 (t, $J = 2.3$ Hz, 2H). ^{13}C NMR (126 MHz, CDCl_3) δ 131.68(2C), 128.21(2C), 128.20, 122.80, 82.48, 81.07, 81.03, 75.75, 14.71, 10.80.

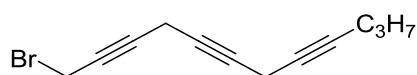


1-bromododeca-2,5-diyne (5e): Yellow oil, 69% yield. ^1H NMR (500 MHz, CDCl_3) δ 3.93 (t, $J = 2.3$ Hz, 2H), 3.23 – 3.22 (m, 2H), 2.16 (tt, $J = 7.2, 2.4$ Hz, 2H), 1.49 (dd, $J = 15.0, 7.4$ Hz, 2H), 1.40 –

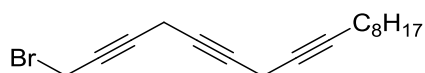
1.36 (m, 2H), 1.30 (ddd, $J = 14.4, 8.8, 2.8$ Hz, 4H), 0.90 (t, $J = 7.0$ Hz, 3H). ^{13}C NMR (126 MHz, CDCl_3) δ 82.08, 81.40, 75.17, 72.71, 31.28, 28.57, 28.49, 22.50, 18.62, 14.82, 14.00, 10.05.



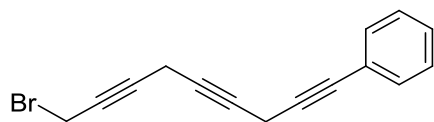
1-bromotetradeca-2,5,8-triyn-1-yl bromide (7a): Yellow oil, 71% yield. ^1H NMR (500 MHz, CDCl_3) δ 3.90 (dd, $J = 3.1, 1.4$ Hz, 2 H), 3.22 (dd, $J = 4.6, 2.2$ Hz, 2 H), 3.12 (dd, $J = 4.7, 2.4$ Hz, 2 H), 2.13 (tt, $J = 7.1, 2.3$ Hz, 2 H), 1.52 – 1.41 (m, 2 H), 1.39 – 1.25 (m, 4 H), 0.88 (t, $J = 7.0$ Hz, 3 H); ^{13}C NMR (125 MHz, CDCl_3) δ 81.34, 81.03, 75.81, 75.60, 73.49, 73.15, 31.06, 28.39, 22.20, 18.65, 14.71, 13.98, 10.12, 9.74.



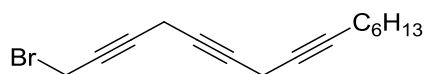
1-bromododeca-2,5,8-triyn-1-yl bromide (7b): Yellow oil, 70% yield. ^1H NMR (300 MHz, CDCl_3) δ 3.89 (t, $J = 2.3$ Hz, 2H), 3.21 (p, $J = 2.3$ Hz, 2H), 3.12 (p, $J = 2.4$ Hz, 2H), 2.11 (tt, $J = 7.1, 2.4$ Hz, 2H), 1.58 – 1.39 (m, 2H), 0.95 (t, $J = 7.4$ Hz, 3H). δ . ^{13}C NMR (75 MHz, CDCl_3) δ 81.27, 80.80, 75.72, 75.50, 73.54, 73.08, 22.05, 20.60, 14.65, 13.43, 10.06, 9.66.



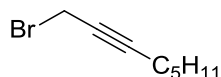
1-bromoheptadeca-2,5,8-triyn-1-yl bromide (7c): Yellow oil, 77% yield. ^1H NMR (300 MHz, CDCl_3) δ 3.90 (t, $J = 2.3$ Hz, 2 H), 3.26 – 3.17 (m, 2 H), 3.17 – 3.05 (m, 2 H), 2.13 (tt, $J = 7.1, 2.4$ Hz, 2 H), 1.46 (dd, $J = 14.6, 7.2$ Hz, 2 H), 1.40 – 1.15 (m, 10 H), 0.87 (t, $J = 6.7$ Hz, 3 H); ^{13}C NMR (126 MHz, CDCl_3) δ 81.33, 81.08, 77.30, 77.04, 76.79, 75.80, 75.57, 73.43, 73.13, 31.84, 29.19, 29.11, 28.90, 28.71, 22.66, 18.70, 14.69, 14.10, 10.14, 9.75.



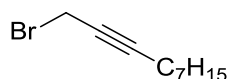
(9-bromonona-1,4,7-triyn-1-yl)benzene (7d): Yellow oil, 77% yield. ^1H NMR (500 MHz, CDCl_3) δ 7.45 – 7.43 (m, 2H), 7.30 (dd, $J = 4.4, 2.1$ Hz, 3H), 3.91 (d, $J = 2.5$ Hz, 2H), 3.40 (d, $J = 2.5$ Hz, 2H), 3.26 (d, $J = 2.5$ Hz, 2H). ^{13}C NMR (126 MHz, CDCl_3) δ 131.55(2C), 128.09(2C), 127.99, 122.83, 83.19, 81.07, 80.64, 75.60, 74.74, 73.67, 14.63, 10.36, 10.02.



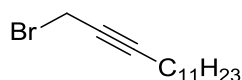
1-bromopentadeca-2,5,8-triyn-1-yl (7e): Yellow oil, 67% yield. ^1H NMR (500 MHz, CDCl_3) δ 3.90 (t, $J = 2.3$ Hz, 2H), 3.23 – 3.22 (m, 2H), 3.13 (d, $J = 3.0$ Hz, 2H), 2.16 – 2.13 (m, 2H), 1.50 – 1.45 (m, 2H), 1.39 – 1.31 (m, 2H), 1.30-1.25 (m, 4H), 0.88 (t, $J = 6.9$ Hz, 3H). ^{13}C NMR (126 MHz, CDCl_3) δ 81.14, 80.86, 75.62, 75.43, 73.28, 72.97, 31.20, 28.52, 28.41, 22.41, 18.53, 14.59, 13.89, 9.95, 9.56.



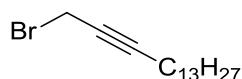
1-bromooct-2-yne (14a): Colourless oil, 97% yield. ^1H NMR (500 MHz, CDCl_3) δ 4.34 (t, $J = 2.3$ Hz, 2H), 2.65 (ddt, $J = 9.3, 4.7, 2.2$ Hz, 2H), 1.94 – 1.91 (m, 2H), 1.77 – 1.72 (m, 4H), 1.31 (t, $J = 7.1$ Hz, 5H). ^{13}C NMR (126 MHz, CDCl_3) δ 88.28, 75.23, 30.92, 27.97, 22.09, 18.87, 15.76, 13.93.



1-bromodec-2-yne (14b): Colourless oil, quantitative yield. ^1H NMR (500 MHz, CDCl_3) δ 3.94 (t, $J = 2.4$ Hz, 2 H), 2.24 (tt, $J = 7.2, 2.3$ Hz, 2 H), 1.56 – 1.46 (m, 2 H), 1.38 (dt, $J = 15.3, 6.8$ Hz, 2 H), 1.34 – 1.23 (m, 6 H), 0.90 (t, $J = 6.9$ Hz, 3 H); ^{13}C NMR (125 MHz, CDCl_3) δ 88.32, 75.27, 31.72, 28.80, 28.78, 28.39, 22.63, 18.96, 15.78, 14.09.



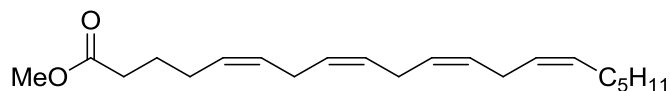
1-bromotetradec-2-yne (14c): Colourless oil, quantitative yield. ^1H NMR (500 MHz, CDCl_3) δ 3.94 (s, 2 H), 2.24 (tt, $J = 7.1, 2.3$ Hz, 2 H), 1.56 – 1.47 (m, 2 H), 1.42 – 1.34 (m, 2 H), 1.30 (d, $J = 24.3$ Hz, 14 H), 0.89 (t, $J = 6.9$ Hz, 3 H); ^{13}C NMR (125 MHz, CDCl_3) δ 88.31, 75.29, 31.94, 29.64 (2 C), 29.53, 29.38, 29.13, 28.86, 28.40, 22.72, 18.98, 15.73, 14.15.



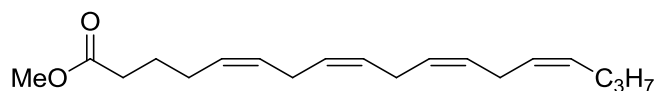
1-bromohexadec-2-yne (14d): Colourless oil, quantitative yield. ^1H NMR (300 MHz, CDCl_3) δ 3.96 (t, $J = 2.2$ Hz, 2 H), 2.27 (tt, $J = 7.0, 2.2$ Hz, 2 H), 1.62 – 1.46 (m, 2 H), 1.46 – 1.16 (m, 20 H), 0.92 (t, $J = 6.6$ Hz, 3 H); ^{13}C NMR (75 MHz, CDCl_3) δ 88.24, 75.17, 31.85, 29.61 (2 C), 29.58, 29.53, 29.42, 29.28, 29.02, 28.75, 28.30, 22.61, 18.87, 15.64, 14.03.

General procedure for the synthesis of 9a-e, 11a-c, 16a-d, 18b-d and 24

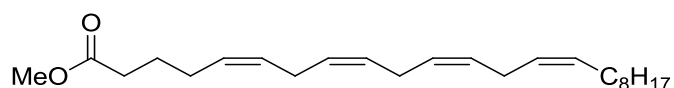
The hydrogenation procedure employed was adapted from the procedure described by Qi *et al.*^{9d} $\text{Ni}(\text{OAc})_2 \cdot 4\text{H}_2\text{O}$ (0.119 g, 0.4773 mmol) was dissolved in a 95% EtOH : 5% 2M NaOH solution and saturated with hydrogen gas through bubbling. 0.4773 mL of 1M NaBH_4 (0.4773 mmol) solution was then added to the $\text{Ni}(\text{OAc})_2 \cdot 4\text{H}_2\text{O}$ mixture under a H_2 atmosphere and stirred vigorously to yield a black suspension. Ethylenediamine (0.032 mL, 0.4773 mmol) was then added to the mixture and H_2 gas was bubbled through it for another 15 – 20 min. The alkyne (0.3182 mmol) was then dissolved in CH_2Cl_2 (2 mL) and added to the reaction mixture. The reaction mixture was stirred under positive hydrogen pressure for 2 h, quenched by passing the mixture through Celite, concentrated and purified via flash column chromatography to afford the respective product as a yellow oil. Prep TLC was utilized whenever necessary.



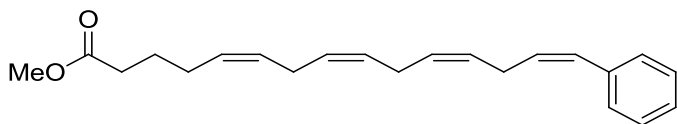
(5Z,8Z,11Z,14Z)-methyl icoso-5,8,11,14-tetraenoate (9a): Yellow oil, 58% yield (over 2 steps), eluent system: 98:2 hexane-EA, ^1H NMR (500 MHz, CDCl_3) δ 5.54 – 5.29 (m, 8 H), 3.68 (s, 3 H), 2.80 – 2.83 (m, 6 H), 2.34 (t, $J = 7.5$ Hz, 2 H), 2.13 (dd, $J = 14.0, 7.1$ Hz, 2 H), 2.07 (dd, $J = 14.2, 7.0$ Hz, 2 H), 1.79 – 1.66 (m, 2 H), 1.45 – 1.23 (m, 6 H), 0.91 (t, $J = 6.8$ Hz, 3 H); ^{13}C NMR (125 MHz, CDCl_3) δ 174.04, 130.48, 128.92, 128.87, 128.57, 128.20, 128.16, 127.86, 127.54, 51.47, 33.43, 31.52, 29.33, 27.22, 26.55, 25.64, 25.63, 25.61, 24.78, 22.58, 14.07.



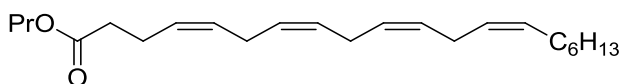
(5Z,8Z,11Z,14Z)-methyl octadeca-5,8,11,14-tetraenoate (9b): Yellow oil, 48% yield (over 2 steps), eluent system: 98:2 hexane-EA, ^1H NMR (500 MHz, CDCl_3) δ 5.67 – 5.18 (m, 8H), 3.67 (s, 3H), 2.82 (dt, $J = 17.1, 5.7$ Hz, 6H), 2.32 (t, $J = 7.5$ Hz, 2H), 2.08 (ddd, $J = 33.9, 13.9, 6.9$ Hz, 4H), 1.83 – 1.62 (m, 2H), 1.39 (dd, $J = 14.8, 7.4$ Hz, 2H), 0.91 (t, $J = 7.4$ Hz, 3H). ^{13}C NMR (75 MHz, CDCl_3) δ 174.05, 130.21, 128.92, 128.88, 128.58, 128.20, 128.17, 127.87, 127.77, 51.46, 33.45, 29.30, 26.56, 25.65, 25.63, 25.61, 24.79, 22.77, 13.77.



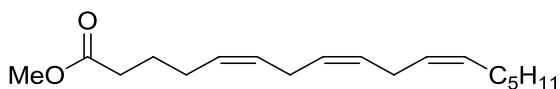
(5Z,8Z,11Z,14Z)-methyl tricoxa-5,8,11,14-tetraenoate (9c): Yellow oil, 50% yield (over 2 steps), eluent system: 98:2 hexane-EA, ^1H NMR (500 MHz, CDCl_3) δ 5.50 – 5.28 (m, 8 H), 3.69 (s, 3 H), 2.85 (dt, $J = 10.3, 5.5$ Hz, 6 H), 2.35 (dd, $J = 9.5, 5.6$ Hz, 2 H), 2.11 (ddd, $J = 28.7, 14.1, 7.0$ Hz, 6 H), 1.79 – 1.66 (m, 2 H), 1.44 – 1.24 (m, 10 H), 0.91 (t, $J = 6.7$ Hz, 1H); ^{13}C NMR (75 MHz, CDCl_3) δ 191.44, 130.37, 129.54, 128.53, 128.29, 128.04, 127.73, 127.64, 127.40, 52.03, 35.47, 33.12, 31.81, 29.56, 29.43, 29.23, 27.16, 25.91, 25.53, 25.49, 22.57, 22.07, 21.89, 13.93.



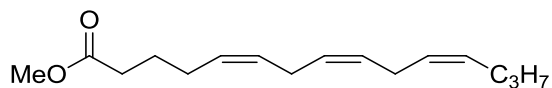
(5Z,8Z,11Z,14Z)-methyl 15-phenylpentadeca-5,8,11,14-tetraenoate (9d): Yellow oil, 46% yield (over 2 steps), eluent system: 98:2 hexane-EA, ^1H NMR (500 MHz, CDCl_3) δ 7.37 (t, $J = 7.6$ Hz, 2H), 7.32 (d, $J = 7.4$ Hz, 2H), 7.29 – 7.21 (m, 1H), 6.51 (d, $J = 11.4$ Hz, 1H), 5.69 (dd, $J = 7.4, 4.1$ Hz, 1H), 5.53 – 5.44 (m, 2H), 5.43 – 5.36 (m, 4H), 3.70 (s, 3H), 3.14 (t, $J = 6.9$ Hz, 2H), 2.84 (t, $J = 5.8$ Hz, 2H), 2.80 (t, $J = 5.2$ Hz, 2H), 2.35 (dd, $J = 9.4, 5.5$ Hz, 2H), 2.13 (dd, $J = 13.3, 6.7$ Hz, 2H), 1.77 – 1.71 (m, 2H). ^{13}C NMR (126 MHz, CDCl_3) δ 173.92, 137.31, 130.53, 129.27, 128.87, 128.77, 128.70, 128.66, 128.23, 128.106, 128.00, 127.90, 126.60, 51.63, 33.63, 26.91, 26.49, 25.67, 25.54, 24.72.



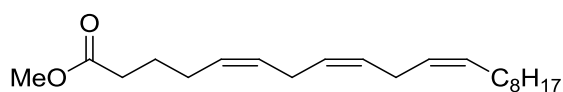
(4Z,7Z,10Z,13Z)-propyl icoso-4,7,10,13-tetraenoate (9e): Yellow oil, 37% yield (over 2 steps), eluent system: 98:2 hexane-EA, ^1H NMR (500 MHz, CDCl_3) δ 5.41 – 5.37 (m, 8H), 4.05 (dd, $J = 8.7, 4.7$ Hz, 2H), 2.86 – 2.79 (m, 6H), 2.42 – 2.37 (m, 4H), 2.09 – 2.05 (m, 2H), 1.67 (dd, $J = 14.2, 7.0$ Hz, 2H), 1.37 – 1.30 (m, 8H), 0.96 (t, $J = 7.4$ Hz, 3H), 0.90 (t, $J = 6.8$ Hz, 3H). ^{13}C NMR (126 MHz, CDCl_3) δ 173.13, 130.42, 129.20, 128.55, 128.28, 127.98, 127.94, 127.80, 127.50, 65.94, 34.22, 31.73, 29.58, 28.94, 27.22, 25.59, 25.55, 22.81, 22.60, 21.96, 14.04, 10.34.



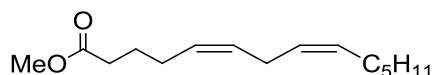
(5Z,8Z,11Z)-methyl heptadeca-5,8,11-trienoate (11a): Yellow oil, 52% yield (over 2 steps), eluent system: 98:2 hexane-EA, ^1H NMR (300 MHz, CDCl_3) δ 5.50 – 5.21 (m, 6 H), 3.65 (s, 3 H), 2.79 (t, $J = 5.4$ Hz, 2 H), 2.31 (t, $J = 7.5$ Hz, 2 H), 2.19 – 1.90 (m, 4 H), 1.69 (dt, $J = 14.4, 7.2$ Hz, 2 H), 1.29 (s, 8 H), 0.88 (t, $J = 6.4$ Hz, 3 H); ^{13}C NMR (75 MHz, CDCl_3) δ 173.93, 130.36, 128.86, 128.75, 128.39, 127.83, 127.46, 51.34, 33.33, 31.42, 29.22, 27.77, 27.12, 26.45, 25.53, 24.69, 22.47, 13.95.



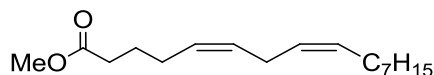
(5Z,8Z,11Z)-methyl pentadeca-5,8,11-trienoate (11b): Yellow oil, 30% yield (over 2 steps), eluent system: 98:2 hexane-EA, ^1H NMR (300 MHz, CDCl_3) δ 5.44 – 5.38 (m, 6H), 3.70 (s, 3H), 2.82 (d, $J = 5.3$ Hz, 4H), 2.36 (t, $J = 7.5$ Hz, 4H), 2.16 – 2.04 (m, 2H), 1.76 – 1.72 (m, 2H), 1.42 (dd, $J = 14.7$, 7.3 Hz, 2H), 0.94 (t, $J = 7.3$ Hz, 3H). ^{13}C NMR (75 MHz, CDCl_3) δ 174.02, 130.14, 128.90, 128.81, 128.45, 127.88, 127.73, 51.42, 33.39, 29.25, 26.50, 25.59, 25.55, 24.74, 22.73, 13.74.



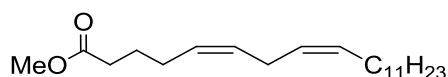
(5Z,8Z,11Z)-methyl icosadeca-5,8,11-trienoate (11c): Yellow oil, 40% yield (over 2 steps), eluent system: 98:2 hexane-EA, ^1H NMR (300 MHz, CDCl_3) δ 5.46 – 5.22 (m, 5H), 3.65 (s, 3H), 2.78 (t, $J = 5.4$ Hz, 1H), 2.31 (t, $J = 7.5$ Hz, 1H), 2.17 – 1.91 (m, 2H), 1.76 – 1.59 (m, 1H), 1.26 (s, 5H), 0.86 (t, $J = 6.3$ Hz, 1H); ^{13}C NMR (75 MHz, CDCl_3) δ 173.95, 130.38, 128.88, 128.77, 128.41, 127.84, 127.46, 51.37, 33.34, 31.83, 29.59, 29.46, 29.25 (2 C), 27.19, 26.47, 25.52 (2 C), 24.70, 22.61, 14.03.



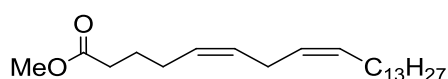
(5Z,8Z)-methyl tetradeca-5,8-dienoate (16a): Pale yellow oil, 29% yield (over 2 steps), eluent system: 98:2 hexane-EA, ^1H NMR (500 MHz, CDCl_3) δ 5.40 – 5.31 (m, 4H), 3.67 (s, 3H), 2.77 (t, $J = 6.7$ Hz, 2H), 2.33 (dd, $J = 9.8$, 5.3 Hz, 2H), 2.13 – 2.09 (m, 2H), 2.06 – 2.03 (m, 2H), 1.72 (dd, $J = 14.9$, 7.5 Hz, 2H), 1.37 – 1.30 (m, 6H), 0.89 (t, $J = 6.8$ Hz, 3H). ^{13}C NMR (126 MHz, CDCl_3) δ 174.01, 130.35, 129.21, 128.58, 127.58, 51.39, 33.40, 31.47, 29.28, 27.16, 26.49, 25.55, 24.76, 22.52, 14.00.



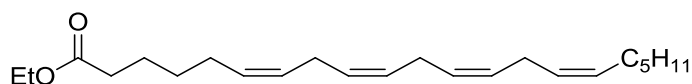
(5Z,8Z)-methyl hexadeca-5,8-dienoate (16b): Yellow oil, 40% yield (over 2 steps), eluent system: 98:2 hexane-EA, ^1H NMR (500 MHz, CDCl_3) δ 5.43 – 5.25 (m, 4 H), 3.65 (s, 3 H), 2.75 (t, $J = 6.7$ Hz, 2 H), 2.36 – 2.25 (m, 2 H), 2.09 (dd, $J = 14.2, 7.1$ Hz, 2 H), 2.03 (dd, $J = 14.0, 7.0$ Hz, 2 H), 1.73 – 1.65 (m, 2 H), 1.38 – 1.19 (m, 10 H), 0.87 (t, $J = 6.8$ Hz, 3 H); ^{13}C NMR (125 MHz, CDCl_3) δ 174.04, 130.39, 129.26, 128.61, 127.60, 51.42, 33.44, 31.86, 29.65, 29.27, 29.22, 27.24, 26.53, 25.59, 24.80, 22.66, 14.08.



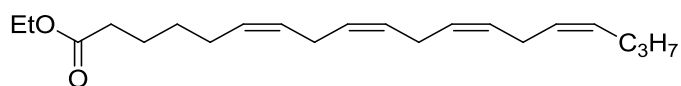
(5Z,8Z)-methyl icoso-5,8-dienoate (16c): Yellow oil, 23% yield (over 2 steps), eluent system: 98:2 hexane-EA, ^1H NMR (500 MHz, CDCl_3) δ 5.45 – 5.25 (m, 4 H), 3.68 (s, 3 H), 2.78 (t, $J = 6.8$ Hz, 2 H), 2.39 – 2.26 (m, 2 H), 2.12 (dd, $J = 14.2, 7.1$ Hz, 2 H), 2.06 (dd, $J = 14.0, 7.0$ Hz, 2 H), 1.78 – 1.62 (m, 2 H), 1.44 – 1.17 (m, 18 H), 0.90 (t, $J = 6.9$ Hz, 3 H); ^{13}C NMR (125 MHz, CDCl_3) δ 174.01, 130.38, 129.26, 128.60, 127.60, 51.40, 33.43, 31.92, 29.68 (2 C), 29.65 (2 C), 29.56, 29.35, 29.32, 27.24, 26.53, 25.59, 24.80, 22.68, 14.08.



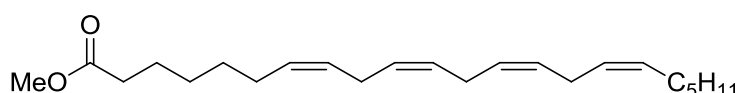
(5Z,8Z)-methyl docosa-5,8-dienoate (16d): Yellow oil, 70% yield (over 2 steps), eluent system: 98:2 hexane-EA, ^1H NMR (500 MHz, CDCl_3) δ 5.49 – 5.27 (m, 4 H), 3.68 (s, 3 H), 2.78 (t, $J = 6.8$ Hz, 2 H), 2.38 – 2.29 (m, 2 H), 2.12 (dd, $J = 14.2, 7.0$ Hz, 2 H), 2.06 (dd, $J = 14.0, 7.0$ Hz, 2 H), 1.77 – 1.67 (m, 2 H), 1.40 – 1.32 (m, 2 H), 1.30 (d, $J = 18.6$ Hz, 20 H), 0.89 (t, $J = 6.9$ Hz, 3 H); ^{13}C NMR (75 MHz, CDCl_3) δ 173.65, 130.13, 129.10, 128.41, 127.46, 51.12, 33.20, 31.82, 29.59 (2 C), 29.55 (2 C), 29.46 (2 C), 29.26 (2 C), 29.21, 27.10, 26.38, 25.45, 24.66, 22.56, 13.92.



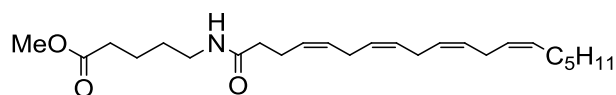
(6Z,9Z,12Z,15Z)-ethyl henicosa-6,9,12,15-tetraenoate (18b): Pale yellow liquid, 48% yield (over 2 steps), eluent system: 98:2 hexane-EA, ^1H NMR (300 MHz, CDCl_3) δ 5.41 – 5.38 (m, 7H), 4.15 (q, $J = 7.1$ Hz, 2H), 2.86 – 2.80 (m, 4H), 2.32 (t, $J = 7.5$ Hz, 2H), 2.10 – 2.05 (m, 6H), 1.70 – 1.62 (m, 2H), 1.40 – 1.33 (m, 4H), 1.32 – 1.25 (m, 7H), 0.92 (t, $J = 6.7$ Hz, 3H). ^{13}C NMR (75 MHz, CDCl_3) δ 173.56, 130.36, 129.60, 128.45, 128.22, 128.06, 128.01, 127.82, 127.49, 60.08, 34.16, 31.45, 29.26, 29.03, 27.15, 27.05, 26.80, 25.56(2C), 24.54, 22.50, 14.17, 13.99.



(6Z,9Z,12Z,15Z)-ethyl nonadeca-6,9,12,15-tetraenoate (18c): Pale yellow liquid, 55% yield (over 2 steps), eluent system: 98:2 hexane-EA, ^1H NMR (500 MHz, CDCl_3) δ 5.40 – 5.38 (m, 8H), 4.15 (q, $J = 7.1$ Hz, 2H), 2.87 – 2.84 (m, 6H), 2.32 (t, $J = 7.5$ Hz, 2H), 2.12 – 2.04 (m, 4H), 1.69 – 1.64 (m, 2H), 1.42 (ddd, $J = 11.8, 7.4, 2.1$ Hz, 4H), 1.28 (t, $J = 7.1$ Hz, 3H), 0.94 (t, $J = 7.4$ Hz, 3H). ^{13}C NMR (126 MHz, CDCl_3) δ 173.63, 130.16, 129.68, 128.54, 128.31, 128.13, 128.10, 127.90, 127.78, 60.14, 34.24, 29.29, 29.08, 26.86, 25.65, 25.63(2C), 24.60, 22.75, 14.22, 13.74.



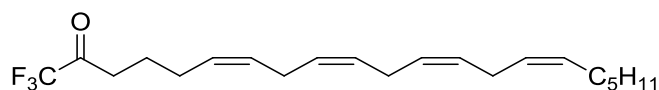
(7Z,10Z,13Z,16Z)-methyl docosa-7,10,13,16-tetraenoate (18d): Yellow liquid, 25% yield (over 2 steps), eluent system: 98:2 hexane-EA, ^1H NMR (500 MHz, CDCl_3) δ 5.39 – 5.34 (m, 8H), 3.67 (s, 3H), 2.85 – 2.77 (m, 6H), 2.31 (t, $J = 7.5$ Hz, 2H), 2.07 – 2.03 (m, 4H), 1.65 – 1.60 (m, 2H), 1.39 – 1.33 (m, 6H), 1.32 – 1.25 (m, 4H), 0.88 (dd, $J = 9.1, 4.7$ Hz, 3H). ^{13}C NMR (126 MHz, CDCl_3) δ 174.20, 130.47, 130.03, 128.53, 128.39, 128.06, 127.93, 127.90, 127.57, 51.43, 34.05, 31.52, 29.32, 29.25, 28.79, 27.22, 27.04, 25.64(3C), 24.86, 22.56, 14.04.



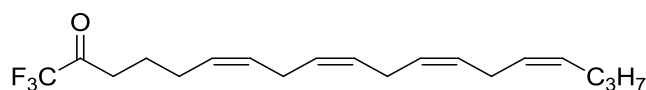
Methyl 5-((4Z,7Z,10Z,13Z)-nonadeca-4,7,10,13-tetraenamido)pentanoate (24): Pale yellow solid, 43% yield (over 2 steps), eluent system: 3:1 hexane-EA, ^1H NMR (500 MHz, DMSO) δ 7.77 – 7.76 (m, 1H), 5.35 – 5.30 (m, 7H), 3.57 (s, 3H), 3.02 – 3.01 (m, 2H), 2.82 – 2.74 (m, 4H), 2.29 (t, $J = 7.4$ Hz, 2H), 2.09 – 2.04 (m, 2H), 2.03 – 1.99 (m, 2H), 1.51 – 1.48 (m, 2H), 1.39 – 1.36 (m, 2H), 1.31 – 1.30 (m, 4H), 1.26 – 1.23 (m, 6H), 0.85 (t, $J = 6.7$ Hz, 3H). ^{13}C NMR (126 MHz, DMSO) δ 173.20, 171.19, 129.92, 128.86, 128.08, 128.03, 128.00, 127.74, 127.66, 127.50, 51.13, 37.91, 35.21, 32.88, 30.85, 28.69, 28.53, 26.57, 25.18, 25.17, 25.13, 23.16, 21.94, 21.84, 13.88. HRMS (ESI): calculated for $\text{C}_{25}\text{H}_{41}\text{NO}_3\text{Na}$ ($\text{M}+\text{Na}$) 426.2979, found 426.2995.

General procedure for the synthesis of **1a-l** and **1n-o**

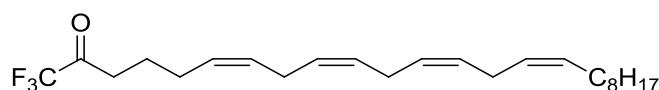
To the respective ester (0.31 mmol) was added 4M NaOH (5 mL) and the reaction mixture was microwaved for 1 h at 120°C. Upon cooling to ambient temperature, the reaction mixture was quenched with 3M HCl (7 mL) and extracted with CH_2Cl_2 (3 x 20 mL). The combined organic phase was dried with anhydrous MgSO_4 , concentrated and used for the next step of the reaction without further purification. Trifluoromethylation was performed by adapting the procedure reported by Ackermann *et al.*^{11b} The acid obtained in the aforementioned reaction (0.31 mmol) was dissolved in CH_2Cl_2 (5 mL). Thereafter, pyridine (0.26 mL, 3.20 mmol) and trifluoroacetic/chlorodifluoroacetic anhydride (0.44 mL, 3.123 mmol) were added. For compounds **1a-h**, the reaction mixture was stirred for 2 h. For compound **1n** and **1o**, the mixture was stirred overnight. Upon completion of reaction (based on TLC), the reaction was quenched by shaking the mixture with saturated NaHCO_3 (50 mL) and subsequently extracting the aqueous layer with ethyl acetate (3 x 20 mL). The combined organic layer was then dried with anhydrous MgSO_4 , concentrated and purified using flash column chromatography with a 98:2 hexane-ethyl acetate eluent system to afford the respective product as a yellow oil.



(6Z,9Z,12Z,15Z)-1,1,1-trifluorohenicosa-6,9,12,15-tetraen-2-one (1a): Yellow oil, 48% yield (over 2 steps). ^1H NMR (500 MHz, CDCl_3) δ 5.57 – 5.26 (m, 8H), 2.97 – 2.79 (m, 6 H), 2.74 (t, $J = 7.1$ Hz, 2 H), 2.23 – 2.12 (m, 2 H), 2.08 (dd, $J = 13.9, 6.8$ Hz, 2 H), 1.80 (dd, $J = 14.4, 7.2$ Hz, 2 H), 1.50 – 1.22 (m, 6 H), 0.94 (t, $J = 6.95$ Hz, 3 H); ^{13}C NMR (125 MHz, CDCl_3) δ 191.42 (d, $J = 3.5$ Hz)^a, 130.51, 129.65, 128.65, 128.41, 128.16, 127.85, 127.76, 127.50, 115.57 (q, $J = 291$ Hz), 35.60, 31.51, 29.31, 27.21, 26.01, 25.63, 25.59 (2 C), 22.55, 22.17, 14.02. HRMS (APCI): calculated for $\text{C}_{21}\text{H}_{32}\text{F}_3\text{O}$ (M+1) 357.2400, found 357.2384.

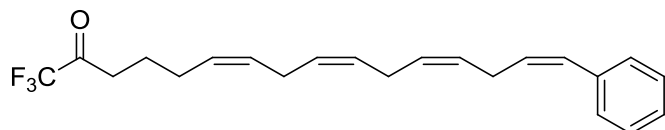


(6Z,9Z,12Z,15Z)-1,1,1-trifluorononadeca-6,9,12,15-tetraen-2-one (1b): Yellow oil, 46% yield (over 2 steps). ^1H NMR (500 MHz, CDCl_3) δ 5.44 – 5.34 (m, 8H), 2.82 (dt, $J = 19.3, 6.7$ Hz, 6H), 2.72 (t, $J = 7.2$ Hz, 2H), 2.14 (dd, $J = 14.4, 7.2$ Hz, 2H), 2.05 (dd, $J = 14.1, 7.1$ Hz, 2H), 1.76 (dd, $J = 14.4, 7.2$ Hz, 2H), 1.38 (dt, $J = 14.6, 7.3$ Hz, 2H), 0.91 (t, $J = 7.3$ Hz, 3H). ^{13}C NMR (126 MHz, CDCl_3) δ 191.40 (d, $J = 34.7$ Hz, 1H), 130.24, 129.67, 128.66, 128.43, 128.16, 127.86, 127.78, 127.75, 115.59 (q, $J = 292.1$ Hz, 2H), 35.62, 29.31, 26.04, 25.66, 25.65, 25.61, 22.76, 22.20, 13.74. HRMS (APCI): calculated for $\text{C}_{19}\text{H}_{28}\text{F}_3\text{O}$ (M+1): 329.2087; found 329.2086.

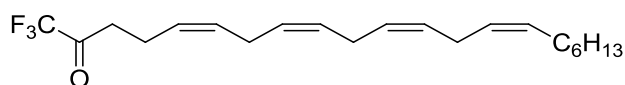


(6Z,9Z,12Z,15Z)-1,1,1-trifluorotetracososa-6,9,12,15-tetraen-2-one (1c): Yellow oil, 52% yield (over 2 steps). ^1H NMR (300 MHz, CDCl_3) δ 5.44 (tt, $J = 8.5, 4.6$ Hz, 8H), 2.96 – 2.67 (m, 6 H), 2.14 (ddd, $J = 19.1, 13.4, 6.5$ Hz, 6 H), 1.81 (dt, $J = 13.6, 6.8$ Hz, 2 H), 1.48 – 1.21 (m, 14 H), 0.93 (t, $J = 8.9, 3$ H); ^{13}C NMR (75 MHz, CDCl_3) δ 191.21 (d, $J = 34$ Hz), 130.37, 129.54, 128.53, 128.29, 128.04, 127.73, 127.64, 127.40, 115.49 (q, $J = 291$ Hz), 35.47, 31.81, 29.56 (2 C), 29.43, 29.23, 27.16, 25.91

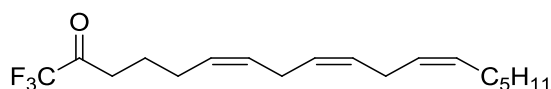
(2 C), 25.53, 25.49, 22.57, 22.07, 13.93. HRMS (APCI): calculated for $C_{24}H_{38}F_3O$ (M+1) 399.2869, found 399.2855.



(6Z,9Z,12Z,15Z)-1,1,1-trifluoro-16-phenylhexadeca-6,9,12,15-tetraen-2-one (1d): Yellow oil, 60% yield (over 2 steps). 1H NMR (500 MHz, $CDCl_3$) δ 7.30 (ddt, $J = 14.5, 7.4, 4.4$ Hz, 5H), 6.49 (d, $J = 11.5$ Hz, 1H), 5.68 (dt, $J = 11.5, 7.5$ Hz, 1H), 5.53 – 5.34 (m, 6H), 3.12 (t, $J = 6.9$ Hz, 2H), 2.83 – 2.71 (m, 6H), 2.14 (dd, $J = 14.5, 7.3$ Hz, 3H), 1.78 (dd, $J = 14.5, 7.2$ Hz, 2H). ^{13}C NMR (126 MHz, $CDCl_3$) δ 191.56 (d, $J = 35$ Hz), 137.35, 130.54, 129.57, 129.32, 128.71, 128.63, 128.15, 128.11, 127.96, 126.64, 115.55 (d, $J = 292$ Hz), 35.58, 26.95, 25.97, 25.71, 25.56, 22.13. HRMS (APCI): calculated for $C_{22}H_{26}F_3O$ (M+1): 363.1930; found 363.1917.

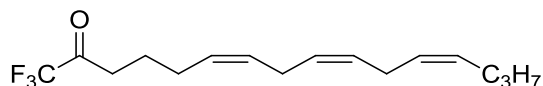


(5Z,8Z,11Z,14Z)-1,1,1-trifluorohenicosa-5,8,11,14-tetraen-2-one (1e): Yellow oil, 64% yield (over 2 steps). 1H NMR (500 MHz, $CDCl_3$) δ 5.41 – 5.32 (m, 8H), 2.85 – 2.77 (m, 6H), 2.47-2.43 (m, 2H), 2.05 (dd, $J = 13.8, 6.9$ Hz, 2H), 1.30– 1.26 (m, 10H), 0.88 (t, $J = 6.7$ Hz, 3H). ^{13}C NMR (126 MHz, $CDCl_3$) δ 190.85 (d, $J = 35.2$ Hz), 130.53, 130.36, 128.70, 128.62, 127.69, 127.61, 127.48, 126.47, 115.52 (d, $J = 292.1$ Hz), 36.33, 31.76, 29.60, 28.98, 27.26, 25.64, 25.63, 25.57, 22.63, 20.30, 14.06. HRMS (APCI): calculated for $C_{21}H_{32}F_3O$ (M+1): 357.2400; found 357.2411.



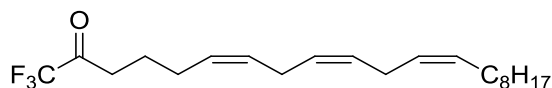
(6Z,9Z,12Z)-1,1,1-trifluorooctadeca-6,9,12-trien-2-one (1f): Yellow oil, 58% yield (over 2 steps). 1H NMR (500 MHz, $CDCl_3$) δ 5.53 – 5.26 (m, 6 H), 2.83 (s, 2 H), 2.75 (t, $J = 7.1$ Hz, 2 H), 2.15 (dt, $J = 12.5, 7.3$ Hz, 2 H), 2.13 – 1.98 (m, 2 H), 1.85 – 1.72 (m, 2 H), 1.42 – 1.22 (m, 8 H), 0.92 (t, $J = 6.7$

Hz, 3 H); ^{13}C NMR (125 MHz, CDCl_3) δ 191.44 (d, $J = 35$ Hz)^c, 130.53, 129.71, 128.69, 128.10, 127.61, 127.44, 115.57 (d, $J = 291$ Hz)^d, 35.59, 31.52, 29.32, 27.22, 25.99, 25.63, 25.58, 22.57, 22.14, 14.03. HRMS (APCI): calculated for $\text{C}_{18}\text{H}_{26}\text{F}_3\text{O}$ (M-1): 315.1941; found 315.1939.



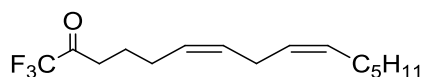
(6Z,9Z,12Z)-1,1,1-trifluorohexadeca-6,9,12-trien-2-one (1g): Yellow oil, 51% yield (over 2 steps).

^1H NMR (500 MHz, CDCl_3) δ 5.44 – 5.33 (m, 6H), 2.82 – 2.79 (m, 4H), 2.72 (t, $J = 7.2$ Hz, 2H), 2.14 (dd, $J = 14.6, 7.3$ Hz, 2H), 2.04 (dd, $J = 14.0, 7.6$ Hz, 2H), 1.76 (m, 2H), 1.39 (dd, $J = 14.7, 7.4$ Hz, 2H), 0.91 (t, $J = 7.4$ Hz, 3H). ^{13}C NMR (126 MHz, CDCl_3) δ 191.41 (q, $J = 34.9$ Hz, 4H), 130.23, 129.71, 128.68, 128.08, 127.65, 127.61, 115.56 (d, $J = 292.3$ Hz, 1H), 35.59, 29.29, 25.99, 25.63, 25.57, 22.73, 22.15, 13.71. HRMS (APCI): calculated for $\text{C}_{16}\text{H}_{24}\text{F}_3\text{O}$ (M+1): 289.1774; found 289.1780.



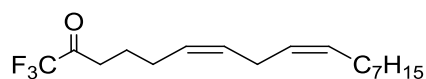
(6Z,9Z,12Z)-1,1,1-trifluorohenicosa-6,9,12-trien-2-one (1h): Yellow oil, 60% yield (over 2 steps).

^1H NMR (300 MHz, CDCl_3) δ 5.49 – 5.24 (m, 6 H), 2.76 (dt, $J = 14.2, 6.7$ Hz, 6 H), 2.10 (ddd, $J = 20.1, 13.7, 6.8$ Hz, 4 H), 1.84 – 1.68 (m, 2 H), 1.19 – 1.41 (s, 12 H), 0.88 (t, $J = 5.8$ Hz, 3 H); ^{13}C NMR (125 MHz, CDCl_3) δ 191.43 (d, $J = 35$ Hz)^e, 130.54, 129.72, 128.70, 128.10, 127.61, 127.43, 115.57 (d, $J = 290$ Hz)^f, 35.60, 31.90, 29.65, 29.52, 29.33, 29.31, 27.26, 26.00, 25.63, 25.59, 22.68, 22.15, 14.08. HRMS (APCI): calculated for $\text{C}_{21}\text{H}_{32}\text{F}_3\text{O}$ (M-1): 357.2411; found 357.2399.

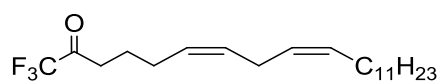


(6Z,9Z)-1,1,1-trifluoropentadeca-6,9-dien-2-one (1i): Pale yellow oil, 75% yield (over 2 steps). ^1H NMR (500 MHz, CDCl_3) δ 5.46 – 5.37 (m, 2H), 5.36 – 5.28 (m, 2H), 2.76 (t, $J = 7.2$ Hz, 2H), 2.72 (t, $J = 7.2$ Hz, 2H), 2.14 (dd, $J = 14.5, 7.2$ Hz, 2H), 2.04 (dd, $J = 14.2, 7.1$ Hz, 2H), 1.76 (p, $J = 7.2$ Hz,

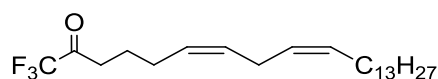
2H), 1.34 – 1.28 (m, 6H), 0.89 (t, $J = 6.7$ Hz, 3H). ^{13}C NMR (126 MHz, CDCl_3) δ 191.45 (d, $J = 34.8$ Hz), 130.61, 130.03, 127.86, 127.30, 115.57 (q, $J = 292.3$ Hz), 35.61, 31.50, 29.28, 27.21, 25.99, 25.58, 22.54, 22.18, 14.01. HRMS (APCI): calculated for $\text{C}_{15}\text{H}_{22}\text{F}_3\text{O}$ (M-1): 275.1628; found 275.1620.



(6Z,9Z)-1,1,1-trifluoroheptadeca-6,9-dien-2-one (1j): Yellow oil, 65% yield (over 2 steps). ^1H NMR (500 MHz, CDCl_3) δ 5.52 – 5.28 (m, 4 H), 2.79 (t, $J = 7.2$ Hz, 2 H), 2.74 (t, $J = 7.2$ Hz, 2 H), 2.16 (dd, $J = 14.3, 7.1$ Hz, 2 H), 2.07 (dd, $J = 14.1, 7.0$ Hz, 2 H), 1.79 (p, $J = 7.2$ Hz, 2 H), 1.42 – 1.22 (m, 10 H), 0.91 (t, $J = 6.9$ Hz, 3 H); ^{13}C NMR (125 MHz, CDCl_3) δ 191.43 (d, $J = 34$ Hz)^h, 130.59, 130.02, 127.85, 127.28, 115.57 (q, $J = 291$ Hz), 35.58, 31.86, 29.62, 29.27, 29.21, 27.25, 25.98, 25.58, 22.65, 22.15, 14.04. HRMS (APCI): calculated for $\text{C}_{17}\text{H}_{26}\text{F}_3\text{O}$ (M-1) 303.1941, found 303.1946.

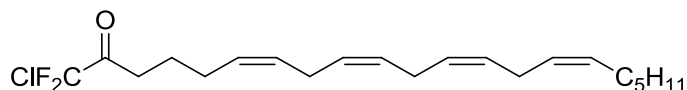


(6Z,9Z)-1,1,1-triflorohenicosa-6,9-dien-2-one (1k): Yellow oil, 47% yield (over 2 steps). ^1H NMR (500 MHz, CDCl_3) δ 5.53 – 5.24 (m, 4 H), 2.77 (dt, $J = 21.1, 7.1$ Hz, 4 H), 2.16 (dd, $J = 14.2, 7.0$ Hz, 2 H), 2.07 (dd, $J = 13.9, 6.9$ Hz, 2 H), 1.83 – 1.73 (m, 2 H), 1.29 (s, 18 H), 0.91 (t, $J = 6.9$ Hz, 3 H); ^{13}C NMR (125 MHz, CDCl_3) δ 191.45 (q, $J = 36$ Hz), 130.62, 130.04, 127.86, 127.28, 115.57 (d, $J = 290$ Hz)ⁱ, 35.60, 31.92, 29.68 (2 C), 29.64 (2 C), 29.56, 29.35, 29.32, 27.26, 25.99, 25.59, 22.69, 22.17, 14.08. HRMS (APCI): calculated for $\text{C}_{21}\text{H}_{34}\text{F}_3\text{O}$ (M-1) 359.2567, found 359.2551.

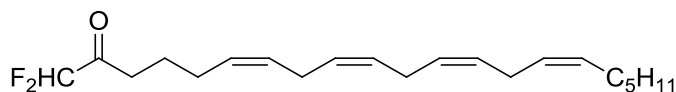


(6Z,9Z)-1,1,1-trifluorotricosa-6,9-dien-2-one (1l): Yellow oil, 46% yield (over 2 steps). ^1H NMR (500 MHz, CDCl_3) δ 5.50 – 5.39 (m, 2 H), 5.39 – 5.29 (m, 2 H), 2.79 (t, $J = 7.2$ Hz, 2 H), 2.74 (t, $J = 7.2$ Hz, 2 H), 2.17 (q, $J = 7.1$ Hz, 2 H), 2.11 – 1.99 (m, 2 H), 1.79 (p, $J = 7.2$ Hz, 2 H), 1.37 (dd, $J = 15.9, 8.5$ Hz, 2 H), 1.31 (d, $J = 19.3$ Hz, 20 H), 0.91 (t, $J = 6.9$ Hz, 3 H); ^{13}C NMR (125 MHz, CDCl_3)

δ 191.42 (q, $J = 34$ Hz), 130.61, 130.04, 127.85, 127.28, 115.58 (q, $J = 291$ Hz), 35.60, 31.92, 29.69 (2 C), 29.67, 29.65, 29.64, 29.63, 29.55, 29.36, 29.32, 27.26, 25.99, 25.59, 22.68, 22.18, 14.07; HRMS (APCI): calculated for $C_{23}H_{38}F_3O$ (M-1) 387.2880, found 387.2863.



(6Z,9Z,12Z,15Z)-1-chloro-1,1-difluorohenicosa-6,9,12,15-tetraen-2-one (1n): Yellow oil, 46% yield. 1H NMR (500 MHz, $CDCl_3$) δ 5.54 – 5.27 (m, 6 H), 2.91 – 2.71 (m, 6 H), 2.16 (dt, $J = 12.1$, 7.5 Hz, 2 H), 2.08 (dd, $J = 14.1$, 7.0 Hz, 2 H), 1.87 – 1.73 (m, 2 H), 1.44 – 1.22 (m, 8 H), 0.88 (t, $J = 3.15$ Hz, 3 H); ^{13}C NMR (125 MHz, $CDCl_3$) δ 191.77, 130.52, 129.58, 128.64, 128.39, 128.25, 127.90, 127.78, 127.51, 119.81 (t, $J = 304$ Hz), 34.36, 31.53, 29.32, 27.23, 26.07, 25.64 (2 C), 25.62, 22.68, 22.57, 14.05. HRMS (APCI): calculated for $C_{21}H_{32}ClF_2O$ (M+1) 373.2104, found 373.2117.

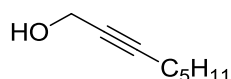


(6Z,9Z,12Z,15Z)-1,1-difluorohenicosa-6,9,12,15-tetraen-2-one (1o): Yellow oil, 51% yield. 1H NMR (500 MHz, $CDCl_3$) δ 5.67 (t, $J = 54.1$ Hz, 1H), 5.40 – 5.34 (m, 8H), 2.85 – 2.80 (m, 6H), 2.69 – 2.66 (m, 2H), 2.15 – 2.12 (m, 2H), 2.06 (t, $J = 7.2$ Hz, 2H), 1.77 – 1.71 (m, 2H), 1.37 – 1.33 (m, 2H), 1.31 – 1.28 (m, 4H), 0.89 (dd, $J = 9.0$, 4.7 Hz, 5H). ^{13}C NMR (75 MHz, $CDCl_3$) δ ^{13}C NMR (126 MHz, $CDCl_3$) δ 199.72, 130.50, 130.36, 129.31, 128.61, 128.54, 128.32, 127.97, 127.80, 127.51, 109.87 (t, $J = 253.0$ Hz, 1H), 35.29, 31.51, 29.31, 29.27, 27.21, 26.22, 25.62, 25.60, 22.56, 22.13, 14.04. HRMS (APCI): calculated for $C_{21}H_{31}F_2O$ (M-1) 337.2348; found 337.2345.

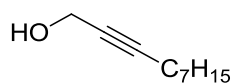
General procedure for the alkylation of 12a-d to form 13a-d.

The general procedure employed was adapted from the protocol reported by Yoshida *et al.*²⁶ To propargyl alcohol (116 μ L, 2.00 mmol) in THF (3 mL) was added HMPA (1.1 mL, 6.3 mmol) and the reaction mixture was cooled to $-78^\circ C$. 2 M n-Butyllithium in cyclohexane (2.0 mL, 4 mmol) was then added to the mixture via a cannula and stirred vigorously. Thereafter, the respective compound **12**

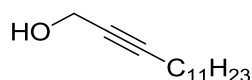
(1.00 mmol) dissolved in THF (3 mL) was transferred to the reaction mixture via a cannula. The temperature of the reaction mixture was allowed to rise to room temperature while stirring overnight. Upon completion of the reaction (based on TLC), the reaction was quenched by adding an equivalent amount of ethyl acetate and washed with saturated NH_4Cl (3 x 20 mL). The organic layer was dried with MgSO_4 , concentrated and purified by flash column chromatography using a 5:1 hexane-ethyl acetate eluent system to afford the respective product as a colourless oil or white solid.



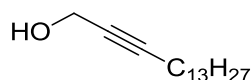
Oct-2-yn-1-ol (13a): Colourless oil, 47% yield. ^1H NMR (300 MHz, CDCl_3) δ 4.24 (t, $J = 2.1$ Hz, 2H), 2.61 (s, 1H), 2.20 (tt, $J = 7.2, 2.1$ Hz, 2H), 1.49 (dd, $J = 14.2, 7.1$ Hz, 2H), 1.41 – 1.28 (m, 4H), 0.89 (t, $J = 6.5$ Hz, 3H). ^{13}C NMR (75 MHz, CDCl_3) δ 86.21, 78.21, 50.98, 30.90, 28.18, 22.05, 18.55, 13.78.



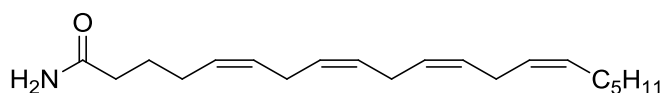
Dec-2-yn-1-ol (13b): Colourless oil, 86% yield. ^1H NMR (500 MHz, CDCl_3) δ 4.21 (s, 2 H), 2.29 (s, 1 H), 2.24 (tt, $J = 7.2, 1.9$ Hz, 2 H), 1.52 – 1.41 (m, 2 H), 1.37 (dt, $J = 15.3, 6.8$ Hz, 2 H), 1.32 – 1.19 (m, 6 H), 0.85 (t, $J = 6.9$ Hz, 3 H); ^{13}C NMR (125 MHz, CDCl_3) δ 87.06, 78.96, 51.81, 32.34, 29.45, 29.41, 29.25, 23.23, 19.34, 14.64.



Tetradec-2-yn-1-ol (13c): White solid, 50% yield. ^1H NMR (500 MHz, CDCl_3) δ 4.22 (s, 2 H), 2.19 (ddd, $J = 9.2, 4.8, 2.0$ Hz, 2 H), 1.89 (d, $J = 5.4$ Hz, 1 H), 1.49 (dt, $J = 14.4, 7.1$ Hz, 2 H), 1.38 – 1.16 (m, 16 H), 0.86 (t, $J = 6.7$ Hz, 3H); ^{13}C NMR (125 MHz, CDCl_3) δ 86.55, 78.31, 51.31, 31.90, 29.62, 29.61, 29.51, 29.33, 29.14, 28.88, 28.62, 22.67, 18.72, 14.07.



Hexadec-2-yn-1-ol (13d): White solid, 65% yield. ^1H NMR (500 MHz, CDCl_3) δ 4.22 (s, 2 H), 2.18 (tt, $J = 7.1, 2.1$ Hz, 2 H), 2.09 (s, 1 H), 1.48 (dt, $J = 15.1, 7.1$ Hz, 2 H), 1.40 – 1.17 (m, 20 H), 0.86 (t, $J = 7.0$ Hz, 3 H); ^{13}C NMR (125 MHz, CDCl_3) δ 86.49, 78.31, 51.26, 31.92, 29.68, 29.66 (2 C), 29.65, 29.53, 29.35, 29.16, 28.89, 28.63, 22.68, 18.72, 14.08.

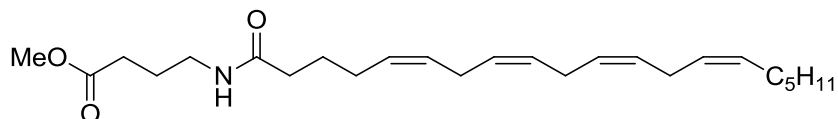


Synthesis of (5Z,8Z,11Z,14Z)-icosa-5,8,11,14-tetraenamide (1m): To **9a** (67 mg, 0.21 mmol) was added 7M ammonia in methanol (0.30 mL, 2.1 mmol) and 7% magnesium methoxide in methanol (0.32 mL, 0.21 mmol) and the reaction mixture was heated in a sealed tube at 80°C overnight. When no starting material was observed, the mixture was cooled to room temperature, quenched with saturated NaCl and extracted with ethyl acetate. The combined organic phase was dried with MgSO_4 , concentrated and purified by flash column chromatography with a gradient elution of 3:1 hexane-ethyl acetate to 1:2 hexane-ethyl acetate system to afford **1m** as a yellow oil (20 mg, 31%). ^1H NMR (500 MHz, CDCl_3) δ 5.62 (s, 1H), 5.42 – 5.29 (m, 8H), 2.84 – 2.79 (m, 4H), 2.24 – 2.21 (m, 2H), 2.16 – 2.11 (m, 2H), 2.05 (dd, $J = 14.0, 6.9$ Hz, 2H), 1.72 (dt, $J = 14.7, 7.4$ Hz, 2H), 1.35 – 1.27 (m, 8H), 0.88 (dd, $J = 8.8, 4.7$ Hz, 3H). ^{13}C NMR (75 MHz, CDCl_3) δ 175.33, 130.53, 129.01, 128.90, 128.62, 128.26, 128.16, 127.86, 127.53, 35.16, 31.51, 29.31, 27.22, 26.58, 25.65(2C), 25.26, 22.56, 14.09, 14.05. HRMS (APCI): calculated for $\text{C}_{20}\text{H}_{34}\text{NO}(\text{M}+1)$ 304.2640; found 304.2645.

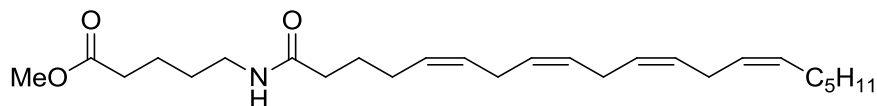
General procedure amidation reaction to afford 2l-m, 20a-k and 22

EDC.HCl (0.029 g, 0.15 mmol), HOBT (0.017 g, 0.120 mmol), the respective compound **19** (30.6 mg, 0.100 mmol), TEA (15 μL , 0.105 mmol) and the respective amine (0.105 mmol) were dissolved in DMF (1.5 mL) and stirred for 3 h at room temperature. Upon the completion of reaction, the reaction was quenched by adding an equivalent amount of ethyl acetate and washed with aqueous NaHCO_3 (3

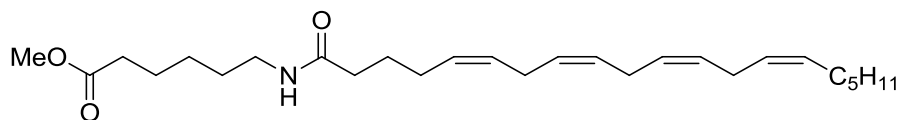
x 20 mL) and brine (3 x 20 mL). The organic layer was dried with MgSO₄ and purified by flash column chromatography.



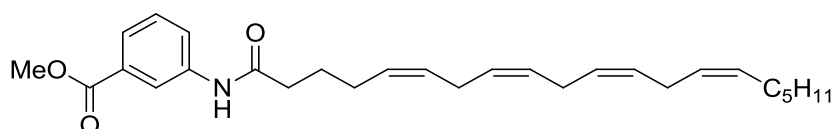
Methyl 4-((5Z,8Z,11Z,14Z)-icosa-5,8,11,14-tetraenamido)butanoate (20a): Pale yellow liquid, 53% yield (over 2 steps), eluent system: 3:1 hexane-ethyl acetate. ¹H NMR (300 MHz, CDCl₃) δ 5.73 (s, 1 H), 5.36 – 5.09 (m, 8 H), 3.66 (s, 3 H), 3.27 (dd, *J* = 12.9, 6.7 Hz, 2 H), 2.92 – 2.64 (m, 6 H), 2.34 (q, *J* = 7.0 Hz, 2 H), 2.09 (ddd, *J* = 22.9, 14.5, 7.1 Hz, 6 H), 1.88 – 1.76 (m, 4 H), 1.69 (dt, *J* = 14.5, 7.4 Hz, 2 H), 1.41 – 1.17 (m, 8 H), 0.87 (t, *J* = 6.7 Hz, 3 H); ¹³C NMR (75 MHz, CDCl₃) δ 173.87, 172.93, 130.47, 129.07, 128.70, 128.55, 128.18, 128.12, 127.81, 127.47, 51.68, 38.86, 36.05, 31.44, 29.72, 29.66, 29.27, 27.17, 26.63, 25.58 (2 C), 25.47, 24.61, 22.52, 14.02. HRMS (ESI): calculated for C₂₅H₄₀NO₃ (M-1) 402.3008, found 402.3019



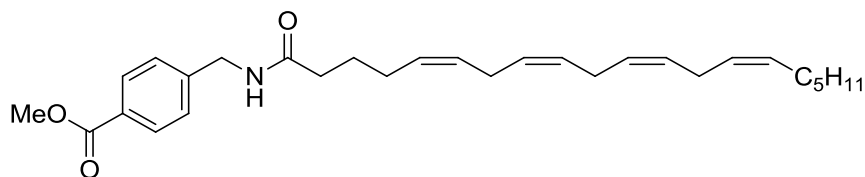
Methyl 5-((5Z,8Z,11Z,14Z)-icosa-5,8,11,14-tetraenamido)pentanoate (20b): Pale yellow liquid, 53% yield (over 2 steps), eluent system: 3:1 hexane-ethyl acetate. ¹H NMR (500 MHz, CDCl₃) δ 5.62 (s, 1 H), 5.47 – 5.29 (m, 8 H), 3.68 (s, 3 H), 3.27 (q, *J* = 6.6 Hz, 2 H), 2.89 – 2.77 (m, 4 H), 2.35 (t, *J* = 7.2 Hz, 2 H), 2.21 – 2.16 (m, 2 H), 2.12 (dd, *J* = 13.4, 6.9 Hz, 2 H), 2.07 (dd, *J* = 14.2, 7.1 Hz, 2 H), 1.73 (dt, *J* = 14.9, 7.5 Hz, 2 H), 1.66 (dd, *J* = 15.2, 7.4 Hz, 2 H), 1.59 – 1.51 (m, 2 H), 1.42 – 1.25 (m, 8 H), 0.90 (t, *J* = 6.7 Hz, 3 H); ¹³C NMR (125 MHz, CDCl₃) δ 173.91, 172.85, 130.51, 129.15, 128.73, 128.60, 128.22, 128.18, 127.86, 127.53, 51.55, 38.96, 36.12, 33.46, 31.50, 29.31, 29.06, 27.21, 26.69 (2 C), 25.63, 25.56 (2 C), 22.55, 22.05, 14.04. HRMS (ESI): calculated for C₂₆H₄₃NO₃ (M-1) 416.3031, found 416.3039



Methyl 6-((5Z,8Z,11Z,14Z)-icosa-5,8,11,14-tetraenamido)hexanoate (20c): Pale yellow liquid, 62% yield (over 2 steps), eluent system: 3:1 hexane- ethyl acetate. ^1H NMR (300 MHz, CDCl_3) δ 5.55 (s, 1H), 5.38 – 5.34 (m, 8H), 3.65 (s, 3H), 3.23 (dd, $J = 13.1, 6.8$ Hz, 2H), 2.82 – 2.80 (m, 6H), 2.30 (t, $J = 7.4$ Hz, 2H), 2.14 (dd, $J = 14.9, 7.0$ Hz, 2H), 2.08 – 2.00 (m, 4H), 1.66 (ddt, $J = 22.6, 15.1, 7.6$ Hz, 4H), 1.52 – 1.47 (m, 2H), 1.36 – 1.28 (m, 8H), 0.87 (t, $J = 6.7$ Hz, 3H). ^{13}C NMR (75 MHz, CDCl_3) δ 174.00, 172.78, 130.46, 129.10, 128.66, 128.54, 128.17, 128.12, 127.80, 127.46, 51.45, 39.14, 36.10, 33.77, 31.45, 29.25(2C), 27.16, 26.63, 26.28, 25.58(3C), 25.52, 24.38, 22.51, 14.01. HRMS (ESI): calculated for $\text{C}_{27}\text{H}_{45}\text{NO}_3\text{Na}$ ($M+23$) 454.3292, found 454.3302.

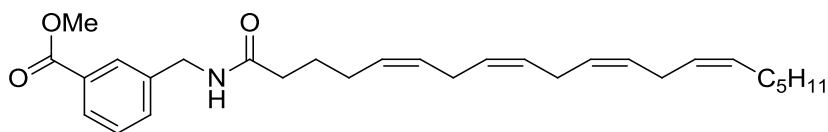


Methyl 3-((5Z,8Z,11Z,14Z)-icosa-5,8,11,14-tetraenamido)benzoate (20d): white solid, 55% yield (over 2 steps), eluent system: 3:1 hexane- ethyl acetate. ^1H NMR (300 MHz, DMSO) δ 10.10 (s, 1H), 8.28 (s, 1H), 7.85 (d, $J = 7.3$ Hz, 1H), 7.62 (d, $J = 7.7$ Hz, 1H), 7.43 (t, $J = 7.9$ Hz, 1H), 5.39 – 5.29 (m, 8H), 3.85 (s, 3H), 2.76 (dd, $J = 11.3, 5.4$ Hz, 5H), 2.34 (t, $J = 7.4$ Hz, 2H), 2.11 – 2.07 (m, 2H), 2.01 – 1.97 (m, 3H), 1.69 – 1.64 (m, 2H), 1.29 – 1.24 (m, 6H), 0.83 (t, $J = 5.6$ Hz, 3H). ^{13}C NMR (75 MHz, DMSO) δ 171.27, 166.09, 139.68, 129.99, 129.87, 129.26, 129.04, 128.19, 128.05, 127.94, 127.75, 127.60, 127.45, 123.48, 123.36, 119.46, 52.09, 35.71, 30.87, 28.70, 26.58, 26.17, 25.16(3C), 24.87, 21.96, 13.87. HRMS (ESI): calculated for $\text{C}_{28}\text{H}_{37}\text{NO}_3$ ($M-1$) 436.2857, found 436.2848.

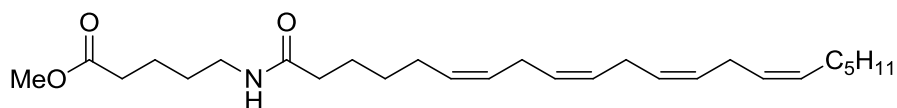


Methyl 4-((5Z,8Z,11Z,14Z)-icosa-5,8,11,14-tetraenamidomethyl)benzoate (20e): Pale yellow solid, 76% yield (over 2 steps), eluent system: 3:1 hexane-ethyl acetate. ^1H NMR (300 MHz, CDCl_3) δ 7.96

(d, $J = 8.3$ Hz, 2H), 7.31 (d, $J = 8.1$ Hz, 2H), 6.02 (s, 1H), 5.39 – 5.34 (m, 8H), 4.46 (d, $J = 5.8$ Hz, 2H), 3.89 (s, 3H), 2.82 – 2.78 (m, 6H), 2.30 – 2.21 (m, 2H), 2.15 – 2.11 (m, 2H), 2.08 – 2.01 (m, 2H), 1.75 (dd, $J = 14.8, 7.4$ Hz, 2H), 1.34 – 1.29 (m, 6H), 0.87 (t, $J = 6.7$ Hz, 3H). ^{13}C NMR (75 MHz, CDCl_3) δ 172.85, 166.74, 143.61, 130.46, 129.89(2C), 129.19, 128.93, 128.78, 128.53, 128.18, 128.04, 127.76, 127.44(3C), 52.04, 43.08, 35.89, 31.43, 29.24, 27.14, 26.59, 25.56(3C), 25.42, 22.49, 14.00, HRMS (ESI): calculated for $\text{C}_{29}\text{H}_{40}\text{NO}_3$ (M-1) 450.3014, found 450.3015.

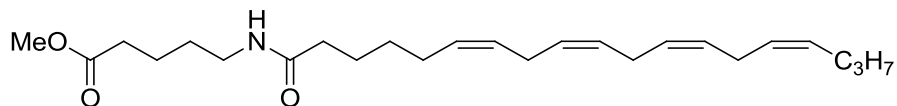


Methyl 3-((5Z,8Z,11Z,14Z)-icosa-5,8,11,14-tetraenamido)methyl)benzoate (20f): Pale yellow solid, 70% yield (over 2 steps), eluent system: 3:1 hexane-ethyl acetate. ^1H NMR (300 MHz, CDCl_3) δ 7.97 (dd, $J = 6.8, 1.4$ Hz, 2H), 7.52 (d, $J = 7.8$ Hz, 1H), 7.43 (dd, $J = 11.2, 4.8$ Hz, 1H), 5.91 (s, 1H), 5.42 – 5.38 (m, 8H), 4.52 (d, $J = 5.8$ Hz, 2H), 3.94 (s, 3H), 2.86 – 2.82 (m, 6H), 2.30 – 2.25 (m, 2H), 2.15 – 2.13 (m, 2H), 2.09 – 2.07 (m, 2H), 1.84 – 1.76 (m, 2H), 1.34 – 1.29 (m, 6H), 0.92 (t, $J = 6.8$ Hz, 3H). ^{13}C NMR (75 MHz, CDCl_3) δ 172.79, 166.82, 138.81, 132.34(2C), 130.50, 129.01, 128.79(2C), 128.66(2C), 128.57, 128.21, 128.10, 127.81, 127.48, 52.15, 43.12, 35.97, 31.47, 29.28, 27.18, 26.63, 25.59(2C), 25.44, 22.53, 14.03. HRMS (ESI): calculated for $\text{C}_{29}\text{H}_{40}\text{NO}_3$ (M-1) 450.3014, found 450.3018.

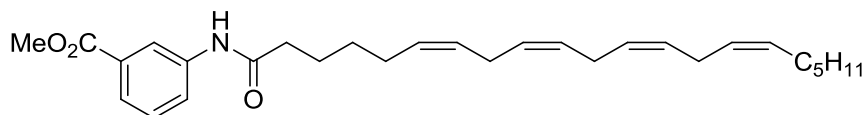


Methyl 5-((6Z,9Z,12Z,15Z)-heneicosa-6,9,12,15-tetraenamido)pentanoate (20g): Pale yellow solid, 45% yield (over 2 steps), eluent system: 3:1 hexane-ethyl acetate. ^1H NMR (500 MHz, CDCl_3) δ 5.67 (s, 1H), 5.35 – 5.34 (m, 8H), 3.65 (s, 3H), 3.23 (dd, $J = 12.9, 6.6$ Hz, 2H), 2.82 – 2.75 (m, 4H), 2.33 (t, $J = 7.2$ Hz, 2H), 2.15 (t, $J = 7.5$ Hz, 2H), 2.07 – 2.01 (m, 6H), 1.65 – 1.61 (m, 4H), 1.53 – 1.50 (m, 2H), 1.39 – 1.35 (m, 2H), 1.34 – 1.27 (m, 6H), 0.87 (t, $J = 6.7$ Hz, 3H). ^{13}C NMR (126 MHz, CDCl_3) δ 173.93, 173.00, 130.43, 129.67, 128.49, 128.25, 128.04(2C), 127.83, 127.48, 51.53, 38.89, 36.63,

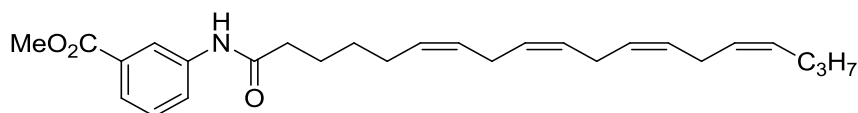
33.39, 31.45, 29.26, 29.19, 28.96, 27.15, 27.07, 26.87, 25.57(2C), 25.34, 22.51, 21.97, 14.01. HRMS (ESI): calculated for $C_{27}H_{44}NO_3$ (M-1) 430.3316, found 4330.3317.



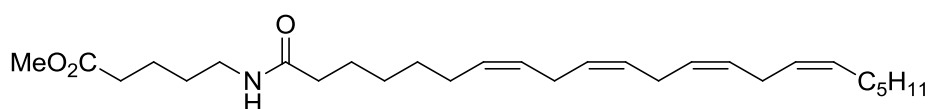
Methyl 5-((6Z,9Z,12Z,15Z)-nonadeca-6,9,12,15-tetraenamido)pentanoate (20h): Pale yellow solid, 41% yield (over 2 steps), eluent system: 3:1 hexane-ethyl acetate. 1H NMR (500 MHz, $CDCl_3$) δ 5.55 (s, 1H), 5.37 – 5.36 (m, 8H), 3.67 (s, 3H), 3.25 (dd, $J = 12.8, 6.6$ Hz, 2H), 2.83 – 2.80 (m, 6H), 2.34 (t, $J = 7.2$ Hz, 2H), 2.16 (t, $J = 7.6$ Hz, 2H), 2.09 – 2.03 (m, 4H), 1.67 – 1.64 (m, 4H), 1.53 (t, $J = 7.0$ Hz, 2H), 1.38 (q, $J = 7.6$ Hz, 4H), 0.91 (t, $J = 7.4$ Hz, 3H). ^{13}C NMR (126 MHz, $CDCl_3$) δ 173.92, 172.97, 130.20, 129.73, 128.56, 128.33, 128.12(2C), 127.90, 127.78, 51.53, 38.96, 36.70, 33.46, 29.30, 29.25, 29.05, 26.93, 25.65, 25.64(2C), 25.38, 22.75, 22.04, 13.75. HRMS (ESI): calculated for $C_{25}H_{41}NNaO_3$ (M+Na) 426.2979, found 426.2989.



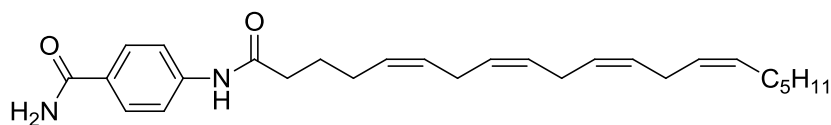
Methyl 3-((6Z,9Z,12Z,15Z)-henicosa-6,9,12,15-tetraenamido)benzoate (20i): Pale yellow solid, 66% yield (over 2 steps), eluent system: 3:1 hexane-ethyl acetate. 1H NMR (300 MHz, $CDCl_3$) δ 8.01 (s, 1H), 7.90 (d, $J = 7.9$ Hz, 1H), 7.77 (d, $J = 7.8$ Hz, 1H), 7.39 (t, $J = 7.9$ Hz, 1H), 5.41 – 5.35 (m, 8H), 3.91 (s, 3H), 2.86 – 2.79 (m, 6H), 2.38 (t, $J = 7.5$ Hz, 2H), 2.13 – 2.02 (m, 4H), 1.76 (dt, $J = 15.3, 7.5$ Hz, 2H), 1.44 (dt, $J = 15.0, 7.5$ Hz, 2H), 1.30 – 1.26 (m, 6H), 0.88 (t, $J = 6.6$ Hz, 3H). ^{13}C NMR (75 MHz, $CDCl_3$) δ 171.28, 166.69, 138.12, 130.91, 130.51, 129.57, 129.17, 128.59, 128.30, 128.27, 128.17, 127.88, 127.54, 125.25, 124.28, 120.53, 52.19, 37.59, 31.51, 29.31, 29.16, 27.22, 26.92, 25.65(3C), 25.09, 22.55, 14.03. HRMS (ESI): calculated for $C_{29}H_{41}NO_3Na$ (M+Na) 474.2979, found 474.2982.



Methyl 3-((6Z,9Z,12Z,15Z)-nonadeca-6,9,12,15-tetraenamido)benzoate (20j): Pale yellow solid, 50% (over 2 steps), eluent system: 3:1 hexane-ethyl acetate. ^1H NMR (500 MHz, CDCl_3) δ 8.01 (s, 1H), 7.91 (d, $J = 7.6$ Hz, 1H), 7.77 (d, $J = 7.7$ Hz, 1H), 7.39 (t, $J = 7.9$ Hz, 1H), 7.29 (s, 1H), 5.39 – 5.37 (m, 8H), 3.91 (s, 3H), 2.84 – 2.81 (m, 6H), 2.38 (t, $J = 7.5$ Hz, 2H), 2.12 (dd, $J = 13.2, 7.1$ Hz, 2H), 2.04 (dd, $J = 14.1, 6.9$ Hz, 2H), 1.76 (dt, $J = 15.3, 7.6$ Hz, 2H), 1.47 (dt, $J = 15.1, 7.5$ Hz, 2H), 1.38 (dd, $J = 14.7, 7.3$ Hz, 2H), 0.91 (t, $J = 7.3$ Hz, 3H). ^{13}C NMR (126 MHz, CDCl_3) δ 171.25, 166.67, 138.16, 130.94, 130.22, 129.57, 129.16, 128.59, 128.32, 128.28, 128.18, 127.89, 127.78, 125.24, 124.30, 120.57, 52.17, 37.59, 29.31, 29.17, 26.92, 25.67(3C), 25.10, 22.76, 13.75. HRMS (ESI): calculated for $\text{C}_{27}\text{H}_{36}\text{NO}_3$ (M-1) 422.2701, found 422.2707.

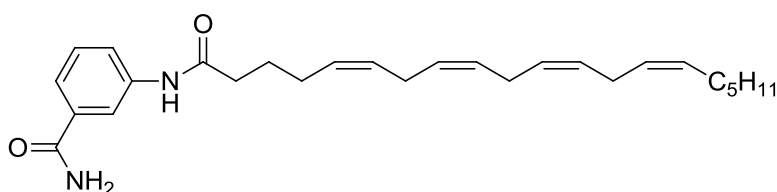


Methyl 5-((7Z,10Z,13Z,16Z)-docosa-7,10,13,16-tetraenamido)pentanoate (20k): Pale yellow solid, 47% yield (over 2 steps), eluent system: 3:1 hexane-ethyl acetate. ^1H NMR (500 MHz, CDCl_3) δ 5.56 (s, 1H), 5.38 – 5.36 (m, 8H), 3.67 (s, 3H), 3.28 – 3.25 (m, 2H), 2.84 – 2.80 (m, 6H), 2.34 (t, $J = 7.2$ Hz, 2H), 2.18 – 2.15 (m, 2H), 2.07 – 2.03 (m, 6H), 1.55 – 1.52 (m, 2H), 1.34 – 1.32 (m, 6H), 1.32 – 1.29 (dd, $J = 11.6, 8.3$ Hz, 4H), 1.28 – 1.27 (m, 2H), 0.89 (t, $J = 6.9$ Hz, 3H). ^{13}C NMR (126 MHz, CDCl_3) δ 178.76, 173.96, 130.49, 130.07, 128.55, 128.39, 128.07, 127.93, 127.88, 127.56, 51.57, 38.99, 36.77, 33.45, 31.51, 29.68, 29.34, 29.32, 29.04, 28.95, 27.22, 27.07, 25.67, 25.64, 25.56, 22.56, 22.02, 14.04, HRMS (ESI): calculated for $\text{C}_{28}\text{H}_{37}\text{NO}_3$ (M-1) 445.3556, found 445.3559.

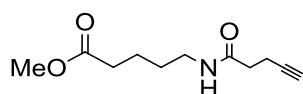


4-((5Z,8Z,11Z,14Z)-icosa-5,8,11,14-tetraenamido)benzamide (2l): Pale yellow solid, 34% yield, eluent system: 1:3 hexane-ethyl acetate. ^1H NMR (500 MHz, MeOD) δ 7.86 (d, $J = 8.8$ Hz, 2 H), 7.70

(d, $J = 8.8$ Hz, 2 H), 5.60 – 5.22 (m, 8 H), 2.98 – 2.71 (m, 6 H), 2.44 (t, $J = 7.4$ Hz, 2 H), 2.20 (dd, $J = 13.2$, 7.3 Hz, 2 H), 2.07 (dd, $J = 13.7$, 6.6 Hz, 2 H), 1.80 (dt, $J = 14.8$, 7.4 Hz, 2 H), 1.55 – 1.20 (m, 8 H), 0.91 (t, $J = 7.0$ Hz, 3 H)¹; ¹³C NMR (126 MHz, CDCl₃) δ 173.22, 170.39, 142.07, 129.80, 128.72, 128.51, 128.37, 128.24 (2 C), 128.04, 127.76, 127.74 (2 C), 127.46, 127.35, 118.82, 35.96, 31.24, 29.04, 26.77, 26.25, 25.19, 25.16, 25.15 (2 C), 22.21, 13.02; HRMS (ESI): calculated for C₂₇H₃₇N₂O₂ (M-1) 421.2861, found 421.2873.



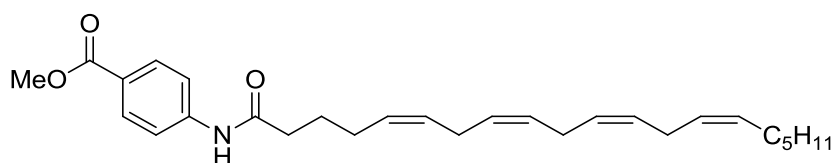
3-((5Z,8Z,11Z,14Z)-icosa-5,8,11,14-tetraenamido)benzamide (2m): white solid, 74% yield (over 2 steps), eluent system: 1:3 hexane-ethyl acetate. ¹H NMR (300 MHz, DMSO) δ 8.04 (s, 1H), 7.76 (dd, $J = 8.1$, 1.0 Hz, 1H), 7.57 (d, $J = 7.8$ Hz, 1H), 7.38 (t, $J = 7.9$ Hz, 1H), 5.42 – 5.38 (m, 2H), 5.37 – 5.31 (m, 5H), 2.85 – 2.77 (m, 4H), 2.41 (t, $J = 7.5$, 2H), 2.19 – 2.15 (m, 2H), 2.06 – 2.02 (m, 3H), 1.80 – 1.75 (m, 2H), 1.37 – 1.30 (m, 6H), 0.89 (t, $J = 6.8$ Hz, 3H). ¹³C NMR (75 MHz, DMSO) δ 174.45, 172.11, 140.23, 135.76, 131.17, 130.12, 129.96, 129.88, 129.43, 129.15, 129.13, 128.86, 128.74, 124.37, 123.95, 120.38, 37.29, 32.65, 30.46, 28.18, 27.68, 26.65, 26.58, 26.54(2C), 23.63, 14.46. HRMS (ESI): calculated for C₂₇H₃₇N₂O₂ (M-1) 421.2861, found 421.2842



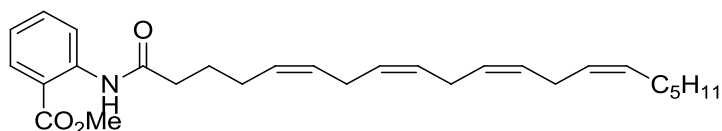
Methyl 5-(pent-4-ynamido)pentanoate (22): Colourless liquid, 96% yield, eluent system: 4:1 hexane-ethyl acetate. ¹H NMR (500 MHz, CDCl₃) δ 6.69 (s, 1H), 3.50 (s, 3H), 3.10 (dd, $J = 13.0$, 6.6 Hz, 2H), 2.35 (dd, $J = 8.8$, 4.7 Hz, 2H), 2.26 (t, $J = 7.2$ Hz, 2H), 2.18 (t, $J = 7.3$ Hz, 2H), 1.88 (t, $J = 2.6$ Hz, 1H), 1.51 (t, $J = 7.4$ Hz, 2H), 1.39 (t, $J = 7.0$ Hz, 2H). ¹³C NMR (126 MHz, CDCl₃) δ 173.53, 170.93, 82.66, 68.90, 51.13, 38.65, 34.79, 33.13, 28.52, 21.75, 14.57. HRMS (ESI): calculated for C₁₁H₁₆NO₃ (M-1) 210.1136, found 210.1135.

General procedure for the synthesis of **20n** and **20o**

The respective acid **19** (0.12mmol) was dissolved in CH₂Cl₂ (3.5 mL). Thereafter, oxalyl chloride (21.2 μL, 0.243 mmol) and 1 drop of DMF were added and the mixture was stirred for 1 h at room temperature. After which, the solvent was removed. The formed acid chloride was re-dissolved in DMF (1.0 mL), the respective amine (0.243 mmol) and TEA (34 μL, 0.243 mmol) and stirred at room temperature overnight. When no more starting material was observed, ethyl acetate and brine were added to quench the reaction. The mixture was extracted with ethyl acetate (3x 20mL) and the organic layer was combined, dried with MgSO₄ and purified by flash column chromatography

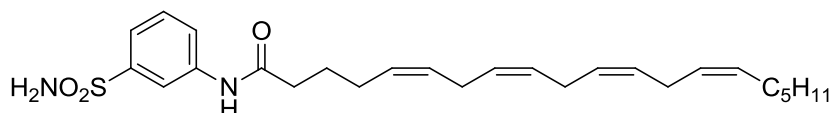


Methyl 4-((5Z,8Z,11Z,14Z)-icosa-5,8,11,14-tetraenamido)benzoate (20n): White solid, 64 % yield (over 2 steps), eluent system: 3:1 hexane-ethyl acetate. ¹H NMR (500 MHz, CDCl₃) δ 7.99 (d, *J* = 8.7 Hz, 2H), 7.59 (d, *J* = 8.5 Hz, 2H), 7.38 (s, 1H), 5.42 – 5.34 (m, 7H), 3.89 (s, 3H), 2.83 – 2.78 (m, 6H), 2.40 – 2.37 (m, 2H), 2.18 – 2.15 (m, 2H), 2.09 – 2.02 (m, 2H), 1.84 – 1.82 (m, 2H), 1.35 – 1.34 (m, 2H), 1.29 – 1.25 (m, 6H), 0.88 (t, *J* = 6.9 Hz, 3H). ¹³C NMR (126 MHz, CDCl₃) δ 171.24, 166.58, 142.08, 130.83(2C), 130.53(2C), 129.12, 128.83, 128.62, 128.31, 128.04, 127.78, 127.48, 125.50, 118.68, 51.98, 37.04, 31.49, 29.29, 27.20, 26.50, 25.65, 25.62(2C), 25.09, 22.55, 14.04. HRMS (ESI): calculated for C₂₈H₃₇NO₃ (M-1) 436.2857, found 436.2838.



Methyl 2-((5Z,8Z,11Z,14Z)-icosa-5,8,11,14-tetraenamido)benzoate (20o): Pale yellow solid, 32% yield (over 2 steps), eluent system: 3:1 hexane-ethyl acetate. ¹H NMR (500 MHz, CDCl₃) δ 11.07 (s, 1H), 8.73 (d, *J* = 8.5 Hz, 1H), 8.03 (d, *J* = 8.0 Hz, 1H), 7.54 (t, *J* = 7.8 Hz, 1H), 7.07 (t, *J* = 7.6 Hz, 1H), 5.42 – 5.34 (m, 8H), 3.93 (s, 3H), 2.81 (dd, *J* = 11.1, 4.8 Hz, 6H), 2.46 (t, *J* = 7.6 Hz, 2H), 2.19 –

2.17 (m, 2H), 2.06 – 2.02 (m, 2H), 1.86 – 1.83 (m, 2H), 1.35 – 1.26 (m, 6H), 0.88 (t, $J = 6.7$ Hz, 3H). ^{13}C NMR (126 MHz, CDCl_3) δ 171.94, 168.77, 141.69, 134.69, 130.79, 130.47, 129.05, 128.90, 128.56, 128.21, 128.19, 127.89, 127.57, 122.31, 120.39, 114.75, 52.29, 38.01, 31.51, 29.69, 29.32, 27.21, 26.64, 25.66, 25.64, 25.30, 22.56, 14.05. HRMS (ESI): calculated for $\text{C}_{28}\text{H}_{37}\text{NO}_3$ (M-1) 436.2857, found 436.2856.

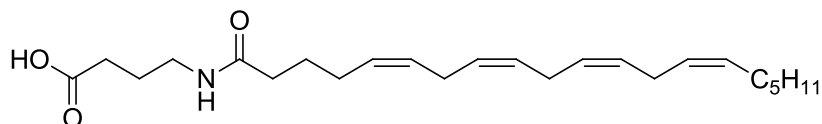


Synthesis of (5Z,8Z,11Z,14Z)-N-(3-sulfamoylphenyl)icosa-5,8,11,14-tetraenamide (2p): EDC.HCl (13 mg, 0.07 mmol), **19a** (18 mg, 0.06 mmol), TEA (9 μL , 0.07 mmol) and 3-aminobenzenesulfonamide (11 mg, 0.07 mmol) were dissolved in MeCN (1.5 mL) and stirred overnight at 4°C. The reaction was quenched with ethyl acetate and the mixture was washed with aqueous NaHCO_3 (3 x 20 mL) and brine (3 x 20 mL). The organic layer was dried, concentrated and purified by flash column chromatography using a 1:1 hexane-ethyl acetate eluent system to yield **2p** as a pale yellow solid (13 mg, 47% yield). ^1H NMR (500 MHz, DMSO) δ 10.18 (s, 1H), 8.17 (s, 1H), 7.76 – 7.74 (m, 1H), 7.48 – 7.46 (m, 2H), 7.34 (s, 2H), 5.40 – 5.31 (m, 8H), 2.82 – 2.77 (m, 6H), 2.35 (t, $J = 7.4$ Hz, 2H), 2.11 (dd, $J = 13.9, 6.9$ Hz, 2H), 2.03 – 2.00 (m, 2H), 1.70 – 1.64 (m, 2H), 1.32 – 1.29 (m, 2H), 1.28 – 1.24 (m, 4H), 0.85 (t, $J = 6.2$ Hz, 3H). ^{13}C NMR (126 MHz, DMSO) δ 171.85, 145.02, 140.05, 130.39(2C), 129.74, 128.67, 128.57, 128.41, 128.29, 128.10, 127.95, 122.24, 120.46, 116.47, 36.24, 31.31, 29.42, 29.13, 27.04, 26.66, 25.66(2C), 25.38, 22.38, 14.33. HRMS (ESI): calculated for $\text{C}_{26}\text{H}_{37}\text{NO}_3\text{S}$ (M-1) 457.2530, found 457.2537.

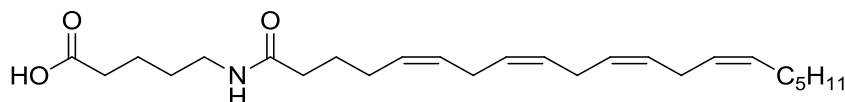
General hydrolysis procedure to yield **2a-k**, **2n-o** and **2q**

The respective ester **20** or **24** (0.03 mmol) was dissolved in 2M methanolic NaOH (2.0 mL) and stirred at room temperature for 3 h. When no more starting material was observed, the reaction was quenched with 1M HCl and then extracted with ethyl acetate (3x20 mL). The organic layer was

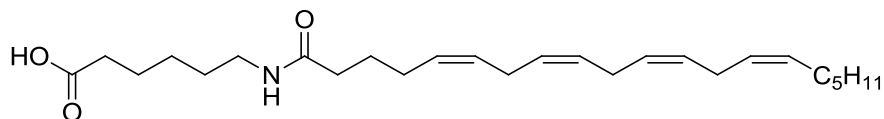
separated and the combined organic layer was dried with MgSO_4 , concentrated and purified by flash column chromatography.



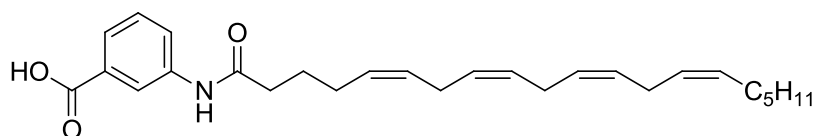
4-((5Z,8Z,11Z,14Z)-icosa-5,8,11,14-tetraenamido)butanoic acid (2a): Pale yellow solid, 59% yield, eluent system: 2:1:0.03 hexane-ethyl acetate-AcOH. ^1H NMR (500 MHz, CDCl_3) δ 5.73 (s, 1 H), 5.83 – 5.33 (m, 8 H), 3.37 – 3.33 (dd, $J = 12.9, 6.7$ Hz, 2 H), 2.92 – 2.64 (m, 4 H), 2.41 (t, $J = 7.0$ Hz, 2 H), 2.09 (ddd, $J = 22.9, 14.5, 7.1$ Hz, 6 H), 1.87 (dt, $J = 14.5, 7.4$ Hz, 2 H), 1.69 (dt, $J = 14.5, 7.4$ Hz, 2 H), 1.41 – 1.17 (m, 8 H), 0.90 (t, $J = 6.7$ Hz, 3 H)^k; ^{13}C NMR (125 MHz, CDCl_3) δ 177.15, 173.72, 130.54, 129.01, 128.87, 128.63, 128.29, 128.14, 127.85, 127.53, 38.83, 36.05, 31.51, 29.69, 29.64, 29.31, 27.22, 26.65, 25.64 (2 C), 25.49, 24.83, 22.57, 14.05. HRMS (ESI): calculated for $\text{C}_{24}\text{H}_{39}\text{NO}_3\text{Na}$ ($\text{M}+\text{Na}$) 412.2822, found 412.2830.



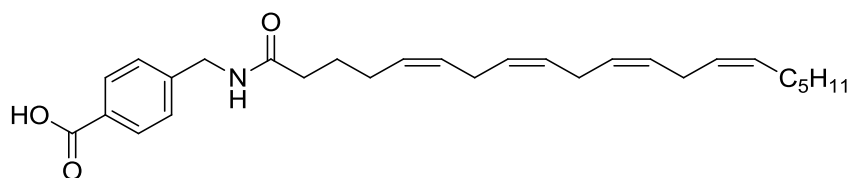
5-((5Z,8Z,11Z,14Z)-icosa-5,8,11,14-tetraenamido)pentanoic acid (2b): Pale yellow solid, 52% yield, eluent system: 2:1:0.03 hexane-ethyl acetate-AcOH. ^1H NMR (500 MHz, CDCl_3) δ 5.67 (s, 1 H), 5.50 – 5.28 (m, 8 H), 3.29 (d, $J = 5.9$ Hz, 2 H), 2.91 – 2.72 (m, 4 H), 2.40 (t, $J = 7.1$ Hz, 2 H), 2.24 – 2.17 (m, 2 H), 2.13 (dd, $J = 13.1, 6.6$ Hz, 2 H), 2.07 (dd, $J = 14.2, 7.1$ Hz, 2 H), 1.71 – 1.62 (m, 4 H), 1.59 (dd, $J = 14.3, 6.9$ Hz, 2 H), 1.44 – 1.24 (m, 8 H), 0.91 (t, $J = 7.0$ Hz, 3 H)^j; ^{13}C NMR (125 MHz, CDCl_3) δ 178.06, 173.30, 130.53, 129.09, 128.79, 128.62, 128.25, 128.17, 127.86, 127.53, 39.05, 36.14, 33.41, 31.51, 29.31, 28.99, 27.22, 26.68, 25.64 (2 C), 25.56 (2 C), 22.56, 21.88, 14.05. HRMS (ESI): calculated for $\text{C}_{25}\text{H}_{42}\text{NO}_3$ ($\text{M}+1$) 404.3159, found 404.3164.



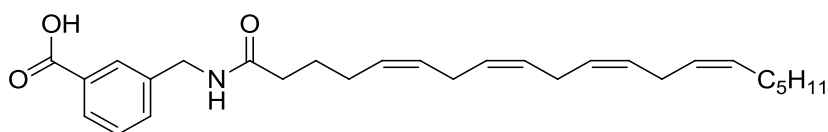
6-((5Z,8Z,11Z,14Z)-icosa-5,8,11,14-tetraenamido)hexanoic acid (2c): Pale yellow solid, 98% yield, eluent system: 2:1:0.03 hexane-ethyl acetate-AcOH. ^1H NMR (500 MHz, CDCl_3) δ 5.57 (s, 1H), 5.38 – 5.34 (m, 8H), 3.25 (dd, $J = 13.3, 6.8$ Hz, 2H), 2.84 – 2.75 (m, 6H), 2.34 (t, $J = 7.3$ Hz, 2H), 2.18 – 2.15 (m, 2H), 2.11 – 2.08 (m, 2H), 2.07 – 2.02 (m, 2H), 1.72 – 1.63 (m, 4H), 1.53 – 1.50 (m, 2H), 1.39 – 1.34 (m, 4H), 1.32 – 1.25 (m, 4H), 0.88 (t, $J = 6.8$ Hz, 3H). ^{13}C NMR (126 MHz, CDCl_3) δ 178.25, 173.14, 130.50, 129.09, 128.73, 128.58, 128.22, 128.14, 127.83, 127.50, 39.25, 36.12, 33.77, 31.48, 29.29, 29.24, 27.19, 26.64, 26.24, 25.61(3C), 25.54, 24.23, 22.54, 14.03. HRMS (ESI): calculated for $\text{C}_{26}\text{H}_{42}\text{NO}_3$ (M-1) 416.3170, found 416.3170.



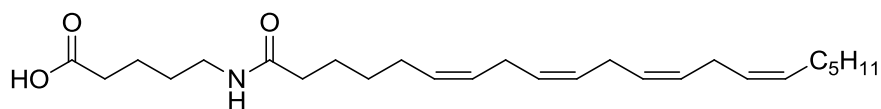
3-((5Z,8Z,11Z,14Z)-icosa-5,8,11,14-tetraenamido)benzoic acid (2d): Pale yellow solid, 63% yield, eluent system: 2:1:0.03 hexane-ethyl acetate-AcOH. ^1H NMR (500 MHz, DMSO) δ 12.91 (s, 1H), 10.05 (s, 1H), 8.22 (s, 1H), 7.82 (d, $J = 8.0$ Hz, 1H), 7.59 (d, $J = 7.7$ Hz, 1H), 7.39 (t, $J = 7.9$ Hz, 1H), 5.39 – 5.31 (m, 7H), 2.77 (dt, $J = 11.5, 5.5$ Hz, 4H), 2.32 (dd, $J = 13.7, 6.3$ Hz, 2H), 2.10 – 2.07 (m, 2H), 2.00 – 1.98 (m, 4H), 1.67 – 1.64 (m, 2H), 1.30 – 1.27 (m, 2H), 1.24 – 1.21 (m, 4H), 0.83 (t, $J = 6.9$ Hz, 3H). ^{13}C NMR (126 MHz, DMSO) δ 171.23, 167.18, 139.51, 131.21, 129.90, 129.29, 128.82, 128.20, 128.07, 127.95, 127.78, 127.62, 127.48, 123.70, 123.04, 119.76, 35.74, 30.86, 28.69, 26.58, 26.19, 25.21(2C), 25.18, 24.91, 21.95, 13.89. HRMS (ESI): calculated for $\text{C}_{27}\text{H}_{36}\text{NO}_3$ (M-1) 422.2701, found 422.2685.



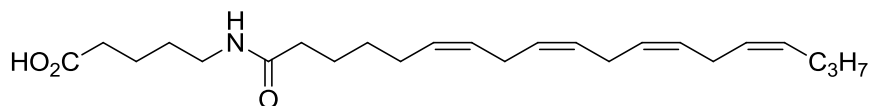
4-((5Z,8Z,11Z,14Z)-icos-5,8,11,14-tetraenamido)methyl)benzoic acid (2e): Pale yellow solid, 95% yield, eluent system: 2:1:0.03 hexane-ethyl acetate-AcOH. ^1H NMR (500 MHz, DMSO) δ 12.83 (s, 1H), 8.37 (s, 1H), 7.88 (d, $J = 8.2$ Hz, 2H), 7.34 (d, $J = 8.3$ Hz, 2H), 5.36 – 5.32 (m, 9H), 4.32 (d, $J = 5.9$ Hz, 2H), 2.82 – 2.77 (m, 6H), 2.16 (t, $J = 7.4$ Hz, 2H), 2.03 (td, $J = 13.9, 7.0$ Hz, 4H), 1.62 – 1.56 (m, 2H), 1.32 – 1.28 (m, 2H), 1.27 – 1.22 (m, 4H), 0.84 (t, $J = 7.0$ Hz, 3H). ^{13}C NMR (126 MHz, DMSO) δ 172.48, 167.59, 145.37, 130.39, 129.83, 129.76, 129.70, 128.57, 128.51, 128.44, 128.24, 128.13, 127.96, 127.57, 42.24, 35.22, 31.31, 29.14, 27.05, 26.74, 25.69, 25.67, 25.65(2C), 22.40, 14.34. HRMS (ESI): calculated for $\text{C}_{28}\text{H}_{37}\text{NO}_3$ (M-1) 436.2587, found 436.2861.



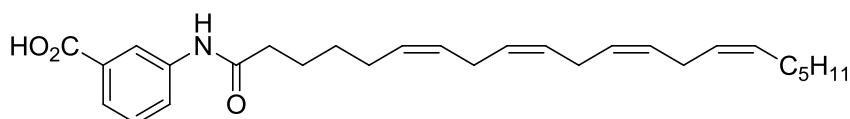
3-((5Z,8Z,11Z,14Z)-icos-5,8,11,14-tetraenamido)methyl)benzoic acid (2f): Pale yellow solid, 98% yield, eluent system: 2:1:0.03 hexane-ethyl acetate-AcOH. ^1H NMR (500 MHz, CDCl_3) δ 8.01 (d, $J = 8.1$ Hz, 2H), 7.53 (d, $J = 7.6$ Hz, 1H), 7.43 (t, $J = 7.7$ Hz, 1H), 5.93 (s, 1H), 5.39 – 5.33 (m, 8H), 4.51 (d, $J = 5.8$ Hz, 2H), 2.83 – 2.79 (m, 6H), 2.28 – 2.25 (m, 2H), 2.12 (dd, $J = 13.3, 6.8$ Hz, 2H), 2.06 – 2.02 (m, 2H), 1.78 – 1.75 (m, 2H), 1.35 – 1.33 (m, 2H), 1.29 – 1.25 (m, 4H), 0.88 (t, $J = 6.9$ Hz, 3H). ^{13}C NMR (126 MHz, CDCl_3) δ 173.21, 170.77, 138.83, 133.02, 130.50, 129.94, 129.27, 129.22, 128.98, 128.90, 128.84, 128.58, 128.23, 128.11, 127.83, 127.49, 43.18, 35.98, 31.48, 29.28, 27.18, 26.64, 25.60(3C), 25.46, 22.53, 14.03. HRMS (ESI): calculated for $\text{C}_{28}\text{H}_{38}\text{NO}_3$ (M-1) 436.2587, found 436.2854.



5-((6Z,9Z,12Z,15Z)-henicosa-6,9,12,15-tetraenamido)pentanoic acid (2g): pale yellow solid, 95% yield, eluent system: 2:1:0.03 hexane-ethyl acetate-AcOH. ^1H NMR (500 MHz, DMSO) δ 11.95 (s, 1H), 7.70 (s, 1H), 5.28 (s, 8H), 2.98 – 2.96 (m, 2H), 2.77 – 2.69 (m, 4H), 2.15 (t, $J = 7.2$ Hz, 2H), 1.99 – 1.98 (m, 8H), 1.45 – 1.42 (m, 4H), 1.35 – 1.32 (m, 2H), 1.29 – 1.24 (m, 2H), 1.22 (s, 6H), 0.81 (t, $J = 6.4$ Hz, 3H). ^{13}C NMR (126 MHz, DMSO) δ 174.33, 171.74, 129.90, 129.73, 129.48, 128.07, 128.02, 127.72, 127.66, 127.49, 40.41, 37.98, 35.27, 33.28, 30.89, 28.72, 28.700, 28.68, 26.61, 26.46, 25.20(2C), 24.99, 21.97, 21.93, 13.89. HRMS (ESI): calculated for $\text{C}_{26}\text{H}_{42}\text{NO}_3$ (M-1) 416.3170, found 416.3165.

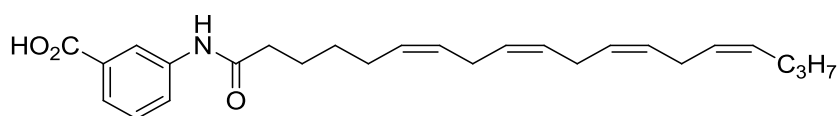


5-((6Z,9Z,12Z,15Z)-nonadeca-6,9,12,15-tetraenamido)pentanoic acid (2h): Pale yellow solid, 95% yield, eluent system: 2:1:0.03 hexane-ethyl acetate-AcOH. ^1H NMR (500 MHz, DMSO) δ 11.99 (s, 1H), ^1H NMR (500 MHz, DMSO) δ 7.74 (m, 1H), 5.38 – 5.33 (m, 8H), 3.02 (q, $J = 6.5$ Hz, 2H), 2.83 – 2.78 (m, 4H), 2.20 (t, $J = 7.3$ Hz, 2H), 2.06 – 2.00 (m, 6H), 1.51 – 1.47 (m, 4H), 1.40 – 1.35 (m, 2H), 1.34 – 1.29 (m, 2H), 1.27 – 1.25 (s, 2H), 0.88 (t, $J = 7.3$ Hz, 3H). ^{13}C NMR (126 MHz, DMSO) δ 174.77, 172.21, 130.20, 130.13, 128.54, 128.50, 128.19(2C), 128.15, 128.08, 38.43, 35.73, 33.75, 29.15, 29.13, 26.90, 25.65, 25.43, 22.65, 22.38, 14.01. HRMS (ESI): calculated for $\text{C}_{24}\text{H}_{38}\text{NO}_3$ (M-1) 388.2857, found 388.2866.

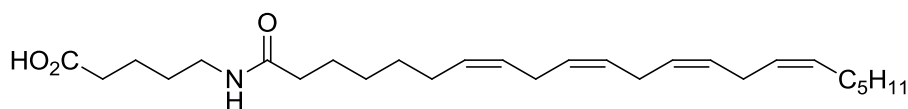


3-((6Z,9Z,12Z,15Z)-henicosa-6,9,12,15-tetraenamido)benzoic acid (2i): Pale yellow solid, 81 % yield, eluent system: 2:1:0.03 hexane-ethyl acetate-AcOH. ^1H NMR (500 MHz, DMSO) δ 12.86 (s, 1H), 10.01 (s, 1H), 8.21 (s, 1H), 7.82 (d, $J = 8.1$ Hz, 1H), 7.59 (d, $J = 7.7$ Hz, 1H), 7.39 (t, $J = 7.9$ Hz,

1H), 5.37 – 5.29 (m, 8H), 2.79 (dt, $J = 17.2, 5.2$ Hz, 6H), 2.32 (t, $J = 7.4$ Hz, 2H), 2.07 (dd, $J = 14.1, 7.0$ Hz, 2H), 2.01 (dd, $J = 13.8, 6.8$ Hz, 2H), 1.61 (dt, $J = 15.1, 7.5$ Hz, 2H), 1.37 (dt, $J = 15.0, 7.6$ Hz, 2H), 1.30 – 1.23 (m, 6H), 0.84 (t, $J = 6.9$ Hz, 3H). ^{13}C NMR (126 MHz, DMSO) δ 171.27, 167.08, 139.43, 131.18, 129.85, 129.59, 128.73, 128.00, 127.93, 127.68, 127.65, 127.59, 127.41, 123.63, 122.99, 119.73, 36.19, 30.77, 28.59(2C), 26.51, 26.40, 25.14, 25.13(2C), 24.63, 21.84, 13.78. HRMS (ESI): calculated for $\text{C}_{28}\text{H}_{37}\text{NO}_3$ (M-1) 436.2587, found 436.2866.

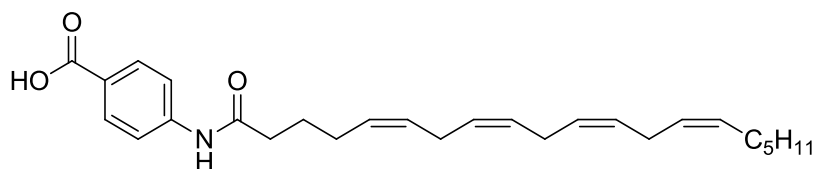


3-((6Z,9Z,12Z,15Z)-nonadeca-6,9,12,15-tetraenamido)benzoic acid (2j): Pale yellow solid, 98% yield, eluent system: 2:1:0.03 hexane-ethyl acetate-AcOH. ^1H NMR (500 MHz, DMSO) δ 12.87 (s, 1H), 10.02 (s, 1H), 8.22 (s, 1H), 7.82 (d, $J = 7.6$ Hz, 1H), 7.60 (d, $J = 7.7$ Hz, 1H), 7.40 (t, $J = 7.9$ Hz, 1H), 5.38 – 5.33 (m, 8H), 2.82 – 2.78 (m, 6H), 2.33 (t, $J = 7.4$ Hz, 2H), 2.10 – 2.06 (m, 2H), 2.04 (dd, $J = 13.4, 6.9$ Hz, 2H), 1.62 (dt, $J = 15.2, 7.5$ Hz, 2H), 1.39 – 1.35 (m, 2H), 1.32 (dd, $J = 14.7, 7.3$ Hz, 2H), 0.86 (d, $J = 7.3$ Hz, 3H). ^{13}C NMR (126 MHz, DMSO) δ 171.27, 167.11, 139.41, 131.35, 129.59, 128.71, 128.01, 127.95, 127.68, 127.66, 127.66, 127.64, 127.61, 123.64, 122.94, 119.74, 36.19, 28.61, 28.59, 26.40, 25.14 (2C), 24.63, 22.10, 13.45. HRMS (ESI): calculated for $\text{C}_{26}\text{H}_{34}\text{NO}_3$ (M-1) 408.2544, found 408.2543.

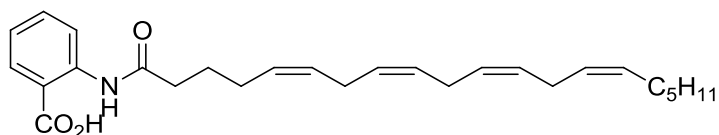


5-((7Z,10Z,13Z,16Z)-docosa-7,10,13,16-tetraenamido)pentanoic acid (2k): Pale yellow solid, 69% yield, eluent system: 2:1:0.03 hexane-ethyl acetate-AcOH. ^1H NMR (500 MHz, DMSO) δ 11.98 (s, 1H), 7.73 (s, 1H), 5.34 – 5.33 (m, 8H), 3.34 (s, 6H), 3.02 (dd, $J = 12.6, 6.5$ Hz, 2H), 2.82 – 2.75 (m, 2H), 2.20 (t, $J = 7.3$ Hz, 2H), 2.04 – 2.02 (m, 4H), 1.50 – 1.47 (m, 4H), 1.40 – 1.36 (m, 2H), 1.33 – 1.25 (m, 10H), 0.86 (t, $J = 6.7$ Hz, 3H). ^{13}C NMR (126 MHz, DMSO) δ 174.76, 172.28, 130.37, 130.32, 128.52, 128.49, 128.16, 128.13, 127.99, 127.95, 38.42, 35.82, 33.74, 31.32, 29.45, 29.26,

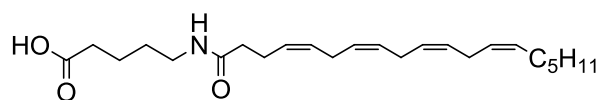
29.23, 29.15, 29.12, 28.75, 27.06, 27.02, 27.00, 25.66, 25.064, 22.38, 14.34. HRMS (ESI): calculated for $C_{28}H_{37}NO_3$ (M-1) 430.3327, found 430.3323.



4-((5Z,8Z,11Z,14Z)-icosa-5,8,11,14-tetraenamido)benzoic acid (2n): Pale yellow solid, 68% yield, eluent system: 2:1:0.03 hexane-ethyl acetate-AcOH. 1H NMR (500 MHz, DMSO) δ 12.65 (s, 1H), 10.18 (s, 1H), 7.86 (d, $J = 8.6$ Hz, 2H), 7.70 (d, $J = 8.3$ Hz, 2H), 5.37 – 5.31 (m, 7H), 2.80 – 2.76 (m, 5H), 2.35 (t, $J = 7.1$ Hz, 2H), 2.10 – 2.08 (m, 2H), 2.01 – 1.98 (m, 3H), 1.67 – 1.64 (m, 2H), 1.30 – 1.26 (m, 2H), 1.24 – 1.23 (m, 4H), 0.83 (t, $J = 6.6$ Hz, 3H). ^{13}C NMR (126 MHz, DMSO) δ 171.54, 166.91, 143.32, 130.30(2C), 129.91, 129.26, 128.23, 128.07, 127.95, 127.77, 127.63, 127.47, 124.81, 118.17(2C), 35.80, 30.85, 28.68, 26.57, 26.16, 25.18(3C), 24.81, 21.94, 13.88. HRMS (ESI): calculated for $C_{27}H_{36}NO_3$ (M-1) 422.2701, found 422.2690.



2-((5Z,8Z,11Z,14Z)-icosa-5,8,11,14-tetraenamido)benzoic acid (2o): Pale yellow solid, 96% yield, eluent system: 2:1:0.03 hexane-ethyl acetate-AcOH. 1H NMR (300 MHz, $CDCl_3$) δ 10.93 (s, 1H), 8.76 (d, $J = 8.5$ Hz, 1H), 8.11 (dd, $J = 8.0, 1.5$ Hz, 1H), 7.62 – 7.57 (m, 1H), 7.14 – 7.09 (m, 1H), 5.44 – 5.33 (m, 8H), 2.84 – 2.77 (m, 6H), 2.47 (t, $J = 7.8$ Hz, 2H), 2.20 – 2.06 (m, 2H), 2.05 – 2.01 (m, 2H), 1.85 (t, $J = 7.4$ Hz, 2H), 1.37 – 1.25 (m, 6H), 0.88 (t, $J = 6.7$ Hz, 3H). ^{13}C NMR (75 MHz, $CDCl_3$) δ 172.13, 171.73, 142.11, 135.61, 131.72, 130.49, 128.97, 128.93, 128.56, 128.21, 128.14, 127.85, 127.53, 122.56, 120.49, 113.74, 37.95, 31.49, 29.30, 27.19, 26.57, 25.64, 25.61(2C), 25.25, 22.55, 14.05. HRMS (ESI): calculated for $C_{27}H_{36}NO_3$ (M-1) 422.2701, found 422.2707.



5-((4Z,7Z,10Z,13Z)-nonadeca-4,7,10,13-tetraenamido)pentanoic acid (2q): Pale yellow solid, 64% yield, eluent system: 2:1:0.03 hexane-ethyl acetate-AcOH. ^1H NMR (500 MHz, DMSO) δ 11.99 (s, 1H), 7.78 – 7.74 (m, 1H), 5.36 – 5.31 (m, 7H), 3.04 – 3.00 (m, 2H), 2.83 – 2.75 (m, 4H), 2.20 (t, J = 7.3 Hz, 2H), 2.08 (dd, J = 8.9, 6.1 Hz, 2H), 2.04 – 2.00 (m, 4H), 1.47 (d, J = 7.3 Hz, 2H), 1.40 – 1.38 (m, 2H), 1.33 – 1.30 (m, 2H), 1.27 – 1.25 (m, 6H), 0.86 (t, J = 6.9 Hz, 3H). ^{13}C NMR (126 MHz, DMSO) δ 174.32, 171.16, 129.92, 128.86, 128.08, 128.03, 128.00, 127.75, 127.67, 127.50, 38.02, 35.21, 33.27, 30.84, 28.68, 28.62, 26.57, 25.18, 25.17, 25.13, 23.16, 21.93, 21.91, 13.88. HRMS (ESI): calculated for $\text{C}_{24}\text{H}_{38}\text{NO}_3$ (M-1) 388.2857, found 388.2841.

2.12 Docking

^bThis part of the project was carried out in collaboration with Prof. Chandra S Verma (Bioinformatics Institute, Agency for Science, Technology and Research (A*STAR)).

Protein modeling

The crystal structure of cPLA₂ in its apo form is available,¹⁴ however the experimental structure has a few missing regions (407 to 414, 431 to 462, 498 to 538 and 626-632). The missing structural regions were modeled using homology and loop modeling methods. The homology models were generated by program Modeller (version 9.12).²⁷ Several models were generated and the models with the best stereochemical properties were refined further using all atom MD simulations.

Ligand preparation

The 3D structures of the test compounds were built using *Maestro* and minimized using the *Macromodel* module employing the OPLS-2005 force field in Schrodinger 9.0.^{28,29} All the inhibitors were then prepared with *Ligprep* that generates low energy tautomers and enumerates realistic protonation states at physiological pH.

Ligand docking

The prepared inhibitors were docked into the binding pockets of the models of cPLA₂ using *Glide*.³⁰ A box of size 10 x 10 x 10 Å for molecular docking centered on the selected active site residue (Ser228) was used to confine the search space of each docked ligand. For the grid generation, the default *Glide* settings were used. A rigid receptor docking (RRD) protocol was used which fixes the protein conformation while allowing the ligands to be flexible. All inhibitors were docked into the active sites of cPLA₂ using this protocol and the docked conformation of each ligand was evaluated using the *Glide* Extra Precision (XP) scoring function. Docking was carried out on several conformational substrates of the Mnk kinases identified by clustering of MD trajectories.

MD simulations

MD simulations were carried out to refine the homology models of cPLA₂ and to generate ensemble of receptor conformations for docking. MD simulations were carried out with the *Sander* module of the program Amber11.³¹ The partial charges and force field parameters for each inhibitor were generated using the *Antechamber* module in Amber. All atom versions of the Amber 03 force field (ff03).³² The *Xleap* module was used to prepare the system for the MD simulations. All the simulation systems were neutralized with an appropriate number of counterions. Each neutralized system was solvated in an octahedral box with TIP3P water molecules, leaving at least 10 Å between the solute atoms and the borders of the box.³³ All MD simulations were carried out in an explicit solvent at 300K. During the simulations, the long-range electrostatic interactions were treated with the particle mesh Ewald method using a real space cutoff distance of 9 Å.³⁴ The Settle algorithm was used to constrain bond vibrations involving hydrogen atoms, which allowed a time step of 2 fs during the simulations.³⁵

Solvent molecules and counterions were initially relaxed using energy minimization with restraints on the protein and inhibitor atoms. This was followed by unrestrained energy minimization to remove any steric clashes. Subsequently the system was gradually heated from 0 to 300 K using MD simulations with positional restraints (force constant: 50 kcal mol⁻¹ Å⁻²) on protein and inhibitors over

a period of 0.25 ns allowing water molecules and ions to move freely. During an additional 0.25 ns, the positional restraints were gradually reduced followed by a 2 ns unrestrained MD simulation to equilibrate all the atoms. For the refinement simulations, three independent MD simulations (assigning different initial velocities) were carried out on each equilibrated cPLA₂ structure for 100 ns with conformations saved every 10 ps. Cluster analysis of the sampled conformations was performed using the *Kclust* program in MMTSB-tools.³⁶ Simulation trajectories were visualized using VMD and figures were generated using Pymol.^{37, 38}

2.13 Experimental - Biology

2.13.1 Enzchek phospholipase A₂ fluorogenic assay (% activity)

The assay was conducted according to the manufacturer's instruction (E10217, Molecular Probes) with slight modification. Briefly, substrate solution was separately prepared by mixing 5 μL of DOPG, 5 μL of DOPC and 5 μL of substrate respectively in 1.5 mL of 1X phospholipase A₂ reaction buffer. The mixture was vortexed vigorously for 3 min before allowing to stand at room temperature for 1 h. 48 μL of 1X phospholipase A₂ reaction buffer were added into each well of a 96-wells plate. This is followed by addition of 1 μL of recombinant cPLA₂ (P4074-03R, US Biological) and 1 μL of 1 mM of the respective compound dissolved in DMSO. The final concentration of the test compound achieved is 10 μM. The reaction is initiated by adding 50 μL of the substrate solution and incubating at room temperature for 1 h. Fluorescence was measured using a Varioskan plate reader by exciting at 485 nm, while fluorescence emission was detected at 515 nm. Positive control was performed when 1 μL of test compound was replaced by vehicle DMSO.

% activity was calculated by the following formula

$$\%activity = \frac{fluorescence\ of\ tested\ well - background}{fluorescence\ of\ positive\ control - background}$$

2.13.2 Enzchek phospholipase A₂ fluorogenic assay (IC₅₀)

The assay was conducted as described above. Instead of adding a fixed concentration of the test compound, various concentrations of compound were reconstituted in DMSO. 48 μL of 1X

phospholipase A₂ reaction buffer were added into each well of a 96-wells plate. This is followed by addition of 1 μL of recombinant cPLA₂ (P4074-03R, US Biological) and 1 μL of the respective concentration of the test compound dissolved in DMSO. The reaction was initiated by adding 50 μL of the substrate solution and incubating at room temperature for 1 h. Fluorescence was measured using a Varioskan plate reader by exciting at 485 nm, while fluorescence emission was detected at 515 nm. Positive control was performed when 1 μL of test compound was replaced by vehicle DMSO.

2.13.3 Enzchek phospholipase A₂ fluorogenic assay (selectivity)

The assay was conducted as described above. Instead of adding cPLA₂, it was replaced by sPLA₂. 48 μL of 1X phospholipase A₂ reaction buffer was added into each well of a 96-wells plate. This is followed by addition of 1 μL of sPLA₂, human recombinant type V (10009563, Cayman Chemical) and 1 μL of 1 mM of the respective compound or thio-etheramidePC dissolved in DMSO [thio-etheramidePC (62750, Cayman Chemical) is a sPLA₂ selective inhibitor]. The reaction was initiated by adding 50 μL of the substrate solution and incubating at room temperature for 1 h. Fluorescence was measured using a Varioskan plate reader by exciting at 485 nm, while fluorescence emission was detected at 515 nm. Positive control was performed when 1 μL of test compound was replaced by vehicle DMSO.

% activity was calculated by the following formula:

$$\%activity = \frac{\text{fluorescence of tested well} - \text{background}}{\text{fluorescence of postive control} - \text{background}}$$

2.13.4 Cell-culture and LPS treatment

Murine BV-2 cells were cultured in DMEM (11965092, ThermoFisher Scientific) supplemented with 10% fetal bovine serum, 100 μg/mL streptomycin and 100 units/mL penicillin. Cells were maintained in an incubator at 37°C, under a 5% CO₂ and in a water saturated environment. When performing LPS treatment, BV-2 cells were plated on a 10 cm dish in 10 mL DMEM at a density of 1x10⁶ cells per dish one day prior to the experiment. After observing that cells are at 90% confluency,

lipopolysaccharide (L6529, Sigma) pre-dissolved in DMEM to achieve a concentration of 2 µg/mL was added to the dish. Different concentrations of test compounds in DMSO were added to the LPS containing medium which was then transferred to the 10 cm dish. DMSO was used as a vehicle control and added to the non-LPS treated control. The cells were incubated for the respective hours at 37°C, under a 5% CO₂. After the respective timepoint, cells were washed once with 1xPBS (10 mL) and scrapped on ice with 8 mL 1xPBS. Collected cells were spun at 800rpm for 3 min at 4°C, before discarding the supernatant. Cells were lysed by RIPA buffer, which contain 1 x protease inhibitor and 1mM PMSF and incubated under ice for 30 min. This was followed by spinning the cell debris at 4°C for 30 min at 13200 rpm before transferring the supernatant to a clean tube and storing the sample at -20°C.

2.13.5 MTS cell proliferation assay

Cells were plated on a 96-wells plate and grown for 24 h to a density of 8000 cells per well for both HEK293T and BV-2 cells. Cells were cultured in an incubator at 37°C under a 5% CO₂ environment in 100 µL of DMEM. Thereafter, the compound of interest dissolved in DMEM at a concentration of 10 µM was added into each well. DMSO was added as vehicle in the control group. 3 biological replicates were performed. The plates were then incubated at 37°C with 5% CO₂ for 48 h and 72 h. At each individual time point, 20 µL of CellTiter 96® AQueous One Solution (MTS reagent) was added into each well and re-incubated at 37°C with 5% CO₂ without light for 3 h. Colorimetric readings were taken at 490 nm using a spectrometer and analysed.

2.13.6 BCA Assay

BCA assay (23225, Pierce BCA Protein Assay Kit) was performed to quantify the concentration of proteins in the cell lysate. 10 µL of test samples (1 µL with 9 µL of lysis buffer) and BSA standards (range from 1.25 to 50 µg/ml) were mixed in a 96 well-plate and incubated with 190 µL of working reagent mixture (Ratio of Reagent A:B used was 50:1) at 37°C for 20 min. The colour intensity that was developed was read at 562 nm using a spectrophotometer. A standard curve of different concentrations of BSA was plotted using the average blank-corrected readings for each standard vs. its

respective concentration ($\mu\text{g/ml}$). This was then used to determine the protein concentration for unknown samples.

2.13.7 Western Blot

The amount of protein in the lysates were normalized by BCA previously. 25 μg of individual protein samples were mixed with an equal volume of 2x Laemmli buffer containing DTT and denatured at 90°C for 10 min. Lysates were loaded into a 10% Tris-Gly Gel. SDS-PAGE was run at a voltage of 100 V for 1.5 h in 1x Running Buffer (10% Tris-Gly-SDS buffer). The protein samples on the gel were then transferred to PVDF membrane assembled in a sandwich soaked in 1x Transfer Buffer (10% Tris-Gly buffer, 10% methanol, 0.1% SDS) at 100V for two hours under ice. The membrane blots were then incubated for one hour at room temperature in a Blocking Buffer containing 5% milk in 1x Tris-Gly buffer and 0.1% TBST, followed by overnight incubation with the respective primary antibody dissolved in 5% milk in 1x Tris-Gly buffer and 0.1% TBST at 4°C. After three washes with 1x Tris-Gly buffer in 0.1% TBST, each of duration 10min, the blot was incubated with a secondary horse-radish peroxidase-conjugated antibody (1:10000) dissolved in 5% milk in 1x Tris-Gly buffer and 0.1% TBST for one hour at room temperature. Three washes with 1x Tris-Gly buffer in 0.1% TBST, each of duration 10min were performed. Enhanced chemiluminescence (ECL) detection of protein bands was performed using ECL Plus Western Blotting detecting system (GB Healthcare). Antibodies used in western blot include rabbit polyclonal anti-NOS2 (Santa-Cruz, sc-651, 1:100), mouse monoclonal anti-cPLA₂ primary antibody (Santa Cruz, sc-454, 1:200), mouse anti-gapdh (Merck, 1:10000), with secondary horse-radish peroxidase-conjugated antibodies (Santa Cruz, 1:10000).

2.13.8 ROS assay

20,000 cells were seeded into a 96-well plate in 100 μL of DMEM and allowed to grow overnight. When a 90% cell confluency was observed, lipopolysaccharide pre-dissolved in DMEM to achieve a concentration of 2 $\mu\text{g/mL}$ was added to each well of the 96 well. Different concentrations of test compounds in DMSO were added to the LPS containing medium and was then transferred to the cells.

DMSO was used as vehicle control and added to the non-LPS treated control. The cells were incubated for 14 h at 37°C, under a 5% CO₂ environment. Medium were removed and washed once with 1x HBSS. 1mM stock solution of CM-H2DCFDA (C6827, Molecular Probes) in DMSO was added into 1x HBSS to achieve a final concentration of 10 µM. 100 µL of CM-H2DCFDA solution was added into each well and incubated at 37°C for 1 h. Fluorescence detection was done by exciting the dye at 485nm and taking emission readings at 525 nm.

2.14 References

1. Burke, J. E.; Dennis, E. A. *Cardiovasc. Drugs Ther.* **2009**, *23*, 49-59.
2. Calder, P. C. *Prostaglandins Leukot. Essent. Fat. Acids* **2008**, *79*, 101-108.
3. (a) Gentile, M. T.; Reccia, M. G.; Sorrentino, P. P.; Vitale, E.; Sorrentino, G.; Puca, A. A.; Colucci-D'Amato, L. *Mol. Neurobiol.* **2012**, *45*(3), 596-604; (b) Last, V.; Williams, A.; Werling, D. *BMC Neuroscience* **2012**, *13*, 106; (c) Stephenson, D.; Rash, K.; Smalstig, B.; Roberts, E.; Johnstone, E.; Sharp, J.; Panetta, J.; Little, S.; Kramer, R.; Clemens, J. *Glia* **1999**, *27*, 110-128; (d) Rao, J. S.; Kellom, M.; Reese, E. A.; Rapoport, S. I.; Kim, H.-W. *J. Affect. Disord.* **2012**, *136*, 63-71. (e) Chalimoniuk, M.; Stolecka, A.; Ziemnska, E.; Stepień, A.; Langfort, J.; Strosznajder, J. B. *J. Neurochem.* **2009**, *110*, 307.
4. (a) Sanchez-Mejia, R. O.; Newman, J. W.; Toh, S.; Yu, G.-Q.; Zhou, Y.; Halabisky, B.; Cisse, M.; Scearce-Levie, K.; Cheng, I. H.; Gan, L.; Palop, J. J.; Bonventre, J. V.; Mucke, L. *Nature Neurosci.* **2008**, *11*, 1311-1318. (b) McKew, J. C.; Lee, K. L.; Shen, M. W. H.; Thakker, P.; Foley, M. A.; Behnke, M. L.; Hu, B.; Sum, F.-W.; Tam, S.; Hu, Y.; Chen, L.; Kirincich, S. J.; Michalak, R.; Thomason, J.; Ipek, M.; Wu, K.; Wooder, L.; Ramarao, M. K.; Murphy, E. A.; Debra G. Goodwin; Albert, L.; Xu, X.; Donahue, F.; Ku, M. S.; Keith, J.; Nickerson-Nutter, C. L.; Abraham, W. M.; Williams, C.; Hegen, M.; Clark, J. D. *J. Med. Chem.* **2008**, *51*, 3388-3413. (c) Seno, K.; Okuno, T.; Nishi, K.; Murakami, Y.; Watanabe, F.; Matsuura, T.; Wada, M.; Fujii, Y.; Yamada, M.; Ogawa, T.; Okada, T.; Hashizume, H.; Kii, M.; Hara, S.-I.; Hagishita, S.; Nakamoto, S.; Yamada, K.; Chikazawa, Y.; Ueno, M.; Teshirogi, I.; Ono, T.; Ohtani, M. *J. Med. Chem.* **2000**, *43*, 1041-1044. (d) Ono, T.; Yamada, K.; Chikazawa, Y.; Ueno, M.; Nakamoto, S.; Okuno, T.; Seno, K. *Biochem. J.* **2002**, *363*, 727-735. (e) Ludwig, J.; Bovens, S.; Brauch, C.; Elfringhoff, A. S.; Lehr, M. *J. Med. Chem.* **2006**, *49*, 2611-2620. (f) Drews, A.; Bovens, S.; Roebrock, K.; Sunderkotter, C.; Reinhardt, D.; Schafers, M.; van der Velde, A.; Elfringhoff, A. S.; Fabian, J.; Lehr, M. *J. Med. Chem.* **2010**, *53*, 5165-5178.

5. (a) A study comparing 4 dose regimens of PLA-695, Naproxen, and Placebo in subjects with osteoarthritis of the knee. <http://clinicaltrials.gov/ct2/show/NCT00396955?term=NCT00396955&rank=1>. (b) Folmer, F.; Jaspars, M.; Schumacher, M.; Dicator, M.; Diederich, M. *Biochem. Pharmacol.* **2010**, *80*, 1793-1800. (c) Yazlovitskaya, E. M.; Linkous, A. G.; Thotala, D. K.; Cuneo, K. C.; Hallahan, D. E. *Cell Death Differ.* **2008**, *15*, 1641-1653. (d) Dennis, E. A.; Norris, P. C. *Nat. Rev. Immunol.* **2015**, *15*, 511-523. (e) <http://adisinsight.springer.com/drugs/800020059>.
6. (a) Fabian, J.; Lehr, M. *J. Pharm. Biomed. Anal.* **2007**, *43*, 601-605. (b) Bovens, S.; Elfringhoff, A. S.; Kaptur, M.; Reinhardt, D.; Schafers, M.; Lehr, M. *J. Med. Chem.* **2010**, *53*, 8298-8308. (c) Drews, A.; Bovens, S.; Roebrock, K.; Sunderkötter, C.; Reinhardt, D.; Schäfers, M.; Velde, A. V. D.; Elfringhoff, A. S.; Jörg, F.; Lehr, M. *J. Med. Chem.* **2010**, *53*, 5165-5178.
7. Ong, W. Y.; Farooqui, T.; Kokotos, G.; Farooqui, A. A. *ACS Chem. Neurosci.* **2015**, *6*, 814-831.
8. Sundaram, J. R.; Chan, E. S.; Poore, C. P.; Pareek, T. K.; Cheong, W. F.; Shui, G.; Tang, N.; Low, C. M.; Wenk, M. R.; Kesavapany, S. *The Journal of Neuroscience* **2012**, *32* (3), 1020 – 1034
9. Huang, W.; Bhavsar, A.; Ward, R. E.; Hall, J. C. E.; Priestley, J. V. & Michael-Titus A. T. *J. Neurotrauma* **2009**, *26*(8), 1429.
10. (a) Lapitskaya, M. A.; Vasiljeva, L. L.; Pivnitsky, K. K. *Synthesis* **1993**, 65-66. (b) Durand, S.; Parrain, J.-L.; Santelli, M. *Synthesis* **1998**, 1015-1018. (c) Jeffery, T.; Gueugnot, S.; Linstrumelle, G. *Tetrahedron Lett.* **1992**, *33*, 5757-5760. (d) Qi, L.; Meijler, M.M.; Lee, S.H.; Sun, C.; Janda, K.D. *Org. Lett.* **2004**, *6*, 1673-1675.
11. (a) Singh, R. P.; Cao G.; Kirchmeier, R. L.; Shreeve, J. M. *J. Org. Chem.* **1999**, *64*, 2873-2876. (b) Krishnamurti, R.; Bellew, D. R.; Prakash, G. K. S. *J. Org. Chem.* **1991**, *56*, 984-989 (c) Reeves, J. T.; Song, J. J.; Tan, Z.; Lee, H.; Yee, N. K.; Senanayake, C. H. *J. Org. Chem.* **2008**, *73*, 9476-9478.

12. (a) Boivin, J.; Kaim, L. E.; Zard, S. Z. *Tetrahedron Lett.* **1992**, *33*, 1285-1288. (b) Ackermann, E. J.; Conde-Frieboes, K.; Dennis, E. A. *J. Biol. Chem.* **1995**, *270*, 445-450.
13. Porter N. A.; Lehman L. S.; Weber B. A.; Smith K. *J. Am. Chem. Soc.*, **1981**, *103*, 6447 – 6455.
14. Connolly, S.; Bennion, C.; Botterell, S.; Croshaw, P.J.; Hallam, C.; Hardy, K.; Hartopp, P.; Jackson, C.G.; King, S.J.; Lawrence, L.; Mete, A.; Murray, D.; Robinson, D.H.; Smith, G.M.; Stein, L.; Walters, I.; Wells, E.; Withnall, W.J. *J. Med. Chem.* **2002**, *45*, 1348 – 1362.
15. Street, I. P.; Lin, H. K.; Laliberte, F.; Ghomashchi, F.; Wang, Z.; Perrier, H.; Tremblay, N. M.; Huang, Z.; Weech, P. K.; Gelb, M. H. *Biochemistry* **1993**, *32*, 5935-5940.
16. Pickard, R. T.; Chiou, X. G.; Striffler, B. A.; DeFelippis, M. R.; Hyslop, P. A.; Tebbe, A. L.; Yee, Y. K.; Reynolds, L. J.; Dennis, E. A.; Kramer, R. M.; Sharp, J. D. *J. Biol. Chem.* **1996**, *271*, 19225-19231.
17. Dessen, A.; Tang, J.; Schmidt, H.; Stahl, M.; Clark, J. D.; Seehra, J.; Somers, W. S. Crystal structure of human cytosolic phospholipase a_2 reveals a novel topology and catalytic mechanism. *Cell* **1999**, *97*, 349-360.
18. Yu, L.; Deems, R. A.; Hajdu, J.; Dennis, E. A. The interaction of phospholipase A_2 with phospholipid analogues and inhibitors. *J. Biol. Chem.* **1990**, *265*, 2657-2664.
19. Di Penta, A.; Moreno, B.; Reix, S.; Fernandez-Diez, B.; Villanueva, M.; Errea, O.; Vandebroek, K.; Comella, J. X.; Villosalada, P. *PLoS One* **2013**, *8*, e54722.
20. Yao, L.; Kan, E. M.; Lu, H.; Hao, A.; Dheen, S. T.; Kaur, C.; Ling E. A. *J. Neuroinflammation* **2013**, *10*, 23.
21. Chuang, D. Y.; Simonyi, A.; Kotzbauer P. T.; Gu, Z.; Sun, G. Y., *J. Neuroinflammation* **2015**, *12*, 199.

22. (a) Hsu, H-Y.; Wen, M-H. *J. Biol. Chem.* **2002**, *277*, 22131-22139. (b) Gao, F.; Chen, D.; Hu, Q.; Wang, G. *PLOS One* **2013**, *8* (8), 72046.
23. Bicker, J.; Alves, G.; Fortuna, A.; Patricio, S.; Falcao, A. *Int. J. Pharm.* **2016**, *501*(1-2), 102-111.
24. <http://www.rcsb.org/pdb/explore/sequence.do?structureId=1CJY>
25. (a) Sun, G. Y.; He, Y.; Chuang, D. Y.; Lee, J. C.; Gu, Z.; Simonyi, A.; Sun, A. Y. *Mol. Neurobiol.* **2012**, *46*(1), 85-95. (b) Love, R. *Lancet Neurol.* **2004**, *3*(4) 199.
26. Yoshida T.; Murai M.; Abe M.; Ichimaru N.; Harada T.; Nishioka T.; Miyoshi H. *Biochemistry* **2007**, 10365 – 10372.
27. Sali, A.; Blundell, T. L. *J Mol Biol.* **1993**, *234*, 779 – 815.
28. Kaminski, G. A.; Friesner, R. A.; Tirado-Rives, J.; Jorgensen, W. L. *J. Phys. Chem. B* **2001**, *105*, 6474 – 6487.
29. *Schrodinger*, version 9.0, Schrödinger, LLC, New York, NY, **2009**.
30. Friesner, R. A.; Banks, J. L.; Murphy, R. B.; Halgren, T. A.; Klicic, J. J.; Daniel, T.; Repasky, M. P.; Knoll, E. H.; Shelley, M.; Perry, J. K. *J. Med. Chem.* **2004**, *47*, 1739 – 1749.
31. Case, D.; Pearlman, D. A.; Caldwell, J. W., *Amber 11*. University of California, San Francisco.
32. Duan, Y.; Wu, C.; Chowdhury, S.; Lee, M. C. K; Xiong, G.; Zhang, W.; Yang, R.; Cieplak, P.; Luo R.; Lee, T.; Caldwell, J.; Wang, J.; Kollman, P. *J. Comp. Chem.* **2003**, *24*, 1999 – 2012.
33. Jorgensen, W. L.; Chandrasekhar, J.; Madura, J. D.; Impey, R.W.; Klein, M. L. *J. Chem. Phys.* **1983**, *79*, 926 – 935.
34. Darden, T.; York, D.; Pedersen, L. *J. Chem. Phys.* **1993**, *98*, 10089 – 10092.

35. Miyamoto, S.; Kollman, P. A. *J. Comp. Chem.* **1992**, *13*, 952 – 962.
36. Feig, M.; Karanicolas, J.; Brooks, C. L. *J. Mol. Graph. Model.* **2004**, *22*, 377 – 395.
37. Humphrey, W.; Dalke, A.; Schulten, K. *J. Mol. Graph. Model.* **1996**, *14*, 33 – 38.
38. De, Lano, W., The PyMOL molecular graphics system. San Carlos CA, USA: De Lano Scientific. **2002**.

CHAPTER 3: CHEMICAL SYNTHESIS AND BIOLOGICAL EVALUATION OF FLUOROGENIC CYTOSOLIC PHOSPHOLIPASE A₂ INHIBITORS AND SUBSTRATE

3.1 Introduction

Arachidonic acid (AA) is a precursor of a family of lipid mediators, including prostaglandins, that regulates a wide variety of physiological responses and disease pathogenesis.¹ The generation of free AA occurs mainly through the activation of phospholipase A₂ (PLA₂) which catalyzes the hydrolysis of the sn-2 acyl ester bond of glycerophospholipids to release AA. Mammalian cells have diverse forms of PLA₂ including the secreted small molecular weight sPLA₂, the larger cytosolic Ca²⁺-dependent cPLA₂ and Ca²⁺-independent iPLA₂. Although sPLA₂ could participate in the release of arachidonate during injury, the main gatekeeper for the enzymatic conversion of arachidonate is cPLA₂.² Given that cPLA₂ is an ubiquitous enzyme which is highly selective for glycerophospholipids containing AA, there has been much interest to design and identify cPLA₂ inhibitors to better understand the molecular mechanism regulating this enzyme and to develop efficacious therapeutics for the treatment of cPLA₂-upregulated diseases.³⁻⁶ To this end, we are interested to identify novel chemical tools, particularly fluorescent probes which could provide a means to monitor cPLA₂ activity. To our knowledge, Chiorazzo *et al* have recently reported a cPLA₂ activatable fluorophore for imaging cPLA₂ in triple negative breast cancer cells.⁷ Herein, we present our works on fluorescent inhibitor and substrate probes for the direct detection of cPLA₂ at cellular level and for the study of cPLA₂ inhibition. We herein present the synthesis of inhibitor probes and substrate probe of cPLA₂ and the investigation of these compounds for (i) inhibition of cPLA₂ (ii) cytotoxicity (iii) specific functionality and (iv) imaging tool.

3.2 Chemical Synthesis

3.2.1 Synthetic Strategy

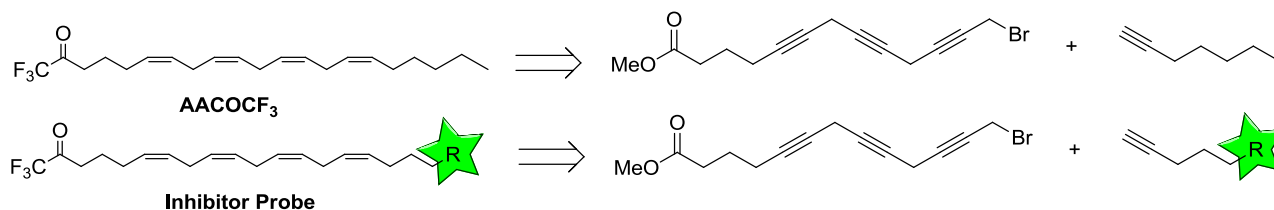


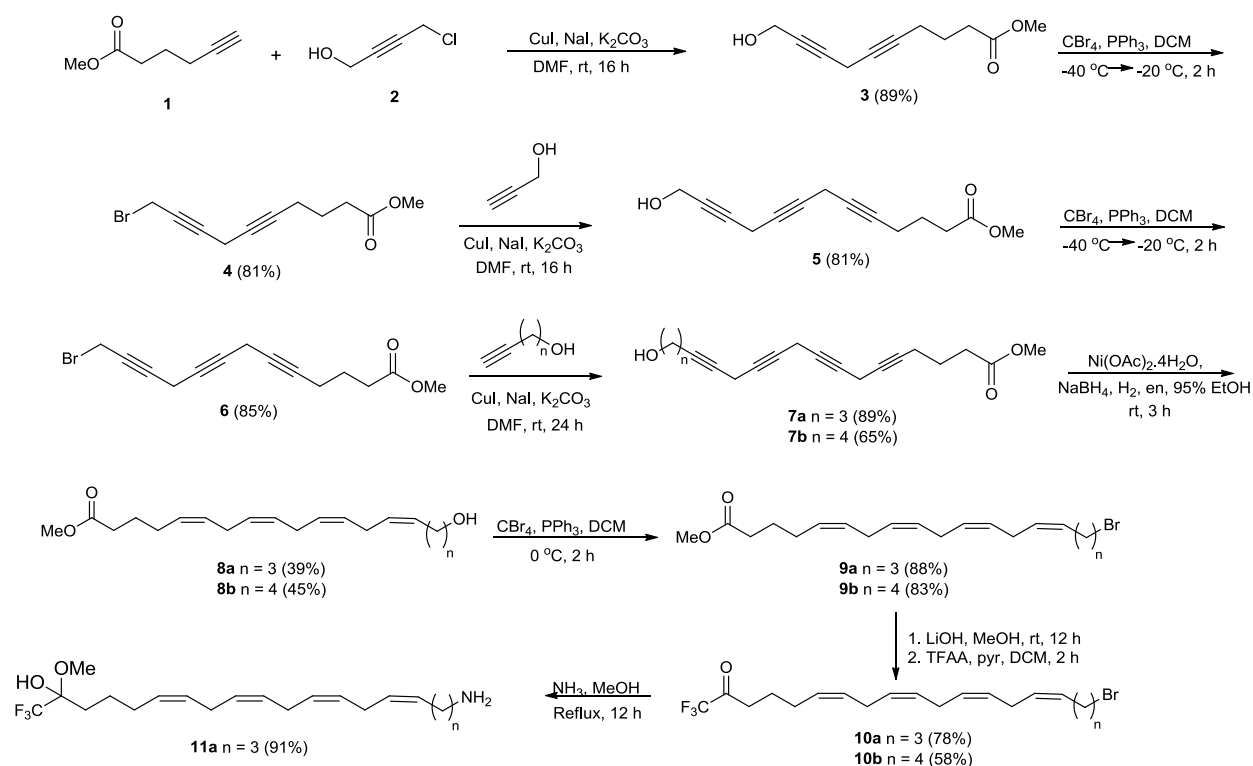
Figure 3-1: Structure of AACOCF₃ and inhibitor probes

Arachidonyl trifluoromethyl ketone (AACOCF₃), a potent inhibitor of cPLA₂ has been shown to cause a reduction in neuronal losses through decreased oxidative stress and inflammation upon inhibiting cPLA₂ in mouse model of spinal cord injury.⁸ This suggests its ability to penetrate the blood-brain barrier and was thus chosen as the scaffold for our cPLA₂ inhibitor probe. In the design of our fluorogenic inhibitor probe (Figure 3-1), the arachidonyl functionality was used to promote enzyme recognition, a trifluoromethylketone moiety was incorporated to inhibit the active site of cPLA₂ and a fluorogenic group was attached to the distal end of the alkyl chain so that it does not hinder interactions with the enzyme's active site. A representative number of inhibitor probes were synthesized and screened for their inhibitory activities. Synthesis of the inhibitor probes mimics the synthesis of compounds in chapter 2 by coupling the main triple alkyne intermediate with a functionalized alkyne instead of heptyne (Figure 3-1). In this way, the functionalized alkyne could be further modified and coupled with various fluorogenic groups to yield inhibitor probes bearing both the trifluoromethylketone and arachidonyl moiety after subsequent transformation.

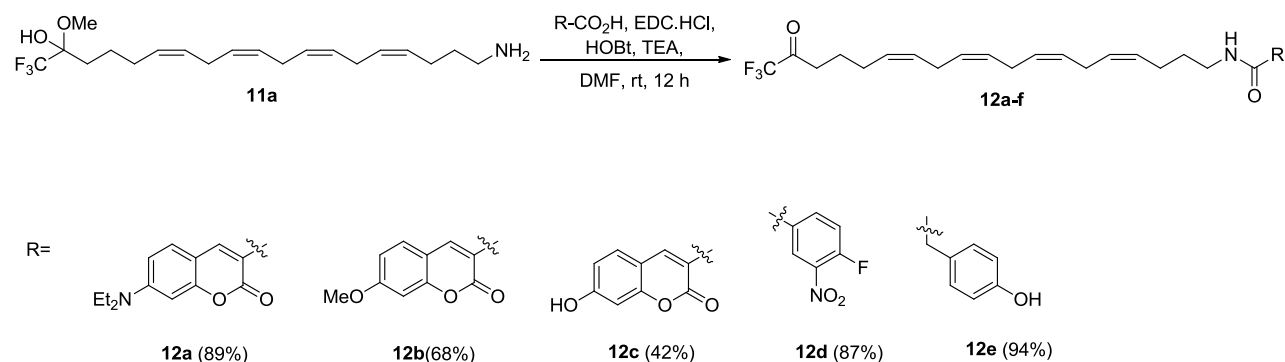
3.2.2 Synthesis of the inhibitor probe

Similar to the previous chapter, the chemical synthesis of these compounds (Scheme 3-1) involved a series of copper-catalyzed coupling and bromination of the alkyne building blocks to achieve a quadruple alkyne intermediate **7a** and **7b**. They were subsequently hydrogenated with Brown's catalyst to form the respective alkene **8a** and **8b**. Upon bromination of the alcohol present in **8** to **9a** and **9b**, the methyl ester was converted into trifluoromethyl ketone by hydrolyzing the ester (**9a** and

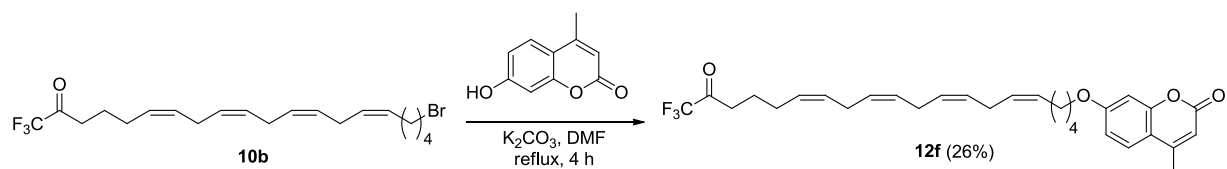
19) to an intermediate carboxylic acid and reacting it with trifluoroacetic anhydride in the presence of pyridine. The alkyl tail end of the alkene, functionalized with either a Br or NH₂ group could then be readily coupled to a fluorophore via Williamson-ether synthesis or an amide coupling reaction (Scheme 3-2 and 3-3). This ensures an efficient synthesis of these relatively complex inhibitor-probes where the synthetic route was made divergent. The scheme's divergence stems from how the various inhibitor probes share a common precursor (**11a**). Six fluorogenic inhibitors (**12a-f**) were synthesized and their inhibitory activities were tested with recombinant cPLA₂ via a PLA₂ assay.



Scheme 3-1. Synthesis of common intermediates before coupling with fluorogenic probes.



Scheme 3-2. Synthesis of inhibitor probes **12a-e** via amide coupling.



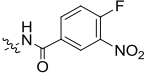
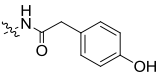
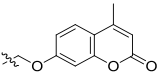
Scheme 3-3. Synthesis of inhibitor probe **12f**.

3.3 Biological Result of cPLA₂ assay and sPLA₂ selectivity

Probe-inhibitors **12a-f** were sent for screening, and their respective % enzymatic activity values are tabulated in Table 3-1. Probe-inhibitors with O-substituted aromatic rings tended to exhibit higher % inhibition and hence higher potency. **7OHCou-AACF3** exhibited the highest potency, with a % inhibition value of 95.8 ± 0.8 at a concentration of $10 \mu\text{M}$. This also suggests that the hydroxyl-coumarin fluorophore would have the best interactions with cPLA₂ if it was incorporated into the substrate-probe at the unsaturated tail. **7OHCou-AACF3** also has an IC₅₀ of $12.5 \pm 1.0 \mu\text{M}$ (Figure 3-2). This is comparable to AACOCF₃ which has an IC₅₀ of $16.5 \pm 3.0 \mu\text{M}$. Selectivity test with recombinant sPLA₂ at $10 \mu\text{M}$ showed that **7OHCou-AACF3** did not give an observable bioactivity with sPLA₂ (Figure 3-3) indicating that it is not sPLA₂ selective.

Table 3-1. % activity towards cPLA₂ in the presence of different test compounds at $10 \mu\text{M}$ were tested in a PLA₂ assay at n=4

Entry	R	% Activity	% Inhibition
1		59.4 ± 4.0	40.6 ± 4.0
2		42.8 ± 7.2	57.2 ± 7.2
3		6.2 ± 0.8	95.8 ± 0.8

4		11.9 ± 1.3	88.1 ± 1.3
5		10.1 ± 1.8	89.9 ± 1.8
6		19.1 ± 3.6	80.9 ± 3.6

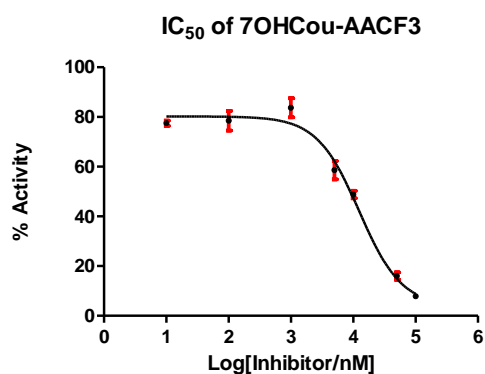


Figure 3-2. IC₅₀ of 7OHCou-AACF3 determined to be $12.5 \pm 1.0 \mu\text{M}$ at $n=4$

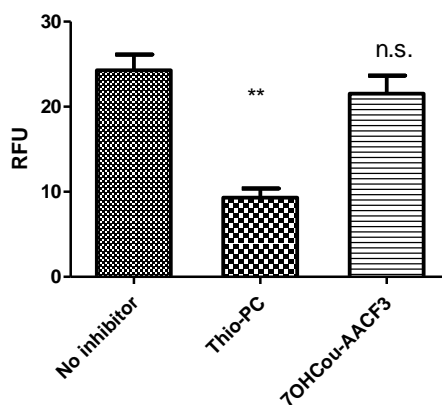


Figure 3-3. Inhibition activity of 7OHCou-AACF3 on sPLA₂ at $10 \mu\text{M}$ compared with sPLA₂ specific inhibitor Thioetheramide-PC (Thio-PC) at $10 \mu\text{M}$. Data analyzed by one-way ANOVA with Bonferroni's Multiple Comparison Test indicated no statistical difference between control (CTR) and 7OHCou-AACF3 while a decrease in activity was observed between CTR and Thio-PC column (** $P < 0.01$).

3.4 Inhibitory ability of 7OHCou-AACF3

Next, we evaluated the inhibitory property of **7OHCou-AACF3** on cPLA₂ in lipopolysaccharide (LPS) stimulated mouse microglial BV-2 cells. Earlier study have shown that BV-2 cells upon LPS insult resulted in an increase in inducible nitric oxide synthase (iNOS) which produces excess nitric oxide (NO) causing neurotoxicity. Upon application of a cPLA₂ specific inhibitor, the protein level of iNOS was found to decrease, demonstrating its ability to mediate the effects of NO. Similarly, when **7OHCou-AACF3** (10 μM) was incubated with BV-2 cells in the presence of LPS, the level of iNOS decreased to less than 20% (Figure 3-4) showing its potential neuroprotective ability through the inhibition of cPLA₂. This is further supported by cell viability assay (*vide infra*).

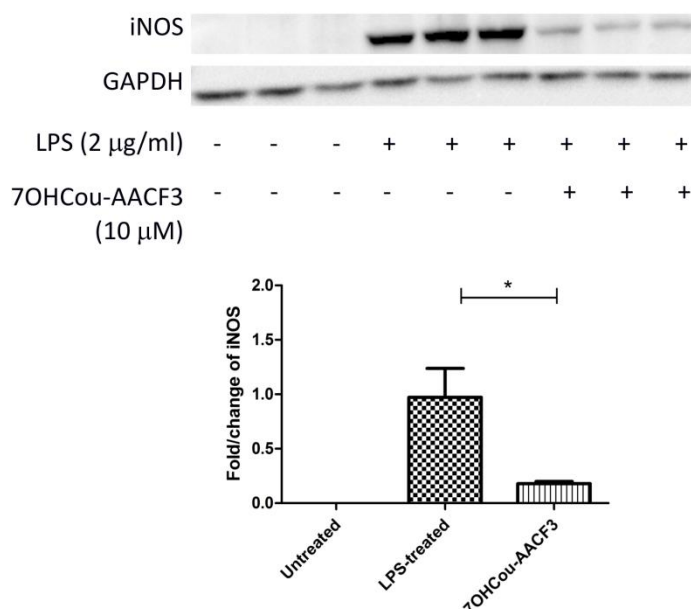
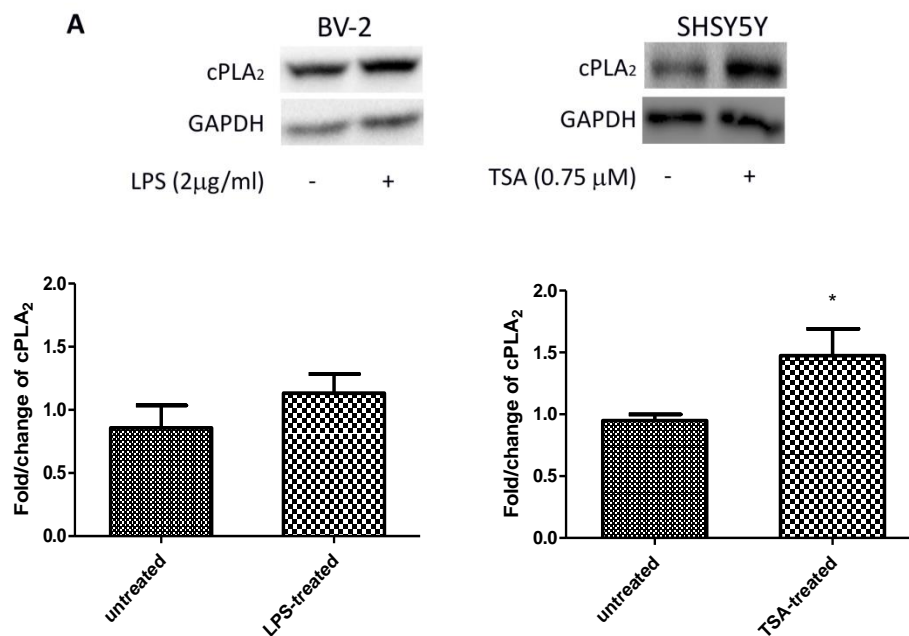


Figure 3-4. Western blot of 3 independent experiments showing protein bands of iNOS and GAPDH when BV-2 cells were stimulated with 2 μg/mL of LPS in the presence or absence of 10 μM **7OHCou-AACF3**. The procedure used was adapted from Chuang *et al.*⁹ Data analyzed by one-way ANOVA with Bonferroni's Multiple Comparison Test indicate statistical difference between LPS-treated and LPS-treated with **7OH-CouAACF3** (*P<0.05).

3.5 7OHCou-AACF3 as a fluorescent dye for imaging

To explore the use of **7OHCou-AACF3** as an imaging tool, two cell lines, BV-2 and SHSY5Y, were treated with different stimulants and stained with **7OHCou-AACF3** (10 μ M) (Figure 3-5). The cPLA₂ levels were found to be not statistically different in the control (untreated BV-2 cells), the LPS-stimulated and **7OHCou-AACF3**-treated LPS-stimulated BV-2 cells whilst in the SHSY5Y cells, the TSA-treated cells were stained more significantly than the non-TSA-treated cells. These results corroborated with the Western blot data (Figure 3-5A(i) and 3-5A(ii)) are in agreement with earlier study which showed that stimulating BV-2 microglial cells with LPS induces cPLA₂ phosphorylation but does not increase the cPLA₂ level⁹ whilst treating SHSY5Y with histone deacetylase inhibitor, trichlorostatin A (TSA) results in an overexpression of cPLA₂.¹⁰



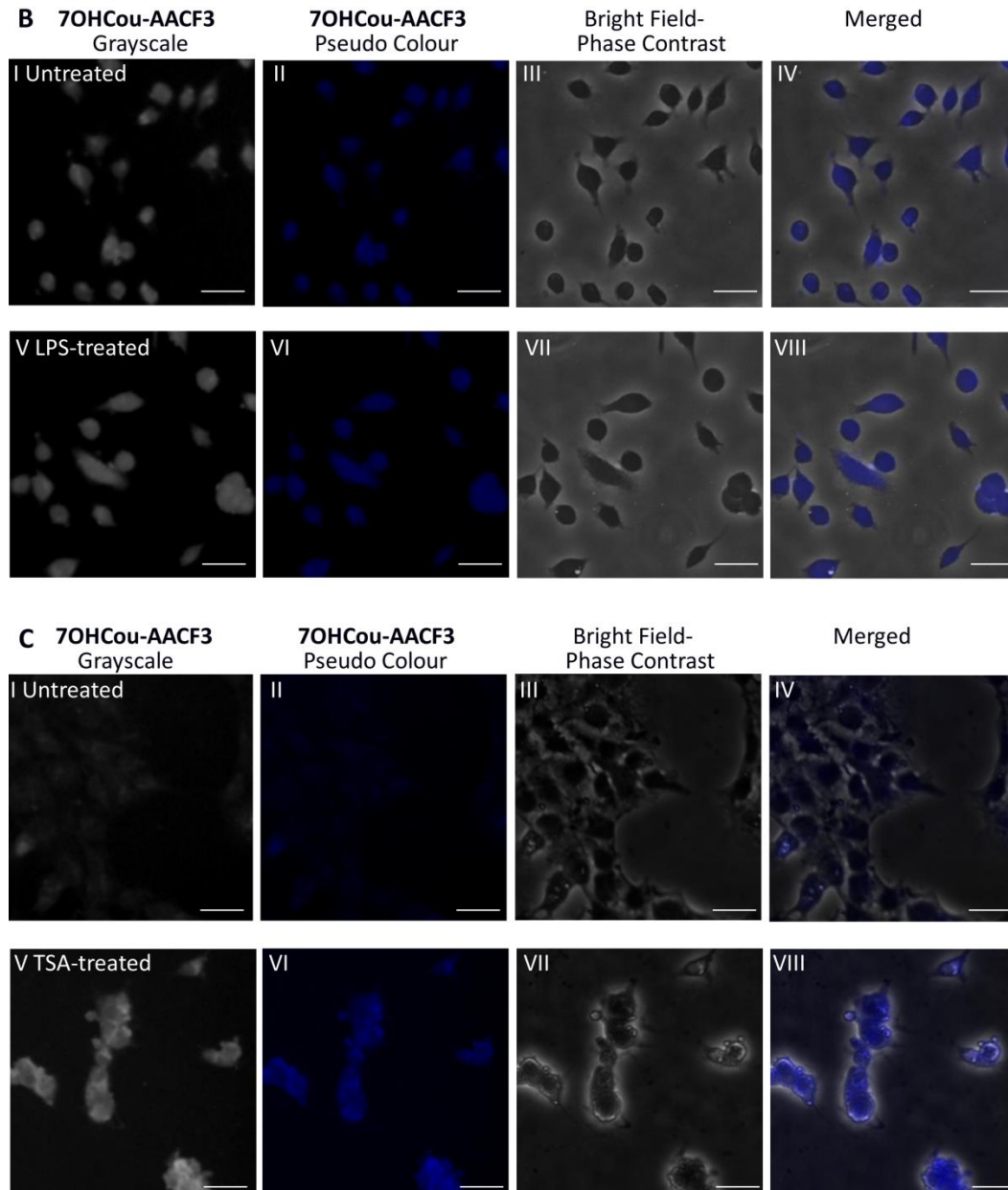


Figure 3-5. Western blot and fluorescence imaging of BV-2 and SHSY5Y cells (A)(i) Representative western blot of 3 independent experiments of cPLA₂ in BV-2 cells stimulated with 2 µg/mL of LPS were normalized with GAPDH. Data analysis by paired t-test indicated no statistical difference between the untreated and LPS-treated cells. (ii) Representative western blot of 3 independent experiments of cPLA₂ in SHSY5Y cells treated with 0.75µM TSA vs control indicate TSA-treated cells have higher level of cPLA₂. Data analysis by paired t-test indicated statistical difference between the untreated and TSA-treated cells (*P<0.05). (B) Imaging of non-treated BV-2 cells vs LPS-treated BV-2 cells after staining with 7OHCou-AACF3 (10µM). No difference in staining

was detected. (C) Imaging of non-treated SHYS5Y cells vs TSA-treated cells after staining with **7OHCou-AACF3** (10 μ M). TSA-treated cells show a larger extent of staining due to higher level of cPLA₂ present compared with the non-treated cells. (I) & (V) Grayscale images with excitation at 358nm. (II) & (VI) Blue pseudo colour images with excitation at 358nm (III) & (VII) Bright-field phase contrast of cells. (IV) and (VIII) Merged images of **7OHCou-AACF3** pseudo colour and bright-field phase contrast images. Images were captured on a LEICA EMCCD camera. Scale bar represent 30 μ m.

3.6 Design and synthesis of substrate probe Flu7OHCou

Despite the varied functions **7OHCou-AACF3** could perform, monitoring the activity of active cPLA₂ would be difficult. Encouraged by the aforementioned results, we decided to expand our studies by developing a substrate probe to measure cPLA₂ activity. The conventional assay of cPLA₂ activity uses 1-palmitoyl-2-[¹⁴C]-arachidonoyl phosphatidylcholine as a substrate. The radiolabeled arachidonate released during the reaction was recovered through aqueous extraction and the released radioactivity was determined by liquid scintillation counting.¹¹⁻¹² However the use of radiometric assays is highly undesirable due to the hazards surrounding radioactive materials. It would thus be desirable to develop a simpler assay which does not use radioisotopes for screening cPLA₂ activities. Various calorimetric and fluorogenic assay kits for the measurement of cPLA₂ activity are now commercially available. However these assays are not selective to cPLA₂ and thus there is a need to develop an alternative probe.¹³

Since **7OHCou-AACF3** has the highest potency amongst the fluorogenic inhibitor probes synthesized, we hypothesized that having the arachidonoyl and 7-hydroxycoumarin moieties in the substrate could potentially lead to stronger binding with cPLA₂. Hence we designed the substrate probe **Flu7OHCou** (Scheme 3-4 to 3-6) to comprise of a glycerylphosphorylcholine (GPC) scaffold attached to an arachionyl moiety to confer selectivity towards cPLA₂. To enable ratiometric measurement, two compatible fluorogenic groups were placed at the alkyl chain end of the fatty acids esterified to the GPC moiety. Since **7OHCou-AACF3** possesses an emission maximum at 447 nm,

fluorescein was chosen as the other fluorophore since its absorption maximum is at 458 nm, making it suitable for Förster resonance energy transfer (FRET) (Figure 3-6). FRET is highly distance-dependent and is disrupted during subsequent cleavage of the substrate (at the acyl ester bond) by cPLA₂, which separates the fluorophore donor-acceptor pair. The resulting changes in fluorescent signal can be tracked and used to measure cPLA₂ activity. FRET substrate-probes showed great promise in measuring enzyme activity, and have been successfully used in past work.¹⁴ Such probes have exceedingly high sensitivities, owing to the accumulative nature and the amplification effects of the enzymatic catalysis.¹⁴ As the substrate-probes incorporate the same arachidonyl backbone and 7-hydroxycoumarin found in **7OHCou-AACF3**, synthesis of the inhibitor-probes facilitates synthesis of the subsequent substrate-probe. The convergence of the substrate-probe's synthetic route, could thus arise from how the compounds are first prepared in separate fragments – the skipped alkene backbone, the phosphate backbone, the fluorophores, and the long alkyl tail – before being coupled together to form the final substrate-probe analogue.

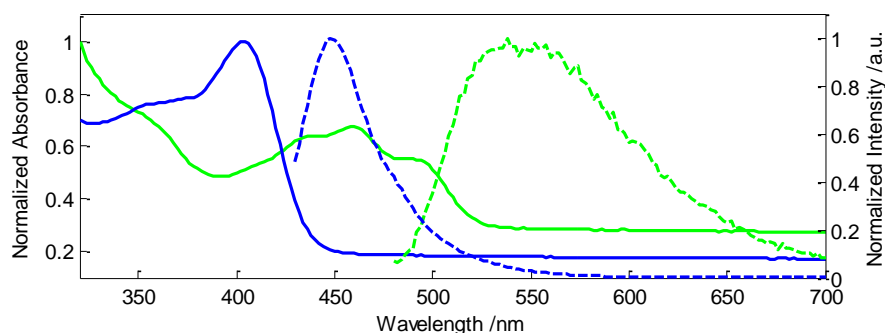
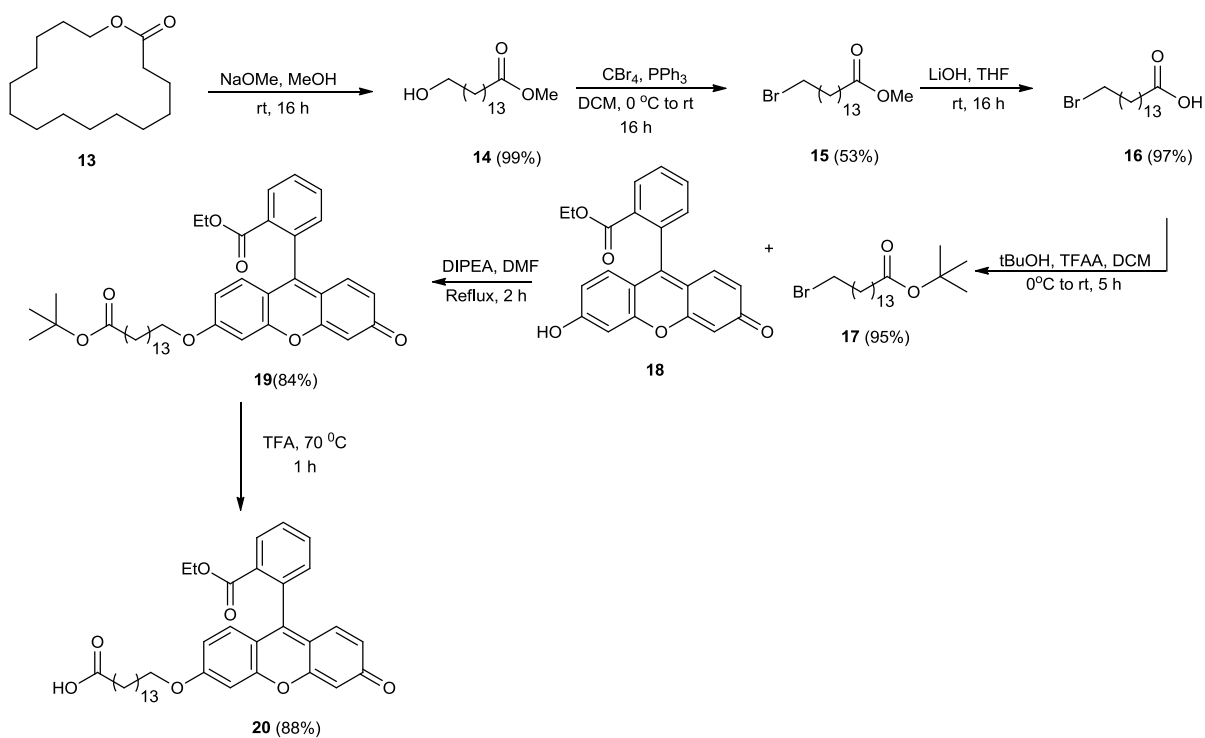
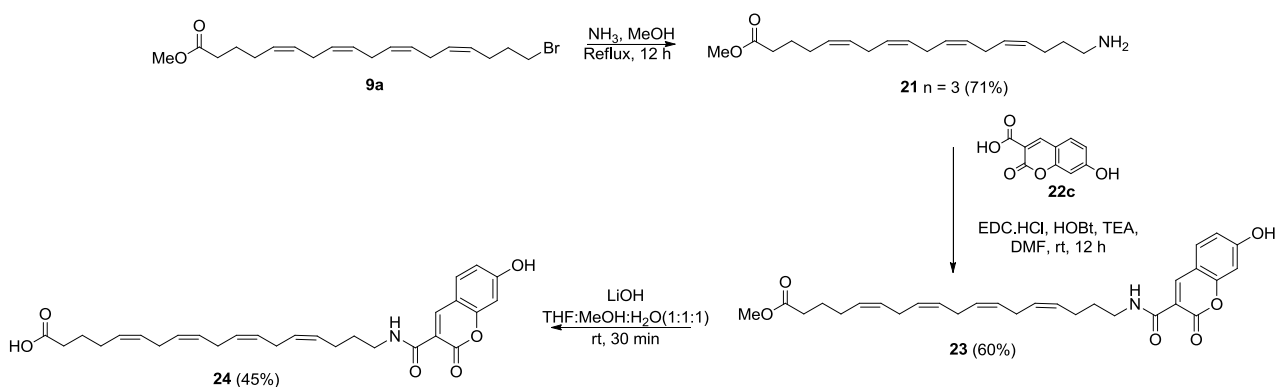


Figure 3-6. Absorbance and Emission graphs of donor and acceptor of the substrate **Flu7OHCou**.

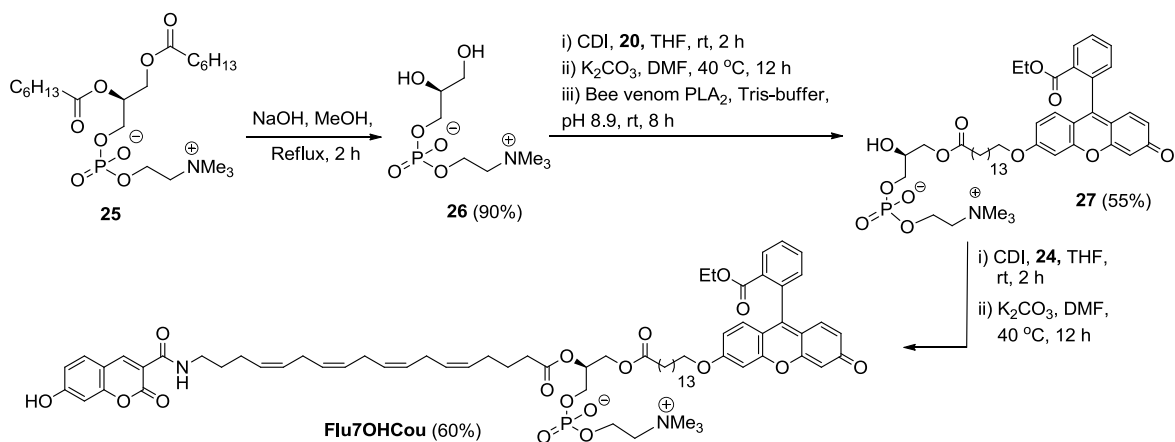
Absorbance (—) and Emission (- -) spectra of 7-hydroxycoumarin (blue) and fluorescein (green) in water.



Scheme 3-4. Synthesis of carboxylic acid **20**



Scheme 3-5. Synthesis of fluorogenic carboxylic acids **24**.



Scheme 3-6. Synthesis of substrate probe **Flu7OHCou**.

Flu7OHCou was prepared by separately synthesizing 3 different fragments of the compound simultaneously and attaching them together via esterification reactions. The fluorogenic carboxylic acid **20** was synthesized by ring opening **13** via a hydrolysis reaction followed by bromination of the alcohol present in **14** into **15**. In order to yield **20**, the ester on **15** needs to be orthogonally hydrolyzed in the presence of the ethyl ester present on the fluorescein moiety. In light of this, **15** was converted into a tert-butyl ester by hydrolyzing it into the carboxylic acid **16** and protecting the acid with tert-butanol to form **17**. This then allowed the fluorescein **18** to be attached to **17** via a S_N2 displacement of the Br followed by selective deprotection of the t-butyl ester by refluxing it in TFA to yield **20** (Scheme 3-4). The unsaturated acid **24** was synthesized by replacing the Br in **9a** into an NH₂ followed by an amidation reaction with 7-hydroxycoumarin **22c**. Hydrolysis of **23** yielded the unsaturated carboxylic acid **24** (Scheme 3-5). To obtain the substrate probe **Flu7OHCou**, 1,2-diheptanoyl-*sn*-glycero-3-phosphocholine **25** was hydrolysed to glycerylphosphorylcholine **26** with methanolic sodium hydroxide. Esterification of the hydroxyl groups on **26** with fluorescein **20** gave predominantly **27** and some di-esterified product. Treating the mixture of **27** and di-esterified product with commercial bee venom PLA₂ selectively hydrolyzed the ester on the secondary alcohol, thus converting the di-esterified product to **27**. Esterification of **27** with **24** provided **Flu7OHCou** in 30% overall yield (Scheme 3-6).

3.7 MTS assay of 7OHCou-AACF3 and Flu7OHCou

7OHCou-AACF3 and **Flu7OHCou** were evaluated for their cytotoxicities against the BV-2 cells after 48 h and 72 h of treatment. Results showed that more than 80% of the cells survived after both the time-points (Figure 3-7), indicating that both compounds are non-cytotoxic.

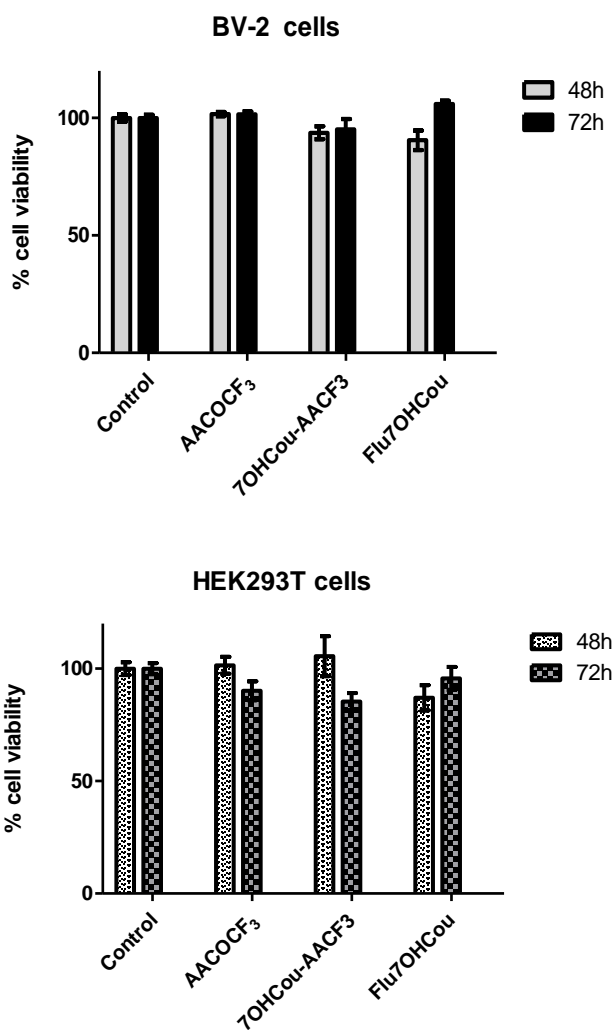


Figure 3-7. MTS assay conducted on AACOCF₃, 7OHCou-AACF₃ and Flu7OHCou on 2 different cell lines at different time points. Compounds were adjusted to final concentration of 10 μ M. Results were obtained from three independent biological repeats (mean \pm SEM). Data analyzed by one-way ANOVA with Bonferroni's Multiple Comparison Test showed no significant difference among the samples. There was no statistical difference among various treatments in both cell lines.

3.8 Flu7OHCou as a substrate for monitoring cPLA₂ activity

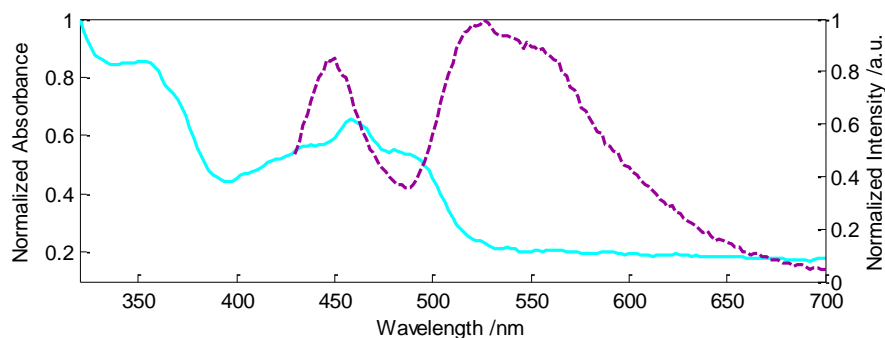


Figure 3-8. Absorbance (—) and Emission (- - -) of the substrate probe **Flu7OHCou** in aqueous Tris-buffer, 1% Triton X.

Next, the photophysical property of **Flu7OHCou** was examined by constituting it in a 20 μM Tris-HCl (50 mM Tris-HCl, 100 mM NaCl, 20 mM CaCl_2) liposomal system containing 1% Triton X-100 at pH 7.3. The liposomes were formed by mixing 10 mM dioleoylphosphatidylcholine (DOPC), 10mM dioleoylphosphatidylglycerol (DOPG) and 20 μM of **Flu7OHCou** together and vigorously vortexed in the Triton X-100 containing buffer. Under these conditions, an appreciable blue fluorescence (447nm) was detected from the donor 7-hydroxycoumarin while the rest of the emission (520nm) came from the green fluorescein acceptor when irradiated at 410 nm (Figure 3-8 and Figure 3-9A). The addition of Triton X-100 enables the formation of small liposomes which facilitate FRET between the 2 fluorophores. When PLA₂-rich bee venom (5 units/mL) was added to the liposomal system containing **Flu7OHCou**, the fluorescence intensity changed from a quantum yield of 0.04 to 0.08. This indicated a successful cleavage of the donor from the substrate, as irradiation at the donor's excitation wavelength lead to successful emission instead of losses due to FRET transfer when the acceptor is no longer at close proximity. The reaction was largely completed within 45min and no further changes were observed in the emission spectra. This demonstrates the potential of **Flu7OHCou** to be used as a PLA₂ substrate probe. These results are also congruent with earlier observations which showed that a membrane-like environment is essential for cPLA₂ to recognize the substrate, highlighting the need to convert the substrate into liposomes.^{11,15}

To investigate if **Flu7OHCou** is a substrate to cPLA₂, the same assay was treated with 0.05 unit/mL of recombinant cPLA₂. No activity was detected even when the pH of the buffer was increased to 8.9 to encourage higher PLA₂ activity (Figure 3-9B(i)).¹⁶ This loss of activity was attributed to Triton X-100 which has been shown previously to abolish cPLA₂ activity.¹⁷ To confirm this hypothesis, a 20 μM liposomal Tris-HCl (50 mM Tris-HCl, 100 mM NaCl, 20 mM CaCl₂, pH 8.9) buffer solution of **Flu7OHCou** without Triton X-100 was prepared and added to 0.05 unit/mL of recombinant cPLA₂. This led to a significant fluorescence increase from 331 to 554 RFU, confirming that Triton X-100 had resulted in the loss of cPLA₂ activity. (Figure 3-9B(ii)) These results also suggest the possibility of developing an assay with **Flu7OHCou** that uses Triton X-100 to isolate out the cPLA₂'s activity without the need of an inhibitor.

To investigate the cPLA₂-selectivity of **Flu7OHCou**, 0.05 unit/mL of cPLA₂ and sPLA₂ were added to the liposomal substrate solution without Triton X-100. A large increase in fluorescence intensity was observed from the liposomal solution containing cPLA₂ while the liposomal solution containing sPLA₂ exhibited only a smaller increase in fluorescence intensity as time increases (Figure 3-9C(i)). The opposite result was observed, where a larger increase in fluorescence intensity for the solution containing sPLA₂ was detected, when 1% Triton X-100 is present (Figure 3-9C(ii)). These results indicate that **Flu7OHCou** has a higher selectivity to cPLA₂ than sPLA₂ in the absence of Triton X-100 while the same result could be reversed in 1% Triton X-100. This suggests the potential of differentiating cPLA₂ and sPLA₂ via an assay with the use of Triton X-100.

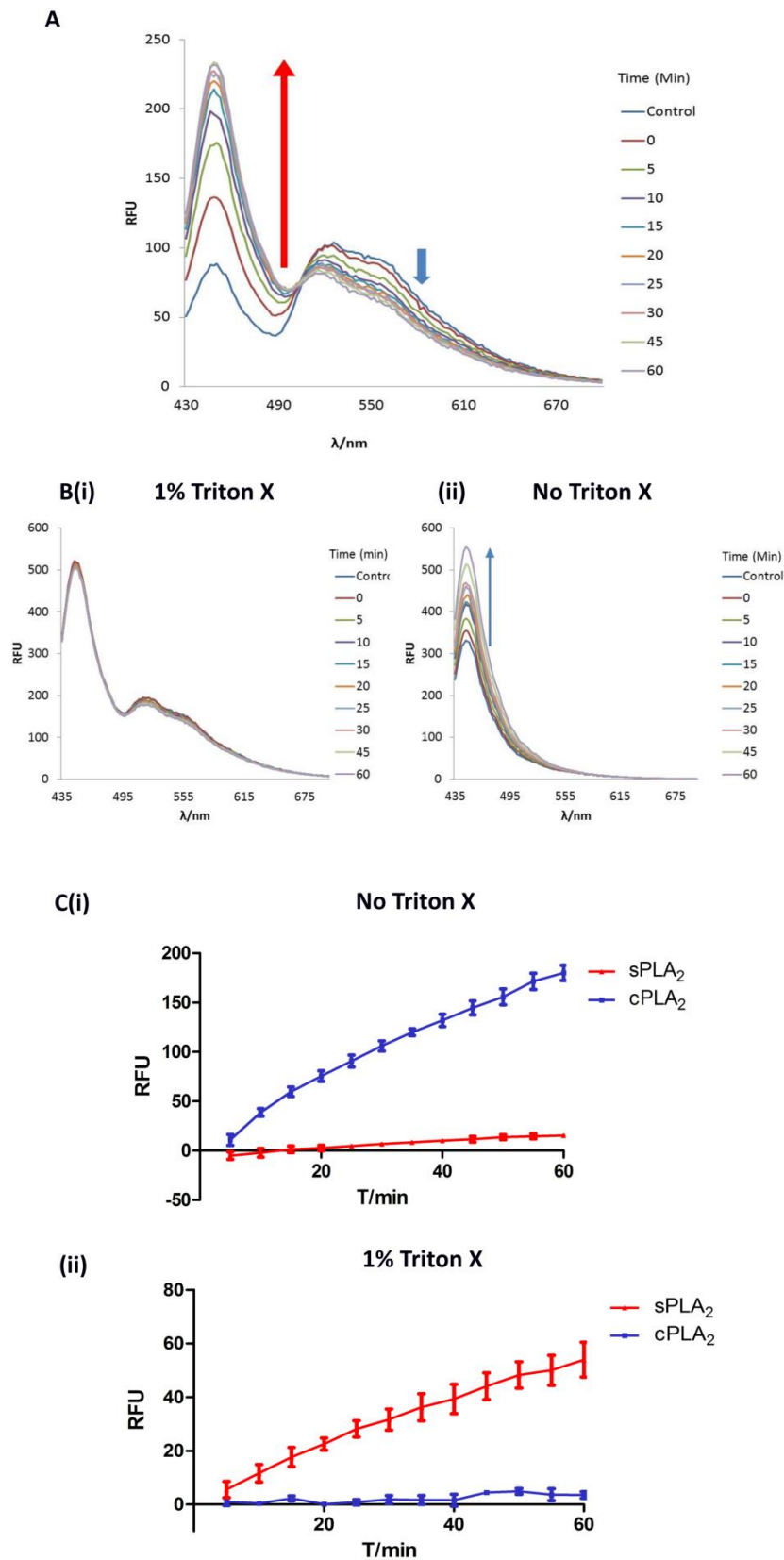


Figure 3-9. Photophysical property of **Flu7OHCou**. (A) - Addition of bee venom (5 units/mL) to 20 μ M **Flu7OHCou** constituted in a liposome formed by vortexing DOPG and DOPC in a Tris-HCl

buffer, pH 7.3 with 1% Triton X-100. Donor peak increases significantly as time increase from 0min to 60min while acceptor peak decrease with time. (B) - Addition of recombinant cPLA₂ (0.05 unit/mL) to 20μM **Flu7OHCou** constituted in a liposome formed by vortexing DOPG and DOPC in a Tris-HCl buffer, pH 8.9 (i) with 1% Triton X-100, (ii) without Triton X-100 (C) - Addition of recombinant cPLA₂ and sPLA₂ (0.05 unit/mL) to 20μM **Flu7OHCou** constituted in a liposome formed by vortexing DOPG and DOPC in a Tris-HCl buffer, pH 8.9 (i) without Triton X-100 (ii) with 1% Triton X-100.

To further examine the possible use of **Flu7OHCou** for inhibitor screening experiments, we proceeded to determine the IC₅₀ of AACOCF₃ by incubating **Flu7OHCou** in a liposomal solution with recombinant cPLA₂ and varying amount of AACOCF₃. By plotting a dose-response curve, the IC₅₀ was found to be 19.0 ± 1.5 μM which is in good agreement with our experimental data of 16.5 ± 3.0 μM determined via the commercial PLA₂ assay (Figure 3-10).

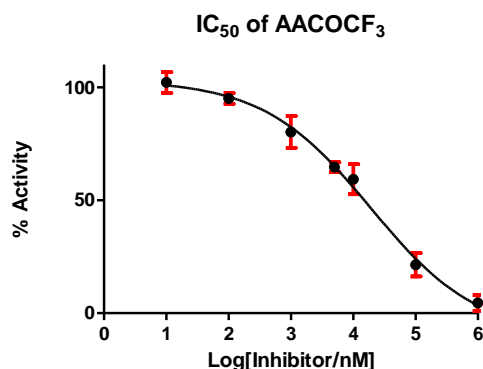


Figure 3-10. IC₅₀ of AACOCF₃ determined from a liposomal substrate solution of **Flu7OHCou**. IC₅₀ was determined to be 19.0 ± 1.5 μM from the assay.

In conclusion, **7OHCou-AACF3**, a fluorogenic inhibitor of cPLA₂ with dual functions of imaging and inhibition has been developed. **7OHCou-AACF3** has an IC₅₀ of 12.5±1.0 μM which is comparable with AACOCF₃. It is able to quench iNOS production via its role as an effective inhibitor

and is capable of imaging the increase in cPLA₂ protein levels. We have also developed **Flu7OHCou**, a cPLA₂-selective fluorogenic substrate and demonstrated its use for inhibitor screening assays.

3.9 Experimental - Chemistry

All air- and moisture-sensitive reactions were performed in an inert N₂ atmosphere, using oven-dried glassware sealed with rubber septa. All reaction mixtures and products had the glassware which contained them wrapped with aluminium foil, due to their light sensitivity. Technical-grade solvents were distilled before use. All commercial-grade reagents and solvents were purchased from Sigma Aldrich, Alfa Aesar and Acros, and were used without further purification. All flash column chromatography was conducted using Merck silica gel 60 and monitored using TLC. Similarly, the progress of all reactions was monitored using TLC. Mass spectra obtained were high resolution mass spectrometry (HRMS) via either atmospheric pressure chemical ionization (APCI) or electrospray ionization (ESI). Bruker Avance 300 (300 MHz) or 400 (400MHz) or 500 (500 MHz) NMR were used to obtain all ¹H and ¹³C and ³¹P spectra. All *J* values are reported in Hz, while chemical shifts (δ) were reported in parts per million.

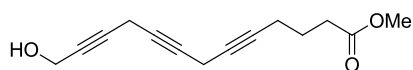
General cross-coupling procedure used in the syntheses of **3**, **5**, **7a**, and **7b**

The overall synthesis route is shown in *Scheme 2*, and was adapted from Qi *et al.*¹⁸ A mixture of **1** (1.76 g, 13.9 mmol), **2** (1.21 g, 11.6 mmol), NaI (2.61 g, 17.4 mmol), CuI (3.31 g, 17.4 mmol), and K₂CO₃ (2.41 g, 17.4 mmol) were dissolved in DMF (30.0 mL), and then stirred for 16 h at room temperature. Quenching of the reaction was done through the addition of 40 mL of water and 30 mL of EA. The bright yellow precipitate that formed upon the addition of water was removed through suction filtration. After the first extraction, two more extractions were conducted on the aqueous phase using 30 mL of ether. The organic layers were combined, dried using anhydrous Na₂SO₄, and then concentrated. The product was isolated using flash column chromatography with a 3:1 Hex:EA eluent to give a yellow oil of **3** at 89% yield (2.01 g). The synthesis of **5** was conducted by reacting bromide **4** with propargyl alcohol. The syntheses of **7a** and **7b** were conducted by reacting bromide **6**

with 5-pentynol and 6-hexynol respectively; due to **7a** and **7b**'s instability, they were immediately hydrogenated without characterisation in the following step.



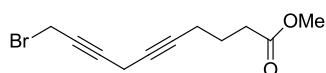
Methyl 10-hydroxydeca-5,8-diynoate 3: Yellow oil, 89% yield (2.01 g); ^1H NMR (500 MHz, CDCl_3) δ 4.22 (t, $J = 3.5$ Hz, 2H), 3.65 (s, 3H), 3.14 (t, $J = 3.5$ Hz, 2H), 2.43 – 2.37 (m, 2H), 2.23 – 2.17 (m, 2H), 1.83 – 1.76 (m, 2H); ^{13}C NMR (75 MHz, CDCl_3) δ 173.67, 80.30, 79.64, 78.54, 74.43, 51.53, 51.01, 32.79, 23.72, 18.05, 9.71.



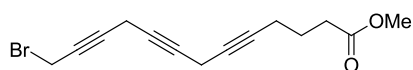
Methyl 13-hydroxytrideca-5,8,11-triynoate 5: Dark brown oil, 81% yield (2.41 g); ^1H NMR (500 MHz, CDCl_3) δ 4.23 (t, $J = 2$ Hz, 2H), 3.65 (s, 3H), 3.18 – 3.16 (m, 2H), 3.10 – 3.09 (m, 2H), 2.41 (t, $J = 7.5$ Hz, 2H), 2.22 – 2.19 (m, 2H), 1.81 – 1.75 (m, 2H); ^{13}C NMR (126 MHz, CDCl_3): δ 173.73, 79.77, 79.50, 78.74, 75.21, 74.62, 73.82, 51.55, 50.99, 32.79, 23.73, 18.07, 9.77, 9.62.

General bromination procedure used in syntheses of **4**, **6**, **9a**, **9b**

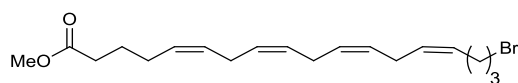
The general protocol was adapted from Qi *et al.*¹⁸ **3** (5.40 g, 27.8 mmol) and CBr_4 (17.58 g, 53.0 mmol) were dissolved in DCM (106.9 mL) and cooled to -40 °C. PPh_3 (13.9 g, 53.0 mmol) was dissolved in DCM (53.4 mL) and then added dropwise via a cannula to the reaction mixture. Upon complete addition of the dissolved PPh_3 , the reaction mixture was stirred for 2 h at -20 °C. When the reaction was completed, hexane was added to the reaction mixture, which caused the precipitation of PPh_3O . The suspension was filtered through Celite and then concentrated. The product, **4**, was then isolated using flash column chromatography with a 25:1 hexane-EA system to give a yellow oil, 81% yield (5.79 g). The synthesis of **6** was conducted using alcohol **5**. The syntheses of **9a** and **9b** were conducted using alcohol **8a** and **8b** respectively at 0 °C.



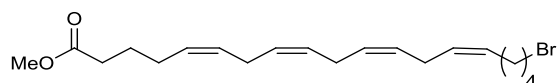
Methyl 10-bromodeca-5,8-diynoate 4: Yellow oil, 81% yield (5.71 g); $^1\text{H NMR}$ (500 MHz, CDCl_3) δ 3.90 (t, $J = 2.4$ Hz, 2H), 3.67 (s, 3H), 3.21 – 3.18 (m, 2H), 2.42 (t, $J = 7.2$ Hz, 2H), 2.26 – 2.20 (m, 2H), 1.80(quin, $J = 7.2$ Hz, 2H); $^{13}\text{C NMR}$ (126 MHz, CDCl_3): δ 173.52, 81.80, 79.96, 75.34, 73.83, 51.51, 32.79, 23.77, 18.10, 14.70, 10.02.



Methyl 13-bromotrideca-5,8,11-triynoate 6: Dark brown oil, 85% yield (1.85 g); $^1\text{H NMR}$ (300 MHz, CDCl_3) δ 3.87 (t, $J = 2.4$ Hz, 2H), 3.64 (s, 3H), 3.20 – 3.18 (m, 2H), 3.10 – 3.08 (m, 2H), 2.39 (t, $J = 7.2$ Hz, 2H), 2.22 – 2.16 (m, 2H), 1.77 (quin, $J = 7.2$ Hz, 2H); $^{13}\text{C NMR}$ (126 MHz, CDCl_3): δ 173.56, 81.14, 79.49, 75.50, 75.40, 74.44, 73.21, 51.48, 32.71, 23.70, 18.02, 14.62, 9.98, 9.59.



(5Z,8Z,11Z,14Z)-methyl 18-bromooctadeca-5,8,11,14-tetraenoate 9a: Brown oil, 88% yield (1.80 g); $^1\text{H NMR}$ (500 MHz, CDCl_3) δ 5.42 – 5.30 (m, 8H), 3.66 (s, 3H), 3.41 (t, $J = 6.5$ Hz, 2H), 2.84 – 2.79 (m, 6H), 2.32 (t, $J = 7.5$ Hz, 2H), 2.23 (t, $J = 7.3$ Hz, 2H), 2.10 (t, $J = 7.0$ Hz, 2H), 1.91 (q, $J = 7.0$ Hz, 2H), 1.70 (q, $J = 7.5$ Hz, 2H); $^{13}\text{C NMR}$ (126 MHz, CDCl_3): δ 173.82, 129.35, 128.81, 128.70, 128.11, 128.05, 128.00, 127.93, 127.83, 51.31, 33.28, 33.14, 32.35, 26.43, 25.58 (2C), 25.53, 25.50, 24.64. HRMS (ESI): calculated for $\text{C}_{19}\text{H}_{30}\text{O}_2\text{Br}$ ($\text{M}+1$) 369.1424, found 369.1419.

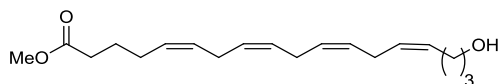


(5Z,8Z,11Z,14Z)-methyl 19-bromononadeca-5,8,11,14-tetraenoate 9b: Brown oil, 83% yield (0.100 g); $^1\text{H NMR}$ (500 MHz, CDCl_3) δ 5.40 – 5.36 (m, 8H), 3.67 (s, 3H), 3.43 – 3.40 (m, $J = 6.8$ Hz, 2H), 2.85 – 2.80 (m, 6H), 2.33 (t, $J = 7.5$ Hz, 2H), 2.14 – 2.10 (m, 4H), 1.87 (q, $J = 7.3$ Hz, 2H), 1.72 (quint, $J = 7.5$ Hz, 2H), 1.55 – 1.54 (m, 2H); $^{13}\text{C NMR}$ (126 MHz, CDCl_3): δ 173.86, 129.28, 128.85,

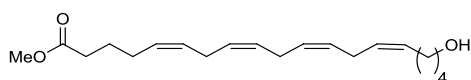
128.72, 128.32 (2C), 128.15, 128.13, 127.98, 51.34, 33.56, 33.32, 32.20, 27.97, 26.46, 26.21, 25.54 (2C), 25.52, 24.67. HRMS (ESI): calculated for C₂₀H₃₂O₂Br (M+1) 383.1580, found 383.1577.

General hydrogenation procedure used in the syntheses of **8a** and **8b**

The general protocol was adapted from Qi *et al.*¹⁸ 95% Ethanol (31.1 mL) was added to Ni(OAc)₂·4H₂O (1.27 g, 5.12 mmol) in a sealed round-bottom flask, and was flushed with H₂ gas for 10 min. 1 M Ethanolic NaBH₄ solution (6.15 mL, 6.15 mmol) was then added, followed by bubbling with H₂ gas for 10 mins. Subsequently, ethylenediamine (2.45 mL, 36.88 mmol) was added, followed by bubbling with H₂ gas for 20 mins. **7a** (1.53 g, 5.12 mmol) was then added, and the mixture was left to stir for 3 h at room temperature, with constant bubbling H₂ gas. A filtration using Celite was conducted, followed by preparative thin layer chromatography using a 4:1 Hex:EA eluent system to afford a yellow oil of **8a**, 39% yield (0.61 g). This protocol was used to synthesise **8b** from **8b**.



(5Z,8Z,11Z,14Z)-methyl 18-hydroxyoctadeca-5,8,11,14-tetraenoate 8a: Yellow oil, 39% yield (0.61 g); ¹H NMR (500 MHz, CDCl₃) δ 5.42 – 5.38 (m, 8H), 3.68 – 3.66 (m, 5H), 2.85 – 2.81 (m, 6H), 2.34 (t, *J* = 7.0 Hz, 2H), 2.20 – 2.12 (m, 4H), 1.75 – 1.63 (m, 4H); ¹³C NMR (126 MHz, CDCl₃): δ 174.11, 129.42, 128.89, 128.82, 128.40, 128.26, 128.18, 128.06, 128.03, 62.38, 51.45, 33.40, 32.44, 26.50 (2C), 25.60 (2C), 24.72, 23.55. HRMS (ESI): calculated for C₁₉H₃₀O₃Na (M+Na) 329.2087, found 329.2093.

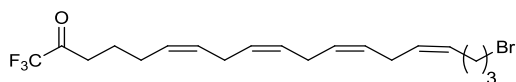


(5Z,8Z,11Z,14Z)-methyl 19-hydroxynonadeca-5,8,11,14-tetraenoate 8b: Yellow oil, 45% yield (0.11 g); ¹H NMR (300 MHz, CDCl₃) δ 5.43 – 5.35 (m, 8H), 3.67 – 3.62 (m, 5H), 2.84 – 2.64 (m, 5H), 2.35 – 2.31 (m, 2H), 2.27 – 2.04 (m, 7H), 1.73 – 1.62 (m, 4H); ¹³C NMR (75 MHz, CDCl₃): δ 174.20, 129.7, 128.94, 128.84, 128.41, 128.32, 128.00, 127.88, 127.68, 58.31, 51.55, 33.46 (2C), 26.54, 25.67,

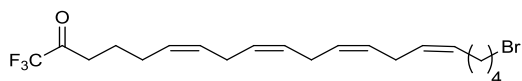
25.65, 25.62, 24.77, 24.33, 18.39. HRMS (ESI): calculated for $C_{20}H_{32}NaO_3$ (M+Na) 343.2224, found 343.2239.

General trifluoromethylation procedure used in the syntheses of **10a** and **10b**

Ester **9a** (0.44 g, 1.2 mmol) dissolved in MeOH (50 mL) was hydrolysed to its corresponding carboxylic acid the addition of 1M LiOH (34 mL). The solution was stirred at room temperature for 12 h and quenched with 1M HCl. After concentrating the mixture was diluted with water and extracted with EA. Organic phase was dried and concentrated to afford a brown liquid without subsequent purification. The acid (1.2 mmol) was dissolved in DCM (35.0 mL), followed by addition of trifluoroacetic anhydride (1.52 mL, 10.7 mmol) and pyridine (1.15 mL, 14.2 mmol).¹⁹ The solution was then stirred at room temperature for 2 h, before being quenched through addition of saturated $NaHCO_3$ solution (40.0 mL). Extraction was conducted with DCM (3 x 30.0 mL). The organic layers were combined and dried using anhydrous Na_2SO_4 , before being concentrated to afford the crude product. The crude product was further purified through flash column chromatography using a 3:1 Hex-EA eluent system to afford a yellow oil of **10a**, 78% yield (0.36 g). This protocol was used to synthesise **10b** from **9b**.



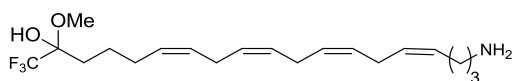
(6Z,9Z,12Z,15Z)-19-bromo-1,1,1-trifluorononadeca-6,9,12,15-tetraen-2-one 10a: Dark brown oil, 78% yield (0.36 g); 1H NMR (500 MHz, $CDCl_3$) δ 5.44 – 5.31 (m, 8H), 3.39 (t, $J = 6.5$ Hz, 2H), 2.85 – 2.79 (m, 6H), 2.71 (t, $J = 7.5$ Hz, 2H), 2.20 (q, $J = 7.0$ Hz, 2H), 2.13 (q, $J = 7.0$ Hz, 2H), 1.91 (quint, $J = 7.0$ Hz, 2H), 1.75 (quint, $J = 7.5$ Hz, 2H); ^{13}C NMR (126 MHz, $CDCl_3$): δ 191.19 (q, $J = 34$ Hz, 1C), 129.46, 129.33, 128.14, 128.08, 127.95, 127.86, 127.82, 118.95, 115.55 (q, $J = 290$ Hz, 1C), 35.47, 33.09, 32.37, 25.89, 25.59, 25.54, 25.51, 25.49, 22.04. HRMS (ESI): calculated for $C_{19}H_{25}BrOF_3$ (M+1) 405.1046, found 405.1031.



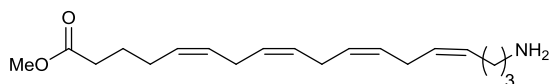
(6Z,9Z,12Z,15Z)-20-bromo-1,1,1-trifluoricoso-6,9,12,15-tetraen-2-one 10b: Pale yellow oil, 58% yield (65 mg); ^1H NMR (500 MHz, CDCl_3) δ 5.41 – 5.38 (m, 8H), 3.45 – 3.35 (m, 2H), 2.86 – 2.81 (m, 1H), 2.72 (t, $J = 7.0$ Hz, 4H), 2.17 – 2.10 (m, 2H), (m, 2H), 1.87 (t, $J = 7.5$ Hz, 2H), 1.76 (t, $J = 7.5$ Hz, 2H), 1.51 (t, $J = 7.5$ Hz, 2H); ^{13}C NMR (126MHz, CDCl_3): δ 191.24 (t, $J = 35$ Hz), 129.99, 129.57, 129.38, 128.35, 128.32, 128.30, 128.26, 128.17, 128.14, 127.94, 127.90, 127.87, 127.85, 127.80, 115.53 (q, $J = 292.1$ Hz, 1C), 72.70, 58.44, 35.56, 33.61, 29.21, 29.18, 28.03, 27.08, 26.98, 26.27, 26.10, 25.97, 25.60. HRMS (ESI): calculated for $\text{C}_{20}\text{H}_{29}\text{BrF}_3\text{O}$ ($M+1$) 421.1348, found 421.1346.

General amination protocol used in the synthesis of 11a, and 21

9a (1.60 g, 4.33 mmol) was dissolved in a 7N methanolic solution of NH_3 (50.0 mL), and heat in a sealed tube for 12 h. The solvent was removed, and flash column chromatography was conducted using a 80:20:1 DCM:MeOH:TEA eluent system to afford a yellow oil of **21**, 71% yield (0.940 g). The synthesis of **11a** was conducted using bromide **10a**.



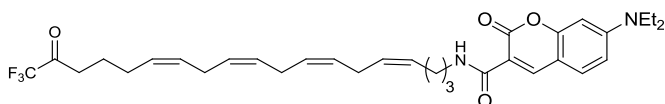
(6Z,9Z,12Z,15Z)-19-amino-1,1,1-trifluoro-2-methoxynonadeca-6,9,12,15-tetraen-2-ol 10a: Yellow oil, 91% yield (0.30 g), eluent system: 98:2 DCM-MeOH; ^1H NMR (500 MHz, CDCl_3) δ 5.98 (s, 3H), 5.36 – 5.35 (m, 8H), 3.47 – 3.44 (m, 3H), 2.97 (t, $J = 7.5$ Hz, 2H), 2.82 – 2.71 (m, 6H), 2.18 – 2.12 (m, 4H), 1.98 – 1.84 (m, 2H), 1.78 – 1.77 (m, 4H); ^{13}C NMR (126 MHz, CDCl_3): δ 191.43 (d, $J = 35$ Hz), 129.52, 129.49, 128.26, 128.17, 128.12, 127.99, 127.88, 127.69, 115.52 (d, $J = 287.9$ Hz, 1C), 50.25, 39.51, 35.53, 27.41, 27.08, 25.92, 25.54, 25.52, 24.16, 22.08. HRMS (ESI): calculated for $\text{C}_{19}\text{H}_{27}\text{O}_2\text{NF}_3$ ($M+1$) 342.2050, found 342.2045.



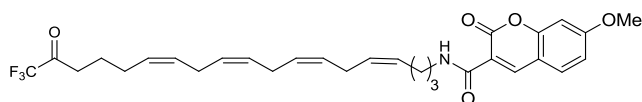
(5Z,8Z,11Z,14Z)-methyl 18-aminooctadeca-5,8,11,14-tetraenoate 21: Yellow oil, 71% yield (0.94 g), eluent system: 90:10:1 DCM:MeOH:TEA; ^1H NMR (500 MHz, CDCl_3) δ 6.98 (s, 5H), 5.36 – 5.31 (m, 8H), 3.62 (s, 3H), 2.96 (s, 2H), 2.80 – 2.76 (m, 6H), 2.28 (t, $J = 7.5$ Hz, 2H), 2.14 (q, $J = 6.8$ Hz, 2H), 2.05 (q, $J = 7.0$ Hz, 2H), 1.82 (t, $J = 7.3$ Hz, 2H), 1.69 (s, 2H); ^{13}C NMR (126 MHz, CDCl_3): δ 173.88, 129.26, 128.72, 128.61, 128.14 (2C), 128.08, 127.78, 127.72, 51.30, 39.72, 33.22, 26.32, 25.46, 25.45 (2C), 25.42, 25.40, 24.55. HRMS (ESI): calculated for $\text{C}_{19}\text{H}_{32}\text{O}_2\text{N}$ (M+1) 306.2428, found 306.2434.

General amidation procedure used in syntheses of 12a-f

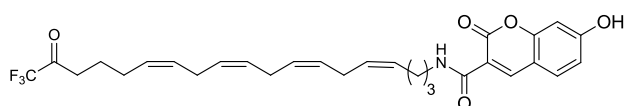
11a (10.0 mg, 0.03 mmol), the respective carboxylic acid (0.03 mmol), EDC.HCl (7.6 mg, 0.04 mmol), HOBt (6.0 mg, 0.04 mmol) and TEA (5.5 μL , 0.04 mmol) were dissolved in DMF (1.2 mL). The mixture was stirred for 12 h at room temperature, and then quenched with brine. Extraction with EA was performed twice on the aqueous layer; the organic layers were combined, dried, and then concentrated. Column chromatography afforded the respective amide **12a-f**.



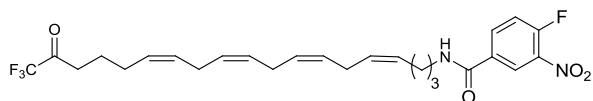
7-(diethylamino)-2-oxo-N-((4Z,7Z,10Z,13Z)-19,19-trifluoro-18-oxononadeca-4,7,10,13-tetraen-1-yl)-2H-chromene-3-carboxamide 12a: Yellow solid, 89% yield (14 mg), eluent system: 3:1 hexane-EA; ^1H NMR (500 MHz, DMSO) δ 8.64 (s, 1H), 7.67 (d, $J = 14$ Hz, 1H), 6.81 – 6.79 (m, 1H), 6.60 (s, 2H), 5.39 – 5.28 (m, 8H), 3.46 (q, $J = 6.5$ Hz, 4H), 3.28 (d, $J = 7.0$ Hz, 2H), 2.79 – 2.73 (m, 4H), 2.10 – 2.03 (m, 2H), 2.02 – 1.99 (m, 2H), 1.60 – 1.54 (m, 2H), 1.51 – 1.46 (m, 2H), 1.31 – 1.23 (m, 4H), 1.14 (t, $J = 7.0$ Hz, 6H); ^{13}C NMR (126 MHz, DMSO): δ 162.07, 161.76, 157.14, 152.36, 147.54, 131.47 (2C), 129.57, 129.11, 128.08, 127.98, 127.75, 127.69, 127.66, 110.07, 109.46, 107.62, 95.81, 44.26 (2C), 38.34, 34.59, 28.96, 26.65, 25.40 (2C), 25.11, 24.14, 21.53, 12.24 (2C). HRMS (ESI): calculated for $\text{C}_{33}\text{H}_{40}\text{F}_3\text{N}_2\text{O}_4$ (M-1) 585.2946, found 585.2948.



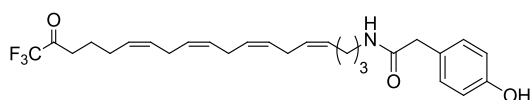
7-methoxy-2-oxo-N-((4Z,7Z,10Z,13Z)-19,19,19-trifluoro-18-oxonadeca-4,7,10,13-tetraen-1-yl)-2H-chromene-3-carboxamide 12b: Pale yellow solid, 68% yield (10 mg), eluent system: 2:1 hexane-EA; ^1H NMR (500 MHz, DMSO) δ 8.83 (s, 1H), 8.74 (s, 1H), 7.57 (d, $J = 2.0$ Hz, 1H), 7.46 (d, $J = 9.0$ Hz, 1H), 7.36-7.34 (m, 1H), 6.61 (s, 1H), 5.41 – 5.30 (m, 8H), 3.84 (s, 3H), 2.85 – 2.76 (m, 5H), 2.16 (s, 2H), 2.12 – 2.06 (m, 3H), 2.03 – 1.98 (m, 3H), 1.62 – 1.59 (m, 2H), 1.24 (m, 6H); ^{13}C NMR (126 MHz, DMSO): δ 162.88, 160.33, 155.93, 148.31, 147.15, 129.58, 129.12, 128.65, 128.12, 127.98, 127.81, 127.75, 127.71, 121.88, 118.89, 117.19 (2C), 111.80, 55.79, 38.62, 35.48, 28.96, 28.80, 28.62, 25.12, 24.13, 21.81, 21.60. HRMS (ESI): calculated for $\text{C}_{30}\text{H}_{33}\text{F}_3\text{NO}_5$ (M-1) 544.2316, found 544.2321.



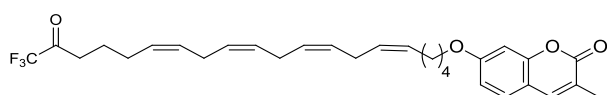
7-hydroxy-2-oxo-N-((4Z,7Z,10Z,13Z)-19,19,19-trifluoro-18-oxonadeca-4,7,10,13-tetraen-1-yl)-2H-chromene-3-carboxamide 12c: Pale yellow, 42% yield (6.0 mg), eluent system: 1:1 hexane-EA; ^1H NMR (500 MHz, DMSO) δ 11.04 (s, 1H), 8.77 (s, 1H), 8.64 (t, $J = 5.5$ Hz, 1H), 7.80 (d, $J = 9.0$ Hz, 1H), 6.88 (dd, $J = 8.5, 2.0$ Hz, 1H), 6.80 (s, 1H), 5.40 – 5.28 (m, 8H), 3.30 (d, $J = 6.5$ Hz, 2H), 2.85 – 2.69 (m, 6H), 2.15 – 2.09 (m, 2H), 2.07 – 2.00 (m, 2H), 1.62 – 1.55 (m, 4H), 1.31 – 1.26 (m, 2H); ^{13}C NMR (126 MHz, CDCl_3): δ 163.52, 161.40, 161.02, 156.18, 147.84, 131.87, 129.63, 129.08, 128.64, 128.57, 128.08, 127.96, 127.79, 127.66, 114.26, 113.70, 111.07, 101.72, 38.50, 35.41, 28.88, 25.41, 25.11 (2C), 25.07, 24.13, 21.62. HRMS (ESI): calculated for $\text{C}_{29}\text{H}_{31}\text{F}_3\text{NO}_5$ (M-1) 530.2160, found 530.2165.



4-fluoro-3-nitro-N-(((4Z,7Z,10Z,13Z)-19,19,19-trifluoro-18-oxonadeca-4,7,10,13-tetraen-1-yl)benzamide 12d: Pale yellow liquid, 87% yield (12 mg), eluent system: 3:1 hexane-EA; ^1H NMR (500 MHz, DMSO) δ 8.79 (d, $J = 5.1$ Hz, 1H), 8.62 (dd, $J = 7.2, 2.0$ Hz, 1H), 8.28 – 8.25 (m, 1H), 7.70 (dd, $J = 11.0, 8.8$ Hz, 1H), 5.40 – 5.29 (m, 8H), 3.31 – 3.27 (m, 2H), 2.86 – 2.75 (m, 6H), 2.15 – 2.04 (m, 4H), 2.03 – 1.99 (m, 2H), 1.64 – 1.57 (dd, $J = 14.1, 7.0$ Hz, 2H), 1.30 – 1.23 (m, 2H); ^{13}C NMR (126 MHz, DMSO) δ 163.03, 156.07 (d, $J = 265.7$ Hz, 1C), 136.59, 135.04 (d, $J = 9.9$ Hz, 1C), 131.38 (d, $J = 3.7$ Hz, 1C), 129.25, 128.64 (d, $J = 11.5$ Hz, 1C), 128.00, 127.79 (d, $J = 9.5$ Hz, 1C), 127.68, 125.11, 125.10, 125.09, 118.67 (d, $J = 21.3$ Hz, 1C), 39.02, 35.43, 28.81, 25.43, 25.14 (2C), 25.10, 24.24, 21.64. HRMS (ESI): calculated for $\text{C}_{26}\text{H}_{29}\text{F}_4\text{N}_2\text{O}_4$ (M-1) 509.2069, found 509.2074.

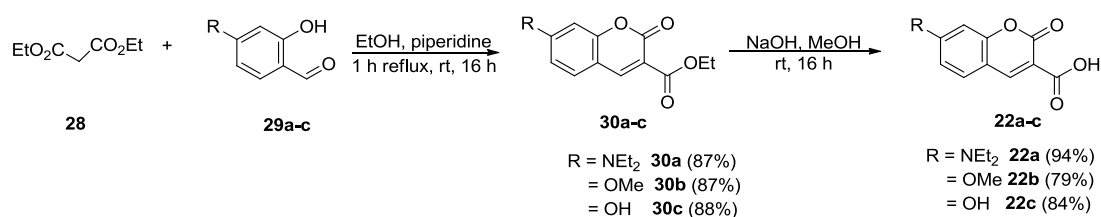


2-(4-hydroxyphenyl)-N-(((4Z,7Z,10Z,13Z)-19,19,19-trifluoro-18-oxonadeca-4,7,10,13-tetraen-1-yl)acetamide 12e: Brown solid, 94% yield (12 mg), eluent system: 99:1 DCM-MeOH; ^1H NMR (500 MHz, DMSO) δ 9.18 (s, 1H), 7.88 (s, 1H), 7.01 (d, $J = 7.9$ Hz, 2H), 6.64 (d, $J = 13.4$ Hz, 2H), 5.37 – 5.32 (m, 8H), 3.24 (s, 2H), 3.04 – 3.00 (m, 2H), 2.87 – 2.70 (m, 6H), 2.08 – 2.01 (m, 4H), 1.63 – 1.60 (m, 2H), 1.46 – 1.30 (m, 2H), 1.23 (s, 2H); ^{13}C NMR (126 MHz, DMSO) δ 170.35, 155.76, 129.70 (2C), 129.61, 129.27, 128.69, 128.60, 128.00, 127.85, 127.70, 126.59, 115.02, 114.87(2C), 41.56, 38.20, 35.41, 29.05, 25.42 (2C), 25.12, 25.09, 24.15, 21.63. HRMS (ESI): calculated for $\text{C}_{27}\text{H}_{33}\text{F}_3\text{NO}_3$ (M-1) 476.2418, found 476.2416.



3-methyl-7-(((5Z,8Z,11Z,14Z)-20,20,20-trifluoro-19-oxoicosa-5,8,11,14-tetraen-1-yl)oxy)-2H-chromen-2-one 12f: **10b** (25 mg, 0.06mmol) was dissolved in DMF (0.5 mL) and added with 4-methylumbelliferone (8.7 mg, 0.049) and K_2CO_3 (20.5 mg, 0.15 mmol). The mixture was refluxed for

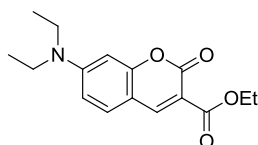
4 h and allowed to cool to room temperature. Mixture was quenched by addition of brine and extraction was performed with EA. The organic phase was separated and dried and concentrated. Flash column chromatography was conducted using a 2:1 Hexane:EA eluent system to afford a brown liquid, 26% yield (8.0 mg); ^1H NMR (500 MHz, DMSO) δ 7.68 (d, J = 8.5 Hz, 1H), 6.96 (m, 2H), 6.21 (s, 1H), 5.38 – 5.33 (m, 8H), 4.09 (t, J = 6.5 Hz, 2H), 2.81 – 2.78 (m, 6H), 2.40 (s, 3H), 2.11 – 2.05 (m, 2H), 2.03 – 2.02 (m, 2H), 1.77 – 1.74 (m, 2H), 1.50 – 1.48 (m, 2H), 1.24 (m, 4H); ^{13}C NMR (126 MHz, DMSO): δ 162.03, 160.09, 154.73, 153.33, 130.29, 129.55, 129.38, 127.99, 127.93, 127.85, 127.68, 126.36 (2C), 112.97, 112.35, 111.00, 101.08, 68.05, 28.96, 28.82, 28.63, 28.54, 27.96, 26.25, 25.39, 25.18, 25.15, 18.05. HRMS (ESI): calculated for $\text{C}_{30}\text{H}_{36}\text{F}_3\text{O}_4$ ($M+1$) 517.2560, found 517.2564.



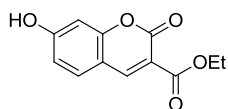
Scheme 3-7. Synthesis of Coumarin analogues

General procedure used in the synthesis of **30a** and **c**

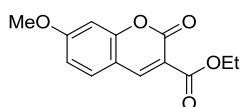
The synthesis of **30c** was adapted from Ma *et al.*²⁰ Aldehyde **29c** (1.51 g, 10.9 mmol), diethyl malonate (2.47 mL, 16.3 mmol), and piperidine (0.80 mL, 8.15 mmol) were dissolved in ethanol (15.6 mL), and then refluxed for 1 h. After that, the reaction mixture was stirred at room temperature for 16 h. The ethanol was removed, and recrystallization was performed using a bi-solvent system of hexane and EA to afford yellow crystals of **30c**, 88% yield (2.26 g). This protocol was used to synthesise **30a** from aldehyde **29a**.



Ethyl 7-(diethylamino)-2-oxo-2H-chromene-3-carboxylate 30a: Brown powder, 87% yield (0.65 g); ^1H NMR (500 MHz, CDCl_3) δ 8.39 (s, 1H), 7.33 (d, $J = 9.5$ Hz, 1H), 6.59 (dd, $J = 9.5, 2.0$ Hz, 1H), 6.42 (d, $J = 2.0$ Hz, 1H), 4.35 (q, $J = 7.0$ Hz, 2H), 3.42 (q, $J = 7.0$ Hz, 4H), 1.37 (t, $J = 7.3$ Hz, 3H), 1.21 (t, $J = 7.0$ Hz, 6H); ^{13}C NMR (126 MHz, CDCl_3): δ 164.03, 158.29, 158.13, 152.74, 149.00, 130.90, 109.44, 108.73, 107.51, 96.52, 60.93, 44.95 (2C), 14.22, 12.27 (2C). HRMS (ESI): calculated for $\text{C}_{16}\text{H}_{19}\text{NO}_4\text{Na}$ ($\text{M}+\text{Na}$) 312.1206, found 312.1213.



Ethyl 7-hydroxy-2-oxo-2H-chromene-3-carboxylate 30c: Yellow solid, 88% yield (2.26 g); ^1H NMR (300 MHz, DMSO) δ 11.09 (s, 1H), 8.67 (s, 1H), 7.75 (d, $J = 8.7$ Hz, 1H), 6.84 (dd, $J = 8.6$ Hz, $J = 2.3$ Hz, 1H), 6.73 (d, $J = 2.1$ Hz, 1H), 4.26 (q, $J = 6.9$ Hz, 2H), 1.29 (t, $J = 7.2$ Hz, 3H); ^{13}C NMR (75 MHz, DMSO): δ 164.04, 162.93, 157.09, 156.39, 149.42, 132.10, 113.99, 112.08, 110.41, 101.78, 60.79, 14.12. HRMS (ESI): calculated for $\text{C}_{12}\text{H}_9\text{O}_5$ ($\text{M}-1$) 233.0455, found 233.0446.

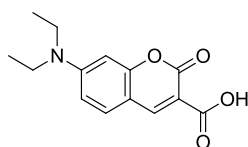


Ethyl 7-methoxy-2-oxo-2H-chromene-3-carboxylate 30b The synthesis of **30b** was adapted from Ma *et al.*²⁰ **29b** (0.500 g, 2.59 mmol), diethyl malonate (0.59 mL, 3.88 mmol), and piperidine (0.19 mL, 1.94 mmol) were dissolved in ethanol (5.2 mL), and then refluxed for 1 h. After that, the reaction mixture was stirred at room temperature for 24 h. The ethanol was removed, and the solid was re-dissolved in EA (30.0 mL). Extraction was carried out using EA (3 x 40.0 mL) and H_2O (30.0 mL), and the organic layer was combined and dried using Na_2SO_4 . The solvent was removed and flash column chromatography was conducted using a 1:1 Hex:EA eluent system to afford a yellow solid of **30b**, 87% yield (0.65 g); ^1H NMR (500 MHz, CDCl_3) δ 8.45 (s, 1H), 7.25 (d, $J = 9.5$ Hz, 1H), 7.21 –

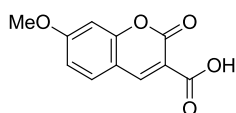
7.18 (m, 1H), 6.99 (d, $J = 7.5$ Hz, 1H), 4.39 (q, , $J = 7.0$ Hz, 2H), 3.84 (s, 3H), 1.38 (t, $J = 7.0$ Hz, 3H); ^{13}C NMR (126 MHz, CDCl_3): δ 163.02, 156.81, 156.20, 149.62, 148.23, 122.50, 118.43, 118.05, 117.73, 110.62, 61.83, 55.82, 14.13. HRMS (ESI): calculated for $\text{C}_{13}\text{H}_{12}\text{NO}_5\text{Na}$ ($\text{M}+\text{Na}$) 271.0577, found 271.0576.

General basic hydrolysis procedure used in the syntheses of 22a-c

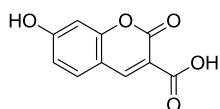
30b (0.65 g, 0.26 mmol) was dissolved in a 0.5M methanolic solution of NaOH (6.0 mL), and left to stir at room temperature for 16 h. Solvent was removed from the reaction mixture and then 1M HCl was added (4.0 mL). The resulting mixture was refrigerated for 24 h, and then filtered and dried to afford a brown powder of **22b**, 79% yield (0.40 g). This protocol was used to synthesise **22a** and **22c** from **30a** and **30c** respectively.



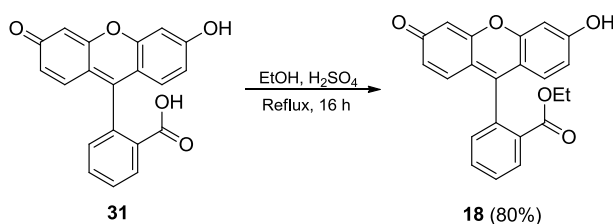
7-(diethylamino)-2-oxo-2H-chromene-3-carboxylic acid 22a: Brown powder, 94% yield (0.55 g); ^1H NMR (500 MHz, DMSO) δ 12.47 (s, 1H), 8.56 (s, 1H), 7.60 (d, $J = 9$ Hz, 2H), 6.76 (d, $J = 8.9$ Hz, 1H), 6.50 (d, $J = 2.1$ Hz, 1H), 3.46 (q, $J = 6.9$ Hz, 4H), 1.25 (t, $J = 7.2$ Hz, 6H); ^{13}C NMR (126 MHz, CDCl_3): δ 164.40, 159.63, 157.82, 152.86, 149.36, 131.78, 110.00, 107.35, 107.04, 95.87, 44.35 (2C), 12.25 (2C). HRMS (ESI): calculated for $\text{C}_{14}\text{H}_{15}\text{NO}_4\text{Na}$ ($\text{M}+\text{Na}$) 284.0893, found 284.091.



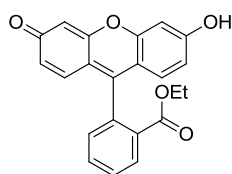
7-methoxy-2-oxo-2H-chromene-3-carboxylic acid 22b: Yellow crystals, 79% yield (0.40 g); ^1H NMR (500 MHz, DMSO) δ 13.22 (s, 1H), 8.69 (s, 1H), 7.47 (d, , $J = 2.5$ Hz, 1H), 7.38 (d, $J = 9$ Hz, 1H) 7.32 (dd, $J = 9.0, 2.8$ Hz, 1H), 3.81 (s, 3H); ^{13}C NMR (126 MHz, DMSO): δ 164.43, 157.43, 156.18, 149.37, 148.52, 122.47, 119.03, 118.84, 117.70, 112.33, 56.26. HRMS (ESI): calculated for $\text{C}_{11}\text{H}_7\text{O}_5$ ($\text{M}-1$) 219.0299, found 219.0294.



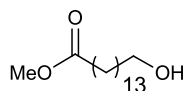
7-hydroxy-2-oxo-2H-chromene-3-carboxylic acid 22c: Yellow crystals, 84% yield (1.89 g); ^1H NMR (300 MHz, DMSO) δ 12.87 (s, 1H), 11.09 (s, 1H), 8.69 (s, 1H), 7.75 (d, $J = 8.7$ Hz, 1H), 6.87 – 6.83 (m, 1H), 6.74 (d, $J = 1.8$ Hz, 1H); ^{13}C NMR (75 MHz, DMSO): δ 164.29, 164.00, 157.67, 157.04, 149.49, 132.08, 114.07, 112.48, 110.67, 101.85. HRMS (ESI): calculated for $\text{C}_{10}\text{H}_5\text{O}_5$ (M-1) 205.0142, found 205.0137.



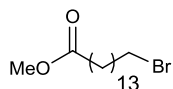
Scheme 3-8. Synthesis of fluorescein **18**



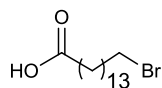
Ethyl 2-(6-hydroxy-3-oxo-3H-xanthen-9-yl)benzoate 18: **31** (1.0 g, 3.0 mmol) was dissolved in EtOH (20.0 mL), followed by addition of H_2SO_4 (1.5 mL, 28.1 mmol) to the solution. The solution was refluxed for 16 h. Solid Na_2CO_3 was added to the solution, which was then filtered. The filtrate was concentrated and the resulting solids that formed were re-dissolved in boiling ethanol. Recrystallization followed by filtration and drying afforded an orange solid of **18**, 80% yield (0.865 g); ^1H NMR (500 MHz, CDCl_3) δ 8.18 (d, $J = 7.5$ Hz, 1H), 7.85 (t, $J = 7.3$ Hz, 1H), 7.77 (t, $J = 7.5$ Hz, 1H), 7.48 (d, $J = 7.5$ Hz, 1H), 6.80 (d, $J = 9.5$ Hz, 2H), 6.57 (d, $J = 7.5$ Hz, 4H), 3.95 (q, $J = 7.0$ Hz, 2H), 0.86 (t, $J = 7.0$ Hz, 3H); ^{13}C NMR (126 MHz, CDCl_3): δ 165.48, 150.90, 134.04, 133.38, 131.09 (2C), 131.00 (2C), 130.55, 130.37, 115.20, 103.75, 61.31, 13.75. HRMS (ESI): calculated for $\text{C}_{22}\text{H}_{17}\text{O}_5$ (M+1) 361.1071, found 361.1078.



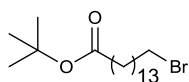
Methyl 15-hydroxypentadecanoate 14: ω -pentadecalactone **13** (5.0 g, 20.8 mmol) was dissolved in MeOH (50.0 mL), and 30% methanolic sodium methoxide (1.54 mL, 8.3 mmol) was added to the solution, which immediately turned from clear to cloudy. The solution was stirred for 16 h at room temperature. Quenching was conducted through addition of water and 3M HCl. The methanol was removed through heating the solution under reduced pressure, which left behind a suspension of solids. The solids were filtered and recrystallized with EA to afford a white solid of **14**, 99% yield (5.64 g); ^1H NMR (500 MHz, CDCl_3) δ 4.85 (s, 1H), 3.64 (s, 3H), 3.61 (t, $J = 6.8$ Hz, 3H), 2.28 (t, $J = 7.5$ Hz, 2H), 1.60 (t, $J = 7.0$ Hz, 2H), 1.54 (t, $J = 7.5$ Hz, 2H), 1.27 (m, 20H); ^{13}C NMR (126 MHz, CDCl_3): δ 174.37, 62.97, 51.38, 34.07, 32.74, 29.55 (2C), 29.51 (2C), 29.38 (2C), 29.19 (2C), 29.09, 25.69, 24.90. HRMS (ESI): calculated for $\text{C}_{16}\text{H}_{32}\text{O}_3\text{Na}$ ($\text{M}+\text{Na}$) 295.2244, found 295.2246.



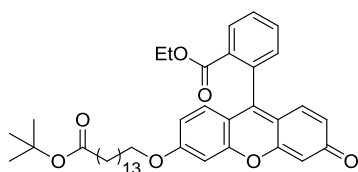
Methyl 15-bromopentadecanoate 15: **14** (4.84 g, 17.8 mmol) was added with CBr_4 (11.2 g, 33.8 mmol) and dissolved in DCM (250 mL). The mixture was cooled to 0°C and PPh_3 (8.85 g, 33.8 mmol) was added in portion to the mixture. The reaction was allowed to warm to room temperature and stirred for 16 h. When the reaction was completed, hexane was added to the reaction mixture, which caused the precipitation of PPh_3O . The suspension was filtered through celite and then concentrated. Flash column chromatography with a 99:1 hexane-EA system to give a pale yellow solid **15**, 53% yield (3.16g), eluent system: 9:1 hexane-EA; ^1H NMR (500 MHz, CDCl_3) δ 3.69 (s, 3H), 3.43 (t, $J = 7.0$ Hz, 2H), 2.32 (t, $J = 7.5$ Hz, 2H), 1.87 (quin, $J = 7.0$ Hz, 2H), 1.65 – 1.62 (m, 2H), 1.46 – 1.43 (m, 2H), 1.26 (m, 20H); ^{13}C NMR (126 MHz, CDCl_3): δ 174.31, 51.40, 34.11, 33.99, 32.85, 29.58, 29.57, 29.55, 29.51 (2C), 29.42, 29.24, 29.14, 28.76, 28.17, 24.95. HRMS (ESI): calculated for $\text{C}_{16}\text{H}_{31}\text{O}_2\text{Br}$ ($\text{M}+\text{Na}$) 334.1507, found 334.1507.



15-bromopentadecanoic acid 16: 15 (1.62 g, 4.8 mmol) was dissolved in THF (50 mL) and add with 1M LiOH (24 mL). The solution was stirred at room temperature for 16 h and quenched with 1M HCl. After concentrating the mixture was diluted with water and extracted with DCM. Organic phase was dried and concentrated to afford a white solid **16** with no additional purification, 97% yield (1.51 g); ^1H NMR (500 MHz, CDCl_3) δ 3.39 (t, $J = 6.9$ Hz, 2H), 2.33 (t, $J = 7.5$ Hz, 2H), 1.87 – 1.81 (m, 2H), 1.63 – 1.60 (m, 2H), 1.42 – 1.39 (m, 2H), 1.27 – 1.25 (m, 18H); ^{13}C NMR (126 MHz, CDCl_3) δ 180.37, 34.06, 33.95, 32.79, 29.54 (2C), 29.51, 29.48, 29.38, 29.36, 29.18, 29.00, 28.72, 28.13, 24.61. HRMS (ESI): calculated for $\text{C}_{15}\text{H}_{28}\text{O}_2\text{Br}$ (M-1) 319.1278, found 319.1283.

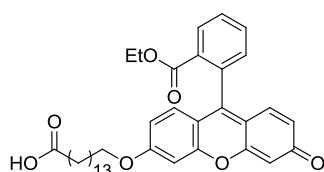


tert-butyl 15-bromopentadecanoate 17: 16 (1.51 g, 4.7 mmol) was dissolved in DCM (15.0 mL) and cooled to 0 °C. Trifluoroacetic anhydride (1.47 mL, 10.4 mmol) was added dropwise to the mixture and the solution was allowed to warm to room temperature for 2 h. Tert-butanol (1.62 mL, 16.9mmol) was added and stirred for an additional 3 h. When no more starting material was detected, the mixture was quenched with water and extracted with diethyl ether. Organic phase was dried and concentrated, flash column chromatography was conducted using a 19:1 Hex:EA eluent system to afford a white solid **17**, 95% yield (1.68g), eluent system: 19:1 hexane-EA; ^1H NMR (500 MHz, CDCl_3) δ 3.39 (t, $J = 6.9$ Hz, 2H), 2.19 (t, $J = 7.5$ Hz, 2H), 1.87 – 1.81 (m, 2H), 1.58 – 1.55 (m, 2H), 1.43 (s, 9H), 1.27 – 1.25 (m, 20H); ^{13}C NMR (126 MHz, CDCl_3) δ 173.14, 79.69, 35.52, 33.77, 32.77, 29.51 (2C), 29.49, 29.45, 29.38, 29.35, 29.21, 29.01, 28.69, 28.10, 28.03(3C), 25.03. HRMS (ESI): calculated for $\text{C}_{19}\text{H}_{37}\text{O}_2\text{Br}$ (M+Na) 399.1869, found 399.1873.



Ethyl 2-(6-((15-(tert-butoxy)-15-oxopentadecyl)oxy)-3-oxo-3H-xanthen-9-yl)benzoate **19: **17****

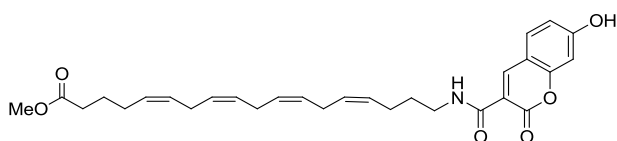
(0.65 g, 1.72 mmol) was dissolved in DMF (5.6 mL) and added with **18** (0.5 g, 1.39 mmol) and DIPEA (0.87 mL, 5.0 mmol). The mixture was refluxed for 2 h and was cooled to room temperature. Following which, the reaction was quenched by the addition of brine while extraction was performed using EA. The organic phase was then dried and concentrated. Flash column chromatography was conducted using a 19:1 DCM:MeOH eluent system to afford an orange solid **19**, 84% yield (0.77 g); ^1H NMR (500 MHz, CDCl_3) δ 8.20 (dd, $J = 7.8, 1.2$ Hz, 1H), 7.69 (td, $J = 7.5, 1.4$ Hz, 1H), 7.63 (td, $J = 7.7, 1.3$ Hz, 1H), 7.27 (dd, $J = 7.5, 1.1$ Hz, 1H), 6.90 (d, $J = 2.2$ Hz, 1H), 6.87 – 6.82 (m, 2H), 6.70 (dd, $J = 8.9, 2.3$ Hz, 1H), 6.49 (dd, $J = 9.7, 1.9$ Hz, 1H), 6.40 (d, $J = 1.9$ Hz, 1H), 4.03 – 3.95 (m, 4H), 2.15 (t, $J = 7.5$ Hz, 2H), 1.79 – 1.76 (m, 2H), 1.54 – 1.51 (m, 2H), 1.43 – 1.40 (m, 11H), 1.31 – 1.30 (m, 18H), 0.92 (t, $J = 7.1$ Hz, 3H); ^{13}C NMR (126 MHz, CDCl_3) δ 185.20, 173.02, 165.09, 163.61, 158.72, 154.12, 150.39, 134.01, 132.32, 130.97, 130.52, 130.17, 130.08, 129.44 (2C), 128.77, 117.26, 114.54, 113.64, 105.39, 100.51, 79.58, 68.76, 61.06, 35.37, 29.37(2C), 29.34 (2C), 29.29, 29.22, 29.08, 29.05, 28.84, 28.70, 27.90 (3C), 25.70, 24.87, 13.37. HRMS (ESI): calculated for $\text{C}_{41}\text{H}_{52}\text{O}_7$ ($\text{M}+\text{Na}$) 679.3605, found 679.3608.



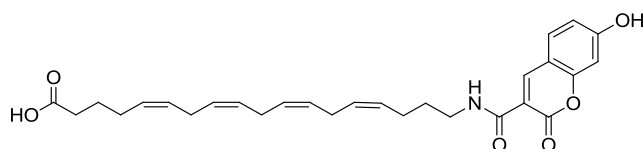
15-((9-(2-(ethoxycarbonyl)phenyl)-3-oxo-3H-xanthen-6-yl)oxy)pentadecanoic acid **20: **19**** (0.46 g,

0.7 mmol) was dissolved in TFA (5.0 mL) and heated at 70 °C for 1 h. When no more starting material was observed, TFA was removed under reduced pressure. Flash column chromatography was conducted using a 19:1 DCM:MeOH eluent system to afford an orange solid **20**, 88% yield (0.37g); ^1H NMR (500 MHz, CDCl_3) δ 8.27 (d, $J = 7.7$ Hz, 1H), 7.74 (dt, $J = 28.2, 7.5$ Hz, 2H), 7.32 (d, $J =$

7.5 Hz, 1H), 6.99 (s, 1H), 6.94 (t, $J=10.5$ Hz, 2H), 6.78 (d, $J = 9.0$ Hz, 1H), 6.65 (d, $J = 10$ Hz, 1H), 6.61 (s, 1H), 4.11 – 4.02 (m, 4H), 2.36 (t, $J = 7.5$ Hz, 2H), 1.87 – 1.84 (m, 2H), 1.67 – 1.64 (m, 2H), 1.50 – 1.47 (m, 2H), 1.28 (s, 18H), 0.97 (t, $J = 7.1$ Hz, 3H); ^{13}C NMR (126 MHz, CDCl_3) δ 185.25, 177.84, 165.15 (2C), 164.16, 159.16, 154.55, 133.98, 132.45, 131.12, 130.55, 130.48, 130.21, 129.67, 129.07 (2C), 117.20, 114.71, 114.32, 105.28, 100.54, 69.00, 61.27, 34.13, 29.48, 29.46, 29.41, 29.37, 29.32, 29.17, 29.14, 29.02, 28.75, 25.81, 25.78, 24.76, 13.47. HRMS (ESI): calculated for $\text{C}_{37}\text{H}_{45}\text{O}_7$ (M+1) 601.3160, found 601.3166.

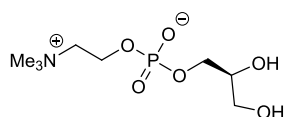


(5Z,8Z,11Z,14Z)-methyl 18-(7-hydroxy-2-oxo-2H-chromene-3-carboxamido)octadeca-5,8,11,14-tetraenoate 23: 21 (58.6 mg, 0.19 mmol) was dissolved in DMF (7.7 mL) and added with **22c** (36.0 mg, 0.17 mmol), EDC.HCl (50.0 mg, 0.26 mmol), HOBt (35.0 mg, 0.26 mmol) and TEA (36.5 μL , 0.26 mmol). The reaction was stirred at room temperature for 12 h and quenched with the addition of brine. Extraction was performed with EA with 1% AcOH. The organic layer was separated, dried and concentrated. Flash column chromatography was conducted using a 2:1 Hexane:EA eluent system to afford a pale yellow solid **23**, 60% yield (52mg); ^1H NMR (500 MHz, CDCl_3) δ 9.01 (s, 1H), 8.79 (s, 1H), 7.53 (d, $J = 8.5$ Hz, 1H), 6.94 (dd, $J = 11.7, 2.9$ Hz, 2H), 5.41 – 5.30 (m, 8H), 3.67 (s, 3H), 3.48 – 3.45 (m, 2H), 2.81 – 2.75 (m, 5H), 2.32 (t, $J = 7.5$ Hz, 2H), 2.19 – 2.15 (m, 2H), 2.11 – 2.08 (m, 2H), 1.74 – 1.66 (m, 4H); ^{13}C NMR (126 MHz, CDCl_3) δ 174.57, 163.57, 162.85, 162.08, 156.72, 148.61, 131.43, 128.90 (2C), 128.80, 128.73, 128.22, 128.15, 128.11, 128.09, 114.94, 113.45, 111.80, 102.83, 51.62, 39.51, 33.48, 29.13, 26.49, 25.58 (2C), 25.55, 24.76, 24.62. HRMS (ESI): calculated for $\text{C}_{29}\text{H}_{34}\text{NO}_6$ (M-1) 492.2392, found 492.2394.

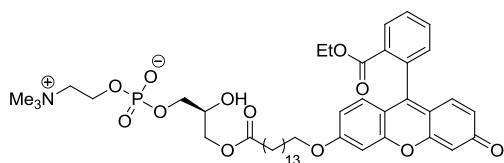


(5Z,8Z,11Z,14Z)-18-(7-hydroxy-2-oxo-2H-chromene-3-carboxamido)octadeca-5,8,11,14-

tetraenoic acid 24: 23 (39 mg, 0.08 mmol) was dissolved in a solution of THF:MeOH: H₂O-1:1:1 (0.6 mL) and added with 1M LiOH (60 μ L). The mixture was stirred for half an hour at room temperature and quenched with 1M HCl. Extraction was performed using EA with 1% AcOH and the subsequent organic phase was separated, dried and concentrated. Flash column chromatography was conducted using a 2:1:0.03 Hexane:EA:AcOH eluent system afford **24** as a pale yellow solid, 45% yield (17 mg); ¹H NMR (500 MHz, CDCl₃) δ 9.04 (d, *J* = 5.5 Hz, 1H), 8.74 (d, *J* = 6.8 Hz, 1H), 7.46 (d, *J* = 8.3 Hz, 1H), 6.89 – 6.84 (m, 2H), 5.40 – 5.34 (m, 8H), 3.45 (d, *J* = 6.3 Hz, 2H), 2.81 – 2.77 (m, 4H), 2.37 (dd, *J* = 15.0, 7.6 Hz, 2H), 2.24 – 2.10 (m, 2H), 2.00 (d, *J* = 6.2 Hz, 2H), 1.74 – 1.62 (m, 4H), 1.31 (m, 2H); ¹³C NMR (126 MHz, CDCl₃) δ 177.70, 163.38, 162.00, 156.60, 148.74, 131.46, 130.89, 129.02, 128.95, 128.73, 128.69, 128.42, 128.15, 128.09, 128.05, 114.92, 113.22, 111.79, 102.79, 39.67, 33.32, 29.67, 29.10, 26.48, 25.64, 24.57, 22.67, 14.08. HRMS (ESI): calculated for C₂₈H₃₃NO₆ (M+Na) 502.2200, found 502.2201.



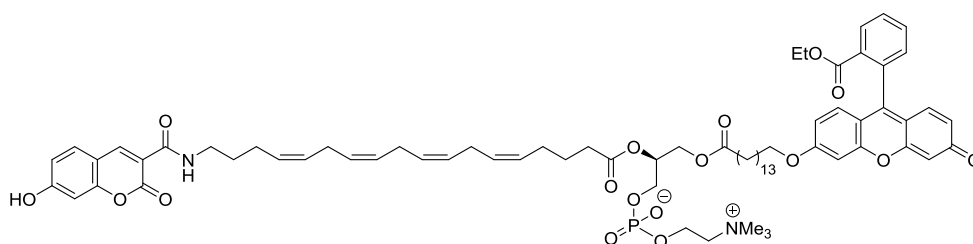
(S)-2,3-dihydroxypropyl (2-(trimethylammonio)ethyl) phosphate 26: 1,2-diheptanoyl-*sn*-glycero-3-phosphocholine **25** (0.5 g, 1.0 mmol) was dissolved in methanol (180 mL) and added with 1 M NaOH (20 mL). The solution was refluxed for 2 h and cooled to room temperature. 2M HCl (10 mL) was added to quench the reaction and the mixture was concentrated. Extraction was performed using EA and water and the aqueous layer was separated and concentrated. Methanol was then added to dissolve the resulting solids in which the residual solids were filtered and discarded while the filtrate was concentrated to afford a white solid **26**, 90% yield (0.24 g); ¹H NMR (500 MHz, MeOD) δ 3.99 (s, 2H), 3.61 (m, 2H), 3.47 (m, 2H), 3.42 (m, 1H), 3.24 (m, *J* = 7.5 Hz, 3H), 3.10 (m, 1H), 3.07 (s, 9H); ¹³C NMR (126 MHz, MeOD): δ 72.74, 67.25, 66.70, 63.59, 59.61, 54.39.



(S)-3-((15-((9-(2-(ethoxycarbonyl)phenyl)-3-oxo-3H-xanthen-6-yl)oxy)pentadecanoyl)oxy)-2-

hydroxypropyl(2-(trimethylammonio) ethyl) phosphate **27 :** Synthesis of **27** was adapted from G.

Borsotti *et al.*²² **20** (177 mg, 0.22 mmol) was first dissolved in THF (2.0 mL) and stirred with CDI (62 mg, 0.38 mmol) at room temperature for 2 h. The mixture was then concentrated and redissolved in DMF (7.0 mL). At the same time, **26** (52 mg, 0.20 mmol) was added into DMF (3.0mL) and sonicated to dissolve the solids before adding into the solution of **20**. K₂CO₃ (54mg, 0.45 mmol) was added and the reaction was heated at 40 °C for 12 h. After the reaction was complete, the solution was extracted with chloroform and water. Organic phase was re-extracted with water and combined aqueous phase was concentrated under reduced pressure. The crude mixture was dissolved in DMSO (20 μL) and added with 20 μL of 1,2-Dioleoyl-sn-glycero-3-phosphocholine(10mM in EtOH), 20 μL of 1,2-Dioleoylphosphatidylglycerol (10mM in EtOH). The mixture was then added to a Tris-buffer solution (6.0 mL), pH 8.9, and stirred vigorously. 60 μL of Bee venom PLA₂ (500 units/mL) was subsequently added and the reaction was stirred at room temperature for 8 h and concentrated. Preparative TLC was performed with the eluent 9:1 DCM:MeOH to afford an orange solid **27**, 55% yield (94 mg); ¹H NMR (500 MHz, MeOD) δ 8.30 (d, *J* = 8 Hz, 1H), 7.87 (td, *J* = 7.5, 1.3 Hz, 1H), 7.80 (td, *J* = 7.7, 1.2 Hz, 1H), 7.45 (d, *J* = 7.5 Hz, 1H), 7.23 (d, *J* = 2.3 Hz, 1H), 7.06 (dd, *J* = 9.3, 5.6 Hz, 2H), 6.95 (dd, *J* = 9.0, 2.3 Hz, 1H), 6.60 (dd, *J* = 9.6, 2.0 Hz, 1H), 6.52 (d, *J* = 2.0 Hz, 1H), 4.32 (d, *J* = 2.3 Hz, 2H), 4.21 – 4.18 (m, 3H), 4.14 – 4.11 (m, 1H), 4.06 – 3.98 (m, 3H), 3.95 -3.91 (m, 2H), 3.67 (dd, *J* = 5.7, 3.2 Hz, 2H), 3.25 (s, 9H), 2.37 (t, *J* = 7.5 Hz, 2H), 1.87 – 1.84 (m, 2H), 1.63 – 1.61 (m, 2H), 1.52 – 1.51 (m, 2H), 1.41 – 1.31 (m, 18H), 0.95 (t, *J* = 7.1 Hz, 3H); ¹³C NMR (126 MHz, MeOD) δ 187.21, 175.36, 166.73, 166.56, 161.50, 156.42, 156.26, 135.15, 133.99, 132.59, 132.20, 131.94, 131.65, 131.29, 130.85, 129.32, 118.12, 116.15, 116.02, 105.46, 101.90, 70.43, 69.89, 67.87, 67.54, 66.24, 62.44, 60.47, 54.71, 34.92, 30.73 (2C), 30.71, 30.64 (2C), 30.59, 30.41, 30.38, 30.22, 30.02, 26.99, 25.99, 13.92; ³¹P NMR (202 MHz, MeOD) δ 0.37. HRMS (ESI): calculated for C₄₅H₆₃NO₁₂P (M+1) 840.4082, found 840.4090.



(S)-3-((15-((9-(2-(ethoxycarbonyl)phenyl)-3-oxo-3H-xanthen-6-yl)oxy)pentadecanoyl)oxy)-2-(((5Z,8Z,11Z,14Z)-18-(7-hydroxy-2-oxo-2H-chromene-3-carboxamido)octadeca-5,8,11,14-tetraenyl)oxy)propyl (2-(trimethylammonio)ethyl) phosphate Flu7OHCou: **24** (17.0 mg, 0.04 mmol) was first dissolved in THF (1.0 mL) and stirred with CDI (6.2mg, 0.04mmol) at room temperature for 2 h. The mixture was then concentrated and redissolved in DMF (2.0 mL). At the same time, **27** (40 mg, 0.05 mmol) dissolved in DMF (0.5 mL) and added into the solution of **24**. K₂CO₃ (5.8mg,0.04 mmol) was added and the reaction was heated at 40 °C for 12 h. The reaction was extracted with chloroform and water. Organic phase was re-extracted with water and combined aqueous phase was concentrated under reduced pressure. Preparative TLC was performed with the eluent 9:1 DCM:MeOH to afford an orange solid, 60 % yield (27.3 mg); ¹H NMR (500 MHz, MeOD) δ 9.03 (s, 1H), 8.74 (s, 1H), 8.30 (d, *J* = 7.0 Hz, 1H), 7.87 (dt, *J* = 7.6, 3.8 Hz, 1H), 7.80 (dt, *J* = 7.7, 6.6 Hz, 1H), 7.74 (dd, *J* = 5.7, 3.3 Hz, 1H), 7.67 – 7.63 (m, 1H), 7.46 (d, *J* = 7.6 Hz, 1H), 7.21 (d, *J* = 2.3 Hz, 1H), 7.06 – 7.04 (m, 2H), 6.93 (dd, *J* = 9.0, 2.3 Hz, 1H), 6.88 (d, *J* = 8.4 Hz, 1H), 6.77 (s, 1H), 6.60 – 6.58 (m, 1H), 6.51 (d, *J* = 1.6 Hz, 1H), 5.44 – 5.26 (m, 8H), 4.44 (dd, *J* = 12.0, 3.1 Hz, 1H), 4.29 (s, 2H), 4.24 (dd, *J* = 5.5, 2.9 Hz, 1H), 4.20 – 4.17 (m, 3H), 4.05 – 3.98 (m, 4H), 3.67 – 3.66 (m, 2H), 3.44 – 3.42 (m, 2H), 3.25 (s, 9H), 2.87 – 2.77 (m, 4H), 2.37 – 2.30 (m, 5H), 2.23 – 2.19 (m, 2H), 2.11 – 2.05 (m, 4H), 1.88 – 1.82 (m, 2H), 1.73 – 1.67 (m, 4H), 1.53 – 1.50 (m, 3H), 1.36 – 1.31 (m, 20H), 0.97 (t, *J* = 7.5 Hz, 3H); ¹³C NMR (101 MHz, MeOD) δ 185.82, 173.53, 173.00, 167.95, 165.34, 165.12, 163.16, 162.00, 160.07, 157.15, 154.99, 154.76, 148.17, 133.75, 132.57, 132.22, 131.48, 131.17, 130.98, 130.80, 130.56, 130.27, 129.87, 129.48, 129.42, 128.58, 128.52, 128.46, 127.97, 127.91, 127.81, 127.76, 127.67, 116.74, 114.75, 114.61, 112.19, 110.96, 104.11, 100.51, 70.47, 69.03, 67.76, 66.14, 63.54, 62.27, 61.04, 59.06, 53.39, 53.35, 53.31, 38.81, 35.14, 33.52, 33.11, 31.65, 30.24, 29.32, 29.22, 28.98, 28.74, 28.63, 26.71, 26.13, 25.60, 25.21, 24.60, 24.26, 23.58, 22.61, 22.30, 12.96,

12.52, 9.99; ³¹P NMR (243 MHz, MeOD) δ -0.43. HRMS (ESI): calculated for C₇₃H₉₂N₂O₁₇P (M-1) 1299.6139, found 1299.6137.

3.10 Experimental - biology

3.10.1 Enzchek Phospholipase A₂ Fluorogenic Assay (% Activity)

The assay was conducted according to the manufacturer's instruction (E10217, Molecular Probes) with slight modification. Briefly, substrate solution was separately prepared by mixing 5 μL of DOPG, 5 μL of DOPC and 5 μL of substrate respectively in 1.5 mL of 1X reaction buffer. The mixture was vortexed vigorously for 3 min before allowing to stand at room temperature for an hour. 48 μL of 1X reaction buffer was added into each well of a 96-wells plate. This was followed by addition of 1 μL of recombinant cPLA₂ (P4074-03R, US Biological) and 1 μL of 1 mM of the respective inhibitor/test compound dissolved in DMSO. The final concentration of the test compound achieved was 10 μM. The reaction was initiated by adding 50 μL of the substrate solution and incubating at room temperature for an hour. Fluorescence was measured using a Varioskan Flash plate reader (ThermoFisher Scientific) at 485 nm excitation and 515nm emission. Positive control was performed when 1 μL of the test compound was replaced by vehicle DMSO. % cPLA₂ activity was calculated by the following formula

$$\% \text{ cPLA}_2 \text{ activity} = \frac{\text{fluorescence of tested well} - \text{background}}{\text{fluorescence of positive control} - \text{background}}$$

3.10.2 Enzchek Phospholipase A₂ Fluorogenic Assay (IC₅₀)

The assay was conducted as described above. Instead of adding a fixed concentration of the inhibitor/test compound, various concentration of **7OHCou-AACF3** was reconstituted in DMSO. 48 μL of 1X reaction buffer were added into each well of a 96-wells plate. This is followed by addition of 1 μL of recombinant cPLA₂ (P4074-03R, US Biological) and 1 μL of the respective concentration of **7OHCou-AACF3** dissolved in DMSO. The reaction was initiated by adding 50 μL of the substrate solution and incubating at room temperature for an hour. Fluorescence was measured using a

Varioskan Flash plate reader (ThermoFisher Scientific) at 485 nm excitation and at 515 nm emission. Positive control was performed when 1 μ L of **7OHCou-AACF3** was replaced by vehicle DMSO.

3.10.3 Enzchek Phospholipase A₂ Fluorogenic Assay (Selectivity)

The assay was conducted as described above. Instead of adding cPLA₂, it was replaced by sPLA₂. 48 μ L of 1X reaction buffer was added into each well of a 96-wells plate. This is followed by addition of 1 μ L of sPLA₂, human recombinant type V (Cat no. 10009563, Cayman Chemical) and 1 μ L of 1 mM of the respective test compound dissolved in DMSO. Thio-etheramidePC is a sPLA₂ selective inhibitor and was purchased from Cayman Chemical (Cat no. 62750). The reaction was initiated by adding 50 μ L of the substrate solution and incubating at room temperature for an hour. Fluorescence was measured using a Varioskan Flash plate reader (ThermoFisher Scientific) by exciting at 485 nm, while fluorescence emission was detected at 515 nm. Positive control was performed when 1 μ L of tested compound was replaced by vehicle DMSO.

% sPLA₂ activity was calculated by the following formula:

$$\% \text{ sPLA}_2 \text{ activity} = \frac{\text{fluorescence of tested well} - \text{background}}{\text{fluorescence of positive control} - \text{background}}$$

3.10.4 Cell-Culture

SHSY5Y human neuroblastoma cells (ATCC CRL-2266) were cultured in DMEM full medium (ThermoFisher Scientific, 11995-065) supplemented with 10% Fetal Bovine Serum, 100 μ g/mL streptomycin and 100 units/mL penicillin. Cells were maintained in an incubator at 37 °C, under a 5% CO₂, water saturated environment. When performing trichostatin A (TSA)-treatment, SHSY5Y cells were plated on 12 wells with density of 0.15x10⁶ cells per well. After observing a 70% confluency, TSA pre-dissolved in DMEM to achieve a final concentration of 0.75 μ M was added to each well and incubated for 24 hours. Cells were then washed once with 1xPBS (1.0 mL) and scrapped on ice with RIPA buffer, which contain 1 x Protease Inhibitor (Roche, 11836153001) and 1 mM PMSF and incubated on ice for 30 min. This was followed by centrifuging the cell debris at 4 °C for 30 min at

13200 rpm before transferring the supernatant to a clean tube and storing the sample at -20 °C for future analyses.

Murine BV-2 cells (ATCC CRL-2540) were cultured in DMEM (ThermoFisher Scientific, 11965092) supplemented with 10% Fetal Bovine Serum, 100 µg/mL streptomycin and 100 units/mL penicillin. Cells were maintained in an incubator at 37 °C, under a 5% CO₂, water saturated environment. When performing LPS treatment, BV-2 cells were plated on 10 cm dish in 10 mL DMEM at a density of 1x10⁶ cells per dish one day prior to the experiment. After observing that cells are at 90% confluency, lipopolysaccharide (Sigma, L6529) pre-dissolved in DMEM to achieve a concentration of 2 µg/mL was added to the dish. 10 µM of **7OHCou-AACF3** were added to the LPS containing medium which was then transferred to the 10 cm dish. DMSO was used as vehicle control and added to the non-LPS treated control. The cells were incubated for 14 hours at 37 °C, under a 5% CO₂. After the respective timepoint, cells were washed once with 1xPBS (10 mL) and scrapped on ice with 8 mL 1xPBS. Collected cells were spun at 800 rpm for 3 min at 4 °C, before discarding the supernatant. Cells were lysed in RIPA buffer, which contains 1 x Protease Inhibitor and 1 mM PMSF and incubated on ice for 30 min. This was followed by spinning the cell debris at 4 °C for 30 min at 13200 rpm before transferring the supernatant to a clean tube and storing the sample at -20 °C for future analyses.

3.10.5 MTS assay

Cells were plated on 96-wells plate and grown for 24 h at a density of 8000 cells per well for both HEK293T (ATCC CRL-3216) and BV-2 cells (ATCC CRL-2540). Cells were cultured in an incubator at 37 °C under a 5% CO₂ environment in 100 µL of DMEM. Thereafter, the compound of interest dissolved in DMEM at a concentration of 10 µM was added into each well. DMSO was added as vehicle in the control group. 3 biological replicates were performed. The plates were then incubated at 37 °C with 5% CO₂ for 48 h and 72 h. At each individual time point, 20 µL of CellTiter 96® Aqueous One Solution (MTS reagent) was added into each well and re-incubated at 37 °C with 5% CO₂ without light for 3 h. Colorimetric readings were taken at 490 nm using a spectrophotometer and analysed.

3.10.6 BCA Assay

BCA assay (Pierce BCA Protein Assay Kit, 23225) was performed to quantify the concentration of proteins in the cell lysate. 10 μ L of sample (1 μ L lysate with 9 μ L of lysis buffer) and BSA standards (range from 1.25 to 50 μ g/ml) were mixed in a 96 well-plate and incubated with 190 μ L of working reagent mixture (ratio of Reagent A:B used was 50:1) at 37 °C for 20 mins. The colour intensity that was developed was read at 562 nm using a spectrophotometer. A standard curve of different concentrations of BSA was plotted using the average blank-corrected readings for each standard vs. its respective concentration (μ g/ml). This was then used to determine the protein concentration for unknown samples.

3.10.7 Western Blot

The amount of protein in the lysates were normalized by BCA previously. 25 μ g of individual protein samples were mixed with an equal volume of 2x Laemmli buffer containing DTT and denatured at 90 °C for 10 mins. Lysates were loaded into a 10% Tris-Gly Gel. SDS-PAGE was ran at a voltage of 100 V for 1.5 hours in 1x Running Buffer (10% Tris-Gly-SDS buffer). The protein samples on the gel were then transferred to PVDF membrane assembled in a sandwich soaked in 1x Transfer Buffer (10% Tris-Gly buffer, 10% methanol, 0.1% SDS) at 100 V for 2 hours under ice. The membrane blots were then incubated for one hour at room temperature in a blocking buffer containing 5% milk in 1xTris-Gly buffer and 0.1% TBST, followed by overnight incubation with the respective primary antibody dissolved in 5% milk in 1xTris-Gly buffer and 0.1 % TBST at 4 °C. After three washes with 1xTris-Gly buffer in 0.1% TBST, each of duration 10 min, the blot was incubated with a secondary horse-radish peroxidase-conjugated antibody (1:10000) dissolved in 5% milk in 1xTris-Gly buffer and 0.1% TBST for one hour at room temperature. Three washes with 1xTris-Gly buffer in 0.1% TBST, each of duration 10 min were performed. Enhanced Chemiluminescence (ECL) detection of protein bands was performed using ECL Plus Western Blotting detecting system (GB Healthcare). Antibodies used in western blot include rabbit polyclonal anti-NOS2 (Santa-Cruz, sc-651, 1:100), mouse monoclonal anti-cPLA₂ primary antibody (Santa Cruz, sc-454, 1:200), mouse anti-GAPDH (Merck, 1:10000),

with secondary horse-radish peroxidase-conjugated antibodies (Santa Cruz, 1:10000). GAPDH was used as the control protein to normalize loading quantity in each lane of the blot.

3.10.8 Cell-staining

The respective treatments were performed as described in the cell-treatment experiment. For these experiments, cells were grown on coverslip coated with 0.1mg/ml PDL. After the respective hours of treatment, 10 μ M of **7OHCou-AACF3** were dissolved in DMEM and incubated with the cells at 37 $^{\circ}$ C for 1 h to stain the cells. Medium was then removed from individual wells and cells were rinse once with 1xPBS (1 mL). 4% formaldehyde (500 μ L) were added for 10 min at room temperature for fixation before rinsing the cells twice with 1xPBS(1 mL). Coverslips were dried for 1 min before mounting it on glass-slides using Prolong Gold Antifade Mountant,(Thermofisher, P36930).

3.10.9 Photophysical property of 7OHCou-AACF3

Quantum yields were measured and calculated by using the following equation and referencing with $\Phi_{fl} = 0.546$ of Quinine sulfate in 0.5M H_2SO_4 solution ($n = 1.35$).

$$QY = QY_{ref} \frac{\eta^2}{\eta_{ref}^2} \frac{I}{A} \frac{A_{ref}}{I_{ref}}$$

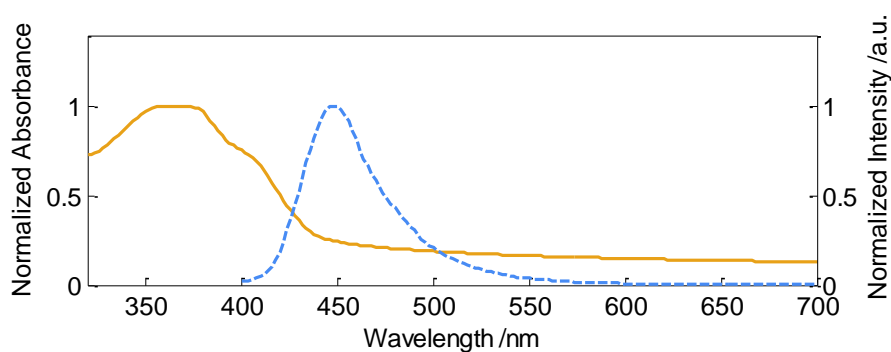


Figure 3-11. Absorbance (—) and Emission (---) of the inhibitor probe **7OHCou-AACF3** in water.

3.10.10 Assay with positive control bee venom PLA₂

6 μL of 10 mM **Flu7OHCou** was mixed with 10 μL of DOPG, 10 μL of DOPC and added into 3 mL of Tris-HCl (50 mM Tris-HCl, 100 mM NaCl, 20 mM CaCl₂, 1% Triton X, pH 7.3) buffer solution. The solution was vortexed vigorously for 3 min before allowing it to stand at room temperature for one hour. 100 μL of the liposomal solution was added into a 96-wells plate. The reaction was initiated by adding 1 μL of Bee venom (E10217), 5 units/ml from EnzChek PLA₂ Assay. Fluorescence was measured using a Varioskan Flash plate reader (ThermoFisher Scientific) by exciting at 410 nm, and measuring the emission spectra at every 5 min intervals. Negative control was performed when 1 μL of bee venom was replaced by the buffer solution.

3.10.11 Assay for cPLA₂ enzyme with and without Triton X-100

6 μL of 10 mM **Flu7OHCou** was mixed with 10 μL of DOPG, 10 μL of DOPC and added into 3 mL of either Tris-HCl (50 mM Tris-HCl, 100 mM NaCl, 20 mM CaCl₂, pH 8.9) or (50 mM Tris-HCl, 100 mM NaCl, 20 mM CaCl₂, 1% Triton X-100, pH 8.9) buffer solution. The solution was vortexed vigorously for 3 min before allowing it to stand at room temperature for one hour. 100 μL of the liposomal solution was added into each well of a 96-wells plate. The reaction was initiated by adding 1 μL of recombinant cPLA₂ (P4074-03R, US Biological). Fluorescence was measured using a Varioskan Flash plate reader (ThermoFisher Scientific) by exciting at 410 nm, and measuring the emission spectra at every 5 min intervals. Negative control was performed when 1 μL of bee venom was replaced by the buffer solution.

3.10.12 Assay for selectivity test with Flu7OHCou

6 μL of 10 mM **Flu7OHCou** was mixed with 10 μL of DOPG, 10 μL of DOPC and added into 3 mL of Tris-HCl (50 mM Tris-HCl, 100 mM NaCl, 20 mM CaCl₂, pH 8.9) or (50 mM Tris-HCl, 100 mM NaCl, 20 mM CaCl₂, 1% Triton X-100, pH 8.9) buffer solution. The solution was vortexed vigorously for 3 min before allowing it to stand at room temperature for one hour. 100 μL of the liposomal solution was added into each well of a 96-wells plate. The reaction was initiated by adding 1 μL of recombinant cPLA₂ (P4074-03R, US Biological) as well as 1 μL of reconstituted sPLA₂ (10009563,

Cayman Chemicals) each having activity of 0.05 unit/mL. Fluorescence was measured using a Varioskan Flash plate reader (ThermoFisher Scientific) by exciting at 410 nm, while fluorescence emission was detected at 447 nm at 5 min intervals. Negative control was performed when 1 μ L of enzyme was replaced by the buffer solution.

3.10.13 Assay to determine IC₅₀ of AACOCF₃ with Flu7OHCou

6 μ L of 10 mM **Flu7OHCou** was mixed with 10 μ L of DOPG, 10 μ L of DOPC and added into 3 mL of Tris-HCl (50 mM Tris-HCl, 100 mM NaCl, 20 mM CaCl₂, pH 8.9) buffer solution. The solution was vortexed vigorously for 3 min before allowing it to stand at room temperature for one hour. 100 μ L of the liposomal solution was added into each well of a 96-wells plate. This is followed by adding 1 μ L of the respective concentration of **AACOCF₃** dissolved in DMSO. The reaction was initiated by adding 1 μ L of recombinant cPLA₂ (P4074-03R, US Biological) and incubating at room temperature for one hour. Fluorescence was measured using a Varioskan Flash plate reader (ThermoFisher Scientific) by exciting at 410 nm, while fluorescence emission was detected at 447 nm. Positive control was performed when 1 μ L of inhibitor/test compound was replaced by vehicle DMSO.

3.11 References

- 1 Yui, K.; Imataka, G.; Nakamura, H.; Ohara N. & Naito, Y. *Curr. Neuropharmacol.* **2015**, *13*(6), 776.
- 2 Gijon, M. A.; Spencer, D. M.; Kaiser, A. L. & Leslie, C. C. *J. Cell Biol.*, **1999** *145*, 1219.
- 3 Dennis, E. A.; Cao, J. ; Hsu, Y. H. ; Magrioti, V. & Kokotos, G. *Chem. Rev.*, **2011** *111*, 6130.
- 4 Farber, S. A.; Olson, E. S.; Clark, I. D. & Halpern, M. E. *J. Biol. Chem.*, **1999** *274*, 19338.
- 5 Bonventre, J. V.; Huang, Z.; Taheri, M. R.; O'Leary, E. ; Li, E.; Moskowitz M. A. & Sapirstein, A. *Nature* **1997**, *390*, 622.
- 6 Desbène, C.; Malaplate-Armand, C.; Youssef, I.; Garcia, P.; Stenger, C.; Sauvée, M.; Fischer, N.; Rimet, D.; Koziel, V.; Escanyé, M. C.; Oster, T.; Kriem, B.; Yen, F. T.; Pillot, T. & Olivier, J. L. *Neurobiol. Aging* **2012**, *33*, 1123.e17.
- 7 Chiorazzo, M. G.; Bloch, N. B.; Popov, A. V. & Delikatny, E. J. *Bioconjugate Chem.* **2015**, *26*, 2360.
- 8 Huang, W.; Bhavsar, A.; Ward, R. E.; Hall, J. C. E.; Priestley, J. V. & Michael-Titus A. T. *J. Neurotrauma* **2009**, *26*(8), 1429.
- 9 Chuang, D. Y.; Simonyi, A.; Kotzbauer, P. T.; Gu, Z. & Sun, G. Y. *J. Neuroinflammation* **2015**, *12*, 199.
- 10 Tan, C. S-H; Ng, Y-K & Ong, W-Y *Mol. Neurobiol.* **2016**, *53*, 3854.
- 11 Stephens, D.; Barbayianni, E.; Constantinou-Kokotou, V.; Peristeraki, A.; Six, D. A.; Cooper, J.; Harkewicz, R.; Deems, R. A.; Dennis, E. A. & Kokotos, G. *J. Med. Chem.* **2006**, *49*, 2821.
- 12 Six, D. A.; Barbayianni, E.; Loukas, V.; Constantinou-Kokotou, V.; Hadjipavlou-Litina, D.; Stephens, D.; Wong, A. C.; Magrioti, V.; Moutevelis-Minakakis, P.; Baker, S. F.; Dennis, E. A. & Kokotos, G. *J. Med. Chem.* **2007**, *50*, 4222.
- 13 Manna, D. & Cho, W. *Methods Enzymol.* **2007**, *434*, 15.
- 14 Wijewickrama, G. T.; Kim, J. H.; Abraham, Y. J.; Oh, Y. S.; Ananthanarayanan, B.; Kwatia, M.; Ackerman, S. J. & Cho, W. J. *J. Biol. Chem.* **2006**, *281*, 10935.

- 15 Connolly, S.; Bennion, C.; Botterell, S.; Croshaw, P. J.; Hallam, C.; Hardy, K.; Hartopp, P.; Jackson, C. G.; King, S. J.; Lawrence, L.; Mete, A.; Murray, D.; Robinson, D. H.; Smith, G. M.; Stein, L.; Walters, I.; Wells, E. & Withnall, W. J. *J. Med. Chem.* **2002**, *45*, 1348
- 16 Fukuda, T.; Kim, D. K.; Chin, M-R.; Hales, C. A. & Bonventre, J. V. *Am. J. Physiol. Lung Cell Mol. Physiol.* **1999**, *277*, 533
- 17 Dennis, E. A.; Reynolds, L. J. & Lin, Y. Assay and substrate for arachidonoyl-specific phospholipase A2, Patent WO1995005479A1, **1995**
- 18 Qi, L.; Meijler, M. M.; Lee, S.H.; Sun, C. & Janda, K. D. *Org. Lett.* **2004**, *6*, 1673 – 1675.
- 19 Ackermann, E. J.; Conde-Frieboes, K. & Dennis, E. A. *J. Biol. Chem.* **1995**, *270*, 445-450.
- 20 Ma, Y.; Luo, W.; Quinn, P. J.; Liu, Z. & Hider, R. C. *J. Med. Chem.* **2004**, *47*, 6349 - 6362.
- 21 Barba-Bon, A.; Costero, A. M.; Gil, S.; Parra, M.; Soto, J.; Martínez-Máñez, R. & Sancenón, F. *Chem. Commun.* **2012**, *48*, 3000-3002
- 22 Borsotti, G.; Battistel, E.; Cellini, F. & Iannaccone, R. Process for the synthesis of Diricinoleylphosphatidylcholine, Patent EP0979825, **2000**

CHAPTER 4: CONCLUSION AND FUTURE PERSPECTIVE

4.1 Conclusion

In this thesis, we have developed a new class of inhibitors of cPLA₂ basing it on AACOCF₃ as scaffold. By devising a synthetic route that is divergent, common intermediates could be identified and used for the synthesis of the compounds. A total of 33 compounds including AACOCF₃ was synthesized and structure activity relationship studies was performed. Among these 33 compounds, we identified one compound, **2i** to be the most potent, non-cytotoxic and a selective and effective inhibitor of cPLA₂. By testing the compound in potential neuroinflammatory model involving LPS-stimulated BV-2 microglial cells, **2i** was able to reduce **ROS** and **iNOS** production. In addition, PAMPA assay showed that **2i** is brain penetrant, further enhancing the potential of **2i** to be a neurological agent for inhibition of cPLA₂ in the CNS. We have also developed **7OHCou-AACF3** as a non-cytotoxic and selective fluorogenic inhibitor of cPLA₂ with dual functions of imaging and inhibition. With an IC₅₀ of 12.5±1.0 μM which is comparable with AACOCF₃, it was demonstrated to quench iNOS production via its role as an inhibitor and is capable of imaging the increase in cPLA₂ protein levels. In addition, **Flu7OHCou**, a cPLA₂-selective fluorogenic substrate was synthesized and demonstrated its use for inhibitor screening assays.

4.2 Future Perspectives

Further modification on the inhibitor scaffold could be directed on the alkyl chain end region, such as changing it to bulky aromatic derivatives to see how flexible the enzyme is at this pocket. In addition, the use of **2i** could be expanded to other neurodegenerative models such as Alzheimer's disease or multiple sclerosis to see the effect it has on disease reversal by reducing cPLA₂'s activity. This could determine the potential of **2i** as a neurological inhibitor of cPLA₂, with upon further studies on its pharmacokinetic properties could assess the feasibility of upgrading **2i** into potential clinical trial.

In terms of developing inhibitor and substrate probe for cPLA₂, a wider range of fluorophore could be attached to the tail end of arachidonyl trifluoromethylketone. The current probe 7-hydroxycoumarin

could potentially be deprotonated at higher pH leading to the formation of a charged moiety. Having a neutral fluorophore allows pH effects to be reduced, hence giving a more stable response. More applications could be performed using the substrate probe **Flu7OHCou** including the use of it to track cPLA₂ activity in tissue slices eg. brain slices. This would pave the path for potential *in vivo* applications.

Lastly, potential functionalization of the alkyl chain end of **2i** could allow the installation of a 7-hydroxycoumarin moiety. The resulting inhibitor probe formed could be more specific to cPLA₂ and the applications similar to what **7OHCou-AACF3** could perform may also be explored.